ABSTRACT

Title of dissertation: SUPERSYMMETRIC INVERSE SEESAW
                           AND ITS PHENOMENOLOGY

                           Paratma Sri Bhupal Dev
                           Doctor of Philosophy, 2012

Dissertation directed by: Professor Rabindra Nath Mohapatra
                           Maryland Center for Fundamental Physics and
                           Department of Physics,
                           University of Maryland,
                           College Park, MD 20742, USA.

The Standard Model (SM) of particle physics, in spite of being spectacularly successful in describing the low-energy physics, cannot be a complete theory of Nature. There are a number of experimental as well as theoretical reasons to believe that there must be some new physics not far above the electroweak scale. This TeV-scale new physics beyond the SM is of enormous current interest as the Large Hadron Collider (LHC) presents an unprecedented opportunity to explore this energy range and shed light on some of the unresolved puzzles of fundamental physics. Although it is not yet clear which new physics scenario is preferred by Nature, supersymmetry is certainly believed to be one of the strongest candidates.

In this work, we propose a Left-Right extension of the Minimal Supersymmetric Standard Model (MSSM) to explain the observed non-zero neutrino masses by the inverse seesaw mechanism. We show that apart from preserving the nice features of MSSM (e.g. gauge coupling unification, radiative electroweak symmetry

breaking, dark matter), this framework provides a natural realization of the resonant leptogenesis mechanism to explain the matter-antimatter asymmetry in the universe, and also provides a natural inelastic dark matter candidate, all linked to the small Majorana mass of the neutrinos. We further show that the collider tests of the inverse seesaw mechanism and the related phenomenology are much more feasible compared to the canonical seesaw, thus extending the scope of the LHC physics search to the neutrino sector as well as to cosmology. We also prove that this TeV-scale scenario can be successfully embedded into a Supersymmetric Grand Unified Theory framework consistent with the proton decay constraints.

SUPERSYMMETRIC INVERSE SEESAW AND ITS PHENOMENOLOGY

by

Paratma Sri Bhupal Dev

Dissertation submitted to the Faculty of the Graduate School of the
University of Maryland, College Park in partial fulfillment
of the requirements for the degree of
Doctor of Philosophy
2012

Advisory Committee:
Rabindra Mohapatra, Professor (Chair)
Kaustubh Agashe, Assistant Professor
Zackaria Chacko, Associate Professor
Carter Hall, Assistant Professor
Massimo Ricotti, Associate Professor (Dean's Representative)
Raman Sundrum, Professor

Acknowledgments

First of all, I would like to thank my advisor, Prof. Rabindra Mohapatra, for his continued guidance, encouragement and support, crucial for the culmination of this project. I would also like to thank Prof. Kaustubh Agashe for carefully reading the thesis and for very useful discussions. Thanks are also due to the other committee members Prof. Raman Sundrum, Prof. Zackaria Chacko, Prof. Massimo Ricotti and Prof. Carter Hall, for being very kind and helpful.

I would like to thank my collaborators on parts of this project, Dr. Haipeng An, Dr. Steve Blanchet, Dr. Chien-Yi Chen, and Dr. Roberto Franceschinni, from whom I have learned a lot of physics as well as computational techniques. Thanks are also due to my colleagues at MCFP for providing me with a nice, friendly and intellectual atmosphere.

I also thank the staff members at MCFP and Physics, especially Yuri Kubota and Jane Hessing, for promptly taking care of the offcial paperwork during my stay at UMD.

I also take this opportunity to express my thanks and gratitude to all my friends who have given me company during times of both happiness and distress, and to family members for their unconditional love, care and support. Special thanks to the Bhakti Yoga Club at UMD which has taught me many valuable lessons in life (usually not taught in any curriculum), apart from providing food for body, mind and soul.

Table of Contents

List of Tables

List of Figures

Chapter 1

Introduction

All the macroscopic forms of matter in our Universe can be traced back to a few basic building blocks of Nature interacting by four fundamental forces: strong (or nuclear), electromagnetic, weak and gravitational [1]. A mathematical framework [1] that describes all the interactions between these fundamental constituents of Nature at the quantum level, except gravity (which is yet to be properly formulated as a quantum phenomenon), is known as the Standard Model (SM) of particle physics [2, 3]. Since the SM explains most of the experimentally observed phenomena with rather high accuracy, it now serves as *the* starting point in the study of elementary particle physics. Except for one (the Higgs mass), all the parameters of the SM have been determined experimentally to an extremely high degree of accuracy over the last three decades or so, in the precision measurements at the Large Electron-Positron (LEP) collider [4], the proton-antiproton collider (Tevatron) [5], and even substantially improved measurements, along with a conclusive proof of the Higgs, are expected from the ongoing experiments at the Large Hadron Collider (LHC) [6]. However, there are strong conceptual as well as experimental indications for the existence of new physics beyond the SM, and much of the current research in elementary particle physics is devoted to exploring this new territory.

---

[1]Gravity is by far the weakest force and is important for macroscopic objects but negligible for nuclear and sub-nuclear particles unless the distance scale is very small ($\sim 10^{-33}$ cm).

In this chapter, we will start with a brief description of the main features of the SM, and discuss the main reasons for going beyond this minimal framework. This will also be the starting point for us in building an extension to the minimal framework in order to address some of the issues raised here.

1.1   The Standard Model

The SM is a non-Abelian Yang-Mills gauge theory [7] based on the gauge group $SU(3)_c \times SU(2)_L \times U(1)_Y$, with the electroweak sector, $SU(2)_L \times U(1)_Y$, spontaneously broken to $U(1)_{\text{em}}$ [8] by a complex scalar field, while the color sector, $SU(3)_c$, remains unbroken and is described by Quantum Chromodynamics (QCD) [9, 10].

1.1.1   Particle Content

The fundamental gauge interactions in the SM are mediated by gauge fields corresponding to spin-one bosons. In the electroweak sector, we have the field B_μ corresponding to the hypercharge generator Y of the Abelian group $U(1)_Y$ and the three fields W_μ^a which correspond to the generators t^a (with $a = 1, 2, 3$) of the non-Abelian group $SU(2)_L$, satisfying the commutation relation $[t^a, t^b] = i\epsilon^{abc}t^c$ where ϵ^{abc} is the anti-symmetric Levi-Civita tensor; these generators are in fact equivalent to the three 2×2 Pauli matrices: $t^a = \frac{\tau^a}{2}$. In the strong interaction sector, there is an octet of gauge boson fields, $G_{\mu\nu}^A$ (with $A = 1, \ldots, 8$), called gluons, which correspond to the eight generators of the $SU(3)_c$ group, satisfying the commutation relations $[T^A, T^B] = if^{abc}T_C$ with $\text{tr}(T^A T^B) = \frac{1}{2}\delta^{AB}$ and f^{ABC} being the structure

constants of the $SU(3)_c$ group [11]; these generators are equivalent to the eight 3×3 Gell-Mann matrices: $T^A = \frac{\lambda^A}{2}$. Note that because of the non-Abelian nature of the $SU(2)$ and $SU(3)$ groups, there are self-interactions between their gauge fields W_μ and G_μ respectively, leading to triple and quartic gauge boson couplings. The precision measurement [4, 5] of these couplings provides a strong evidence for the underlying gauge structure of the SM (for recent results, see e.g. Ref. [12]).

The elementary building blocks of matter are spin-half particles (fermions), called quarks and leptons, which come in three generations in the SM. In order to have the experimentally determined chiral structure for the weak interactions [13], the left- and right-handed components of quark and lepton fields are assigned to different representations of the electroweak gauge group: the left-handed (LH) fermions f_L are in weak iso-doublets, while the right-handed (RH) fermions f_R are in weak iso-singlets, with weak iso-spin $I_f^{3L,3R} = \pm\frac{1}{2}, 0$ respectively for $f_{L,R} = \frac{1}{2}\left(1 \mp \gamma^5\right) f$, where γ^5 is the product of all the Dirac γ-matrices. The electric charge of the fermion in units of the proton charge $+e$ is given by $Q_{\text{em}} = I^{3L} + \frac{Y}{2}$, where Y is the $U(1)_Y$ hypercharge.

The gauge quantum numbers of the SM fields are summarized in Table 1.1. It can be seen that for these quantum number assignments of fermions, $\sum_f Q_{\text{em}}^f = \sum_f Y_f = 0$ which ensures the cancellation of chiral anomalies [14] within each generation, and thus, preserving [15] the renormalizability of the electroweak theory [16].

The basic SM Lagrangian, invariant under the local $SU(3)_c \times SU(2)_L \times U(1)_Y$

Field Content		$SU(3)_c$	$SU(2)_L$	$U(1)_Y$
Gauge	G_A	**8**	**1**	0
	W_a	**1**	**3**	0
	B	**1**	**1**	0
Lepton	$L_i = \begin{pmatrix} \nu_L \\ e_L \end{pmatrix}_i$	**1**	**2**	-1
	e_{R_i}	**1**	**1**	-2
Quark	$Q_i = \begin{pmatrix} u_L \\ d_L \end{pmatrix}_i$	**3**	**2**	$\frac{1}{3}$
	u_{R_i}	**3**	**1**	$\frac{4}{3}$
	d_{R_i}	**3**	**1**	$-\frac{2}{3}$
Scalar	$\Phi = \begin{pmatrix} \phi^+ \\ \phi^0 \end{pmatrix}$	**1**	**2**	1

Table 1.1: The field content (gauge, fermion and and scalar fields) of the SM along with the gauge quantum numbers. Here $i = 1, 2, 3$ denotes the generation index; in other words, $e_i = e, \mu, \tau$; $u_i = u, c, t$ and $d_i = d, s, b$ respectively. $A = 1, \cdots, 8$ for the 8 gluons fields and $a = 1, 2, 3$ for the weak gauge bosons. Each of the particles has an associated anti-particle, with the same mass and spin, but opposite charge. gauge transformation, involving the gauge bosons and matter fermions is given by

$$\mathcal{L}_{\text{gauge}} + \mathcal{L}_{\text{matter}} = -\frac{1}{4} G_{\mu\nu}^A G_A^{\mu\nu} - \frac{1}{4} W_{\mu\nu}^a W_a^{\mu\nu} - \frac{1}{4} B_{\mu\nu} B^{\mu\nu}$$

$$+i\left[\bar{L}_i\,\not{D}L_i + i\bar{e}_{R_i}\,\not{D}e_{R_i} + \bar{Q}_i\,\not{D}Q_i + \bar{u}_{R_i}\,\not{D}u_{R_i} + \bar{d}_{R_i}\,\not{D}d_{R_i}\right], \qquad (1.1)$$

where $\not{D} \equiv D_\mu \gamma^\mu$ (γ^μ are the Dirac γ-matrices) and D_μ is the covariant derivative through which the matter fields f minimally couple to the gauge fields G_μ, W_μ, B_μ:

$$D_\mu f \equiv \left(\partial_\mu - ig_3 \frac{\lambda_A}{2}G_\mu^A - ig_2 \frac{\tau_a}{2}W_\mu^a - ig_1 \frac{Y}{2}B_\mu\right)f, \qquad (1.2)$$

where g_3, g_2 and g_1 are the coupling constants of $SU(3)_c, SU(2)_L$ and $U(1)_Y$ respectively. The field strengths in Eq. (1.1) are given by

$$\begin{aligned}
G_{\mu\nu}^A &= \partial_\mu G_\nu^A - \partial_\nu G_\mu^A + g_3 f_{ABC}G_\mu^B G_\nu^C, \\
W_{\mu\nu}^a &= \partial_\mu W_\nu^a - \partial_\nu W_\mu^a + g_2 \epsilon_{abc}W_\mu^b W_\nu^c, \\
B_{\mu\nu} &= \partial_\mu B_\nu - \partial_\nu B_\mu
\end{aligned} \qquad (1.3)$$

1.1.2 Higgs Mechanism and Particle Masses

In Eq. (1.1), all the fermion and gauge fields are massless. The simplest way to generate the gauge boson and the fermion masses without violating the local gauge invariance is by the Higgs mechanism of spontaneous symmetry breaking [17]. In this mechanism, a complex $SU(2)_L$ doublet scalar field Φ is introduced (see Table 1.1) and the following invariant terms are added to the SM Lagrangian given by Eq. (1.1):

$$\mathcal{L}_{\text{Higgs}} = (D^\mu\Phi)^\dagger(D_\mu\Phi) - \mu_\Phi^2\Phi^\dagger\Phi - \lambda_\Phi(\Phi^\dagger\Phi)^2. \qquad (1.4)$$

For $\mu_\Phi^2 < 0$, the neutral component of the doublet field Φ acquires a non-zero vacuum expectation value (vev),

$$\langle\Phi\rangle = \frac{1}{\sqrt{2}}\begin{pmatrix} 0 \\ v \end{pmatrix} \quad \text{with } v = \sqrt{-\frac{\mu_\Phi^2}{\lambda_\Phi}}, \qquad (1.5)$$

thus spontaneously breaking the electroweak symmetry $SU(2)_L \times U(1)_Y$ to $U(1)_{\text{em}}$. In this process, three of the four degrees of freedom of the doublet scalar field are absorbed by three linear combination of the electroweak gauge fields to form their longitudinal polarization and to acquire masses, whereas the fourth field, corresponding to the unbroken $U(1)$ symmetry still remains massless. We identify this massless mode as the photon (A) which is the mediator of the long-range electromagnetic interaction, whereas the three massive modes are the $W^\pm$ and Z vector bosons which mediate the short-range weak interaction. In terms of the original fields W_μ^a, B_μ:

$$W_\mu^\pm = \frac{1}{\sqrt{2}}(W_\mu^1 \mp iW_\mu^2), \quad Z_\mu = \frac{g_2 W_\mu^3 - g_1 B_\mu}{\sqrt{g_2^2 + g_1^2}}, \quad A_\mu = \frac{g_1 W_\mu^3 + g_2 B_\mu}{\sqrt{g_2^2 + g_1^2}} \tag{1.6}$$

and the corresponding masses are

$$m_W = \frac{1}{2}vg_2, \quad m_Z = \frac{1}{2}v\sqrt{g_2^2 + g_1^2}, \quad m_A = 0 \tag{1.7}$$

Now the fermion masses can also be generated using the same scalar field Φ with hypercharge $Y = 1$, and its iso-doublet, $\tilde{\Phi} = i\tau_2 \Phi^*$ with $Y = -1$, by introducing the following Yukawa interaction Lagrangian:

$$\mathcal{L}_{\text{Yukawa}} = -y_{e_{ij}} \bar{L}_i \Phi e_{R_j} - y_{d_{ij}} \bar{Q}_i \Phi d_{R_j} - y_{u_{ij}} \bar{Q}_i \tilde{\Phi} u_{R_j} + \text{h.c.}, \tag{1.8}$$

and after Φ gets the vev, the corresponding fermion mass matrices are given by

$$M_e = \frac{vy_e}{\sqrt{2}}, \quad M_d = \frac{vy_d}{\sqrt{2}}, \quad M_u = \frac{vy_u}{\sqrt{2}} \tag{1.9}$$

Note that since the neutrinos do not have a right-handed counterpart, $M_\nu = 0$ in the SM.

After three of the four degrees of freedom of the scalar field Φ are absorbed by the gauge fields, the remaining one is called the Higgs boson (h). In the unitary gauge, the neutral component of the field Φ is given by

$$\Phi(x) = \frac{1}{\sqrt{2}} \begin{pmatrix} 0 \\ v + h(x) \end{pmatrix}, \tag{1.10}$$

and from the Lagrangian given by Eq. (1.4), we obtain

$$\mathcal{L}_h = \frac{1}{2}(\partial^\mu h)(\partial_\mu h) - \lambda_\Phi v^2 h^2 - \lambda_\Phi v h^3 - \frac{\lambda_\Phi}{4} h^4, \tag{1.11}$$

from which we can read off the Higgs mass:

$$m_h = \sqrt{2\lambda_\Phi v^2} = \sqrt{-2\mu_\Phi^2} \tag{1.12}$$

1.1.3 Electroweak Interactions

It is more convenient to express the interactions in terms of the physical eigenstates. Eqs. (1.6) for the field rotation which lead to the physical gauge bosons define the electroweak mixing angle (Weinberg angle):

$$\begin{pmatrix} Z_\mu \\ A_\mu \end{pmatrix} = \begin{pmatrix} \cos\theta_W & -\sin\theta_W \\ \sin\theta_W & \cos\theta_W \end{pmatrix} \begin{pmatrix} W_\mu^3 \\ B_\mu \end{pmatrix}, \tag{1.13}$$

with $\sin\theta_W = \frac{g_1}{\sqrt{g_2^2 + g_1^2}}$ and $m_W = m_Z \cos\theta_W$. The covariant derivative, Eq. (1.2), in terms of the physical fields is given by

$$\begin{aligned} D_\mu f \;\equiv\; & \left(\partial_\mu - ig_3 \frac{\lambda_A}{2} G_\mu^A - i\frac{g_2}{\sqrt{2}} \left(W_\mu^+ t^+ + W_\mu^- t^- \right) \right. \\ & \left. -i\frac{g_2}{\cos\theta_W} Z_\mu \left(t^3 - \sin^2\theta_W Q_f \right) - ieQ_f A_\mu \right) f \end{aligned} \tag{1.14}$$

where $t^{\pm} = t^1 \pm it^2$ and the electric charge $e = g_2 \sin\theta_W = g_1 \cos\theta_W$ so that the matching condition for couplings is satisfied at the electroweak breaking scale:

$$\frac{1}{g_2^2} + \frac{1}{g_1^2} = \frac{1}{e^2} \tag{1.15}$$

Using the fermionic part of the Lagrangian in Eq. (1.1), now written in terms of the physical fields, Eq. (1.14), we can write the neutral- and charged-current interactions as

$$\begin{aligned}
\mathcal{L}_{\text{neutral}} &= -e\sum_f Q_f \bar{f}\gamma^\mu f A_\mu - \frac{g_2}{\cos\theta_W}\sum_f \bar{f}\gamma^\mu \left[I_f^{3L}\frac{(1-\gamma^5)}{2} - Q_f \sin^2\theta_W\right]f Z_\mu, \\
\mathcal{L}_{\text{charged}} &= -\frac{g_2}{\sqrt{2}}\sum_f \left[\bar{f}_u\gamma^\mu\frac{(1-\gamma^5)}{2}V_{\text{CKM}}f_d W_\mu^+ + \bar{f}_\nu\gamma^\mu\frac{(1-\gamma^5)}{2}f_\ell W_\mu^+ + \text{h.c.}\right]
\end{aligned} \tag{1.16}$$

where $f_{u(d)}, f_{\nu(\ell)}$ are the up (down) -type fermions of weak isospin $I_f^{3L} = +(-)\frac{1}{2}$. Note that we have introduced a unitary matrix V_{CKM} in the charged-current interaction for quarks; this is because for more than one generation case, the current eigenstates for quarks are not identical to the mass eigenstates[2]. If we start with the u-type quarks in their mass eigenstates, the down-type quark mass eigenstates d are connected to their flavor eigenstates d' by the unitary transformation

$$\begin{pmatrix} d' \\ s' \\ b' \end{pmatrix} = V_{\text{CKM}}\begin{pmatrix} d \\ s \\ b \end{pmatrix} = \begin{pmatrix} V_{ud} & V_{us} & V_{ub} \\ V_{cd} & V_{cs} & V_{cb} \\ V_{td} & V_{ts} & V_{tb} \end{pmatrix}\begin{pmatrix} d \\ s \\ b \end{pmatrix} \tag{1.17}$$

where V_{CKM} is a 3×3 unitary matrix, known as the Cabibbo-Kobayashi-Maskawa (CKM) matrix [18]. It can be parameterized by three mixing angles and one *CP*-

---

[2]There is no analogous mixing matrix for the lepton sector since in the SM, the neutrinos are assumed to be massless.

violating phase [19], or by four real parameters [20]:

$$V_{\text{CKM}} = \begin{pmatrix} 1 - \frac{1}{2}\lambda^2 & \lambda & A\lambda^3\left(\rho - i\eta\right) \\ -\lambda & 1 - \frac{1}{2}\lambda^2 & A\lambda^2 \\ A\lambda^3(1 - \rho - i\eta) & -A\lambda^2 & 1 \end{pmatrix} + \mathcal{O}(\lambda^4) \qquad (1.18)$$

Defining $\bar{\rho} = \rho\left(1 - \frac{1}{2}\lambda^2 + \cdots\right)$ and similarly for $\bar{\eta}$, we note that

$$\bar{\rho} + i\bar{\eta} = -\frac{V_{ud}V_{ub}^*}{V_{cd}V_{cb}^*} \qquad (1.19)$$

which is phase-convention independent, and ensures that the CKM matrix given by Eq. (1.18) is unitary to all orders in λ. The unitarity of V_{CKM} ensures that the neutral currents are diagonal in both mass and flavor bases; this is necessary for explaining the natural absence of flavor changing neutral currents (FCNC) at the tree-level in the SM, also known as the Glashow-Illiopoulos-Maiani (GIM) suppression mechanism [21].

1.1.4 Parameters of the SM

The SM has 18 parameters[3]: masses of the six quarks and three charged leptons, three quark mixing angles and one phase, three gauge coupling constants, Higgs quadratic coupling and self-coupling strengths None of these parameter values are predicted by the model, and they must be determined from experiments. The current experimental values of these parameters are summarized in Table 1.2 [22].

In the scalar sector, there are two parameters in the SM, namely μ_Φ and λ_Φ in Eq. (1.4), or equivalently, the Higgs vev v in Eq. (1.5) and the Higgs mass in

---

[3]Sometimes, the phase θ_{QCD} in the CP-violating term added to the QCD Lagrangian is considered to be an additional parameter which is assumed to be zero in the SM.

Parameter	Experimental value	Comment
m_e	0.510998910 (13) MeV	Scheme-independent
m_μ	105.6583668 (38) MeV	"
m_τ	1.77682 (16) GeV	"
m_u	$2.49^{+0.81}_{-0.79}$ MeV	$\overline{\text{MS}}$ scheme at $Q = 2$ GeV
m_d	$5.05^{+0.75}_{-0.95}$ MeV	"
m_s	101^{+29}_{-21} MeV	"
m_c	$1.27^{+0.07}_{-0.09}$ GeV	$\overline{\text{MS}}$ scheme at $Q = m_c$
m_b	$4.19^{+0.18}_{-0.06}$ GeV	$\overline{\text{MS}}$ scheme at $Q = m_b$
m_t	173.2 ± 0.9 GeV	Latest Tevatron result [23]
λ	0.2253 ± 0.0007	CKMfitter result [24]
A	$0.808^{+0.022}_{-0.015}$	"
$\bar{\rho}$	$0.132^{+0.022}_{-0.014}$	"
$\bar{\eta}$	0.341 ± 0.013	"
α_3	0.1184 ± 0.0007	at $Q^2 = m_Z^2$
α_2	$0.033493^{+0.000042}_{-0.000038}$	"
α_1	$0.016829(17)$	"
G_F	$1.16637(1) \times 10^{-5}$ GeV^{-2}	from Ref. [25]
m_h	unknown	see Ref. [26] for exclusion limits

Table 1.2: Parameters of the SM and their current experimental values [22].

Eq. (1.12). However, the value of the vev can be obtained from the Fermi coupling constant G_F which is determined experimentally [25] from muon decay mediated in the SM by W-boson exchange:

$$\frac{G_F}{\sqrt{2}} = \frac{g_2^2}{8m_W^2}, \quad \text{or,} \quad v = \left(\frac{1}{\sqrt{2}G_F}\right)^{1/2} \simeq 246 \text{ GeV} \tag{1.20}$$

This leaves the Higgs mass as the only parameter in the SM whose value is not yet known experimentally [27]. The direct searches at LEP have excluded the SM Higgs mass below 114.4 GeV [4], whereas the most recent combined results from CDF and D0 experiments at Tevatron exclude the mass range of 147 - 179 GeV at 95% C.L. [28]. On the other hand, the combined results from ATLAS and CMS experiments at the LHC have excluded 127 - 600 GeV with 5 fb^{-1} data [26].

1.2 Why beyond the SM?

Even though the SM is remarkably consistent with all the precision measurements so far [29], just finding the Higgs boson will not make it a complete theory of Nature. There are strong experimental as well as conceptual indications that the SM is just a low-energy effective field theory and there must exist some new physics beyond the SM, not far above the electroweak scale.

The major experimental indications for beyond SM physics are the following:

1. *Neutrino Masses and Mixing:* The experiments with solar, atmospheric, reactor and accelerator neutrinos have provided solid evidences for neutrino flavor oscillations [30, 31] which imply nonzero neutrino masses and mixing. All existing neutrino oscillation data can be described in a minimal three-flavor

basis which is consistent with the LEP result for the number of light neutrino species, $N_\nu = 2.9840 \pm 0.0082$ [4]. In this basis, assuming that the charged leptons are in their mass eigenstates, the leptonic part of the charged current weak interaction in Eq. (1.16) can be written similar to the quark part:

$$
\begin{aligned}
\mathcal{L}_{\text{charged}}^{\text{lepton}} &= -\frac{g_2}{\sqrt{2}} \sum_{\ell=e,\mu,\tau} \bar{\nu}_\ell \gamma^\mu \frac{(1-\gamma^5)}{2} \ell W_\mu^+ + \text{h.c.} \\
&= -\frac{g_2}{\sqrt{2}} \sum_{\ell=e,\mu,\tau} \sum_{\alpha=1,2,3} \bar{\nu}_\alpha U_{\ell\alpha}^\dagger \gamma^\mu \frac{(1-\gamma^5)}{2} \ell W_\mu^+ + \text{h.c.} \quad (1.21)
\end{aligned}
$$

where U is now a 3×3 unitary neutrino mixing matrix, analogous to the CKM mixing matrix in the quark sector, and is known as the Pontecorvo-Maki-Nakagawa-Sakata (PMNS) matrix [32]. This can also be parameterized by three Euler angles and a phase, as in the CKM, but there are two additional phases if the neutrinos are Majorana particles [33]:

$$
U_{\text{PMNS}} = \begin{pmatrix}
c_{12}c_{13} & s_{12}c_{13} & s_{13}e^{-i\delta} \\
-s_{12}c_{23} - c_{12}s_{23}s_{13}e^{i\delta} & c_{12}c_{23} - s_{12}s_{23}s_{13}e^{i\delta} & s_{23}c_{13} \\
s_{12}s_{23} - c_{12}c_{23}s_{13}e^{i\delta} & -c_{12}s_{23} - s_{12}c_{23}s_{13}e^{i\delta} & c_{23}c_{13}
\end{pmatrix}
$$
$$
\times \operatorname{diag}\left(1, e^{i\alpha_{21}/2}, e^{i\alpha_{31}/2}\right), \quad (1.22)
$$

where $s_{ij} = \sin\theta_{ij}, c_{ij} = \cos\theta_{ij}$, δ is the Dirac CP-violating phase, and α_{21}, α_{31} are the Majorana CP- violating phases. Thus, we have 7 (9 for Majorana) additional parameters, namely the three neutrino masses, three mixing angles, and one (three) CP-violating phases, in addition to those in the SM given by Table 1.2. The existing neutrino oscillation data allow us to determine some of these parameters, namely the two mass-squared differences, Δm_{21}^2 and $|\Delta m_{31}^2|$, the solar and atmospheric mixing angles θ_{12} and θ_{23}, and the reactor mixing

angle θ_{13}. The best fit as well as 3σ values are shown in Table 1.3 [34]. Note that the global analysis provides $> 3\sigma$ evidence for non-zero θ_{13} which was recently confirmed by the Daya Bay [35] and RENO [36] reactor neutrino experiments at 5.2σ and 6.3σ C.L., respectively. A natural explanation of the remarkable smallness but non-vanishing nature of neutrino mass and large neutrino mixing requires some new physics beyond the SM [37].

Parameter	Best Fit	3σ range
Δm^2_{21}	7.58×10^{-5} eV^2	$(6.99 - 8.18) \times 10^{-5}$ eV^2
$|\Delta m^2_{31}|$	2.35×10^{-3} eV^2	$(2.06 - 2.67) \times 10^{-3}$ eV^2
$\sin^2 \theta_{12}$	0.312	$0.265 - 0.364$
$\sin^2 \theta_{23}$	0.42	$0.34 - 0.64$
$\sin^2 \theta_{13}$	0.025	$0.005 - 0.050$

Table 1.3: The neutrino oscillation parameters values obtained from the global 3ν oscillation analysis [34]. It includes all the existing neutrino data, except the most recent Daya Bay [35] and RENO [36] results.

2. *Baryon Asymmetry:* Our Universe appears to be populated exclusively with matter rather than antimatter. The asymmetry between matter and anti-matter is usually characterized in terms of the baryon-to-photon ratio $\eta_B = (n_B - n_{\bar{B}})/n_\gamma$ where $n_{B(\bar{B})}$ is the number density of baryons (anti-baryons) and n_γ is the number density of photons in the Universe. Historically, this ratio was determined using the abundance of light elements in Big Bang Nucleosyn-

thesis (BBN) [38]. However, in the last few years, the Wilkinson Microwave Anisotropy Probe (WMAP) data has provided a more accurate measurement of η_B [39]:

$$\eta_B = (6.19 \pm 0.15) \times 10^{-10} \qquad \text{(68\% C.L. value)} \qquad (1.23)$$

The mechanism by which this non-zero baryon asymmetry could be produced dynamically, starting from a baryon-symmetric universe, is known as "baryogenesis" [40], and it requires to satisfy the three Sakharov conditions [41]: baryon number (B) violating interactions, C and CP violation, and a departure from thermal equilibrium. In principle, all these conditions could be satisfied within the SM: baryon number is violated by sphalerons through non-perturbative effects [42]; parity is maximally violated in weak interactions, and CP violation exists in the CKM matrix; the out of equilibrium condition could be satisfied during electroweak phase transition. However, a more quantitative analysis shows that it is not possible to have the observed baryon asymmetry in the SM because the CKM CP violation is much too small $\sim 10^{-20}$ [43] and the electroweak phase transition is not sufficiently strong first order unless the SM Higgs mass, $m_h < 80$ GeV [44] which is already excluded by LEP [4]. Thus we must have additional sources of CP violation beyond the SM in order to explain the observed baryon asymmetry in the universe [40].

3. *Dark Matter and Dark Energy:* There is overwhelming astrophysical and cosmological evidence [45] that most of the matter in our universe does not absorb or emit electromagnetic radiation (hence the name "dark") and most of this

dark matter (DM) is not composed of baryons or any of the known particles. The measurements of the Cosmic Microwave Anisotropy (CMB) anisotropy and of spatial distribution of galaxies yield the DM density [39]

$$\Omega_{\text{DM}} h^2 = 0.110 \pm 0.006, \tag{1.24}$$

where h is the Hubble constant in units of 100 km.s^{-1}.Mpc^{-1}. Candidates for non-baryonic DM must satisfy several conditions: they must be stable over cosmological time scales ($\gtrsim 10^{18}$ sec), they must be electrically neutral and interact only weakly (and gravitationally) with ordinary matter, and they must have the right relic density given by Eq. (1.24). Moreover, analyses of structure formation in the universe indicate that most of the DM should be non-relativistic (or "cold") [46]. All these arguments rule out the only SM candidate for DM (neutral and stable), i.e. neutrinos, which are highly relativistic and have relic density $\Omega_\nu h^2 \leq 0.0067$ at 95% CL [39]. Thus we must consider beyond SM scenarios for viable DM candidates.

The discovery of accelerated expansion of the universe [47] suggests that the bulk of the energy density of the universe is in the form of "dark energy" with exotic physical properties which cannot be accounted for in the SM. The 7-year WMAP data yields the Dark Energy density of the universe to be [39]

$$\Omega_\Lambda = 0.725 \pm 0.016. \tag{1.25}$$

A compelling theoretical explanation for the Dark Energy must come from some beyond SM physics involving gravity [48].

4. *Anomalies:* In addition to these major experimental evidences for physics beyond SM, there are always some experimental "anomalies" that do not agree with the SM predictions. At present, the most persistent ones are: (i) the muon anomalous magnetic moment which disagrees with the SM prediction at 3.4σ level [49], and (ii) top quark forward-backward asymmetry which shows deviations of more than 3σ from the SM expectations in the region of large $t\bar{t}$ invariant mass [50].

Apart from the major experimental evidences listed above, there are also conceptual reasons [51] that suggest the incompleteness of the SM as a fundamental theory of Nature. Some of them are listed below:

1. *The Naturalness Problem:* The structure of the SM does not naturally explain the relative smallness of the electroweak symmetry breaking scale $v \sim 1/\sqrt{G_F} \sim 100$ GeV compared to the natural scale in the theory, i.e. the Planck scale $M_{\mathrm{Pl}} \equiv \sqrt{\hbar c/G_N} \sim 10^{19}$ GeV. This "hierarchy problem" [52] becomes worse for the Higgs mass in the SM due to quantum corrections which are quadratically divergent with respect to the cut-off scale Λ:

$$m_h^2(\text{physical}) = m_h^2(\text{tree}) + \Delta m_h^2, \quad \text{where } \Delta m_h^2 \sim \frac{\lambda_\Phi^2}{16\pi^2}\Lambda^2. \qquad (1.26)$$

Thus, if we assume that the SM is valid all the way up to the Planck scale, then in order to prevent the physical Higgs mass given by Eq. (1.26) from being pulled up to $\Lambda = M_{\mathrm{Pl}}$, the tree-level mass parameter $m_h^2(\text{tree})$ given by Eq. (1.12) has to be fine-tuned to 1 part in 10^{28} to cancel the large radiative correction Δm_h^2 and to yield a physical Higgs mass at the weak scale. While

16

this is not strictly impossible, it is technically unnatural and is known as the "naturalness problem" in the SM [52, 53]. This problem could be eliminated by making the cut-off scale slightly above the electroweak scale, i.e. $\Lambda \sim \mathcal{O}$ (TeV) which implies there must be new degrees of freedom that manifest themselves at this scale [54].

2. *Electroweak Symmetry Breaking:* The SM does not provide any insight into the mechanism of electroweak symmetry breaking (EWSB). Although we can achieve EWSB spontaneously by introducing a complex scalar field, this is done in the SM by an arbitrary scalar potential. There is no dynamical understanding of why the mass-squared parameter for the Higgs field becomes negative in Eq. (1.4). A precise understanding of the EWSB is one of the major goals of beyond SM physics [55].

3. *Grand Unification Problem:* This is the problem of trying to understand the strong and electroweak interactions in the SM as different manifestations of a single underlying force, thus unifying the three coupling strengths at a higher energy scale known as the Grand Unified Theory (GUT) scale. The SM field content does not lead to the unification of the three gauge couplings at high energy (see Section 2.3).

4. *The Flavor Puzzle:* The SM does not explain the masses and mixing pattern in the fermion sector. There appears to be a hierarchy between the fermion mass scales, ranging from 0.5 MeV to about 200 GeV (see Table 1.2), and it gets worse if we include the neutrino masses ($<$ eV). Note however that this

hierarchy between fermion masses and weak scale is not as serious problem as the hierarchy between the Planck scale and weak scale for the Higgs mass because the fermion masses are protected by chiral symmetry.

Although the experimental and theoretical arguments given above all imply the existence of new physics beyond the SM, most likely at the TeV scale, they do not by themselves provide any hints for the exact nature of the new physics. There exist a number of possible extensions of the SM some of which are mentioned in the following Section.

1.3 New Physics at TeV Scale

In order to solve the hierarchy problem, we must introduce new degrees of freedom near the electroweak scale. The main ideas for new physics scenarios can be divided into two broad classes of models:

1. There are no elementary scalar fields in Nature (and hence no associated fine-tuning problem), and the Higgs boson is a composite of fermions. It duplicates the QCD picture (at weak scale) that the low energy degrees of freedom are baryons and mesons while at high energy these are quarks and gluons. This idea is the basis of all technicolor, top-color and offspring models [56].

   It was also realized that this strong dynamics at the weak scale is dual to the warped extra dimensional models [57] via the AdS/CFT correspondence [58], thus providing a natural solution of the gauge hierarchy problem.

2. Unlike the above idea which invokes new strong interactions at the TeV scale,

one could keep the elementary scalars and maintain perturbativity up to much higher energies if the quantum corrections are canceled to all orders in perturbation theory, due to some deeper symmetry. This is known as "supersymmetry (SUSY)" [59, 60] which relates the bosonic and fermionic degrees of freedom, and ensures the desired cancellation to all orders in perturbation theory by exploiting the sign difference between bosonic and fermionic loops.

From experimental point of view, none of these ideas are completely disfavored, and with more data from the ongoing LHC, we might be able to decide very soon the exact nature of new physics chosen by Nature. At present, however, we find SUSY as one of the leading candidates, due to several theoretical as well as experimental arguments in its favor (see Section 2.1).

The plan of this thesis is as follows: In Chapter 2, we start with a brief review of the Minimal Supersymmetric extension of the SM (MSSM), gauge coupling unification in this model and its extension for neutrino masses by seesaw mechanism. In Chapter 3, after a review of the seesaw scale, we discuss a different realization of the seesaw mechanism, namely the inverse seesaw, and its general phenomenological aspects. Then we introduce a realistic inverse seesaw model based on Supersymmetric Left-Right (SUSYLR) gauge group and show that it can be realized as a TeV-scale effective theory of an $SO(10)$ SUSY-GUT. In Chapter 4, we discuss the generation of baryon asymmetry in the universe from lepton asymmetry ("leptogenesis") in general, and also in the case of Left-Right (LR) models with inverse seesaw, and show that leptogenesis is consistent with TeV-scale LR symmetry. In Chapter 5,

after an overview of the Weakly Interacting Massive Particles (WIMPs) as a viable DM candidate and a discussion of the WIMP candidate in MSSM, namely the neutralino, we show that in SUSYLR models, there exists a new scalar DM candidate which is naturally inelastic due to the small Majorana mass in inverse seesaw and it is allowed to be very light, unlike the neutralino in MSSM. In Chapter 6, we discuss the collider and other low-energy tests of the inverse seesaw models. In Chapter 7, we discuss various proton decay operators in SUSY models and then present a calculation for the decay rates in the SUSYLR models discussed earlier. Finally, a summary is given in Chapter 8. Appendix A explicitly gives the masses of the $SO(10)$ Higgs multiplets for the GUT embedding of SUSYLR with inverse seesaw. In Appendix B, we present all the Renormalization Group Equations (RGEs) for fermion masses and mixing in SUSYLR, and in Appendix C, the RGEs for soft-SUSY breaking sector of SUSYLR. Appendix D shows an analytic derivation of the CP-asymmetry for inverse seesaw for specific forms of the Majorana singlet mass matrix. Appendix E gives the analytic formulas for sfermion spectrum in SUSYLR.

Chapter 2

Low-Scale Supersymmetry: the Minimal Model and Beyond

2.1 Why SUSY?

Supersymmetry [59, 60] predicts the existence of a new spin-1/2 particle for every known spin-0 and spin-1 particles of the SM, and similarly, a new spin-0 particle for every SM fermion, with degenerate masses. These supersymmetric particles serve as the new perturbatively coupled degrees of the freedom that cancel the quadratic divergences in the SM [61]. However, since we have not yet observed any of these superpartners, SUSY must be a broken symmetry at low-energy. It turns out that if broken appropriately (or "softly") [62], this does not reintroduce the quadratic divergences. These softly-broken SUSY theories have a number of theoretical virtues as well as phenomenological arguments which make them a strong candidate for new physics at TeV-scale:

1. The supersymmetric transformations linking bosons and fermions, together with translations, rotations and boosts, form the super-Poincaré group, whose direct product with the internal symmetry group generate the most general symmetries of the S-matrix allowed in a Quantum Field Theory [63].

2. The scalar potential in SUSY models is stable under radiative corrections, provided the SUSY scale is around $4\pi m_h \sim$ TeV. Thus, TeV-scale SUSY

models solve the naturalness problem with only $\mathcal{O}(1)$ tuning between the bare scalar mass and multiplicatively renormalized quantum corrections. Moreover, the weak scale SUSY theories do not reintroduce the hierarchy problem since they are technically natural and the dynamical SUSY breaking can be realized due to non-perturbative effects [64].

3. Gravity can be incorporated into SUSY theories if supersymmetric transformations are made local. This results in a gauge theory of gravity, known as the "supergravity" [59, 60, 65], which could be elevated to superstring theories [66], so far the only viable candidates for a consistent quantum theory of gravity.

4. If we assume SUSY in the range of 100 GeV-10 TeV, the three SM gauge couplings unify remarkably well at the scale $M_G \sim 2 \times 10^{16}$ GeV, thus strongly suggesting a SUSY-GUT at that scale [67, 68].

5. Soft SUSY-breaking offers a somewhat natural understanding of the electroweak symmetry breaking (EWSB) by the mechanism of radiative EWSB [69] in which the renormalization effects drive one of the Higgs squared mass parameters to negative values while keeping all other SUSY mass squared parameters positive. This mechanism occurs naturally if the top mass is close to the electroweak scale, $m_t \sim 100 - 200$ GeV which is indeed the case [23].

6. In order to enforce lepton and baryon number conservation in a simple way, the minimal SUSY models are usually required to have a discrete symmetry,

called R-parity [70]. A major consequence is that the lightest supersymmetric particle is absolutely stable. A stable LSP is usually required to be electrically and color neutral in order to be consistent with cosmological constraints [71], thus making it a promising candidate for cold dark matter [72].

2.2   The Minimal Supersymmetric Standard Model

The most economical version of a low-energy SUSY theory is known as the Minimal Supersymmetric Standard Model (MSSM) [59, 60] which is based on the SM gauge group $SU(3)_c \times SU(2)_L \times U(1)_Y$ and contains the smallest number of new particles and new interactions consistent with SM phenomenology.

Each of the SM gauge boson (spin-1) requires a real Majorana fermion (spin-1/2) with the same quantum numbers as its superpartner (gaugino) to form a vector supermultiplet, and each SM fermion requires a complex scalar boson (sfermion) with the same quantum numbers to form a chiral superfield [73]. Finally, the Higgs doublet requires the presence of its fermion superpartner, the Higgsino, to form two chiral superfields with hypercharges ± 1; note that two Higgs doublets with opposite hypercharge are required to cancel the triangle anomalies [14] and also to give masses to the isospin $+1/2$ and $-1/2$ fermions in a SUSY invariant way [74]. Note that the introduction of an additional Higgs doublet leads to five Higgs particles after EWSB: two CP-even (h, H), a CP-odd (A) and two charged $(H^\pm)$ Higgs bosons [75]. Their fermionic superpartners (higgsinos) will mix with the partners of $SU(2)_L$ and $U(1)_Y$ gauge bosons (winos and bino) to give the mass eigenstates: 2 charginos $(\chi^\pm)$

and 4 neutralinos ($\chi^0_{1,2,3,4}$). The field content of the MSSM is given in Table 2.1.

Superfield		Boson field	Fermion field	$SU(3)_c$	$SU(2)_L$	$U(1)_Y$
Gauge	$\hat{G}_A$	G^μ_A	$\widetilde{G}_A$	**8**	**1**	0
	$\hat{W}_a$	W^μ_a	$\widetilde{W}_a$	**1**	**3**	0
	$\hat{B}$	B^μ	$\widetilde{B}$	**1**	**1**	0
Lepton	$\hat{L}_i = \begin{pmatrix} \hat{\nu}_L \\ \hat{e}^-_L \end{pmatrix}_i$	$\left(\widetilde{\nu}_L, \widetilde{e}^-_L\right)_i$	$\left(\nu_L, e^-_L\right)_i$	**1**	**2**	-1
	$\hat{E}^c_i$	$\widetilde{e}^-_{Ri}$	e^-_{Ri}	**1**	**1**	-2
Quark	$\hat{Q}_i = \begin{pmatrix} \hat{u}_L \\ \hat{d}_L \end{pmatrix}_i$	$(\widetilde{u}_L, \widetilde{d}_L)_i$	$(u_L, d_L)_i$	**3**	**2**	$\frac{1}{3}$
	$\hat{U}^c_i$	$\widetilde{u}_{Ri}$	u_{Ri}	**3**	**1**	$\frac{4}{3}$
	$\hat{D}^c_i$	$\widetilde{u}_{Ri}$	d_{Ri}	**3**	**1**	$-\frac{2}{3}$
Higgs	$\hat{H}_d = \begin{pmatrix} \hat{h}^0_d \\ \hat{h}^-_d \end{pmatrix}$	(h^0_d, h^-_d)	$(\widetilde{h}^0_d, \widetilde{h}^-_d)$	**1**	**2**	-1
	$\hat{H}_u = \begin{pmatrix} \hat{h}^+_u \\ \hat{h}^0_u \end{pmatrix}$	(h^+_u, h^0_u)	$(\widetilde{h}^+_u, \widetilde{h}^0_u)$	**1**	**2**	1

Table 2.1: The field content of the MSSM and the corresponding gauge quantum numbers. Here $i = 1, 2, 3$ for 3 generations of SM fermions, $a = 1, 2, 3$ for the 3 W-bosons and $A = 1, \cdots, 8$ for the 8 gluons. For each supermultiplet, there is a corresponding anti-particle multiplet of charge-conjugated SM particles and their superpartners.

The most general MSSM superpotential, compatible with gauge invariance, renormalizability and R-parity is given by [59, 60]

$$W = \mu \epsilon^{ab} \hat{H}_{u_a} \hat{H}_{d_b} + \sum_{i,j=1}^{3} \epsilon^{ab} \left[-y_{u_{ij}} \hat{Q}_{ia} \hat{H}_{u_b} \hat{U}_j^c + y_{d_{ij}} \hat{Q}_{ia} \hat{H}_{d_b} \hat{D}_j^c + y_{e_{ij}} \hat{L}_{ia} \hat{H}_{d_b} \hat{E}_j^c \right], \quad (2.1)$$

where $a, b = 1, 2$ are the $SU(2)_L$ indices, and $y_{u,d,e}$ are the 3×3 Yukawa coupling matrices, similar to those given in Eq. (1.8). The particle masses are generated after the EWSB by the vevs of neutral components of the Higgs doublets:

$$\langle H_u \rangle = \frac{1}{\sqrt{2}} \begin{pmatrix} 0 \\ v_u \end{pmatrix}, \quad \langle H_d \rangle = \frac{1}{\sqrt{2}} \begin{pmatrix} v_d \\ 0 \end{pmatrix} \quad \left(\text{with } \frac{v_u}{v_d} \equiv \tan \beta \right) \quad (2.2)$$

The soft SUSY-breaking terms are given by

$$\begin{aligned}
-\mathcal{L}_{\text{soft}} =& \; m_{H_u}^2 H_u^\dagger H_u + m_{H_d}^2 H_d^\dagger H_d + B\mu(\epsilon^{ab} H_{u_a} H_{d_b} + \text{h.c.}) \\
&+ \sum_{i,j=1}^{3} \left[m_{Q_{ij}}^2 \tilde{Q}_i^\dagger \tilde{Q}_j + m_{U_{ij}}^2 \tilde{u}_{Ri}^\dagger \tilde{u}_{Rj} + m_{D_{ij}}^2 \tilde{d}_{Ri}^\dagger \tilde{d}_{Rj} + m_{L_{ij}}^2 \tilde{L}_i^\dagger \tilde{L}_j + m_{E_{ij}}^2 \tilde{e}_{Ri}^\dagger \tilde{e}_{Rj} \right. \\
&\left. + \epsilon^{ab} \left(A_{u_{ij}} y_{u_{ij}} \tilde{Q}_{ia} H_{u_b} \tilde{u}_{Rj}^\dagger + A_{d_{ij}} y_{d_{ij}} \tilde{Q}_{ia} H_{d_b} \tilde{d}_{Rj}^\dagger + A_{e_{ij}} y_{e_{ij}} \tilde{L}_{ia} H_{d_b} \tilde{e}_{Rj}^\dagger + \text{h.c.} \right) \right] \\
&+ \frac{1}{2} \left[M_1 \bar{\tilde{B}} \bar{\tilde{B}} + M_2 \sum_{a=1}^{3} \bar{\tilde{W}}^a \bar{\tilde{W}}_a + M_3 \sum_{A=1}^{8} \bar{\tilde{G}}^A \bar{\tilde{G}}_A + \text{h.c.} \right] \\
&+ \frac{i}{2} \left[M_1' \bar{\tilde{B}} \gamma^5 \bar{\tilde{B}} + M_2' \sum_{a=1}^{3} \bar{\tilde{W}}^a \gamma^5 \bar{\tilde{W}}_a + M_3' \sum_{A=1}^{8} \bar{\tilde{G}}^A \gamma^5 \bar{\tilde{G}}_A + \text{h.c.} \right] \quad (2.3)
\end{aligned}$$

These soft SUSY-breaking terms introduce 105 unknown parameters, in addition to the 19 SM parameters, and makes any meaningful phenomenological analysis very difficult [76]. However, many of these parameters lead to severe phenomenological problems [77], e.g. unacceptably large FCNCs, CP violation, lepton flavor violation (LFV) etc. which results in a more restricted parameter space for the MSSM. One version in the bottom-up approach is known as the phenomenological MSSM (pMSSM) [78], based on Minimal Flavor violation (MFV) [79], which has only 22

parameters and has much more predictability [80]. A more restrictive scenario in the top-down approach is known as the constrained MSSM (cMSSM) [78], or more commonly known as minimal supergravity (mSUGRA) [81, 82] inspired by local SUSY-GUT, and has only 5 parameters. For simplicity, we will mostly limit our discussions to mSUGRA-based models in this work, but the results can be easily extended to a more generalized parameter space.

2.3   Gauge Coupling Unification

In a renormalizable quantum field theory, the coupling constants and mass parameters of the theory are replaced by their running values depending on the energy scale. The scale dependence of the parameters is specified by the renormalization group (RG) equations [1]. In particular, the RG evolution of a coupling constant g with renormalization scale Q is governed by the Callan-Symanzik β-function [83]

$$\beta(g) = Q\frac{\partial g}{\partial Q} \tag{2.4}$$

The one-loop β-function for a general non-supersymmetric gauge theory is given by [84]

$$\beta(g) = \frac{g^3}{16\pi^2}\left[-\frac{11}{3}C(G) + \frac{2}{3}n_F S(R_F) + \frac{1}{3}n_H S(R_H)\right], \tag{2.5}$$

where $C(G)$ is the quadratic Casimir for the adjoint representation of the associated Lie algebra [11], $S(R_{F(H)})$ is the Dynkin index for representation $R_{F(H)}$ of the fermion (scalar) fields, and $n_{F(H)}$ is the number of fermion (complex scalar) fields. For an $SU(N)$ gauge theory, $S(R) = 1/2$ for both fermions and scalars in the fundamental N-dimensional representation, whereas $C(G) = N$. For $U(1)_Y$, $S(R) = 1$

26

and $C(G) = 0$. For small values of n_F, the β-function is negative which leads to the asymptotic freedom of non-Abelian gauge theories [10].

For the SM particle content (see Table 1.1), the coefficients b_i given by the square bracket term in Eq. (2.5) are

$$(b_1, b_2, b_3) = \left(\frac{41}{10}, -\frac{19}{6}, -7\right) \tag{2.6}$$

for $U(1)_Y, SU(2)_L$ and $SU(3)_c$ respectively, and we have used the "GUT normalization"[1] for $U(1)_Y$ coupling $g_1 = \sqrt{5/3}g'$ [68]. The running behavior of the SM gauge couplings with respect to the energy scale $t = \log Q$ is shown in Figure 2.1 (thin lines), where we have used the experimental values at $Q = m_Z$ (see Table 1.2) as inputs. It is clear that from Figure 2.1 that the three couplings in the SM fail to unify.

In the MSSM, the β-function given by Eq. (2.5) will get modified by the additional degrees of freedom, namely gauginos, higgsinos and sfermions. Using $S(R) = N$ for the adjoint representation in $SU(N)$, the one-loop β-function in a SUSY theory can be written as [85]

$$\beta(g) = \frac{g^3}{16\pi^2} \left[-3C(G) + S(R)\right] \tag{2.7}$$

where the Dynkin index $S(R)$ is now summed over all the matter and Higgs fields, and their superpartners. For the MSSM particle content (see Table 2.1), the coefficients of the β-function in Eq. (2.7) are given by

$$(b_1, b_2, b_3) = \left(\frac{33}{5}, 1, -3\right) \tag{2.8}$$

---

[1]We must use this normalization if each chiral family is to be embedded in a representation of the unified group.

The corresponding RG evolution is shown in Figure 2.1 (thick lines) from which it is clear that the three gauge couplings do unify with satisfactory precision at a point $\alpha_U \simeq 0.04$, thus defining a SUSY-GUT scale $M_{\text{GUT}} \sim 2 \times 10^{16}$ GeV, as well as confirming the validity of perturbativity of the theory.
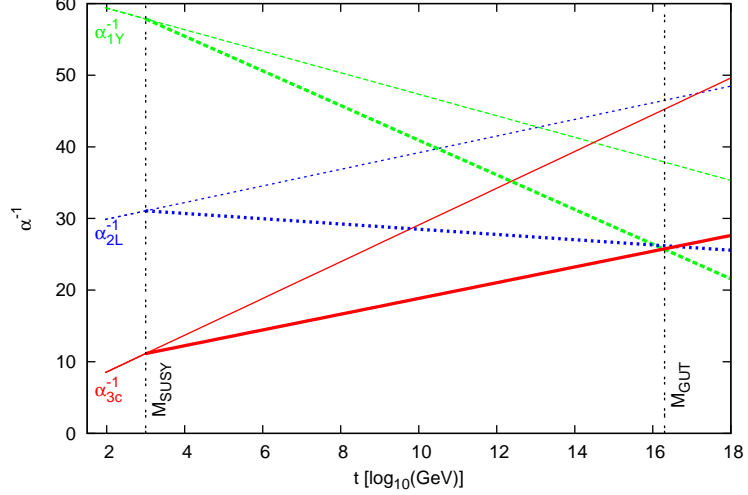
Figure 2.1: The RG evolution of the gauge coupling strengths $\alpha_i^{-1} \equiv (g_i^2/4\pi)^{-1}$ for the SM gauge group $U(1)_Y \times SU(2)_L \times SU(3)_c$. With only the SM valid up to the Planck scale, they (thin lines) fail to unify, whereas introducing MSSM at TeV-scale leads to their unification (thick lines) at GUT-scale, $M_{\text{GUT}} \sim 2 \times 10^{16}$ GeV.

To summarize, the MSSM solves some of the major inadequecies of the SM listed in Section 1.2, namely, the gauge hierarchy problem, grand unification problem and dark matter problem. Also, it is possible to have successful electroweak baryogenesis in MSSM [40]. However, just like in the minimal SM, neutrinos are massless in MSSM. Given the solid evidence for neutrino masses and mixing [31], we must extend the MSSM sector to incorporate neutrino masses, while preserving its other nice features. One such viable mechanism is discussed in the following section.

2.4 Neutrino Mass

In the SM, the LH neutrinos are massless due to the absence of their RH counterparts (hence no Dirac mass) as well as the conservation of a global $(B-L)$ symmetry (hence no Majorana mass). Therefore, in order to generate non-zero neutrino masses, one must extend the SM sector by either adding three RH neutrinos (one per family) or by introducing $(B-L)$-breaking fields or both [30]. If we just add RH neutrinos (N) while keeping the $(B-L)$ symmetry unbroken, then the observed smallness of LH-neutrino masses requires that the new Yukawa couplings (y_ν) must be extremely small, i.e. $y_\nu \lesssim 10^{-12}$ for sub-eV LH neutrino mass. In the absence of any obvious compelling arguments for such a tiny Yukawa coupling, the alternative path of generating non-zero neutrino masses by breaking $(B-L)$ symmetry seems more natural.

2.4.1 Seesaw Mechanism

The simplest way to parameterize the $(B-L)$ breaking effects in SM extensions is through Weinberg's dimension-5 operator [86]

$$\mathcal{L}_{\text{eff}} = \lambda_{ij} \frac{L_i L_j \Phi \Phi}{M} \quad (i, j = e, \mu, \tau) \tag{2.9}$$

added to the SM Lagrangian, where M is the scale of new physics. After EWSB, due to the Higgs vev given by Eq. (1.5), this operator leads to a non-zero neutrino mass of the form $m_\nu = \lambda v^2 / M$.

There are both tree- and loop-level realizations of the dimension-5 operator given by Eq. (2.9) to generate non-zero neutrino masses [87]. The tree-level realiza-

tion is the so-called *seesaw mechanism* [37] in which the heavy particles associated with the new physics, after being integrated out, lead to the effective operator in Eq. (2.9). The simplest such model is the type I seesaw [88] in which the heavy particles are SM singlet Majorana fermions, usually known as the RH neutrinos (N), which couple to LH-doublets through Dirac Yukawa:

$$\mathcal{L}_\nu = \sum_{i,j=1}^{3} \left[y_{\nu_{ij}} \bar{L}_i \Phi N_j + \text{h.c.} \right] + \frac{1}{2} \sum_{i=1}^{3} M_{N_i} N_i N_i, \tag{2.10}$$

and M_N is the Majorana mass of N which we have chosen to be diagonal, without loss of generality. After EWSB, this leads to the neutrino mass matrix of the form

$$\mathcal{M}_\nu = \begin{pmatrix} 0 & M_D \\ M_D^T & M_N \end{pmatrix}, \tag{2.11}$$

where $M_D = v y_\nu$. The light mass eigenvalues are given by

$$m_\nu = -v^2 y_\nu M_N^{-1} y_\nu^T. \tag{2.12}$$

Note that a second way to write the Weinberg operator in Eq. (2.9) is $(L^T \vec{\tau} L) \cdot (H^T \vec{\tau} H)/M$ where τ^i's are the usual Pauli matrices. This can be implemented by adding an $SU(2)_L$ bosonic triplet $\vec{\Delta} \equiv (\Delta^{++}, \Delta^+, \Delta^0)$ coupled to SM leptons through Majorana type couplings. This is known as the type II seesaw mechanism [89]. Yet another way to write the effective Weinberg operator in Eq. (2.9) is $(L^T \vec{\tau} H)^2/M$ which can be implemented by adding an $SU(2)_L$ fermionic triplet ($\vec{\Sigma}$) coupled to leptons through Dirac Yukawas, just like the singlet ones in type I. This is known as the type III seesaw [90]. However, we do not discuss these variations further in this work.

2.4.2 Supersymmetric Seesaw

In the supersymmetric extension of the SM, the seesaw mechanism can be incorporated [91] by introducing three gauge singlet RH neutrino superfields[2] in $\hat{N}_i^c$ ($i = 1, 2, 3$) which couple to the other MSSM superfields given by Table 2.1 via the superpotential

$$W = W^{\text{MSSM}} + \sum_{i,j=1}^{3} y_{\nu_{ij}} \epsilon^{ab} \hat{L}_{ia} \hat{H}_{u_b} \hat{N}_j^c + \frac{1}{2} \sum_{i=1}^{3} M_{N_i} \hat{N}_i^c \hat{N}_i^c, \tag{2.13}$$

where W^{MSSM} is given by Eq. (2.1). The light neutrino masses are given by the type-I seesaw formula, Eq. (2.12).

The soft SUSY-breaking terms in Eq. (2.3) must also be augmented by adding the following terms:

$$-\mathcal{L}_{\text{soft}}^{\text{seesaw}} = \sum_{i,j=1}^{3} \left[m_{N_{ij}}^2 \widetilde{\nu}_{Ri}^{\dagger} \widetilde{\nu}_{Rj} + \epsilon^{ab} \left(A_{\nu_{ij}} y_{\nu_{ij}} \widetilde{L}_{ia} H_{u_b} \widetilde{\nu}_{Rj}^{\dagger} + \frac{1}{2} B_{\nu_{ij}} \widetilde{\nu}_{Ri} \widetilde{\nu}_{Rj} + \text{h.c.} \right) \right] \tag{2.14}$$

These new neutrino-sector superpotential and soft SUSY-breaking parameters in general lead to enhancement in LFV decay rates through slepton and sneutrino loops [93], and hence, are strongly constrained by experiments.

The massive neutrinos can also be incorporated in supersymmetric models with the minimal particle content given in Table 2.1, but by giving up R-parity conservation [94]. In R-parity violating (RPV) models with L violation, both $\Delta L = 1$ and $\Delta L = 2$ phenomena are allowed, leading to neutrino masses and mixing [95] and various other L-violating phenomena [96]. However, we will not discuss RPV models in this work.

---

[2]For SUSY models of neutrino mass without the seesaw mechanism, see e.g. Ref. [92].

Chapter 3

Inverse Seesaw

3.1   Scale of Seesaw Physics

As discussed in Section 2.4.1, a simple paradigm for understanding the small-ness of neutrino masses is the seesaw mechanism [88] where one introduces three $SU(2)_L \times U(1)_Y$ singlet RH neutrinos with Majorana masses M_{N_i}, usually assumed to be much larger than the weak scale, thereby providing a natural way to under-stand the tiny LH neutrino masses (hence the name "seesaw"). A great deal of attention has been devoted to testing this idea the prospects of which depend on the seesaw scale as well as any associated physics that comes with it at that scale. A key question of interest is whether there are any theoretical guidelines for the seesaw scale. This is certainly not possible within the SM gauge group under which the RH neutrino fields are neutral. Therefore, it is natural to look for extended gauge groups containing the RH neutrinos whose masses could be generated via Higgs mechanism by spontaneous symmetry breaking of this extended gauge group and be protected by the extended gauge symmetry. Also note that in the seesaw-extended SM, lep-ton number is broken due to the $\Delta L = 2$ Majorana mass term in the Lagrangian, Eq. (2.10). Consequently, the seesaw-extended MSSM superpotential in Eq. (2.13) conserves R-parity. It is therefore desirable to seek supersymmetric theories where, just like in the SM, baryon and lepton number conservation (or R-parity) is guar-

anteed by the field content and gauge symmetry.

The simplest extension is the supersymmetric version [97] of the Left-Right (LR) model based on the gauge group $SU(2)_L \times SU(2)_R \times U(1)_{B-L}$ that provides a natural explanation of the seesaw scale as connected to the $SU(2)_R \times U(1)_{B-L}$-breaking scale [98], apart from restoring the parity symmetry at high energy. Also, the smallness of the neutrino mass is connected to the extent to which the RH-current is suppressed at low energy. Thus, the LR-symmetry provides a well-defined theory of neutrino masses [30] and can be used as a guide to study seesaw physics at colliders provided the LR symmetry breaking scale is $\mathcal{O}(\text{TeV})$ [99]. Moreover, it provides a very attractive low-energy realization of $SO(10)$ [100, 68], which is arguably the simplest GUT scenario for seesaw mechanism [37] as it automatically predicts the existence of RH neutrinos (along with the SM fermions) in a single multiplet.

An advantage of GUT embedding of the seesaw mechanism is that the constraints of GUT symmetry tend to relate the Dirac neutrino mass M_D in Eq. (2.11) to the charged fermion masses thereby making a prediction for the seesaw scale M_N from low-energy experiments. For type I seesaw GUT embedding, typical values for the M_N are very large, usually in the range of 10^{10} - 10^{14} GeV, which are far beyond the reach of colliders. Note that the key feature that leads to such restrictions in type I seesaw case is the close link between the *large* $(B - L)$-breaking RH neutrino Majorana mass and the *smallness* of the LH neutrino masses. So the question is to know if there exists a seesaw mechanism whose GUT embedding is consistent with TeV scale RH neutrinos. This is the main theme of this chapter.

33

3.2 Inverse Seesaw Mechanism

A completely different realization [101] of the seesaw mechanism is characterized by a *small* effective lepton number violating Majorana mass μ_S which is directly proportional to the small LH neutrino mass. This is known as the "inverse seesaw" mechanism. The original motivation behind this formulation was to understand small neutrino mass in SUSY-GUT models where no Higgs representation is available to generate the RH neutrino mass, e.g. in supersymmetric E_6 models inspired by superstring theory [102]. The original implementation of this mechanism required two sets of SM singlet neutrino superfields $\hat{N}_i^c$, $\hat{S}_i$ ($i = 1, 2, 3$ for three generations)[1], added to the MSSM field content (see Table 2.1). The resulting superpotential is given by [101]

$$W = W^{\text{MSSM}} + \sum_{i,j=1}^{3} \left[\epsilon_{ab} y_{\nu_{ij}} \hat{L}_i^a \hat{H}_u^b \hat{N}_j^c + M_{N_{ij}} \hat{N}_i^c \hat{S}_j + \frac{1}{2} \mu_{S_{ij}} \hat{S}_i \hat{S}_j \right], \qquad (3.1)$$

where W^{MSSM} is the MSSM superpotential given by Eq. (2.1). In a non-supersymmetric version of the model, the corresponding Lagrangian is given by[2]

$$\mathcal{L}_\nu = \mathcal{L}^{\text{SM}} + \sum_{i,j=1}^{3} \left[\left(y_{\nu_{ij}} \bar{L}_i \Phi N_j + M_{N_{ij}} \bar{N}_i S_j + \text{h.c.} \right) + \frac{1}{2} \mu_{S_{ij}} S_i S_j \right] \qquad (3.2)$$

---

[1]It was shown in Ref. [103] that in a minimal supersymmetric inverse seesaw model, only one pair of singlets is sufficient to satisfy the neutrino oscillation data. However, we consider three sets of singlets as required by $SO(10)$ symmetry [100].

[2]A similar construction with $SU(2)_L \times SU(2)_R \times U(1)_{B-L}$ gauge group was done in Ref. [104].

3.2.1 Light Neutrino Mass

After electroweak symmetry breaking, we obtain the following 9×9 neutrino

mass matrix in the basis $\{\nu, N^c, S\}$:

$$\mathcal{M}_\nu = \begin{pmatrix} 0 & M_D^T & 0 \\ M_D & 0 & M_N^T \\ 0 & M_N & \mu_S/2 \end{pmatrix}, \tag{3.3}$$

where we have suppressed the family index for brevity. Here $M_D \equiv v_u y_\nu$ and M_N

are arbitrary 3×3 complex matrices in flavor space, whereas μ_S is a 3×3 complex

symmetric matrix that breaks the lepton number. The 9×9 mass matrix in Eq. (3.3)

can be diagonalized by a unitary mixing matrix $\mathcal{V}$:

$$\mathcal{V}^T \mathcal{M}_\nu \mathcal{V} = \text{diag}\left(m_{\nu_i}, m_{N_j}, m_{N_k'}\right), \quad (i, j, k = 1, 2, 3) \tag{3.4}$$

thus yielding nine mass eigenstates, three of which correspond to the observed light

neutrinos with masses m_{ν_i}, and three pairs of two-component leptons (N_j, N_j') com-

bining to form three heavy quasi-Dirac neutrinos with masses M_{N_i}. The mixing

between the light and heavy states is roughly $\theta_{\nu N} \simeq M_D M_N^{-1}$ for $M_D \ll M_N$,

similar to the type I case.

In the limit $\mu \ll M_D \ll M_N$, the diagonalization of Eq. (3.3) results in the

following effective Majorana mass matrix for light neutrinos:

$$m_\nu \simeq \left(M_D M_N^{-1}\right) \mu_S \left(M_D M_N^{-1}\right)^T, \tag{3.5}$$

where μ_S breaks the lepton number. Because of the presence of this new mass scale

μ_S in this theory, the seesaw scale M_N can be as low as $\mathcal{O}(\text{TeV})$ even for "large"

Dirac masses, unlike in the type I case [Eq. (2.12)].

3.2.2 Smallness of μ_S

In the limit $\mu_S \to 0$, there are exactly conserved lepton numbers $(1, -1, 1)$ for (ν, N^c, S) respectively. Then the three light neutrinos are massless Weyl fermions as in the SM and the six heavy neutrinos combine exactly into three Dirac fermions. Thus, the smallness of μ_S is technically natural (in the 't Hooft sense) [105], since $\mu_S \to 0$ restores a larger symmetry (a global $U(1)$ in this case).

The typical size of μ_S can be estimated from Eq. (3.5) (for one generation):

$$\left(\frac{m_\nu}{0.1 \text{ eV}} \right) = \left(\frac{M_D}{100 \text{ GeV}} \right)^2 \left(\frac{\mu_S}{1 \text{ keV}} \right) \left(\frac{M_N}{10 \text{ TeV}} \right)^{-2} \tag{3.6}$$

Thus for $M_R \sim$ a few TeV and large Dirac mass $M_D \sim 100$ GeV, the observed light neutrino masses are obtained with μ_S in the keV range. In models where lepton number is spontaneously broken by a vev $\langle \sigma \rangle$ [106], $\mu_S = y_\nu \langle \sigma \rangle$ [107]. For typical Yukawas $y_\nu \sim 10^{-1} - 10^{-3}$, $\mu_S = 1$ keV corresponds to the lepton number violation scale of $\langle \sigma \rangle \sim 10$ keV $- 1$ MeV. However, such a low scale may not be protected by SUSY from radiative corrections, though gauge loops may not destabilize it since it is a gauge singlet and interacts with gauge bosons only through its mixing. However, the smallness of μ_S can be explained by some other mechanism, e.g. radiative corrections [108], or extra dimensions [109].

3.2.3 Phenomenology

The inverse seesaw mechanism leads to a rich phenomenology which can be used to test it in energy, intensity and cosmic frontiers. Here we present a brief summary of various signatures of this mechanism in a model-independent manner,

and in subsequent chapters, we elaborate on these topics.

1. *Direct Collider Signatures:* In the inverse seesaw mechanism, since the $(B-L)$-breaking RH neutrino mass is decoupled from the smallness of the neutrino mass by the new small Majorana mass scale μ_S, the RH neutrino mass could be easily allowed to be in the TeV-range, which should be kinematically accessible at the LHC to be produced on-shell by gauge boson exchange. In particular, if the Dirac Yukawa is large, it allows for a large mixing effect $|\theta_{\nu N}|^2 \sim \left(M_D M_N^{-1}\right)^2$ between the light and heavy neutrinos, thus making the collider test of this mechanism much more feasible (see Section 6.1 for a more detailed discussion). This is in contrast with the type I case where the mixing effects are usually of order $\sim m_\nu M_N^{-1}$ and hence suppressed by the small neutrino mass unless there are cancellations to get small neutrino masses from large Dirac masses using some symmetries (see e.g. Ref. [110, 111]).

Once produced, these heavy neutrinos will decay to multi-lepton final states as their striking collider signatures [112]. Due to their pseudo-Dirac nature in inverse seesaw, the "smoking gun" signal for type I seesaw, namely the lepton number violating same-sign dilepton signal [112, 113, 114, 111], is absent. Instead, the lepton-flavor violating trilepton signal [112, 115, 116, 117] can be used to test the inverse seesaw models at the LHC. We showed in Ref. [116] that this could be used to distinguish type I from inverse seesaw at the LHC, and also the heavy gauge boson W_R could be discovered in this process.

2. *Non-unitarity Effects:* Apart from directly producing the RH neutrinos at col-

liders, a different way to test the seesaw mechanism at the intensity frontier follows from the observation that the mixing of the LH neutrinos with the RH ones in general leads to violation of unitarity of the PMNS mixing matrix [118] that describes only the mixing of the three light neutrinos. Due to large mixing being allowed in inverse seesaw models, the non-unitarity effects could be sizable [119, 120] and could be searched for in neutrino oscillation experiments [118, 121] and weak decays [118]. Note that these effects are usually suppressed by the light neutrino masses in canonical type I seesaw [122].

One may recall here that for the analogous mixing matrix in the quark sector, namely the CKM matrix, deviations from unitarity are considered a good window for physics beyond the SM and the unitarity triangle has been extensively studied in that case [123]. The need for similar studies in the leptonic sector should also be emphasized [124].

3. *CP Violation:* The large mixing and non-unitarity effects could give rise to leptonic *CP* violation [125] (for a review, see e.g. Ref. [126]). Note that the *CP* violation in inverse seesaw models [119, 120] can occur even when the light neutrinos are strictly massless [127], and could be large provided $\sin^2\theta_{13}$ and the Dirac *CP* phase are non-zero. As $\sin^2\theta_{13}$ is indeed found to be large [35, 36], the possibility of large leptonic *CP* violation becomes stronger now.

4. *LFV Signatures:* The large mixing between the light and heavy neutrinos in the charged current sector leads to enhanced rates for the LFV processes $\ell_\alpha^- \to \ell_\beta^- + \gamma$, $\mu \to eee$ and $\mu \to e$ conversion in nuclei and $\tau \to eee, e\mu\mu$ [128, 129,

38

130]. Note that these LFV processes can occur in inverse seesaw irrespective of the light neutrino mass and the SUSY spectrum [128]. This is in contrast with the canonical type I seesaw where the LFV decay rates are usually suppressed by the light neutrino mass [131] and are enhanced only by SUSY effects [93, 132].

Note that due to the small lepton number breaking in inverse seesaw, the important lepton number violating signal for Majorana neutrinos, i.e. neutrinoless double beta decay ($0\nu2\beta$) cannot be used to test the inverse seesaw [133].

5. *Dark Matter:* In SUSY seesaw models, the scalar superpartner of the RH neutrino, with a small admixture of the LH counterpart, could be a possible DM candidate, apart from the usual MSSM candidate, viz. the neutralino. Moreover, if the DM turns out to be very light ($\lesssim 20$ GeV or so), as suggested by some recent experiments and observations (for a recent review, see Ref. [134]), the mixed sneutrino DM could be a preferred candidate than the neutralino (see Chapter 5 for more details). Various models of such sneutrino DM have been constructed for extensions of MSSM with type I [135] as well as inverse seesaw [136, 137, 138, 139, 140]. We showed in Ref. [140] that the small Majorana mass term in inverse seesaw leads to a keV-scale mass splitting of the lightest complex scalar sneutrino, thus providing a natural framework for "inelastic" DM [141]. This could be used to test the inverse seesaw mechanism in DM direct detection experiments, when combined with the results from collider searches for a sneutrino DM [103, 117, 142].

6. *Leptogenesis:* One of the attractive features of the seesaw mechanism is that it provides a way to understand the origin of matter in the Universe via leptogenesis [143] (for recent reviews, see Ref. [144]). In the canonical type I seesaw models with extended gauge groups (required to explain the RH neutrino mass scale), low-scale leptogenesis is found to be in conflict with the observed baryon asymmetry unless the extra gauge boson (W' and/or Z') masses are above several TeVs [145, 146]. On the other hand, for inverse seesaw, we find these constraints to be rather weak [147] due to large Dirac Yukawa couplings and very small lepton number breaking (see Chapter 4 for details), which allow the masses of heavy gauge bosons to be in the "LHC-friendly" energy range. Hence, the discovery of heavy gauge bosons at the LHC will be considered as a strong indication for inverse seesaw if leptogenesis is indeed the mechanism for origin of matter.

These are some generic, model independent qualitative features of the inverse seesaw phenomenology. However, for making more precise and quantitative predictions, we need to be somewhat model-dependent. As we discussed earlier, in order to have a complete model of BSM physics, the seesaw mechanism must be embedded into either the SM or an extended gauge group. In the bottom-up approach, we would like to examine whether a TeV-scale inverse seesaw model is compatible with any other existing new physics scenarios. In particular, we are interested in TeV-scale supersymmetric inverse seesaw models.

3.2.4   Model Building

Current literature on the SUSY inverse seesaw discusses a few classes of such models: (i) Originally, the minimal inverse seesaw structure given by Eq. (3.3) was considered within the framework of MSSM [101] and some of its phenomenology was explored in details later [103, 129, 136, 148]. However, in these models, since both N and S are singlet fields, the MSSM gauge symmetry does not forbid terms like LH_uS and NN in the superpotential given by Eq. (3.2), and these extra terms have to be omitted "by hand" in order to obtain the minimal structure given by Eq. (3.3). (ii) The second class of inverse seesaw models extend the gauge symmetry of the model to $SU(2)_L \times U(1)_Y \times U(1)_{B-L}$ [149] so that the seesaw mass matrix arises from a $(B-L)$ gauge symmetry and given rise to some interesting phenomenology [137, 150]. However, the $(B-L)$ gauge symmetry discussed in Ref. [149] does not arise from a GUT, and thus, the nice features of SUSY-GUT might be lost in this framework. (iii) Yet another class of models uses global $(B-L)$ symmetry to restrict the inverse seesaw matrix to the desired form [139].

We proposed an alternative realization of TeV scale supersymmetric inverse seesaw [120, 151] by extending the MSSM gauge group to the supersymmetric Left-Right (SUSYLR) gauge group $SU(2)_L \times SU(2)_R \times U(1)_{B-L}$. Apart from rendering the inverse seesaw matrix in Eq. (3.3) naturally protected by gauge symmetry, this scenario has many interesting features such as (i) a full set of heavy gauge bosons $(W_R^{\pm}, Z')$ for the $SU(2)_R$ sector, thus restoring parity symmetry at TeV scale, while being consistent with low-scale leptogenesis [147] (see Chapter 4), (ii) inelastic sneu-

41

trino dark matter [140] which is allowed to be very light ($5 - 20$ GeV range, as suggested by some direct detection experiments) satisfying cosmological and collider constraints (see Chapter 5), (iii) enhanced tri-lepton signal at the LHC [116] due to on-shell production of a heavy RH neutrino via W_R exchange (see Chapter 6), (iv) gauge coupling unification and a successful embedding into an $SO(10)$ GUT [120] (see section 3.3) while being consistent with the current proton decay constraints [151] (see Chapter 7). The GUT-embedding allows us to fully determine the Yukawa couplings and the Dirac neutrino mass matrix from $SO(10)$ relations between quark and lepton mass matrices, which makes the model very predictive for the non-unitarity and LFV effects in inverse seesaw [120] (see section 6.2).

3.3   A Realistic Model based on SUSYLR

The Left-Right symmetry [98], based on the gauge group $SU(2)_L \times SU(2)_R \times U(1)_{B-L}$, has the appealing feature of restoring parity symmetry in weak interactions asymptotically, apart from explaining the neutrino mass naturally via seesaw mechanism [88]. A key question is whether this extended symmetry could co-exist with SUSY close to the weak scale, and if so, whether a TeV-scale $SU(2)_R \times U(1)_{B-L}$ breaking (and hence the seesaw scale) is consistent with coupling unification. As a generic possibility, the SUSYLR is quite consistent with current low energy observations [152]. Whether a TeV Scale $SU(2)_R$ symmetry is compatible with supersymmetric coupling unification has been extensively investigated in literature [153, 154]. While it is possible with a judicious choice of Higgs multiplets [153], it is very hard

to reconcile with TeV scale type I seesaw and related phenomenology [154]. On the other hand, as we showed in Ref. [120], it is possible to achieve gauge coupling unification with TeV scale inverse seesaw, which gives rise to interesting phenomenology. Moreover, our SUSYLR model could be easily embedded into an $SO(10)$ GUT and fermion masses and mixing arise in a simple manner[3], unlike in Ref. [153] which does not give rise to a realistic fermion mass spectrum.

3.3.1   Particle Content of the SUSYLR Model

Here we consider only the doublet implementation of the SUSYLR model, i.e. we use only $SU(2)$ doublet Higgs fields (from the $\mathbf{16}_H \oplus \overline{\mathbf{16}}_H$ multiplet of $SO(10)$) to break the $(B-L)$ symmetry. In order to keep the model general, we allow for an arbitrary number of these doublet fields, to be denoted by n_L and n_R respectively for $SU(2)_L$ and $SU(2)_R$ doublets. Likewise we have n_{10} Higgs bi-doublets (from $\mathbf{10}_H$ multiplet) which, on acquiring vevs, give masses to the fermions through Yukawa couplings. We also allow for an arbitrary number n_S of singlet fields S^α, as required by inverse seesaw. These are the essential multiplets in a generic SUSYLR model with inverse seesaw.

However, it turns out that with this minimal set of particles, it is not possible to obtain the gauge coupling unification at a scale higher than $\sim 10^{15}$ GeV as required from current bounds on proton decay lifetime, $\tau_p \gtrsim 10^{34}$ years [156]. As we have shown below, unification is possible after adding the contribution from the

---

[3]An $SO(10)$ embedding for inverse seesaw along somewhat similar lines to ours was also considered in Ref. [155].

color triplets $\left[\left(3, 1, \frac{4}{3}\right) + \text{c.c.}\right]$ (which come from the $\mathbf{45}_H$ multiplet). The lightness of these Higgs multiplets, while consistently keeping all other multiplets heavy, is justified in Appendix A.

The most general field content in our SUSYLR model is given in Table 3.1. The electric charges of the fields must obey the relation $Q_{\text{em}} = I^{3L} + I^{3R} + \frac{B-L}{2}$.

3.3.2 Gauge Coupling Unification

The running of the gauge couplings is given by Eq. (2.4) and the one-loop β-function in a supersymmetric theory is given by Eq. (2.7). With $C(G) = N$ for a fundamental representation of $SU(N)$, we can write the coefficients of β_i in Eq. (2.7) as [157]

$$b_i^{\text{SUSY}} = 2n_g - 3N + T_H(S_N) \tag{3.7}$$

for n_g generations of fermions, and the complex Higgs representation parametrized by $T_H(S_N)$. For $U(1)$ gauge group, $N = 0$ in Eq. (3.7) and the $(B - L)$ gauge coupling is GUT-normalized as $g_1 = \sqrt{\frac{2}{3}} g_{B-L}$ [68].

For the particle content given by Table 3.1, the Higgs contributions to Eq. (3.7) are explicitly given by

$$T_{2L} = n_{10} + n_L, \ T_{2R} = n_{10} + n_R, T_{3c} = 1, \ \text{and } T_{B-L} = 4 + \frac{3}{2}\left(n_L + n_R\right) \tag{3.8}$$

Hence for three fermion generations, the coefficients of the β-functions in our SUSYLR model are

$$b_i^{\text{SUSYLR}} = \left(10 + \frac{3}{2}n_L + \frac{3}{2}n_R, \ n_{10} + n_L, \ n_{10} + n_R, \ -2\right), \tag{3.9}$$

	Superfield	$SU(3)_c$	$SU(2)_L$	$SU(2)_R$	$U(1)_{B-L}$
Gauge	$\hat{G}^A$	**8**	**1**	**1**	0
	$\hat{W}_L^a$	**1**	**3**	**1**	0
	$\hat{W}_R^a$	**1**	**1**	**3**	0
	$\hat{B}$	**1**	**1**	**1**	0
Quark	$\hat{Q}_i = \begin{pmatrix} \hat{u}_i \\ \hat{d}_i \end{pmatrix}$	**3**	**2**	**1**	$\frac{1}{3}$
	$\hat{Q}_i^c = \begin{pmatrix} \hat{d}_i^c \\ -\hat{u}_i^c \end{pmatrix}$	**3̄**	**1**	**2**	$-\frac{1}{3}$
Lepton	$\hat{L}_i = \begin{pmatrix} \hat{\nu}_i \\ -\hat{e}_i \end{pmatrix}$	**1**	**2**	**1**	-1
	$\hat{L}_i^c = \begin{pmatrix} \hat{e}_i^c \\ -\hat{\nu}_i^c \end{pmatrix}$	**1**	**1**	**2**	1
Singlet	$\hat{S}_i^\alpha$	**1**	**1**	**1**	0
Higgs	$\hat{\phi}_u^p = \begin{pmatrix} \hat{\phi}_u^{+p} \\ \hat{\phi}_u^{0p} \end{pmatrix}$	**1**	**2**	**1**	1
	$\left(\hat{\phi}^c\right)_u^q = \begin{pmatrix} \hat{\phi}_u^{c^{0q}} \\ -\hat{\phi}_u^{c^{+q}} \end{pmatrix}$	**1**	**1**	**2**	-1
	$\hat{\phi}_d^p = \begin{pmatrix} \hat{\phi}_d^{0p} \\ \hat{\phi}_d^{-p} \end{pmatrix}$	**1**	**2**	**1**	-1
	$\left(\hat{\phi}^c\right)_d^q = \begin{pmatrix} \hat{\phi}_d^{c^{-q}} \\ -\hat{\phi}_u^{c^{0q}} \end{pmatrix}$	**1**	**1**	**2**	1
	$\hat{\Phi}_r = \begin{pmatrix} \hat{\varphi}_{d_r}^0 & \hat{\varphi}_{u_r}^+ \\ \hat{\varphi}_{d_r}^- & \hat{\varphi}_{u_r}^0 \end{pmatrix}$	**1**	**2**	**2**	0
	$\hat{\delta}$	**3**	**1**	**1**	$\frac{4}{3}$
	$\hat{\delta}^c$	**3̄**	**1**	**1**	$-\frac{4}{3}$

Table 3.1: The superfield content of our SUSYLR model and their $\mathbf{3}_c\mathbf{2}_L\mathbf{2}_R\mathbf{1}_{B-L}$ quantum numbers. Here $i = 1, 2, 3$ is the generation index, $a = 1, 2, 3$ and $A = 1, \cdots, 8$ are the **2** and **3** gauge indices, $r = 1, ..., n_{10}$, $p = 1, ..., n_L$, $q = 1, ..., n_R$ and $\alpha = 1, ..., n_S$.

where i stands for $\mathbf{1}_{B-L}$, $\mathbf{2}_L$, $\mathbf{2}_R$ and $\mathbf{3}_c$ respectively.

For illustrative purposes, we assume the SUSY scale $M_{\mathrm{SUSY}} = 300$ GeV and the $SU(2)_R \times U(1)_{B-L}$-breaking scale $M_R = 1$ TeV. Also we take the number of Higgs bi-doublets, $n_{10} = 2$ which is the minimum number required to get a realistic fermion mass and mixing pattern for an $SO(10)$-GUT [68]. However, the number of Higgs doublets can be arbitrary and we choose the minimum number of them which gives successful unification. We start with the weak scale experimental values of the couplings for $\mathbf{1}_Y$, $\mathbf{2}_L$ and $\mathbf{3}_c$ given in Table 1.2 and run them up to the SUSY scale M_{SUSY} using the SM β-functions given by Eq. (2.5) with the coefficients given by Eq. (2.6). Similarly, the running between the SUSY scale and the $SU(2)_R$-breaking scale is determined by the MSSM β-functions given by Eq. (2.7) with the coefficients given by Eq. (2.8). And finally, the running between the $SU(2)_R$-breaking scale and the GUT-scale is determined by the SUSY β-functions given by Eq. (2.7) with the coefficients obtained in Eq. (3.9). Also we use the matching condition [68] at $Q = M_R$ where the $U(1)_Y$-gauge coupling gets merged into $SU(2)_R \times U(1)_{B-L}$:

$$\alpha_{1Y}^{-1}(M_R) \;=\; \frac{3}{5}\alpha_{2R}^{-1}(M_R) + \frac{2}{5}\alpha_{B-L}^{-1}(M_R) \tag{3.10}$$

As shown in Figure 3.1, the gauge coupling unification is obtained for $n_L = 0$ and $n_R = 2$, with the unification scale parameters

$$M_G \simeq 4 \times 10^{16} \text{ GeV}, \quad \text{and} \quad \alpha_U(M_G) \simeq 0.05 \tag{3.11}$$

As the running behavior is mostly controlled by the SUSYLR sector, the scales M_{SUSY} and M_R can be relaxed a little bit, still preserving unification, as long as M_{SUSY} is not too far from the weak scale (for reasons already discussed in Chapter

46
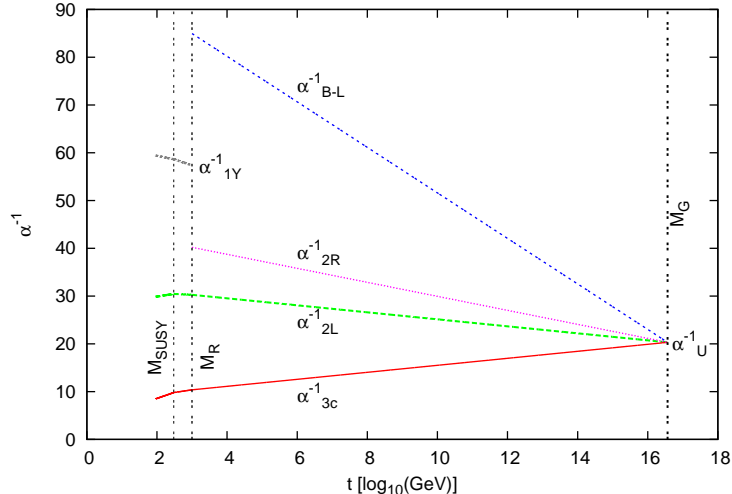
Figure 3.1: Gauge coupling unification in the SUSYLR model. We have used $n_{10} = 2$, $n_L = 0$, $n_R = 2$, $M_{\text{SUSY}} = 300$ GeV and $M_R = 1$ TeV.

2). Note that the unification scale obtained here is slightly higher than the usual SUSY-GUT scale. Moreover, unification occurs irrespective of the value of the intermediate scale M_R, and when the unified coupling is extrapolated back to the weak scale, the Weinberg angle $\sin^2 \theta_W(m_Z)$ and the strong coupling constant $\alpha_3(m_Z)$ are independent of M_R. This is an important feature of $SO(10)$ GUT [158].

It should be emphasized here that the choice of two Higgs bi-doublets is the minimum possible choice since one bi-doublet does not give a realistic fermion mass spectrum in $SO(10)$. Also, the choice of the number of Higgs doublets is unique for the field content given by Table 3.1, since changing any of them will spoil the unification. However, as we realized later (see Appendix A in Ref. [147]), there is an alternative and somewhat better choice of Higgs fields which also leads to coupling unification with TeV-scale W_R and Z'. We found that if we add one set of $SU(2)_R$ triplets $\Delta(1, 1, 3, 0)$ (coming from the $\mathbf{45}_H$ field) to the field content in Table 3.1,

47

then we can achieve unification with only one $SU(2)_R$ doublet, instead of two as shown in Figure 3.1. This model has two nice features over the one presented here: (i) all the Higgs fields required for unification are connected to breaking of separate gauge symmetries and there is no arbitrariness in the number of fields, and (ii) the presence of the $SU(2)_R$ triplet enables us to decouple the mass scales M_{W_R} and $M_{Z'}$ which are otherwise related in usual Left-Right models with $M_{Z'} > M_{W_R}$. However, the other low-energy effects to be discussed in subsequent chapters are more or less independent of this choice of one or two RH-doublets.

We should also comment on the asymmetry between n_L and n_R. As shown in Appendix A, since the vev of the $\mathbf{45}_H$ Higgs breaks D-parity and decouples it from the $SU(2)_R$ breaking scale [159], it is possible to have only the right-handed doublets and no left-handed ones below the GUT scale. This leads to the asymmetry between α_{2L} and α_{2R}, with $\frac{\alpha_{2L}}{\alpha_{2R}} \simeq 1.3$ at TeV-scale in our case (see Figure 3.1).

3.3.3   Fermion masses and mixing

The RG evolution of the fermion masses and mixing have been extensively studied for both the SM and the MSSM cases [84, 85, 160], but not for the SUSYLR model, even though the analytical expressions for the Yukawa couplings had already been derived in Ref. [161]. In this section, we present a detailed RG analysis of our SUSYLR model and numerically solve them to obtain the quark and lepton masses and the CKM matrix elements at the unification scale M_G.

The general R-parity conserving superpotential in the SUSYLR model is given

by

$$
\begin{aligned}
W^{\text{SUSYLR}} &= iy_a\hat{Q}^T\hat{\Phi}_a\hat{Q}^c + iy_a'\hat{L}^T\tau_2\hat{\Phi}_a\hat{L}^c + iy_S'^{\alpha p}\hat{S}^\alpha\hat{L}^T\tau_2\hat{\phi}_u^p + iy_S^{\alpha q}\hat{S}^\alpha\hat{L}^{cT}\tau_2\hat{\phi}_u^{cq} \\
&\quad + y_\Phi^{\alpha ab}\hat{S}^\alpha\mathrm{Tr}\left(\hat{\Phi}_a^T\tau_2\hat{\Phi}_b\tau_2\right) + iy_\phi^{\alpha pq}\hat{S}^\alpha\left(\hat{\phi}_u^p\right)^T\tau_2\hat{\phi}_d^q + iy_{\phi^c}^{\alpha pq}\hat{S}^\alpha\left(\hat{\phi}_u^{cp}\right)^T\tau_2\hat{\phi}_d^{cq} \\
&\quad + i\lambda_{apq}\left(\hat{\phi}_u^p\right)^T\tau_2\hat{\Phi}_a\left(\hat{\phi}_u^{cq}\right) + i\bar{\lambda}_{apq}\left(\hat{\phi}_d^p\right)^T\tau_2\hat{\Phi}_a\hat{\phi}_d^{cq} \\
&\quad + i\mu_\phi^{pq}\left(\hat{\phi}_u^p\right)^T\tau_2\hat{\phi}_d^q + i\mu_{\phi^c}^{pq}\left(\hat{\phi}_u^{cp}\right)^T\tau_2\hat{\phi}_d^{cq} + \mu_\Phi^{ab}\mathrm{Tr}\left(\Phi_a^T\tau_2\Phi_b\tau_2\right) \\
&\quad + \frac{1}{2}\mu_S^{\alpha\beta}\hat{S}^\alpha\hat{S}^\beta + \frac{1}{6}Y_S^{\alpha\beta\gamma}\hat{S}^\alpha\hat{S}^\beta\hat{S}^\gamma
\end{aligned}
\tag{3.12}
$$

where we have suppressed the generational and $SU(2)$ indices. Also we have ignored all non-renormalizable terms in the superpotential as their contributions to the RGEs are suppressed by M_R/M_G. We note that the superpotential given by Eq. (3.12) has two additional terms of the form $SL\phi_u$ and $SL^c\phi_u^c$ (as required by the inverse seesaw model) as compared to that given in Ref. [161]. Also note that since the δ, δ^c fields in Table 3.1 do not couple to any of the matter fields, they do not enter the superpotential and do not affect the RG running of fermion mass parameters (they only affect the color gauge coupling evolution).

We have seen from the previous section that the gauge coupling unification requires that we should not have any $SU(2)_L$ doublet of Higgs fields in the low-energy spectrum. Hence, we can drop the $\phi_{u,d}$ terms altogether from the superpotential of Eq. (3.12) to get the following working superpotential for our model:

$$
\begin{aligned}
W &= iy_a\hat{Q}^T\hat{\Phi}_a\hat{Q}^c + iy_a'\hat{L}^T\tau_2\hat{\Phi}_a\hat{L}^c + iy_S^{\alpha q}\hat{S}^\alpha\hat{L}^{cT}\tau_2\hat{\phi}_u^{cq} + y_\Phi^{\alpha ab}\hat{S}^\alpha\mathrm{Tr}\left(\hat{\Phi}_a^T\tau_2\hat{\Phi}_b\tau_2\right) \\
&\quad + iy_{\phi^c}^{\alpha pq}\hat{S}^\alpha\left(\hat{\phi}_u^{cp}\right)^T\tau_2\hat{\phi}_d^{cq} + i\mu_{\phi^c}^{pq}\left(\hat{\phi}_u^{cp}\right)^T\tau_2\hat{\phi}_d^{cq} + \mu_\Phi^{ab}\mathrm{Tr}\left(\Phi_a^T\tau_2\Phi_b\tau_2\right) \\
&\quad + \frac{1}{2}\mu_S^{\alpha\beta}\hat{S}^\alpha\hat{S}^\beta + \frac{1}{6}Y_S^{\alpha\beta\gamma}\hat{S}^\alpha\hat{S}^\beta\hat{S}^\gamma
\end{aligned}
\tag{3.13}
$$

49

where $a = 1, 2$, $p, q = 1, 2$ and $\alpha = 1, 2, 3$ corresponding to the two bi-doublets, RH-doublets and three fermion singlets, respectively, and we have suppressed other $SU(2)$ indices for brevity.

The RGEs for the Yukawa couplings y_a and y'_a in Eq. (3.13) are given by

$$16\pi^2 \frac{dy_a}{dt} = y_a \left[2y_b^\dagger y_b - \frac{16}{3} g_3^2 - 3g_{2L}^2 - 3g_{2R}^2 - \frac{1}{6} g_{B-L}^2 \right]$$
$$+ y_b \left[\text{Tr} \left(3y_b^\dagger y_a + y_b'^\dagger y'_a \right) + 2y_b^\dagger y_a + 4 \left(\mu_\alpha^{\Phi\dagger} \mu_\alpha^\Phi \right)_{ba} \right] \quad (3.14)$$

$$16\pi^2 \frac{dy'_a}{dt} = y'_a \left[2y_b'^\dagger y'_b - 3g_{2L}^2 - 3g_{2R}^2 - \frac{3}{2} g_{B-L}^2 \right]$$
$$+ y'_b \left[\text{Tr} \left(3y_b^\dagger y_a + y_b'^\dagger y'_a \right) + 2y_b'^\dagger y'_a + 4 \left(\mu_\alpha^{\Phi\dagger} \mu_\alpha^\Phi \right)_{ba} + y_S^{\alpha\dagger} y_S^\alpha \delta_{ba} \right] (3.15)$$

where the repeated indices are summed over. Note that we have an additional contribution to the RGE of the lepton Yukawa coupling y'_a as compared to those given in Ref. [161] which comes from the $S\phi_u^c L^c$ term in the superpotential. Note also the presence of the y_b terms in the second line in both the Yukawa RGEs even for $a \neq b$, which are characteristics of left-right models, arising from the Higgs self-energy effects, and are absent in case of MSSM [157].

The fermion masses arise through the Yukawa couplings y_a and y'_a in the superpotential given by Eq. (3.13) when the two Higgs bi-doublets $\Phi_{1,2}$ acquire vevs. In general, a linear combination of y_1 and y_2 will give masses to the up-type quarks, and similarly different linear combinations for the other masses. The dynamics of the superpotential can be chosen in such a way that the bi-doublets acquire vevs in the following simple manner:

$$\langle \Phi_1 \rangle = \frac{1}{\sqrt{2}} \begin{pmatrix} v_d & 0 \\ 0 & 0 \end{pmatrix}, \quad \langle \Phi_2 \rangle = \frac{1}{\sqrt{2}} \begin{pmatrix} 0 & 0 \\ 0 & v_u \end{pmatrix} \quad (3.16)$$

and we identify the ratio $v_u/v_d \equiv \tan\beta$ as in Eq. (2.2). To obtain the RGEs for the mass matrices, we choose the renormalization method where the Yukawa couplings and the Higgs vevs run separately [160]. The RGEs for the Higgs vevs are obtained from the gauge and scalar self-energy contributions:

$$16\pi^2 \frac{dv_u}{dt} = v_u \left[\frac{3}{2}g_{2L}^2 + \frac{3}{2}g_{2R}^2 - \mathrm{Tr}\left(3y_2^\dagger y_2 + y_2'^\dagger y_2'\right) - 4\left(\mu_\alpha^{\Phi\dagger}\mu_\alpha^\Phi\right)_{22} \right] \quad (3.17)$$

$$16\pi^2 \frac{dv_d}{dt} = v_d \left[\frac{3}{2}g_{2L}^2 + \frac{3}{2}g_{2R}^2 - \mathrm{Tr}\left(3y_1^\dagger y_1 + y_1'^\dagger y_1'\right) - 4\left(\mu_\alpha^{\Phi\dagger}\mu_\alpha^\Phi\right)_{11} \right] \quad (3.18)$$

Using Eqs. (3.14, 3.15) for $\dot{y}_a$, $\dot{y}_a'$ and Eqs. (3.17, 3.18) for $\dot{v}_u$, $\dot{v}_d$, we have explicitly derived the RGEs for the physical fermion masses and the quark mixing in our SUSYLR model in Appendix B. Using the initial values for the mass and mixing parameters at weak scale from Table 1.2 and the SM and MSSM Yukawa RGEs [160] for m_Z to M_{SUSY} and M_{SUSY} to M_R respectively, we numerically solve the SUSYLR RGEs given in Appendix B to obtain the running quark and lepton masses and the CKM matrix elements at the unification scale M_G:

$$m_u(M_G) = 0.0017 \text{ GeV}, \; m_c(M_G) = 0.1910 \text{ GeV}, \; m_t(M_G) = 77.8035 \text{ GeV};$$

$$m_d(M_G) = 0.0013 \text{ GeV}, \; m_s(M_G) = 0.0263 \text{ GeV}, \; m_b(M_G) = 1.7092 \text{ GeV};$$

$$m_e(M_G) = 0.0004 \text{ GeV}, m_\mu(M_G) = 0.0911 \text{ GeV}, \; m_\tau(M_G) = 1.7096 \text{ GeV};$$

$$V_{\mathrm{CKM}}(M_G) = \begin{pmatrix} 0.9793 & 0.2023 + 0.0018i & 0.0005 - 0.0057i \\ -0.2023 + 0.0016i & 0.9791 & 0.0240 \\ 0.0044 - 0.0056i & -0.0236 - 0.0013i & 0.9997 \end{pmatrix}$$

$$\tan\beta(M_G) = 7.0 \quad (3.19)$$
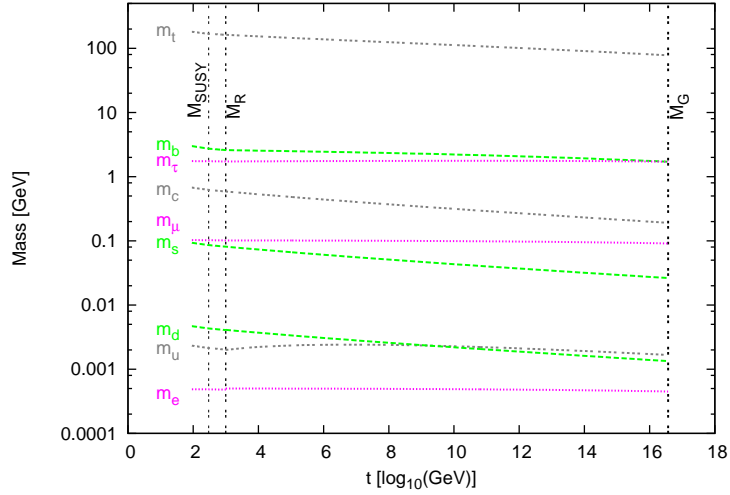
Figure 3.2: Running of fermion masses in our SUSYLR model for $M_{\mathrm{SUSY}} = 300$ GeV and $M_R = 1$ TeV. Note the $b - \tau$ unification which is a generic feature of $SO(10)$ GUT.
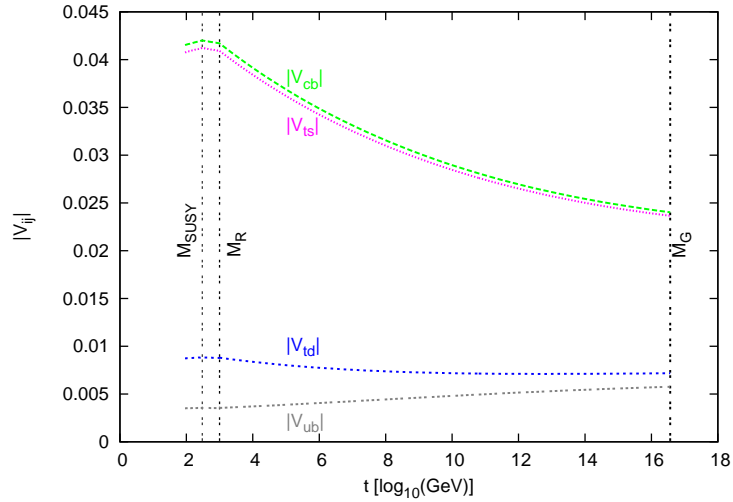
Figure 3.3: Running of the CKM mixing elements involving third generation in our SUSYLR model for $M_{\mathrm{SUSY}} = 300$ GeV and $M_R = 1$ TeV. The running of other CKM elements, being small, is not shown here.

Figure 3.2 shows the running of the quark and charged lepton masses up to the unification scale M_G. Note that we are able to generate the fermion mass spectrum at the GUT scale with

$$\frac{m_b}{m_\tau} \simeq 1, \ \frac{m_\mu}{m_s} \simeq 3, \ \frac{m_e}{m_d} \simeq \frac{1}{3} \tag{3.20}$$

which are characteristics of $SO(10)$-GUT spectrum [100], thus validating our RG analysis presented here. Figure 3.3 shows the running of the CKM elements involving only the third generation. Note that in addition to the significant running for the third generation CKM elements $V_{ub, \ cb, \ td, \ ts}$, we have a relatively milder running for the other elements as well [cf. Eq. (3.19)], even in the third-generation dominance approximation. This is a characteristic of the Left-Right model, in contrast with the MSSM case where in the third generation dominance, the first and second generation elements do not run at the one-loop level [160].

3.3.4   Symmetry breaking by radiative corrections

In this section, we propose a way to break both the $SU(2)_R \times U(1)_{B-L}$ as well as the SM symmetry via radiative corrections from renormalization group extrapolation of the scalar Higgs masses from the GUT to TeV scale [151]. As is well known, the large top quark coupling enables one to achieve a similar goal in the case of MSSM [69]. However, the simple generalization of that procedure cannot work in our model since the bidoublet Higgs of LR models contains both the $H_{u,d}$ components of MSSM, and as a result, large top quark coupling will necessarily turn both their masses negative and this will not to give a stable vacuum.

Our proposal [151] is that we use a domain of parameter space for the soft SUSY-breaking mass squares for the RH Higgs doublets $\phi_{u,d}^c$ where the mass square of one of them turns negative, by RG running to the TeV scale due to the $L^c \phi_d^c S$ Yukawa coupling being large. This leads to a breaking of the $SU(2)_R$ and $(B-L)$ symmetry. The mass square of the ϕ_u^c remains positive throughout but it acquires an induced vev. The differences in their vevs, via the D-term [162], can make the mass square of the H_u field negative while keeping the mass square of H_d positive as in the case of MSSM, thereby also giving rise to the EWSB. The main point is that both symmetry breakings owe their origin to one radiative correction.

In order to show that it is indeed possible to achieve negative mass square for one of the RH Higgs doublets while keeping all other soft mass squares positive, we need to examine the RG running of all the soft mass parameters from the GUT to TeV scale. In this regime, the model is SUSYLR for which the soft SUSY-breaking Lagrangian is given by [161]

$$
\begin{aligned}
\mathcal{L}_{\text{soft}} \;=\; & -\frac{1}{2}\left(M_3 \widetilde{G}\widetilde{G} + M_{2L}\widetilde{W}_L\widetilde{W}_L + M_{2R}\widetilde{W}_R\widetilde{W}_R + M_1 \widetilde{B}\widetilde{B} + \text{h.c.}\right) \\
& -\left[iA_{u_a}\widetilde{Q}^T \tau_2 \Phi_a \widetilde{Q}^c + iA_{e_a}\widetilde{L}^T \tau_2 \Phi_a \widetilde{L}^c + iA_{\phi_u^c}^\alpha S^\alpha \phi_u c^T \tau_2 \phi_{u^c} + iA_{L^c}^\alpha \widetilde{S}^\alpha \widetilde{L}^{cT} \tau_2 \phi_u^c \right. \\
& \left. +\frac{1}{6}A_S^{\alpha\beta\gamma}S^\alpha S^\beta S^\gamma + A_{\Phi_{ab}}^\alpha S^\alpha \text{Tr}\left(\Phi_a^T \tau_2 \Phi_b \tau_2\right) + \text{h.c.}\right] \\
& -\left[iB_{\phi^c}\phi_u^{cT}\tau_2 \phi_d^c + B_{ab}\text{Tr}\left(\Phi_a^T \tau_2 \Phi_b \tau_2\right) + \frac{1}{2}B_S^{\alpha\beta}S^\alpha S^\beta\right] \\
& -\left[m_Q^2 \widetilde{Q}^\dagger \widetilde{Q} + m_{Q^c}^2 \widetilde{Q}^{c\dagger}\widetilde{Q}^c + m_L^2 \widetilde{L}^\dagger \widetilde{L} + m_{L^c}^2 \widetilde{L}^{c\dagger}\widetilde{L}^c + m_{\phi_u^c}^2 \phi_u^{c\dagger}\phi_u^c + m_{\phi_d^c}^2 \phi_d^{c\dagger}\phi_d^c \right. \\
& \left. +m_{\Phi_{ab}}^2 \text{Tr}\left(\Phi_a^\dagger \Phi_b\right) + m_{S_{\alpha\beta}}^2 S^\alpha S^\beta\right]
\end{aligned}
\tag{3.21}
$$

where we have suppressed the generational and $SU(2)$ indices, and $a, b = 1, 2$ (for two bidoublets), and $\alpha, \beta, \gamma = 1, 2, 3$ (for three gauge singlets). Note that we do

54

not have any $\phi_{u,d}$-term in these expressions as there is no $SU(2)_L$ Higgs doublet in our model. Also we have an additional term in the superpotential (the $SL^c\phi_u^c$ term) and a corresponding trilinear term in the soft breaking Lagrangian (the $\widetilde{S}\widetilde{L}^c\phi_u^c$ term) as compared to the expressions given in Ref. [161]; this additional term in the superpotential is required for the inverse seesaw mechanism to work. Moreover, if we assume R-parity conservation, then the $S\phi_u^c\phi_d^c$ and $S\Phi\Phi$ terms are not allowed in the superpotential and also in the soft-breaking Lagrangian, i.e. the couplings μ_{ϕ^c} and μ_Φ as well as Y_{abc} in Eq. (3.12) and the corresponding terms in Eq. (3.21) are set to zero and y_{ϕ^c} is the only non-zero coupling in Eq. (3.12) which can be fixed by requiring $b - \tau$ unification at the GUT-scale. In this section, we work with this assumption.

Now we analyze the RG evolution of the gaugino and soft mass parameters from GUT to TeV scale. It is well known that in minimal SUSY GUTs, the β-function for the gaugino mass is proportional to the β-function for the corresponding gauge coupling [157]. Explicitly, the RGEs for the gaugino mass parameters are given by

$$\frac{dM_i}{dt} = \frac{b_i}{8\pi^2} M_i g_i^2 \qquad (3.22)$$

where the β-function coefficients in our SUSYLR model are given by Eq. (3.9). This implies that the three gaugino masses, like the three gauge couplings, must unify at $Q = M_G$. In order to solve Eq. (3.22), we adopt the universality hypothesis at the GUT scale (as in typical mSUGRA type models) [82]

$$M_1 = M_{2L} = M_{2R} = M_3 \equiv m_{1/2}, \qquad (3.23)$$

together with the initial condition

$$g_1^2 = g_{2L}^2 = g_{2R}^2 = g_3^2 \equiv 4\pi\alpha_U, \tag{3.24}$$

where α_U is given by Eq. (3.11). Using these initial conditions, we can obtain the running masses for the gauginos at TeV scale, starting with a given value $m_{1/2}$ at the GUT scale, as shown in Fig. 3.4 for an illustrative value of $m_{1/2} = 200$ GeV. The value of M_3 increases, since it has a negative β-function, while the other gaugino masses decrease as we go down the energy scale. Thus the gluino is much heavier than the other gauginos at the weak scale.
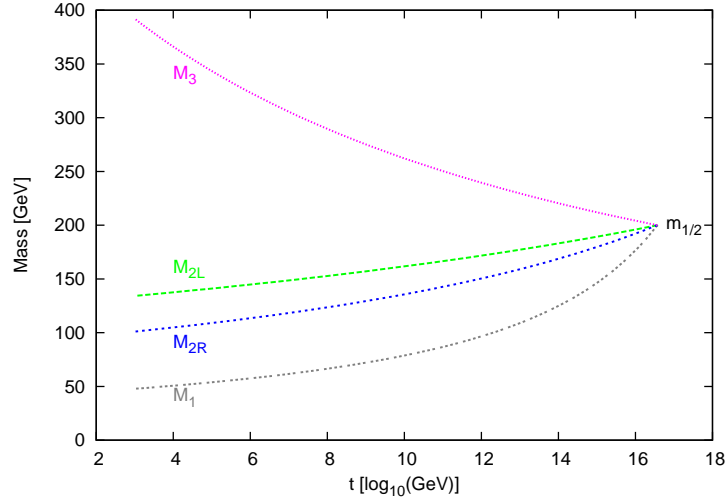
Figure 3.4: RG evolution of gaugino masses from GUT to TeV scale for $m_{1/2} = 200$ GeV.

The one-loop RGEs for the soft SUSY-breaking mass parameters are given in Appendix C. As initial conditions, we assume universality and reality of the soft fermion and Higgs masses at the GUT-scale, i.e.

$$\left(m_Q^2\right)_{ij} = \left(m_{Q^c}^2\right)_{ij} = \left(m_L^2\right)_{ij} = \left(m_{L^c}^2\right)_{ij} \equiv m_0^2\delta_{ij},$$

56

$$m_{\phi_u^c}^2 = m_{\phi_d^c}^2 = m_{\phi_0}^2, \quad \left(m_\Phi^2\right)_{ab} = m_{\Phi_0}^2 \delta_{ab},$$

$$\left(m_S^2\right)_{\alpha\beta} = m_{S_0}^2 \delta_{\alpha\beta} \tag{3.25}$$

Note that in principle, we can choose a different mass scale for the Higgs bidoublets and even different generations of fermions as well. The only constraint due to the $SO(10)$ symmetry requires us to have the same mass for each generation of fermions. Also note that all the off-diagonal soft SUSY breaking scalar masses have been set to zero. The inter-generation mixing at the low energy scale then occurs only via the superpotential Yukawa couplings. With these initial conditions, we solve the coupled RGEs for the soft masses given in Appendix C, along with the Yukawa RGEs given by Eqs. (3.14) and (3.15) to get the running soft masses at the low scale.

Fig. 3.5 illustrates such a scenario for the choice $m_{1/2} = 200$ GeV, $m_0 = m_{\phi_0} = m_{\Phi_0} = 1.2$ TeV and $m_{S_0} = 1.27$ TeV. We have chosen the $SL^c\phi_u^c$ coupling $y_S = 0.7$ to achieve a realistic fermion mass spectrum, and in particular, the $b - \tau$ unification at the GUT scale. Note that the RH slepton masses evolve much more rapidly than their LH counterparts due to this large coupling y_S. The value of m_{S_0} is chosen such that all the other eigenvalues (especially $m_{L_3^c}^2$ and m_S^2) remain positive at the TeV scale. Note that the low energy values of $m_{L_3^c}^2$ and m_S^2 are of order $(10 \text{ GeV})^2$. However the physical masses of these particles also receive a contribution from the $\langle \phi_d^c \rangle$ which pushes the masses upto a TeV scale. As far as the squark masses are concerned, they evolve more than the slepton masses due to the strong interaction loop contributions to their RGEs. The small intra-generational mass splitting is
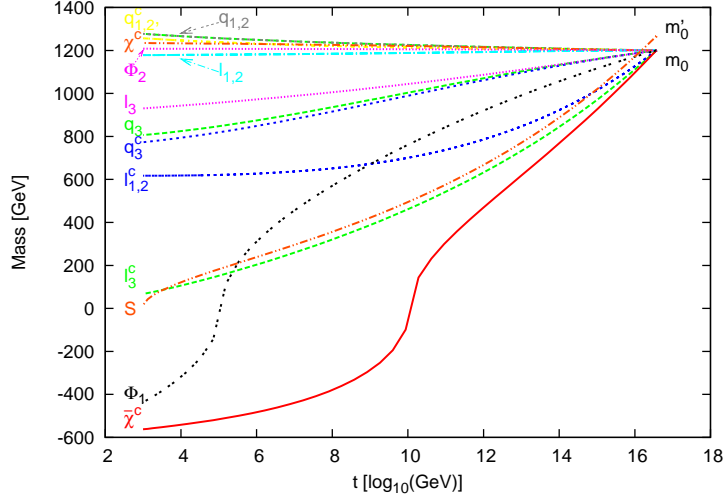
Figure 3.5: Evolution of the scalar mass parameters for $m_{1/2} = 200$ GeV, $m_0 = m_{\phi_0} = m_{\Phi_0} = 1.20$ TeV, $m_{S_0} = 1.27$ TeV and $y_{\phi^c} = 0.7$. For the scalar masses, we actually plot $\text{sign}(m^2) \cdot \sqrt{|m^2|}$, so that the negative values on the curves correspond to negative values of m^2.

due to the differences in their electroweak interaction. We can see clearly that at the weak scale, the values of $m^2_{\phi^c_d}$ and $m^2_{\Phi_1}$ are negative, thus triggering the $SU(2)_R$ and electroweak symmetry breaking respectively. Note that we need not have both the bidoublet mass squares to be negative, as one negative value will induce the symmetry breaking via the cross terms of the type $\Phi_1\Phi_2$ in the Lagrangian.

We also verify that the low-energy values of the sfermion mass square matrices satisfy all the FCNC constraints [77], due to the smallness of the off-diagonal entries. As an example, we give the values here for the parameter values shown in Figure 3.5:

$$
m_Q^2 = \begin{pmatrix} 1.63 \times 10^6 & -1.45 \times 10^1 + 8.64 \times 10^1 i & -4.79 \times 10^2 + 3.57 \times 10^3 i \\ -1.45 \times 10^1 - 8.64 \times 10^1 i & 1.63 \times 10^6 & -2.31 \times 10^4 + 1.68 i \\ -4.79 \times 10^2 - 3.57 \times 10^3 i & -2.31 \times 10^4 - 1.68 i & 6.51 \times 10^5 \end{pmatrix} \text{GeV}^2,
$$

58

$$
m_{Q^c}^2 = \begin{pmatrix} 1.58 \times 10^6 & -1.45 \times 10^1 + 8.64 \times 10^1 i & -4.79 \times 10^2 + 3.57 \times 10^3 i \\ -1.45 \times 10^1 - 8.64 \times 10^1 i & 1.58 \times 10^6 & -2.31 \times 10^4 + 1.68 i \\ -4.79 \times 10^2 - 3.57 \times 10^3 i & -2.31 \times 10^4 - 1.68 i & 5.99 \times 10^5 \end{pmatrix} \text{GeV}^2,
$$

$$
m_L^2 = \begin{pmatrix} 1.39 \times 10^6 & -7.28 + 8.39 \times 10^1 i & -2.59 \times 10^2 + 3.45 \times 10^3 i \\ -7.28 - 8.39 \times 10^1 i & 1.39 \times 10^6 & -1.25 \times 10^4 + 7.45 \times 10^{-1} i \\ -2.59 \times 10^2 - 3.45 \times 10^3 i & -1.25 \times 10^4 - 7.45 \times 10^{-1} i & 8.66 \times 10^5 \end{pmatrix} \text{GeV}^2,
$$

$$
m_{L^c}^2 = \begin{pmatrix} 3.81 \times 10^5 & -7.18 + 8.24 \times 10^1 i & -2.57 \times 10^2 + 3.41 \times 10^3 i \\ -7.18 - 8.24 \times 10^1 i & 3.81 \times 10^5 & -1.24 \times 10^4 + 7.75 \times 10^{-1} i \\ -2.57 \times 10^2 - 3.42 \times 10^3 i & -1.24 \times 10^4 - 7.75 \times 10^{-1} i & 5.00 \times 10^3 \end{pmatrix} \text{GeV}^2.
$$

3.4 Embedding into $SO(10)$ GUT

In order to embed the inverse seesaw mechanism into a supersymmetric $SO(10)$ theory, we have to break the $(B-L)$ symmetry by using a $\mathbf{16} \oplus \overline{\mathbf{16}}$ pair rather than a $\mathbf{126} \oplus \overline{\mathbf{126}}$ pair of Higgs representation. In this context, there are two symmetry breaking chains that are particularly interesting:

1. $SO(10) \xrightarrow{M_G} \mathbf{3}_c \mathbf{2}_L \mathbf{2}_R \mathbf{1}_{B-L} \xrightarrow{M_R} \mathbf{3}_c \mathbf{2}_L \mathbf{1}_Y (\text{MSSM})$

   $\xrightarrow{M_{\text{SUSY}}} \mathbf{3}_c \mathbf{2}_L \mathbf{1}_Y (\text{SM}) \xrightarrow{M_Z} \mathbf{3}_c \mathbf{1}_Q$ [153]

2. $SO(10) \xrightarrow{M_G} \mathbf{3}_c \mathbf{2}_L \mathbf{2}_R \mathbf{1}_{B-L} \xrightarrow{V_R} \mathbf{3}_c \mathbf{2}_L \mathbf{1}_{I_{3R}} \mathbf{1}_{B-L} \xrightarrow{v_R} \mathbf{3}_c \mathbf{2}_L \mathbf{1}_Y (\text{MSSM})$

   $\xrightarrow{M_{\text{SUSY}}} \mathbf{3}_c \mathbf{2}_L \mathbf{1}_Y (\text{SM}) \xrightarrow{M_Z} \mathbf{3}_c \mathbf{1}_Q$ [163]

In this paper, we consider only the former (and simpler) case of $SO(10)$ breaking chain. We also need at least two $\mathbf{10}_H$ and a $\mathbf{45}_H$ to have a realistic fermion mass spectrum. With this minimum set of Higgs multiplets $\{\mathbf{10}_H, \ \mathbf{16}_H, \ \overline{\mathbf{16}}_H, \ \mathbf{45}_H\}$, several $SO(10)$ models have been constructed [164]. All these models require various

dimension-5 operators to get right fermion masses: in principle, they are also present in our model. However, most of them e.g. $\frac{h_{ij}}{M}\mathbf{16}_i\mathbf{16}_j\mathbf{16}_H\mathbf{16}_H$, are suppressed by the factor $\frac{M_R}{M_{\text{Pl}}} \sim 10^{-15}$ as the $\mathbf{16}_H$ Higgs acquires only TeV-scale vev. The only other dimension-5 operator that can make significant contribution to fermion masses is $\frac{h'_{ij}}{M}\mathbf{16}_i\mathbf{16}_j\mathbf{10}_H\mathbf{45}_H$; we assume its effects to be small in our model and keep the dimension six operator

$$\frac{f_{ij}}{M^2}\mathbf{16}_i\mathbf{16}_j\mathbf{10}_H\mathbf{45}_H\mathbf{45}_H \tag{3.26}$$

This operator is suppressed only by $\left(\frac{M_G}{M_{\text{Pl}}}\right)^2 \sim 10^{-4}$ as the $\mathbf{45}_H$ acquires a vev at the scale M_G and plays an important role in the fermion mass fitting given below.

The fermion mass splitting is obtained by the completely antisymmetric combination of the operator given by the expression (3.26), i.e. in the notation of Ref. [165]

$$\langle\psi_+^*|B[\Gamma_i\Gamma_j\Gamma_k\Gamma_l\Gamma_m]A_{ij}A_{kl}\Phi_m|\psi_+\rangle \tag{3.27}$$

with $B = \prod_{\mu=\text{odd}}\Gamma_\mu$ and $[...]$ denoting the completely antisymmetric combination. Here Φ and A denote the $\mathbf{10}_H$ and $\mathbf{45}_H$ fields respectively. When the following vevs are non-zero:

$$\langle\Phi_{9,10}\rangle \neq 0, \quad \langle A_{12,34,56}\rangle \neq 0, \tag{3.28}$$

this antisymmetric combination acts as an effective $\mathbf{126}_H$ operator which gives the mass relation $m_e = -3m_d$ and $m_\nu = -3m_u$ due to the vevs $\langle A_{ij}\rangle$, while m_u and m_d are split in the usual manner by the two $\mathbf{10}_H$ vevs, $\langle\phi_{9,10}\rangle$. To obtain a realistic fermion mass spectrum, we construct the following model using the Higgs multiplets $\{\mathbf{10}_H, \mathbf{45}_H, \mathbf{54}_H\}$. The $SO(10)$ symmetry breaking to $\mathbf{3}_c\mathbf{2}_L\mathbf{2}_R\mathbf{1}_{B-L}$ is obtained by

a combination of the $\mathbf{45}_H$ and $\mathbf{54}_H$, with the following vevs in an $SU(5)$ basis:

$$\langle \mathbf{45} \rangle \propto \text{diag}(a, a, a, 0, 0),$$

$$\langle \mathbf{54} \rangle \propto \text{diag}(2a, 2a, 2a, 2a, 2a, 2a, -3a, -3a, -3a, -3a) \qquad (3.29)$$

In this model, the fermion mass matrices at the GUT-scale have the following form:

$$M_u = \tilde{h}_u + \tilde{f}, \quad M_d = \tilde{h}_d + \tilde{f}, \quad M_e = \tilde{h}_d - 3\tilde{f}, \quad M_D = \tilde{h}_u - 3\tilde{f} \qquad (3.30)$$

where the $h_{u,d}$ matrices come from the usual Yukawa terms $h_{ij}\mathbf{16}_i\mathbf{16}_j\mathbf{10}_H(\mathbf{10}'_H)$ and the f matrix comes from the $\mathbf{45}_H$ contribution given by the expression (3.26), where we have assumed the same coupling for both the $\mathbf{10}_H$ fields. The tilde denotes the normalized couplings with mass dimensions where the vevs have been absorbed. We know the nine eigenvalues of the quark and charged lepton mass matrices at the scale M_G from our RG analysis in the previous section [cf. Eqs. (3.19)]; however, we have 18 unknowns (for 3 hermitian matrices) to fit into Eq. (3.30). Hence a unique fit is not possible; we just give here one sample fit that is consistent with all the masses and mixing at the GUT scale obtained from the RGEs.

We work in a basis in which the charged lepton mass matrix is diagonal, i.e.

$$M_e = \begin{pmatrix} m_e(M_G) & 0 & 0 \\ 0 & m_\mu(M_G) & 0 \\ 0 & 0 & m_\tau(M_G) \end{pmatrix} = \begin{pmatrix} 0.0004 & 0 & 0 \\ 0 & 0.0911 & 0 \\ 0 & 0 & 1.7096 \end{pmatrix} \text{GeV}$$

This immediately implies from Eq. (3.30) that

$$\tilde{h}_{d,ij} = 3\tilde{f}_{ij}. \quad (i \neq j) \qquad (3.31)$$

61

For simplicity, let us choose the $\tilde{f}$-matrix to be diagonal. Then Eq. (3.31) implies that $\tilde{h}_d$ is also a diagonal matrix. We also have the following relations:

$$\tilde{h}_{d,\alpha\alpha} + \tilde{f}_{\alpha\alpha} = m_\alpha, \quad \tilde{h}_{d,\beta\beta} - 3\tilde{f}_{\beta\beta} = m_\beta \tag{3.32}$$

where $m_\alpha = (m_d, \ m_s, \ m_b)$ are the eigenvalues of M_d and $m_\beta = (m_e, \ m_\mu, \ m_\tau)$ the eigenvalues of M_e. These six equations (3.32) now fix the h_d and f matrices completely:

$$\tilde{f} = \begin{pmatrix} \frac{1}{4}(m_d - m_e) & 0 & 0 \\ 0 & \frac{1}{4}(m_s - m_\mu) & 0 \\ 0 & 0 & \frac{1}{4}(m_b - m_\tau) \end{pmatrix}$$

$$= \begin{pmatrix} 2.25 \times 10^{-4} & 0 & 0 \\ 0 & -0.0162 & 0 \\ 0 & 0 & -0.0001 \end{pmatrix} \text{GeV},$$

$$\tilde{h}_d = \begin{pmatrix} \frac{1}{4}(3m_d + m_e) & 0 & 0 \\ 0 & \frac{1}{4}(3m_s + m_\mu) & 0 \\ 0 & 0 & \frac{1}{4}(3m_b + m_\tau) \end{pmatrix}$$

$$= \begin{pmatrix} 0.0011 & 0 & 0 \\ 0 & 0.0425 & 0 \\ 0 & 0 & 1.7093 \end{pmatrix} \text{GeV} \tag{3.33}$$

The $\tilde{h}_u$ matrix can now be determined by fitting to M_u which, in this basis, is given by

$$M_u = V_{\text{CKM}} M_u^{\text{diag}} V_{\text{CKM}}^\dagger$$

$$
= \begin{pmatrix} 0.0120 & 0.0384 - 0.0103i & 0.038 - 0.4433i \\ 0.0384 + 0.0103i & 0.2280 & 1.8623 + 0.0002i \\ 0.038 + 0.4433i & 1.8623 - 0.0002i & 77.7569 \end{pmatrix} \text{GeV} \quad (3.34)
$$

Then from Eq. (3.30) the $\tilde{h}_u$ matrix is given by

$$
\tilde{h}_u = \begin{pmatrix} 0.0118 & 0.0384 - 0.0103i & 0.038 - 0.4433i \\ 0.0384 + 0.0103i & 0.2442 & 1.8623 + 0.0002i \\ 0.038 + 0.4433i & 1.8623 - 0.0002i & 77.757 \end{pmatrix} \text{GeV} \quad (3.35)
$$

Hence the Dirac neutrino mass matrix is given by

$$
M_D = \begin{pmatrix} 0.0111 & 0.0384 - 0.0103i & 0.038 - 0.4433i \\ 0.0384 + 0.0103i & 0.2928 & 1.8623 + 0.0002i \\ 0.038 + 0.4433i & 1.8623 - 0.0002i & 77.7573 \end{pmatrix} \text{GeV} \quad (3.36)
$$

It may be noted here that even though the specific form of the Dirac neutrino mass matrix may depend on the choice of the particular basis we have chosen, the individual values of the matrix elements are more or less fixed by the up-type quark mass values, due to the mass relation (3.30), and hence, do not depend on the basis so much. Therefore, all the predictions of the model that follow from the form of M_D given by Eq. (3.36) will be independent of the initial choice of our basis, upto a few %. We will use this Dirac mass matrix in phenomenological studies as a representative value for our model.

With this Dirac neutrino mass, we can easily fit the observed neutrino oscillation data in Table 1.3 by fixing the singlet mass matrix μ_S in Eq. (3.5). As an example, for a normal hierarchy of neutrino masses, and assuming a diagonal degenerate structure for the RH neutrino mass matrix M_N with eigenvalue 1 TeV, we

can fit the observed neutrino oscillation data in Table 1.3 for the following choice of μ_S:

$$\mu_S = \begin{pmatrix} -1.5934 + 0.0283\mathrm{i} & 0.2244 - 0.0063\mathrm{i} & -0.0044 + 0.0092\mathrm{i} \\ 0.2244 - 0.0063\mathrm{i} & -0.0322 + 0.0012\mathrm{i} & 0.0006 - 0.0013\mathrm{i} \\ -0.0044 + 0.0092\mathrm{i} & 0.0006 - 0.0013\mathrm{i} & (4.0 + 5.1\mathrm{i}) \times 10^{-5} \end{pmatrix} \mathrm{GeV} \quad (3.37)$$

Note that this can be regarded as one drawback of the inverse seesaw mechanism as μ_S is an arbitrary mass matrix, and hence, we lose the predictability in the neutrino sector, unlike other seesaw schemes embedded in $SO(10)$ GUT. However, recently there has been some progress in ameliorating this situation in inverse seesaw by using some discrete symmetries [166] though its validity in $SO(10)$ GUT is yet to be tested.

Chapter 4

Low-Scale Leptogenesis

4.1 The General Framework of Leptogenesis

Leptogenesis [143] is an elegant framework to understand the origin of matter-antimatter asymmetry of the Universe [39]. Another attractive feature of this mechanism is that this is the cosmological consequence of the seesaw mechanism [88] and is intimately related to the Majorana nature of the neutrino masses. In particular, successful leptogenesis yields an upper bound on all light neutrino masses of 0.1eV [167] which could be tested by future laboratory experiments and also by cosmology.

In the standard paradigm of leptogenesis (for reviews, see e.g. Ref. [144]), the three Sakharov conditions [41] for dynamically generating the baryon asymmetry (see Section 1.2) are satisfied as follows:

1. The heavy RH neutrinos (required by seesaw mechanism) decay into lepton and Higgs doublets to produce lepton number violation, which is transferred to baryon number violation through $(B+L)$-violating sphaleron interactions [168, 143].

2. CP violation also occurs in the decays of the heavy neutrinos through their

Yukawa couplings. The *CP* asymmetry parameter is defined as

$$\epsilon_i \equiv \frac{\sum_\alpha \Gamma(N_i \to \ell_\alpha \Phi^\dagger) - \sum_\alpha \Gamma(N_i \to \bar{\ell}_\alpha \Phi)}{\sum_\alpha \Gamma(N_i \to \ell_\alpha \Phi^\dagger) + \sum_\alpha \Gamma(N_i \to \bar{\ell}_\alpha \Phi)}, \tag{4.1}$$

where $\alpha = e, \mu, \tau$ is the flavor index. This parameter can be computed from the interference between the tree-level diagram and the two one-loop diagrams, namely the vertex correction and self-energy diagrams, as shown in Figure 4.1, which yields [169]

$$\epsilon_i = \frac{1}{8\pi} \frac{\sum_{j \neq i} \text{Im}\left[(y^\dagger y)_{ij}^2\right]}{\sum_\alpha |y_{i\alpha}|^2} f\left(\frac{M_{N_j}^2}{M_{N_i}^2}\right), \tag{4.2}$$

where $f(x) = \sqrt{x}\left[1 - (1 + x)\log\left(\frac{1+x}{x}\right)\right]$ is the Fukugita-Yanagida loop function [143].
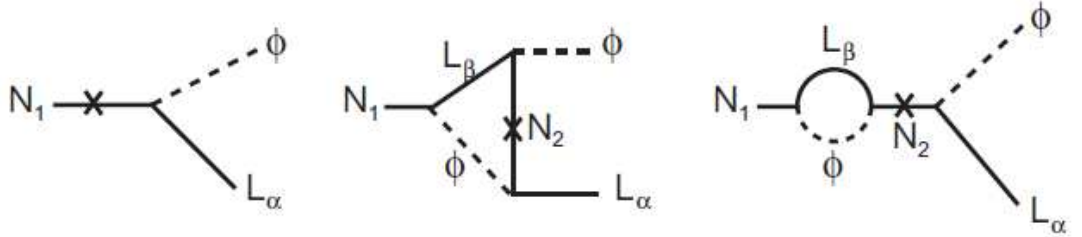
Figure 4.1: The Feynman diagrams for the *L*-violating decays of the heavy RH neutrino. Note that we need at least two of them to produce a non-zero *CP* asymmetry.

3. The out-of-equilibrium condition is provided by the expansion of the universe when the *L*-violating interaction rates become slower than the Hubble expansion rate. Thus a naive out-of-equilibrium condition is

$$\Gamma_{D,i} < H(T = M_{N_i}), \tag{4.3}$$

where $\Gamma_{D,i}$ is the total decay rate of the heavy neutrino N_i,

$$\Gamma_{D,i} = \sum_\alpha \Gamma(N_i \to \ell_\alpha \Phi^\dagger) + \sum_\alpha \Gamma(N_i \to \bar{\ell}_\alpha \Phi) = \frac{(y_\nu^\dagger y_\nu)_{ii} M_{N_i}}{8\pi}, \tag{4.4}$$

and H is the usual Hubble expansion rate of the universe,

$$H(T) = 1.66 g_*^{1/2} \frac{T^2}{M_{\text{Pl}}} \tag{4.5}$$

where g_* is the number of relativistic degrees of freedom in the thermal bath [170]. A more sophisticated way to parameterize the out-of-equilibrium condition is through the decay parameter K_i [171]

$$K_i \equiv \frac{\Gamma_{D,i}}{H(T = M_{N_i})} \tag{4.6}$$

The parameter range for which $K \ll 1$ is known as the "weak washout" regime and $K \gtrsim 3$ is known as "strong washout" [171]. Eq. (4.6) can be conveniently expressed in terms of two mass parameters [172]:

$$\begin{aligned}
\widetilde{m}_i &\equiv \frac{8\pi v^2}{M_{N_i}^2} \Gamma_{D,i} = \frac{(y^\dagger y)_{ii} v^2}{M_{N_i}}, \\
m_* &\equiv \frac{8\pi v^2}{M_{N_i}^2} H(T = M_{N_i}) \simeq 1.08 \times 10^{-3} \text{ eV}
\end{aligned} \tag{4.7}$$

Both these masses are of the order of the light neutrino masses. m_* is known as the "equilibrium neutrino mass" and $\widetilde{m}_i$ is known as the "effective neutrino mass" which should be larger than the lightest neutrino mass [173].

4.1.1 The Boltzmann Equations

The theory of leptogenesis is very similar to classical GUT baryogenesis [170], where the departure from thermal equilibrium is provided by some heavy particle

decay resulting in the deviation of its distribution function from the equilibrium value. This non-equilibrium deviation is usually computed by solving the classical Boltzmann equations [174]. Here we only discuss the "vanilla leptogenesis" scenario in which the baryon asymmetry is thermally produced by the decay of heavy singlet neutrinos.

The various relevant processes[1] for the out-of-equilibrium distribution are [176, 177]:

1. Decays and inverse decays: $N_i \leftrightarrow \ell \Phi^\dagger$ and the conjugate process $N_i \leftrightarrow \bar{\ell} \Phi$.

2. $\Delta L = 2$ scattering processes $\ell \Phi \leftrightarrow \bar{\ell}' \Phi^\dagger$ (s-channel) and $\ell\ell \leftrightarrow \Phi^\dagger \Phi^\dagger$ (u- and t-channel) mediated by N_i.

3. $\Delta L = 1$ scattering processes mediated by Higgs (e.g. $\ell N_i \leftrightarrow Q_3 \bar{t}$) and gauge bosons (e.g. $\ell N_i \leftrightarrow \Phi^\dagger V$).

The decay process was shown in Figure 4.1, and the other processes, collectively known as the "washout processes" are shown in Figure 4.2. Neglecting the thermal corrections [176], the Boltzmann equations can be written as [169, 177]

$$\frac{dN_{N_i}}{dz} = -(D_i + S_i)(N_{N_i} - N_{N_i}^{\text{eq}}), \tag{4.8}$$

$$\frac{dN_{B-L}}{dz} = \sum_i \epsilon_i (D_i + S_i)(N_{N_i} - N_{N_i}^{\text{eq}}) - N_{B-L}W, \tag{4.9}$$

where $z \equiv M_{N_1}/T$, N_1 being the lightest heavy neutrino. N_{N_i} and N_{B-L} are the number densities (abundance per RH neutrino) in a comoving volume containing one photon at temperature $T \gg M_1$, so that the relativistic equilibrium number density

[1]We have neglected the spectator processes [175] for simplicity.
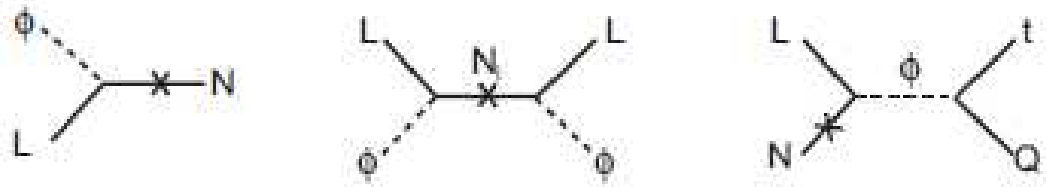
Figure 4.2: The Feynman diagrams for the washout processes: inverse decays, $\Delta L = 2$ and $\Delta L = 1$ scatterings. There are also t-channel contributions to the last diagram, as well as those involving gauge bosons.

is given by $N_{N_1}^{\text{eq}}(z \ll 1) = 3/4$ [170]. The decay term $D_i \equiv \Gamma_{D,i}/(Hz)$ accounts for both decays and inverse decay, whereas S_i represents the $\Delta L = 1$ scattering. The decays also yield the 1st term in Eq. (4.9) which is the source term for generating the $B - L$ asymmetry. All the other processes, namely the inverse decay and $\Delta L = 1, 2$ scatterings contribute to the total washout, denoted by W.

4.1.2 Baryon Asymmetry

The final $B - L$ asymmetry can be obtained by solving the Boltzmann equations, Eqs. (4.8) and (4.9) [170]:

$$N_{B-L}^{\text{f}}(z) = N_{B-L}^{\text{i}}\exp\left(-\sum_i \int_{z_i}^{z} dz' W_i(z')\right) + \frac{3}{4}\sum_i \epsilon_i \kappa_i^{\text{f}}(z), \qquad (4.10)$$

where N_{B-L}^{i} denotes any possible pre-existing asymmetry at the onset of leptogenesis at $z = z_i$. In the strong washout regime, such initial asymmetry is completely erased before the lightest heavy neutrino decay [167], and hence, the final asymmetry is independent of the initial conditions. On the other hand, in the weak washout regime, the final asymmetry does depend on the initial conditions; however, in the

standard "thermal leptogenesis" scenario, it is usually assumed that $N^{\rm i}_{B-L} = 0$ [171].

The $B - L$ production from the decay of N_i is expressed by the final efficiency factor $\kappa^{\rm f}_i \equiv \kappa_i(z \to \infty)$ [178] in Eq. (4.10) which is given by

$$\kappa^{\rm f}_i(z) = \frac{4}{3} \int_{z_i}^{\infty} dz' \frac{D_i(z')}{D_i(z') + S_i(z')} \frac{dN_{N_i}}{dz'} \exp\left(-\sum_i \int_{z'}^{z} dz'' W_i(z'')\right) \tag{4.11}$$

Eq. (4.11) is normalized such that $\kappa^{\rm f}_i \to 1$ in the limit of thermal initial abundance of the heavy neutrinos, $N_{N_i} = N^{\rm eq}_{N_i}$ and no washout ($W_i = 0$); in general, for $N_{N_i} \leq N^{\rm eq}_{N_i}$, $\kappa^{\rm f}_i \leq 1$.

The final baryon asymmetry, which is to be compared with the measured value at recombination, Eq. (1.23), is given by [171]

$$\eta_B = \frac{3}{4} \frac{a_{\rm sph}}{f} N^{\rm f}_{B-L} \tag{4.12}$$

where $a_{\rm sph} = N_B/N_{B-L}$ accounts for the fraction of $B-L$ asymmetry converted into baryon asymmetry by sphaleron processes, and its value is $28/79$ if the electroweak sphalerons go out of equilibrium before electroweak phase transition [179][2]. $f = N^{\rm rec}_\gamma/N^{\rm i}_\gamma = 2387/86$ [170] is the dilution factor for the photon number density from the onset of leptogenesis till recombination. Using these values for $a_{\rm sph}$ and f in Eq. (4.12), and ignoring the $N^{\rm i}_{B-L}$ term in Eq. (4.10), the final baryon asymmetry is given by

$$\eta_B \simeq 0.96 \times 10^{-2} \sum_i \epsilon_i \kappa^{\rm f}_i \tag{4.13}$$

---

[2]If the sphalerons remain in equilibrium until slightly after the electroweak phase transition, $a_{\rm sph} = 12/37$ [180]. Both the values are of order $1/3$ and, for definiteness, we use the previous value.

4.1.3   Lower Bounds on RH Neutrino Mass and T_{reheat}

Comparing the theoretical prediction for the baryon asymmetry, Eq. (4.13), with the measured value, Eq. (1.23), we obtain the required CP-asymmetry (assuming that only the lightest heavy neutrino N_1 decay contributes significantly):

$$\epsilon_1^{\mathrm{WMAP}} \simeq \left(6.4 \times 10^{-8}\right) \left(\kappa_1^{\mathrm{f}}\right)^{-1} \tag{4.14}$$

The maximal CP-asymmetry [181] in general depends on the mass of the heavy neutrino M_{N_1}, the effective neutrino mass $\widetilde{m}_1$ [cf. Eq. (4.7)] and the light neutrino mass spectrum. For a normal hierarchy of neutrino mass with $m_1 = 0$, the maximal CP-asymmetry is only a function of M_{N_1} and is given by [182]

$$\epsilon_1^{\mathrm{max}}(M_{N_1}) = \frac{3}{16\pi} \frac{M_{N_1} \sqrt{\Delta m_{\mathrm{atm}}^2}}{v^2} \simeq 10^{-7} \left(\frac{M_{N_1}}{10^9 \ \mathrm{GeV}}\right) \left(\frac{\sqrt{\Delta m_{\mathrm{atm}}^2}}{0.05 \ \mathrm{eV}}\right) \tag{4.15}$$

Comparing Eqs. (4.14) and (4.15), and using the atmospheric neutrino oscillation mass parameter from Table 1.3, we obtain an absolute lower bound on the heavy neutrino mass for successful vanilla leptogenesis, known as the *Davidson-Ibarra bound* [182]:

$$M_{N_1} > M_N^{\mathrm{min}} \simeq 4 \times 10^8 \ \mathrm{GeV} \tag{4.16}$$

This translates into a lower bound on the initial temperature of leptogenesis,

$$T_{\mathrm{in}} > T_{\mathrm{in}}^{\mathrm{min}} \simeq 1.5 \times 10^9 \ \mathrm{GeV} \tag{4.17}$$

The main point is that for hierarchical heavy RH neutrinos, leptogenesis makes it impossible for them to be observed at colliders. Moreover, assuming a period of inflation [183] at early states of the expansion, the minimum initial temperature $T_{\mathrm{in}}^{\mathrm{min}}$

that allows for successful leptogenesis can be identified with the minimal reheating temperature $T_{\text{reheat}}^{\min}$ after inflation [170]. This leads to the "gravitino problem" [184] in local supersymmetric theories, as the abundant production of gravitinos during the reheating phase may overclose the universe. If the gravitino is the stable LSP, as in most supergravity models, in order for it not to exceed the DM relic abundance, the reheat temperature should be below $10^7 - 10^9$ GeV [185]; on the other hand, if the gravitinos are unstable, their decay during or after BBN may lead to a large entropy production which puts stronger bounds on the reheating temperature, $T_{\text{reheat}} \lesssim 10^6$ GeV [186].

4.2   Resonant Leptogenesis

As we discussed in the previous section, the vanilla leptogenesis scenario is not compatible with supergravity. On the other hand, from the point of view of the seesaw mechanism itself, one can envisage the new physics scale to be anywhere between TeV to 10^{14} GeV. Hence, it is interesting to explore the possibilities of a "low-scale leptogenesis" which could be tested at the LHC. Several ways to relax the constraints of leptogenesis and to overcome the gravitino problem have been proposed in the literature [144]. Here we focus on one such possibility, namely the enhancement of the *CP* asymmetry by allowing the RH neutrinos to be quasi-degenerate; this mechanism is known as the "resonant leptogenesis" [187].

The idea of resonant leptogenesis came from the observation that self-energies dominate the lepton asymmetry provided $|M_{N_i} - M_{N_j}| \ll M_{N_{i,j}}$ [188]. It leads to

72

important qualitative as well as quantitative differences from the vanilla leptogenesis scenario discussed earlier. For example, flavor effects [189] due to neutrino Yukawa couplings play an important role here. Also, we have to include the heavy neutrino width effects in order to obtain a well-behaved analytic expression for the CP asymmetry. The CP asymmetry generated during the decay $N_i \to \ell_\alpha \Phi^\dagger$ (and its conjugate process $N_i \to \bar{\ell}_\alpha \Phi$) is now given by [190]

$$\epsilon_{i\alpha} = \frac{1}{8\pi} \sum_{j \neq i} \left\{ \frac{\text{Im}\left[\left(y_{i\alpha}^* y_{j\alpha} \left(\sum_\beta y_{i\beta}^* y_{j\beta} \right) \right) \right]}{\sum_\gamma |y_{i\gamma}|^2} f_{ij}^v + \frac{\text{Im}\left[\left(y_{i\alpha}^* y_{j\alpha} \left(\sum_\beta y_{i\beta} y_{j\beta}^* \right) \right) \right]}{\sum_\gamma |y_{i\gamma}|^2} f_{ij}^c \right\} \quad (4.18)$$

where f^v is the L-violating self-energy and vertex loop factor and f^c is the L-conserving self-energy loop factor. In the quasi-degenerate limit of the (i, j) pair, namely $M_{N_i} \simeq M_{N_j}$, only the self-energy correction is relevant and

$$f_v^{i,j} \simeq -f_v^{j,i} \simeq f_c^{i,j} \simeq -f_c^{j,i} \equiv f_{\text{self}}^{i,j} \quad (4.19)$$

with [191]

$$f_{\text{self}}^{ij} = \frac{(M_{N_j}^2 - M_{N_i}^2) M_{N_i}^2}{(M_{N_j}^2 - M_{N_i}^2)^2 + (M_{N_j} \Gamma_j - M_{N_i} \Gamma_i)^2}, \quad (4.20)$$

where $\Gamma_i \simeq \Gamma_j$ is the width of the quasi-degenerate pair.

Similarly, the efficiency factors receive separate contributions for each degenerate N_i, and the final efficiency is given by

$$\kappa_{i\alpha}^{\text{f}}(z \to \infty) \simeq \kappa \left(\sum_j K_{j\alpha} \right), \quad (4.21)$$

where the function $\kappa(K_1)$ is defined as [171]

$$\kappa(K_1) = \frac{2}{K_1 z_B(K_1)} \left[1 - \exp\left(-\frac{1}{2} K_1 z_B(K_1) \right) \right], \quad (4.22)$$

where z_B is the central value around which the effective $B - L$ asymmetry is generated (for $z_B - 2 < z < z_B + 2$) [192]:

$$z_B(K_1) \simeq 2 + 4K_1^{0.13}\exp\left(-\frac{2.5}{K_1}\right). \tag{4.23}$$

and the decay parameter K_1 is defined in Eq. (4.6).

The final $B - L$ asymmetry is then given by

$$N_{B-L}^{\mathrm{f}} = \sum_\alpha \left[\left(\sum_i \epsilon_{i\alpha}\right)\kappa\left(\sum_j K_{j\alpha}\right)\right] \tag{4.24}$$

Note that the sums i and j run over all degenerate heavy neutrinos $N_{i,j}$, i.e. if all 3 of them are degenerate, then $i, j = 1, 2, 3$, whereas if only N_1 and N_2 are degenerate, then $i, j = 1, 2$.

4.3   Low-scale Leptogenesis with LR Symmetry

Theoretically, it will be nice to have an understanding of the quasi-degeneracy of the RH neutrinos in resonant leptogenesis. In seesaw models for RH neutrinos, a higher gauge symmetry, e.g. $B-L$, is usually called for to make the model "natural". An attractive gauge symmetry that embeds the $B - L$ symmetry and also provides a way to understand the origin of parity violation in low-energy weak interactions is the Left-Right (LR) gauge group $SU(2)_L \times SU(2)_R \times U(1)_{B-L}$ [98]. As discussed in previous chapter, in addition to providing a compelling reason for the inclusion of the RH neutrinos to guarantee anomaly cancellation, in the type I case, it can also be used to understand why the seesaw scale is so much lower than the GUT scale, whereas, in the inverse seesaw case, it stabilizes the zeros in the (ν, N^c, S)

mass matrix that leads to the doubly-suppressed seesaw formula. An important question that arises in these models is: What is the scale of parity invariance? In particular, if it is in the TeV range and if at the same time leptogenesis generates the desired matter-anti-matter asymmetry, then the LHC could be probing neutrino mass physics as well as shed light on one of the deepest mysteries of cosmology.

Since Sakharov's out-of-equilibrium condition [41] must be satisfied in order to generate a baryon asymmetry, the existence of new interactions inherent to the LR models make it a nontrivial task to check whether a TeV-scale W_R, Z' is indeed compatible with leptogenesis as an explanation of the origin of matter. Specifically, the efficiency of leptogenesis crucially depends on the number of RH neutrinos that decay out of equilibrium to produce a leptonic asymmetry. As discussed earlier in this chapter, this number is set by two things: First, it depends on the relative magnitudes of the decay rate and the (CP-conserving) gauge scattering rates of the RH neutrino, since this can lead to a dilution of the number of "useful" RH neutrinos. Second, the washout processes, primarily inverse decays, should drop out of equilibrium early enough, otherwise the number of RH neutrinos gets suppressed at an exponential rate.

4.3.1 With Type I Seesaw

The above issues have been analyzed for the type-I case within LR symmetric models [145] as well as only $(B - L)$ models [146]. It was found that for the full LR models with TeV-scale parity restoration and RH neutrino masses, gauge scattering

rates induced by W_R exchange largely dominate the decay and inverse decay rates because the Yukawa couplings are small for the standard type-I seesaw at the TeV scale. These facts lead to a huge dilution of the number of RH neutrinos which decay out of equilibrium and in a CP asymmetric manner. Moreover, the gauge scattering interactions also wash out lepton number at a very large rate, much larger than the inverse decays. Altogether, these two effects lead to a very stringent constraint on the mass scale of W_R for successful leptogenesis, $M_{W_R} \geq 18$ TeV [145], which would imply that the discovery of a W_R at the LHC is incompatible with thermal leptogenesis as the origin of matter. On the other hand, in the case of a simple $(B - L)$ theory, successful leptogenesis only implies that $M_{Z'} \geq 2.5$ TeV in the "collider-friendly" region of parameter space where the RH neutrino mass is less than half the Z' mass [146][3]. We note that there exist bounds on the W_R mass from low energy observations [194] and they allow W_R mass to be as low as 2.5 TeV.

4.3.2 With Inverse Seesaw

In this section we summarize the main features of leptogenesis within the class of LR inverse seesaw models discussed in Chapter 3 [147][4]. We want to make it clear that while we have used the $SO(10)$ framework to make the results definite and somewhat more predictive, our discussion is very general and applies also to the case of TeV-scale Left-Right symmetry without grand unification and even without

---

[3]For a discussion of low scale leptogenesis in an $SO(10)$ model where only the doubly charged Higgs boson is in the TeV range, see Ref. [193].

[4]For other low-scale leptogenesis scenarios in inverse-seesaw-related frameworks, see Ref. [195].

SUSY.

Two features distinguish the inverse seesaw mechanism from the type-I seesaw: (i) the Dirac Yukawa couplings of the RH neutrino N can be much larger ($\sim 10^{-1} - 10^{-2}$) than for the type-I case (where they are typically of order $\sim 10^{-6}$ for TeV-scale RH neutrino masses) and (ii) the lepton-number-violating parameter (the Majorana mass μ_S of the left-right singlet lepton S, which measures the "pseudo-Diracness" of N) is much smaller than the Dirac mass of N. As a result, first, the decay rate of N can be much larger than the W_R exchange scattering rate at the baryogenesis epoch, and second, the wash-out processes are suppressed by the small Majorana mass μ_S. Consequently, we find that both the W_R and Z' can be in the TeV range and hence accessible at the LHC [147]. This result should make the case for searching the W_R and Z' at LHC stronger [116, 196, 197, 198].

Note that in inverse seesaw models, the quasi-degeneracy of the RH neutrinos are natural since they are related to the smallness of the Majorana neutrino mass and they become exactly degenerate in the limit of massless neutrinos. We expect that the lepton-number-violating washout will also go to zero in the limit of vanishing μ_S. As a matter of fact, as explicitly shown in Ref. [199], the all-important $\Delta L = 2$ washout process $\ell \Phi \to \bar{\ell} \Phi^\dagger$ vanishes as δ_i^2, with

$$\delta_i = \frac{|M_i - M_j|}{\Gamma_i} \simeq \frac{\mu_{ii}}{\Gamma_i}, \tag{4.25}$$

where Γ_i is the total decay rate of N_i into lepton and Higgs (and antiparticles), and $M_{i,j}$ are the masses of the quasi-Dirac RH neutrino pair $N_{i,j}$ (with $\Gamma_i \simeq \Gamma_j$). Note that we denote by M_i ($i = 1, \ldots, 6$) the heavy neutrino mass eigenvalues. As shown

in the Appendix D, the leading order contribution to the mass splitting for each quasi-Dirac pair comes from the diagonal elements of the μ_S matrix. Therefore, as expected, the washout tends to zero in the limit of vanishing μ_S. The suppression of the washout can be shown to occur through the destructive interference of one member of a quasi-Dirac pair with the other [199]. It is instructive to show numerically how the washout is kept under control in this family of models with more than one pair of RH neutrinos. Plugging in numbers, we find that with Yukawa couplings of order 10^{-1} and a RH neutrino mass of order 1 TeV, the decay parameter K in Eq. (4.6) is of order 10^{12}, which would naively imply strong washout! However, the suppression of the washout is also very large, being proportional to δ^2 with $\delta \ll 1$ due to the smallness of μ_S, as required to get the right scale for the light neutrinos. Specifically, for the example of Eq. (3.37), we find that $\delta \sim 10^{-5}$ and therefore the effective decay parameter $K^{\text{eff}} \simeq \delta^2 K \sim 100$, which is reasonably small.

In the LR model we are considering, there are other processes contributing to the washout of lepton number, for instance, $N_R e_R \leftrightarrow \bar{u}_R d_R$. More precisely, this process destroys RH lepton number, but in the temperature range of interest to us (TeV scale) every individual RH lepton flavor equilibrates with the LH lepton flavor one, thanks to the Yukawa interactions. Does this process also turn off in the limit of lepton number conservation? It can be easily shown that, including the production of the RH neutrino by an inverse decay, followed by the scattering process mentioned above, there is also a destructive interference within the quasi-Dirac pair which leads exactly to the same kind of δ^2-suppression as for the process $\ell \Phi \to \bar{\ell} \Phi^\dagger$.

Another feature of inverse seesaw models is that they typically lead to lepton flavor equilibration [200] because of the large Yukawa couplings. More precisely, it can be shown that the process $\ell_\alpha \Phi \leftrightarrow \ell_\beta \Phi$, which does not change lepton number, but changes lepton flavor, is deep in thermal equilibrium for the TeV temperatures (see, for instance, Ref. [192]). Consequently, the Boltzmann equations for leptogenesis can be written as only one equation for the sum of the lepton flavors [200]. In other words, flavor effects [189] are not important in our framework.

The CP asymmetry is given by Eq. (4.18). Note that this was derived assuming heavy neutrino mass eigenstates. Therefore, it is necessary to make a basis transformation from the "flavor" basis where

$$\mathcal{M}_{\mathrm{RH}} = \begin{pmatrix} 0 & M_N \\ M_N^T & \mu_S/2 \end{pmatrix},\tag{4.26}$$

to the diagonal mass basis with real and positive eigenvalues M_i $(i = 1, 2, \ldots, 6)$, grouped into three quasi-degenerate pairs with mass splittings in each pair of order μ_{kk} $(k = 1, 2, 3)$. Analytically, the exact diagonalization of the full 6×6 mass matrix $\mathcal{M}_{\mathrm{RH}}$ to get a closed form expression for the Yukawa couplings, $y_{i\alpha}$, in terms of the known parameters, namely M_D, M_N and μ_S, is extremely involved. In Appendix D, we show the analytical expressions up to first order in μ_S for some simpler cases with only two quasi-Dirac pairs and show explicitly that the CP-asymmetry indeed vanishes in the L-conserving limit $\mu_S \to 0$, as expected. For the general case with three quasi-Dirac pairs, we numerically evaluate the CP-asymmetry in the next section. We note that the three-pair case reduces to the two-pair case discussed in Appendix D if one of the masses is much heavier than the other two and hence

decouples from the rest.

For numerical results, the Yukawa couplings are fixed by the $SO(10)$ symmetry. The μ_S matrix can be deduced from the knowledge of the light neutrino masses and mixing angles as a function of the RH neutrino mass matrix M_N, which can be taken to be diagonal without loss of generality. Varying the RH neutrino mass eigenvalues input then leads to different μ_S matrices, keeping the light neutrino mass matrix such that its mass eigenvalues and mixing angles satisfy the neutrino oscillation data within 3σ. Once we know the explicit form of the RH neutrino mass matrix given by Eq. (4.26), we can define the quasi-Dirac pairs by transforming to a basis in which this mass matrix is diagonal with real and positive eigenvalues. We then calculate the CP-asymmetry and efficiency factors for the decay of the lightest RH neutrino pair and scan the parameter space to match the calculated baryon asymmetry (Eq. (4.13)) with the measured value (Eq. (1.23). Note that we only consider the asymmetry generated by decay of the lightest RH neutrino pair as the asymmetry generated by the heavy pairs is washed out very rapidly (due to large exponential suppression), and for these washouts not to affect the asymmetry generated by the lightest pair, we require the lightest pair to be at least 3 times smaller than the next heavy pair [201].

To calculate the efficiency factor given by Eq. (4.11), we first write down the thermally averaged rates for $N \to \ell\Phi$ decay and the corresponding inverse decay [171]:

$$D(K_i, z) = \frac{\mathcal{K}_1(z)}{\mathcal{K}_2(z)} K_i z,$$

$$W_{\mathrm{ID}}(K_i, z) = \frac{1}{4} K_i \mathcal{K}_1(z) z^3. \tag{4.27}$$

with $\mathcal{K}_a$, $a = 1, 2$ denoting the modified Bessel function of the ith type. The thermally averaged rate D_{W_R} for the W_R-mediated N-decay, $N \to \ell q_R \bar{q}'_R$, is given by

$$D_{W_R}(z) = \frac{\gamma_N^{(W_R)}}{n_N^{\mathrm{eq}} H z} \tag{4.28}$$

where n_N^{eq} is the RH neutrino equilibrium number density, $n_N^{\mathrm{eq}}(z) = \frac{3}{4} n_\gamma(z) N_{N_i}^{\mathrm{eq}}(z)$ with $n_\gamma = \frac{2\zeta(3)}{\pi^2} T^3$, and γ_N is the reaction density:

$$\gamma_N^{(W_R)} = n_N^{\mathrm{eq}}(z) \frac{\mathcal{K}_1(z)}{\mathcal{K}_2(z)} \Gamma_N^{(W_R)}, \tag{4.29}$$

where $\Gamma_N^{(W_R)}$ is the total three body decay width of N, given by [145]

$$\Gamma_N^{W_R} = \frac{3 g_R^4}{2^9 \pi^3 M_N^3} \int_0^{M_N^2} ds \, \frac{(M_N^6 - 3 M_N^2 s^2 + 2 s^3)}{(s - M_{W_R}^2)^2 + M_{W_R}^2 \Gamma_{W_R}^2}. \tag{4.30}$$

with the W_R total decay width $\Gamma_{W_R} = \frac{g_R^2}{4\pi} M_{W_R}$.

The various scattering rates $S_{W_R, Z'}$ appearing in Eq. (4.11) are also defined as in Eq. (4.28) where the corresponding scattering reaction density is related to the reduced cross section as follows (see, for instance, Ref. [176]):

$$\gamma(ab \leftrightarrow cd) = \frac{M_N^4}{64\pi^4 z} \int_{x_{\mathrm{thr}}}^\infty dx \sqrt{x} \hat{\sigma}(x) \mathcal{K}_1(z\sqrt{x}) \tag{4.31}$$

with $x = s/M_N^2$ and the threshold value $x_{\mathrm{thr}} = \frac{1}{M_N^2} \max[(m_a + m_b)^2, (m_c + m_d)^2]$. The reduced cross sections for various W_R exchange diagrams were computed in Ref. [145]:

$$\hat{\sigma}_{Ne_R \leftrightarrow \bar{u}_R d_R}(x) = \frac{9 g_R^4}{48\pi x} \frac{(1 - 3x^2 + 2x^3)}{\left[\left(x - \frac{M_{W_R}^2}{M_N^2} \right)^2 + \frac{M_{W_R}^2 \Gamma_{W_R}^2}{M_N^4} \right]}, \tag{4.32}$$

$$\hat{\sigma}_{N\bar{u}_R \leftrightarrow e_R \bar{d}_R}(x) = \frac{9g_R^4}{8\pi x} \int_{1-x}^{0} du \frac{(x+u)(x+u-1)}{\left(u - \frac{M_{W_R}^2}{M_N^2}\right)^2}, \tag{4.33}$$

$$\hat{\sigma}_{N d_R \leftrightarrow e_R u_R}(x) = \frac{9g_R^4}{8\pi} \frac{M_N^2}{M_{W_R}^2} \frac{(1-x)^2}{\left(x + \frac{M_{W_R}^2}{M_N^2} - 1\right)}, \tag{4.34}$$

Here we have ignored the t-channel process $NN \to \ell\ell$ as the rate for this process falls off very rapidly for the region of interest, viz. $z > 1$ [145].

The reduced cross section for the Z' exchange diagram is given by [169]

$$\hat{\sigma}_{NN \leftrightarrow \ell\bar{\ell}, q\bar{q}}(x) = \frac{13 g_{B-L}^4}{6\pi} \frac{\sqrt{x(x-4)^3}}{\left(x - \frac{M_{Z'}^2}{M_N^2}\right)^2 + \frac{M_{Z'}^2 \Gamma_{Z'}^2}{M_N^4}}, \tag{4.35}$$

with the total Z' decay width

$$\Gamma_{Z'} = \frac{g_{B-L}^2}{24\pi} M_{Z'} \left[13 + 3\left(1 - \frac{4M_N^2}{M_{Z'}^2}\right)^{3/2}\right]. \tag{4.36}$$

Before calculating the efficiency factor, it is instructive to compare all the reaction rates appearing in Eq. (4.11) to get a clear idea of various contributions. As an illustration, we consider the case with the RH Majorana neutrino mass eigenvalues $(3.5, 3, 1)$ TeV (as in Eq. (3.37)). The flavor-summed washout parameter for the decay of the lightest quasi-Dirac pair in this case is given by $K_3 \simeq 4 \times 10^{11}$ whereas the effective washout parameter is given by $K_3^{\rm eff} \simeq \delta_3^2 K_3 \simeq 168$ which is reasonable. For comparison, the corresponding values for the two heavy pairs are $K_1^{\rm eff} \simeq K_2^{\rm eff} = 8 \times 10^7$ which, when exponentiated in the washout term in Eq. (4.11), leads to a huge suppression, thus making the efficiency in those channels practically negligible. Hence, from now on, we will consider the decay of only the lightest pair.

In Fig. 4.3, we show the various thermally averaged decay and scattering rates as a function of $z \equiv M_{N_3}/T$, for the above choice of the RH neutrino masses and for
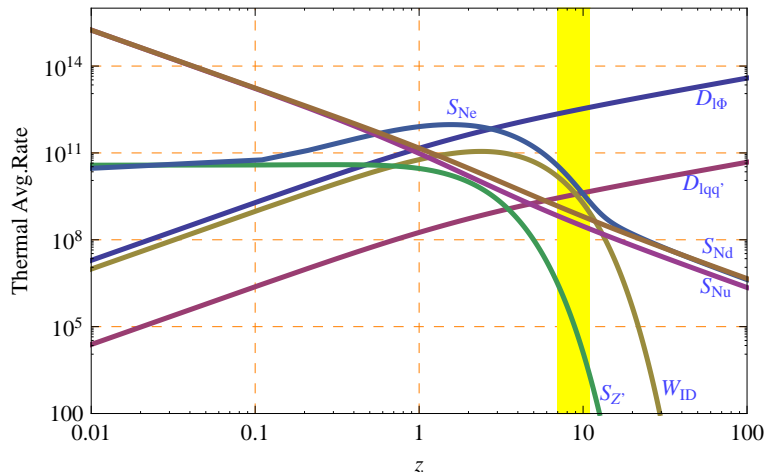
Figure 4.3: Various N decay and scattering rates (thermally averaged) as a function of $z = M_{N_3}/T$ for a particular choice of RH neutrino masses, $(M_{N_1}, M_{N_2}, M_{N_3}) = (3.5, 3, 1)$ TeV and $M_{W_R} = M_{Z'} = 2$ TeV. The yellow shaded region is where the asymmetry is generated.

$M_{W_R} = M_{Z'} = 2$ TeV. The yellow shaded region shows the asymmetry production time, approximately when $z_B - 2 < z < z_B + 2$ with z_B given by Eq. (4.23) [5]. We note that in this range, the $N \to \ell\Phi$ decay rate, $D_{\ell\Phi}$, dominates over the three-body decay rate as well as all the scattering rates by several orders of magnitude. Hence in the efficiency factor, Eq. (4.11), the dilution term $D/(D+S)$ is very close to unity and is essentially independent of M_{W_R} and $M_{Z'}$. The enhanced $N \to \ell\Phi$ decay rate is due to the large Yukawa couplings in the inverse seesaw scenario. We also note that as the W_R-mediated three-body N decay rate is much smaller than

___

[5]Here we have assumed that the production of asymmetry stops immediately after the temperature drops below the sphaleron freeze-out temperature, $T_{\text{sph}} \simeq 130$ GeV for a Higgs mass $m_H = 120$ GeV [202].

the $N \to \ell\Phi$ decay rate, the washout term W_{W_R} in Eq. (4.11) arising due to the process $\ell\Phi \to N \to \bar{\ell}q\bar{q}'$ which is proportional to the branching ratio of $N \to \bar{\ell}q\bar{q}'$ will be suppressed compared to the inverse decay term W_{ID}. Thus we find that the efficiency factor is also essentially independent of both W_R and Z' masses for a wide range of parameter space. Of course, the W_R and Z' scattering terms will start to dominate for very low values of their masses; however, we estimated this lower bound to be well below the current collider bounds on M_{W_R} and $M_{Z'}$ which are roughly a TeV or so [203].
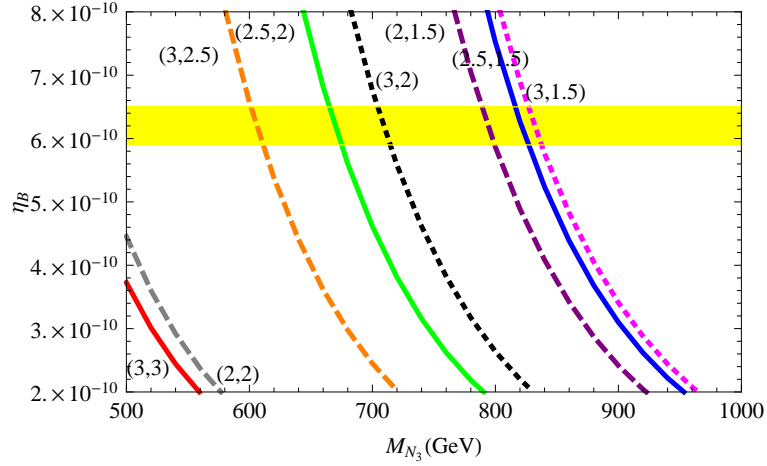
Figure 4.4: Correlation between the baryon asymmetry and the lightest RH neutrino mass for various heavy mass pairs (M_{N_1}, M_{N_2}) in TeV. The yellow shaded region is the observed value of η_B within 2σ C.L..

Fig. 4.4 shows the baryon asymmetry η_B as a function of the lightest RH neutrino mass M_{N_3} for different choices of the heavy RH neutrino masses (M_{N_1}, M_{N_2}) from $1.5 - 3$ TeV. The calculated value of η_B is to be compared with the observed 68% C.L. value, $\eta_B = (6.2 \pm 0.15) \times 10^{-10}$ [39]. It is clear from the figure that for a
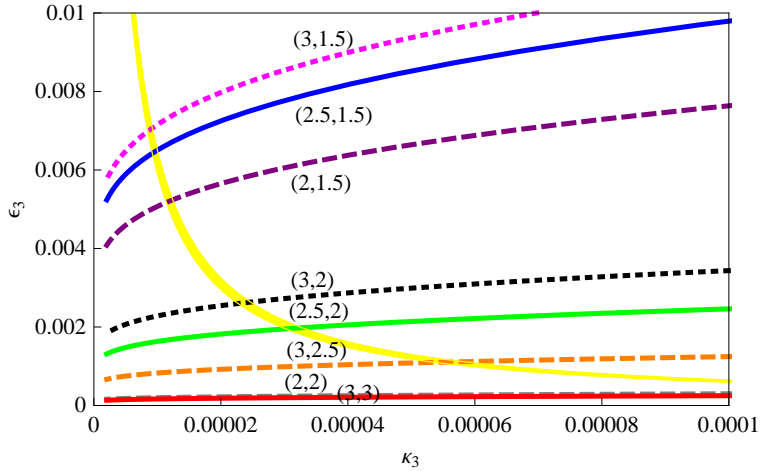
Figure 4.5: Correlation between the efficiency factor and the flavor-summed CP-asymmetry for the lightest pair for various values of the heavy mass pair (M_{N_1}, M_{N_2}) in TeV. The yellow shaded region corresponds to the observed value of η_B within 2σ C.L..

given heavy mass pair, there is a narrow range of values allowed for M_{N_3} satisfying the observed baryon asymmetry (the yellow shaded region). We note that for fixed M_{N_1}, the allowed range of M_{N_3} decreases with increasing M_{N_2}, while for fixed M_{N_2}, the allowed range of M_{N_3} increases with increasing M_{N_1}. Also note that when the heavy pairs have degenerate mass, the baryon asymmetry gets suppressed (e.g. the lower two lines in Fig. 4.4) due to the suppression in the CP-asymmetry. Finally, we note that for a given set of heavy mass pairs, $\eta_B \propto M_{N_3}^{-3}$.

Fig. 4.5 shows the correlation between the efficiency factor and the flavor-summed CP asymmetry for various channels. The different lines correspond to different values of the heavy mass pair, (M_{N_1}, M_{N_2}) in TeV, starting from (3,1.5) TeV at the top to (3,3) TeV at bottom. We note that for fixed M_{N_1}, the lines move

down as we increase M_{N_2} while for fixed M_{N_2}, they move up with increasing M_{N_1}. The yellow shaded region shows the observed value of η_B which is essentially the product of κ and ϵ, summed over all pairs. As we have pointed out earlier, only the lightest pair contribution is significant, while the efficiency is too small for the other two pairs.

In summary, we have shown that a TeV-scale Left-Right symmetry can be compatible with the understanding of the origin of matter via leptogenesis provided small neutrino masses are understood using the inverse seesaw mechanism.

Chapter 5

Dark Matter

The existence of Dark Matter in our universe is by now well-established [45] from various astrophysical and cosmological observations, e.g. galactic rotation curves, spatial distribution of galaxies, gravitational lensing and CMB anisotropy. The current relic abundance of the DM is measured by the fraction of its density $\Omega_{\mathrm{DM}} = \rho_{\mathrm{DM}}/\rho_c$ where ρ_c is the critical closure density,

$$\rho_c = \frac{3H_0^2}{8\pi G_N} \simeq 1.88 \times 10^{-29} h^2 \ \mathrm{g.cm}^{-3}, \tag{5.1}$$

where h is a dimensionless scaling constant used to parameterize the Hubble parameter today, $H_0 = 100h\mathrm{km.s}^{-1}.\mathrm{Mpc}^{-1}$, and its measured value is $h = 0.72 \pm 0.03$ [204]. The current most accurate determination of Ω_{DM} comes from global fits of cosmological parameters [204] to a number of observations (e.g., CMB, Baryonic Acoustic Oscillations, Type Ia Supernovae) and yields Eq. (1.24): $\Omega_{\mathrm{DM}}h^2 = 0.110 \pm 0.006$ [39]. This actually refers to the relic density of "cold, non-baryonic" DM [204]:

$$\Omega_{\mathrm{CDM}} = \Omega_{\mathrm{m}} - \Omega_{\mathrm{b}} - \Omega_{\nu} = 0.110(6)h^{-2} = 0.21 \pm 0.02, \tag{5.2}$$

which is deduced from the total matter density $\Omega_{\mathrm{m}} = 0.26(2)$, total "baryonic" matter density $\Omega_{\mathrm{b}} = 0.044(4)$, and the light neutrino density $\Omega_{\nu} < 0.013$.

Another important parameter in Dark Matter physics is the "local DM halo density", i.e. the DM density in the neighborhood of our solar system; the estimates based on the "Standard Halo Model" give $\rho_{\mathrm{local}} \simeq 0.3$ GeV.cm^{-3} [205].

5.1 WIMPs

A number of possible DM candidates exist in literature [206], with masses ranging from 10^{-5} eV to 10^{60} GeV. However, as the observational data indicate [cf. Eq. (5.2)], most of the DM in our universe must be "cold" (non-relativistic) and non-baryonic. Hence, we will not further discuss about the baryonic DM candidates (e.g. MACHOs and molecular gas clouds) and "hot" (relativistic) DM candidates (e.g. light neutrinos). The leading "cold" DM candidates are axions [207] and WIMPs (Weakly Interacting Massive Particles) [208]. WIMP candidates are theoretically motivated by the so-called "WIMP Miracle" (discussed below); also from experimental point of view, the nature and properties of a WIMP can be directly probed via its scattering against different target nuclei [209] as well as from indirect signals through its annihilation in space [210].

5.1.1 Relic Density

The thermal relic density of WIMPs (henceforth denoted by χ) can be calculated reliably within the standard Friedmann-Robertson-Walker (FRW) cosmology by assuming that they were in thermal and chemical equilibrium with other elementary particles in the early universe when the temperature of the universe was larger than the WIMP mass (m_χ). As the universe expands and cools to a temperature $T < m_\chi$, the equilibrium abundance becomes exponentially (Boltzmann) suppressed $\sim e^{-m_\chi/T}$ until its interaction rates fall below the Hubble expansion rate, at which point it drops out of equilibrium ("freeze out"). After freeze out, the comoving

WIMP density remains essentially constant and can be determined by solving the Boltzmann equation in an expanding universe [170]:

$$\frac{dn_\chi}{dt} + 3Hn_\chi = -\langle \sigma_A v_{\rm rel} \rangle \left[n_\chi^2 - \left(n_\chi^{\rm eq} \right)^2 \right],$$

(5.3)

where n_χ is the number density of WIMPs, $H = \frac{1}{a}\frac{da}{dt}$ is the Hubble expansion rate, a is the scale factor of the universe, and $\langle \sigma_A v_{\rm rel} \rangle$ is the thermally averaged total annihilation cross section times the relative velocity. $n_\chi^{\rm eq} = \frac{g}{(2\pi)^3} \int d^3\mathbf{p} f(\mathbf{p})$ is the equilibrium number density, where g is the number of relativistic degrees of freedom and $f(\mathbf{p})$ is the statistical distribution function. The second term on left in Eq. (5.3) represents a diminution of number density as the universe expands, while the first term on right accounts for depletion due to annihilation, and the second term due to creation of WIMPs from inverse reactions.

In the absence of number-changing interactions, the right side of Eq. (5.3) is zero, and the solution is $n_\chi \propto a^{-3}$ as for a matter-dominated universe. In presence of the right side term, there is no closed-form analytic solution; however, we can obtain an analytic approximation to within 10% accuracy by assuming that the annihilation cross section is energy independent. Using the freeze-out condition that the annihilation rate $\Gamma = n_\chi \langle \sigma_A v_{\rm rel} \rangle$ is equal to the Hubble expansion rate $H = 1.66 g_*^{1/2} T^2 / M_{\rm Pl}$ (which occurs at temperature $T_{\rm f} \simeq m_\chi/20$ almost independently of the WIMP properties), and the fact that the comoving number density n_χ/s remains constant after freeze out, where $s \simeq 0.4 g_* T^3$ is the entropy density, we obtain [170]

$$\begin{aligned} \left(\frac{n_\chi}{s} \right)_{\rm today} = \left(\frac{n_\chi}{s} \right)_{\rm freeze-out} &\simeq \frac{100}{M_{\rm Pl} g_*^{1/2} m_\chi \langle \sigma_A v_{\rm rel} \rangle} \\ &\simeq 10^{-8} \left(\frac{1 \text{ GeV}}{m_\chi} \right) \left(\frac{10^{-27} \text{ cm}^3\text{s}^{-1}}{\langle \sigma_A v_{\rm rel} \rangle} \right) \end{aligned}$$

(5.4)

Using the current entropy density $s_0 \simeq 4000$ cm^{-3}, and the critical density from Eq. (5.1), we obtain [170]

$$\Omega_\chi h^2 = \frac{m_\chi n_\chi}{\rho_c} \simeq \frac{3 \times 10^{-27} \text{ cm}^3\text{s}^{-1}}{\langle \sigma_A v_{\text{rel}} \rangle} \equiv \frac{0.1 \text{ pb}}{\langle \sigma_A v_{\text{rel}} \rangle} \tag{5.5}$$

Thus, the relic density of the WIMP is independent of its mass (except for logarithmic corrections) and is inversely proportional to its annihilation cross section which happens to be the typical size of weak interaction cross sections $\mathcal{O}(1 \text{ pb})$ in order to reproduce the measured relic density, Eq. (5.2). This is known as the "WIMP miracle".

As noted above, the typical freeze out temperature $T_{\text{f}} \simeq m_\chi/20$ which means the WIMPs are already non-relativistic at freeze out. Hence, the total annihilation cross section can be written in powers of their velocities ($v \ll 1$):

$$\langle \sigma_A v_{\text{rel}} \rangle = a + bv^2 + \mathcal{O}(v^4), \tag{5.6}$$

where the first term comes from s-wave annihilation and the second term from both s- and p-wave annihilation. Hence, the simplest (energy independent) case considered above is true only if the s-wave annihilation is unsuppressed. For s-wave suppression case, we need to consider the velocity-dependent term in Eq. (5.6) and the final relic density given by Eq. (5.5) has to be modified accordingly to take this effect into account [170], which can be done with high accuracy by numerically solving the Boltzmann equation, Eq. (5.3).

5.1.2 LSP as WIMP

As discussed in Chapter 2, in R-parity conserving SUSY models, the LSP is absolutely stable. If it is a color and electrically neutral massive particle, it can serve as a WIMP candidate. The lightest neutralino is the most popular WIMP candidate in SUSY models [72]. In fact, in MSSM, this is the only possible DM candidate, as the other natural candidate, namely the scalar superpartner of the LH neutrino, is completely ruled out by relic density, direct detection and invisible Z-decay width constraints [211]. More precisely, the LH sneutrinos are weakly charged and typically annihilate too rapidly via Z-mediated s-channel diagrams. This results in a too small relic density [cf. Eq. (5.5)] compared to the observed value, Eq. (5.2). In order to suppress the annihilation rate, the sneutrinos must be either very light of order GeV [212] or very heavy of order TeV [213]. A very light sneutrino is excluded by the measurement of the Z-invisible decay width at LEP [4] whereas a very heavy sneutrino is excluded from constraints on the direct detection cross section (for the latest exclusion limits, see e.g. Ref. [214]).

In the constrained MSSM, the lightest neutralino has the desired relic density given by Eq. (5.2) in a few narrow regions (for a recent updated analysis, see Ref. [215]).

1. The *bulk annihilation region* which occurs at low $(m_0, m_{1/2})$ where neutralino annihilation mainly occurs via $\chi_1^0 \chi_1^0 \to \ell\bar{\ell}$ via t-channel slepton exchange. As m_0 increases, the slepton masses also increase, thus suppressing the annihilation cross section and increasing the relic density beyond the observed value.

2. The *co-annihilation region* where the lighter stau and other sleptons bring the relic density into measured range [1]. At large $\tan\beta$, this region extends into a *funnel region* when $2m_\chi$ is close to the mass of the *CP*-odd Higgs boson so that direct-channel Higgs resonances are dominant. There is also a narrow strip at low $m_{1/2}$ where the annihilation via light Higgs resonance occurs; however, this region is already ruled out by the LHC SUSY searches [216].

3. The *focus point region* at large m_0 where the neutralino is mostly Higgsino like (since $|\mu|$ is small) and annihilates dominantly into WW, ZZ and Zh states.

The neutralino relic density allowed regions in $(m_0, m_{1/2})$ plane are narrow strips for fixed values of A_0 and $\tan\beta$ [217, 215] from which we conclude that the parameter space for neutralino DM is highly constrained in the cMSSM.

Also, the relic density puts strong constraints on the MSSM neutralino LSP mass. If we assume gaugino mass unification, the absolute lower limit on the neutralino mass from LEP searches is 47 GeV [219]. Even if we do not assume gaugino or scalar mass unification, the WMAP constraints, together with the LEP bounds on chargino mass, require that $m_{\chi_1^0} > 18$ GeV [218]. Thus, if the WIMP DM turns out to be as light as $5 - 15$ GeV, as suggested by some recent experiments [220], we need to go beyond the universal MSSM scenario. Since MSSM is anyway not a complete theory and needs to be extended to accommodate observed small neutrino masses, it would be interesting to see if these extensions can also provide viable light dark matter candidate while satisfying both collider and relic density constraints. In

---

[1]At large A_0, the stop co-annihilation is also important.

this chapter, we examine [140] these issues in the inverse seesaw extension discussed before.

5.2   Sneutrino DM in Inverse Seesaw

In this section, we focus on the supersymmetric inverse seesaw models [101] discussed before where one adds two SM singlet fermions N and S per family to generate small neutrino masses while still keeping the S and N masses in the TeV range. These models give three lepton number carrying electrically neutral fermions per family, namely (ν, N^c, S). If a linear combination of the super-partners of these fields turns out to be the LSP, then it could be a candidate for dark matter [136, 137, 138, 139, 140]. As discussed earlier, we consider the SUSYLR gauge group to stabilize the zeros of the inverse seesaw mass matrix. The presence of left-right gauge symmetry endows special dynamical properties to the dark matter particle than other inverse seesaw sneutrino models. We showed in Ref. [140] that this can lead to a light inelastic dark matter particle in the 5-20 GeV mass range with the correct relic abundance and also satisfying the current XENON100 bounds for spin-independent scattering cross section.

Working within this LR class of models, we find the following results [140]: (i) The LSP dark matter, a linear combination of the superpartners of the new SM singlet fermions, can have mass from a few GeV up to about 100 GeV without running into conflict with known low energy observations. (ii) The S-fermion, which is given a small lepton number violating mass to understand small neutrino masses,

leads to a splitting of the above complex scalar LSP into two closely-spaced real scalar fields[2], the lighter of which (we'll denote it by χ_1) is the true dark matter field and is accompanied by its slightly heavier partner field (χ_2) with a mass difference of order keV. A consequence of this is that the direct detection process involves a dominantly inelastic scattering mode with the nucleus ($\mathcal{N}$) where $\chi_1 + \mathcal{N}(\mathcal{A}, \mathcal{Z}) \rightarrow \chi_2 + \mathcal{N}(\mathcal{A}, \mathcal{Z})$ [141], and can therefore be tested in direct dark matter detection experiments [222]. The inelastic property arises naturally since the gauge Noether current coupling to the Z (and Z' in models with extended gauge symmetries) necessarily connects χ_1 to χ_2; also, any possible elastic contribution (mostly through the Higgs mediation) is highly suppressed due to small Yukawa couplings to light quarks. We believe that this important point was emphasized for the first time in Ref. [140]. (iii) The new TeV scale gauge dynamics in these models leads to new annihilation diagrams for dark matter in the early Universe responsible for its current relic density. (iv) Finally, we also note a collider signature which is specific to sneutrino combination rather than the neutralino being the dark matter.

In the SUSYLR model, the sneutrino mass matrix in the basis of $\{\widetilde{\nu}, \widetilde{\nu}^{c\dagger}, \widetilde{S}\}$ is given by

$$
\mathcal{M}_{\widetilde{\nu}} = \begin{pmatrix} m^2_{\widetilde{\nu}^\dagger \widetilde{\nu}} & m^2_{\widetilde{\nu}^\dagger \widetilde{\nu}^{c\dagger}} & m^2_{\widetilde{\nu}^\dagger \widetilde{S}} \\ \left(m^2_{\widetilde{\nu}^\dagger \widetilde{\nu}^{c\dagger}} \right)^\dagger & m^2_{\widetilde{\nu}^c \widetilde{\nu}^{c\dagger}} & m^2_{\widetilde{\nu}^c \widetilde{S}} \\ \left(m^2_{\widetilde{\nu}^\dagger \widetilde{S}} \right)^\dagger & \left(m^2_{\widetilde{\nu}^c \widetilde{S}} \right)^\dagger & m^2_{\widetilde{S}^\dagger \widetilde{S}} \end{pmatrix}
\tag{5.7}
$$

where the various entries are described in Appendix E. The lightest sneutrino mass eigenstate, which will be the dark matter candidate, turns out to be mostly $\widetilde{S}$ and

---

[2]For a similar idea connecting inelastic splitting to neutrino masse, see Ref. [221]

with little admixtures of $\widetilde{\nu}$ and $\widetilde{\nu}^{c\dagger}$ in this model. Note that the $\widetilde{\nu}$ component is anyway required to be very small for a light DM as it is severely constrained by the invisible Z-decay width. The $\widetilde{\nu}$, $\widetilde{\nu}^c$ components are crucial for the direct detection of the DM because these are the only parts interacting with the observable sector via gauge bosons and gauginos. However, the relic density will be mostly determined by the $\widetilde{S}$ component of the DM as explained in Section 5.2.3.

5.2.1 Constraints in the $\widetilde{\nu}$ Sector

Most of the collider and flavor constraints are only on the left-sneutrino component, $\widetilde{\nu}_L$, due to its interaction with the SM-sector. However, if we assume sfermion mass universality at the GUT scale, some indirect bounds on the other components of sneutrino could be derived. Assuming that only one $\widetilde{\nu}$ state can be lighter than half Z mass, the Z decay width to two $\widetilde{\nu}$s is given by

$$\Gamma(Z \to \widetilde{\chi}_1 \widetilde{\chi}_2) \;\; = \;\; |C_0|^4 \frac{\Gamma_\nu}{2} \left[1 - \left(\frac{2M_\chi}{m_Z} \right)^2 \right]^{3/2} \Theta(m_Z - 2m_1) \qquad (5.8)$$

where C_0 is the fraction of LH component and $\Gamma_\nu = \frac{e^2 m_Z}{24\pi \sin^2 2\theta_W} = 167$ MeV is the partial decay width of Z into one invisible $\nu\bar{\nu}$ mode in the SM. The current bound on the width of any additional invisible decay is 2.3 MeV (experimental uncertainty [4]). This constrains the LH component c_0 as shown in Figure 5.1. We note here that for a purely LH-sneutrino, the invisible Z-decay width puts a lower bound on the sneutrino mass around 44 GeV [22]. Roughly speaking, for light mass dark matter that contains the left sneutrino ($M_\chi \leq 44$ GeV), the $\widetilde{\nu}$-fraction must be less than 40%
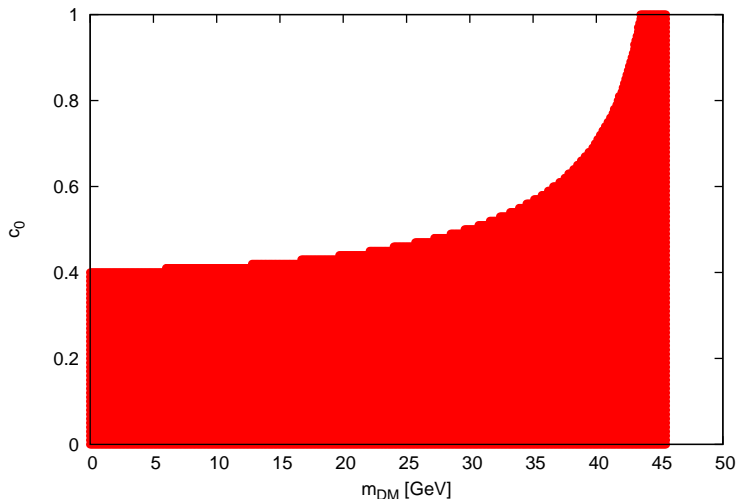
Figure 5.1: LH sneutrino component constrained by the invisible Z-decay width as a function of the DM mass. Red region is the allowed domain.

5.2.2 Sneutrino as Inelastic Dark Matter

Neglecting the keV scale lepton number violation effect, the sneutrino mass eigenstates are complex scalars in the basis of $(\widetilde{\nu}, \widetilde{N}^\dagger, \widetilde{S})$, and the lightest sneutrino eigenstate can be written as

$$\widetilde{\chi}_1 \;=\; \sum_{i=1}^{3}(U^\dagger)_{1\nu_i}\widetilde{\nu}_i + (U^\dagger)_{1N_i}\widetilde{N}_i^\dagger + (U^\dagger)_{1S_i}\widetilde{S}_i \tag{5.9}$$

where U is a 9×9 unitary matrix that diagonalizes the full neutrino mass matrix given by Eq. (3.3). When the lepton number violation is invoked, the splitting terms $\sum_{m,n=1}^{9} A_{mn}\widetilde{\chi}_m\widetilde{\chi}_n$ are generated in the sneutrino sector, through the F-term [223] potential

$$\left|\frac{\partial W}{\partial \hat{\Phi}}\right|^2_{\hat{\Phi}=S} = \left|\mu_S\widetilde{S} + y_S v_{Rd}\widetilde{\nu}^c\right|^2 \tag{5.10}$$

The interference term, $y_S\mu_S v_{Rd}\widetilde{S}^\dagger\widetilde{\nu}^c+$ h.c., generates the mass splitting between the imaginary and real part of the mass eigenstates $\widetilde{\chi}_i$.

Up to leading order in the lepton number violating mass term μ_S, the mass splitting of the lightest mass eigenstate can be written as

$$\delta M_\chi = \frac{4|A_{11}|}{M_\chi}, \tag{5.11}$$

where generically $A_{11} \sim \mu_S M_{\mathrm{SUSY}}$. If M_χ is also of order of the SUSY breaking scale (assumed to be around TeV), the splitting is of order μ_S, and if M_χ is much lower than M_{SUSY} as in some region of parameter space in SUSYLR, the splitting can be enhanced.

A consequence of this mass splitting is that in the direct detection process, the scattering of the DM particle off nuclei mediated by gauge bosons will be an inelastic scattering mode. The inelastic property arises naturally since the gauge Noether current coupling to the Z (and Z' in this model) necessarily connects χ_1 to χ_2. Moreover, any possible elastic contribution (mostly through the Higgs mediation) is highly suppressed due to small Yukawa couplings to light quarks, as discussed in Section 5. Hence, a sneutrino LSP in supersymmetric inverse seesaw naturally leads to an inelastic DM, as we pointed out in Ref. [140].

5.2.3 Relic Abundance

From Eq. (5.9), we see that the sneutrino DM is a linear combination of the $(\tilde{\nu}, \tilde{N}^\dagger, \tilde{S})$ fields. Therefore, as shown in Fig. 5.2, its annihilation channels involve three major contributions, one from each component. Note that the second and third channels are the new contribution in SUSYLR. To leading order, the expressions for

the annihilation cross sections in the s- and t-channel are respectively given by

$$\sigma_s \simeq \frac{g_{2L}^4 \kappa_f N_c}{96\pi \cos^4\theta_W} \frac{sv}{(s-M_Z^2)^2 + M_Z^2\Gamma_Z^2} \left[c_0^2 + c_1^2 \left(\frac{g_{2R}}{g_{2L}}\right)^4 \left(\frac{\cos^{12}\theta_W}{\cos^2 2\theta_W}\right)\right.$$

$$\left(\frac{(s-M_Z^2)^2 + M_Z^2\Gamma_Z^2}{(s-M_{Z'}^2)^2 + M_{Z'}^2\Gamma_{Z'}^2}\right) + 2c_0 c_1 \left(\frac{g_{2R}}{g_{2L}}\right)^2 \frac{\cos^8\theta_W}{\cos 2\theta_W}$$

$$\times \left.\left(\frac{(s-M_Z^2)(s-M_{Z'}^2) + M_Z M_{Z'}\Gamma_Z\Gamma_{Z'}}{(s-M_{Z'}^2)^2 + M_{Z'}^2\Gamma_{Z'}^2}\right)\right]$$

$$\sigma_t \simeq \frac{y_S^4 c_2^2}{96\pi} \frac{sv}{\left(M_{\tilde\phi_R}^2 - M_\chi^2\right)^2} \tag{5.12}$$

where $\kappa_f = (I_{3f} - Q_f \sin^2\theta_W)^2 + (Q_f \sin^2\theta_W)^2$, $N_c = 3(1)$ for quarks (leptons), $v = \sqrt{1 - 4M_\chi^2/s}$ is the speed of the DM particle in the center-of-mass frame, and $c_{(0,1,2)} = \sum_{i=1}^3 |U_{(\nu,N,S)_{i1}}|^2$. We note that both s- and t-channel annihilations in our case are p-wave scattering, as expected from symmetry arguments. For low-mass DM ($M_\chi < 20$ GeV), and assuming $y_S \sim \mathcal{O}(1)$ and $M_{\tilde\phi_R} \lesssim 500$ GeV, the t-channel involving only leptonic final states turns out to be the dominant contribution in our case (Fig. 5.3). For this reason, we do not show the interference term between s- and t-channels for leptonic final states in Eq. (5.12).
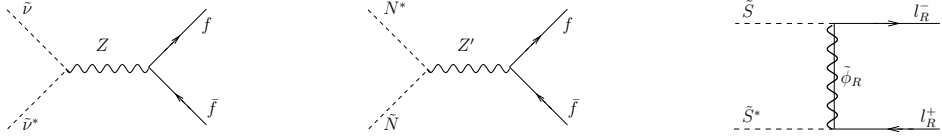
Figure 5.2: The dominant annihilation channels of the sneutrino DM in SUSYLR model.

The annihilation cross section for the Z' channel is suppressed compared to the Z-channel by a factor $(c_1/c_0)^2 (M_Z/M_{Z'})^4$. Also, we find that the correct DM relic density is obtained only for $c_0 < 0.16$, as shown in the left-panel of Fig. 5.4. This also agrees with the invisible Z-decay width constraint (as shown by the vertical line in Fig. 5.4).
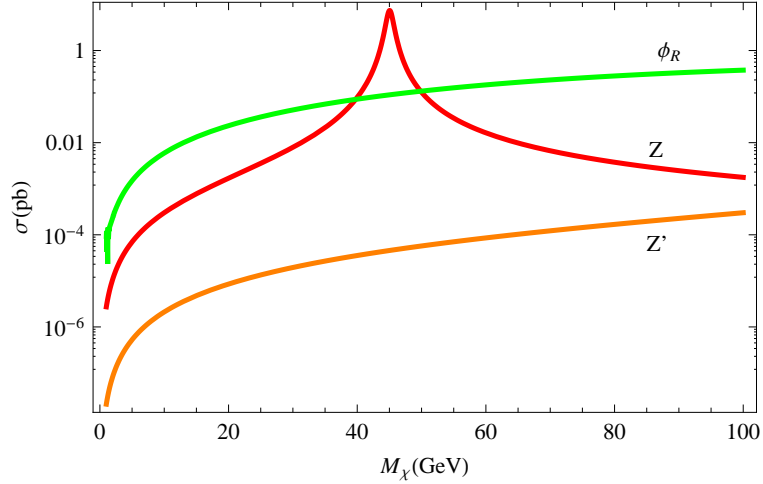
Figure 5.3: The dominant annihilation cross sections in our SUSYLR model. We have chosen $M_{\widetilde{\phi}_R} = 500$ GeV and $M_{Z'} = 1$ TeV. Also $c_0 = 0.16$ and $c_1 = 0.5$.
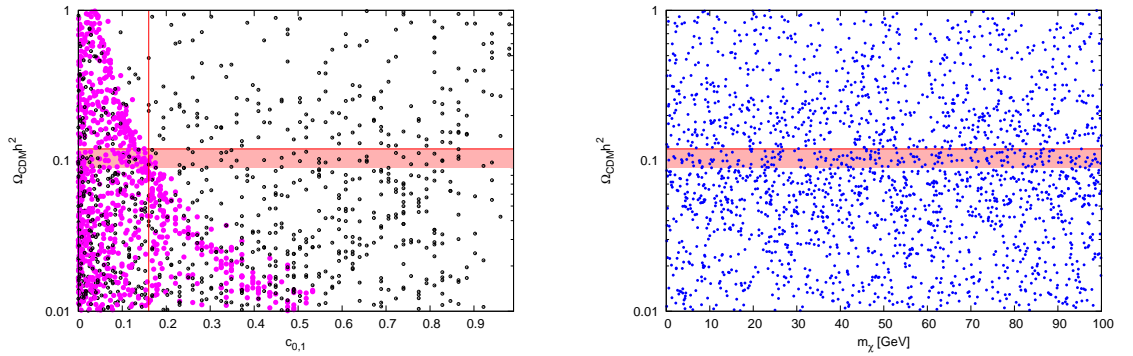
Figure 5.4: In the left-panel, the purple (black) points correspond to the allowed values in the $c_{0(1)}$-relic density plane, for the mixed sneutrino DM in our model; the vertical line shows the upper limit for c_0 from invisible Z-width constraint. The right-panel shows the scatter plot of relic density prediction for light LSP mass. The horizontal shaded region is the 2σ limit obtained from 7-year WMAP data.

The right panel of Fig.5.4 shows the the scatter plot of the predictions for the LSP relic density, calculated numerically using `MicroMEGAS` [224] taking into account all relevant annihilation channels; we find enough parameter range where the correct relic density is reproduced for a light DM.

5.2.4 Direct Detection

As the sneutrino dark matter ($\widetilde{\chi}_1$) in inverse seesaw is a real scalar field accompanied by its slightly heavier partner field, it has both elastic and inelastic interaction with nuclei in direct detection experiments.

The direct detection channel mediated by the SM-like Higgs boson is due to the interaction term $\lambda h_0 \widetilde{\chi}_1^\dagger \widetilde{\chi}_1$, where λ is mainly the D-term [162] contribution which can be simplified to $(g_1^2 + g_2^2) v_{\mathrm{wk}} c_0 / 4$ for MSSM and $(g_{2L}^2 c_0 + g_{2R}^2 c_1) v_{\mathrm{wk}} / 4$ for SUSYLR assuming the coupling limit of the MSSM Higgs mixing angles, i.e. large $\tan\beta$ and $\alpha \simeq \beta - \pi/2$ [225]. After invoking the lepton number violation effect, a mass splitting is generated between χ_1 and χ_2, and the interaction term can be rewritten as $\frac{\lambda}{2} h_0 (\chi_1^2 + \chi_2^2)$ which is clearly an elastic interaction.

The direct detection channel contributed by gauge boson exchanges can be written as

$$\frac{i}{2\cos\theta_W} \left(c_0 g_{2L} Z^\mu + c_1 \frac{\cos^2\theta_W}{\sqrt{\cos 2\theta_W}} g_{2R} Z'^\mu \right) \tag{5.13}$$

where θ_W is the Weinberg angle, and in the MSSM version, only the first term exists (i.e. $c_1 = 0$). After invoking lepton number violation effect, the interaction term is of the form $iZ^\mu(\chi_1 \partial_\mu \chi_2 - \chi_2 \partial_\mu \chi_1)$. Therefore, the collisions between χ_1 and nucleus conducted by gauge bosons is inelastic.

The differential scattering rate of dark matter particle on target nucleus in direct detection experiment can be written as

$$\frac{dR}{dE_r} = \frac{\rho_{\chi_1}}{M_\chi} \int_{|\mathbf{v}|>v_{\min}} d^3\mathbf{v} \frac{A_{\text{eff}}^2 \bar{\sigma}_N}{2\mu_{\chi N}|\mathbf{v}|} F^2(|\mathbf{q}|) f(\mathbf{v}) \ , \tag{5.14}$$

where E_r is the nuclear recoil energy, ρ_{χ_1} is the local mass density of DM, M_χ is the mass of the DM particle, σ_N is the DM-nucleon cross section, and $\mu_{\chi N}$ is the reduced mass of DM and the target nucleus. $\bar{\sigma}$ and A_{eff} are defined as $\bar{\sigma} = (\sigma_p + \sigma_n)/2$ and $A_{\text{eff}} = \sum_{i\in\text{isotopes}} 2r_i[\mathcal{Z}\cos\theta_N + (A_i - \mathcal{Z})\sin\theta_N]^2$, where r_i are relative abundances of isotopes, and $\tan\theta_N = \mathcal{M}_n/\mathcal{M}_p$, $\mathcal{M}_{n,p}$ being the DM scattering amplitudes off neutron and proton respectively [226]. $F(|\mathbf{q}|)$ is the nuclear form factor and $f(\mathbf{v})$ is the velocity distribution of the local galaxy. $v_{\min}$ is the minimal velocity needed to generate the nuclear recoil energy E_r, which can be written as [141]

$$v_{\min} = \frac{1}{\sqrt{2M_N E_r}} \left(\frac{M_N E_r}{\mu_{\chi N}} + \delta \right) \tag{5.15}$$

where δ is the mass gap, and $\delta = 0$ corresponds to the case of elastic scattering.

In the case of elastic scattering contributed by the Higgs boson exchange, σ_N in Eq. (5.14) is the total scattering cross section which can be written as

$$\sigma_N^{\text{el}} = \frac{\lambda^2 (M_N^2 \sum_q \langle N|m_q\bar{q}q|N\rangle)^2}{4\pi v_{\text{wk}}^2 M_h^4 (M_N + M_\chi)^2} \ , \tag{5.16}$$

whereas in the case of inelastic scattering, σ_N can be written as

$$\sigma_{p,n}^{\text{in}} = \frac{g_{2L}^4 \kappa_{p,n}}{4\pi \cos^4\theta_W M_Z^4} \frac{M_{p,n}^2 M_{\chi_1}^2}{(M_{\chi_1} + M_{p,n})^2} \left[c_0^2 + c_1^2 \left(\frac{g_{2R}}{g_{2L}}\right)^4 \left(\frac{M_Z}{M_{Z'}}\right)^4 \frac{\cos^{12}\theta_W}{\cos^2 2\theta_W} \right] , \tag{5.17}$$

where the first term in the bracket is induced by Z boson whereas the second term is due to the Z' boson exchange in SUSYLR. The factors $\kappa_p = \left(\frac{3}{4} - \sin^2\theta_W\right)^2$ and $\kappa_n = \left(\frac{3}{4}\right)^2$ are due to the different coupling of the vector bosons to proton and neutron respectively.
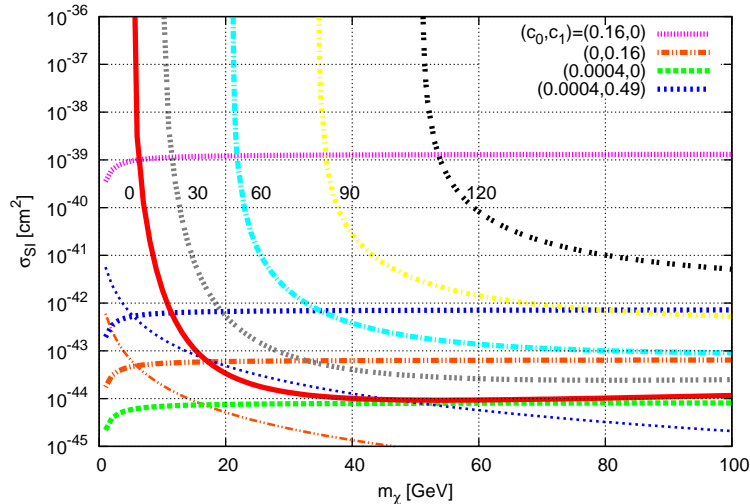
Figure 5.5: The model prediction for the inelastic scattering cross section of the sneutrino dark matter off a nucleon as a function of its mass, for various choices of the left and right sneutrino components. Also shown are the XENON100 constraints for mass gap $\delta = (0,\ 30,\ 60,\ 90,\ 120)$ keV which were obtained by Feldman-Cousins method [227] using the 100 days of live data [228].

It is important to note here that for large fractions of the left sneutrino component ($c_0 \gtrsim 10^{-3}$), the scattering is mostly dominated by the Z-exchange, and is hence inelastic. The Z' contribution to the inelastic channel is always suppressed by its mass, and similarly, the elastic cross section is 4-5 orders of magnitude smaller than the Z-dominated inelastic contribution because the coupling of the Higgs to nucleon is suppressed by light quark masses. However, for $c_0 \lesssim 10^{-4}$ and large c_1, the inelastic contribution, suppressed by the Z'-mass, becomes either smaller than or comparable to the elastic counterpart. This is shown in Fig. 5.5, where we have plotted the cross section as a function of the DM mass for various values of c_0 and c_1. One can see that for small c_0 and large c_1 values (blue and orange horizontal curves), the cross section is dominated by the elastic channel for

102

low mass DM and by inelastic channel (mediated by Z') for $M_\chi \gtrsim 10$ GeV, whereas for small or zero c_1 component (pink and green curves), the scattering is always dominated by the inelastic channel (mediated by Z). It is interesting to note here that the current XENON data constrains most of the parameter space of the model and for large c_0, puts an upper bound on the DM mass. This can be seen clearly from Fig. 5.5 where we have shown the XENON100 limits on scattering cross section for various values of the mass gap, starting from zero on the left (red solid curve, corresponding to the elastic case) to $\delta = 30$, 60, 90 and 120 keV cases. We note that for small mass gaps of order a few keV (as expected in this model), the XENON100 constraints leave only the low mass iDM (below 20 GeV) open in this model. Similar constraints on the iDM mass can be obtained using the existing data from other direct detection experiments [229], but the XENON100 constraints are found to be the most stringent.

The nuclear recoil energy in both elastic and inelastic scattering has a maximum determined by the escape velocity of DM in the local galaxy, and a minimum determined by the mass gap for inelastic case. Therefore, the topology of the differential scattering rate for inelastic scattering is very different from the elastic scattering, which can be used to determine whether the DM is inelastic or not. Furthermore, for inelastic scattering, if the mass gap is comparable to the kinetic energy of DM, for certain nuclear recoil energy, due to Eq. (5.15), the required velocity is pushed to the tail end of the velocity distribution where the motion of the earth has a larger effect and therefore the DM annual modulation signal gets enhanced.

The predicted normalized differential scattering rate and annual modulation for Germanium- and Xenon-based detectors are shown in Fig. 5.6 with different choices for parameters of the SUSYLR model. The mass of Z' is taken to be 1 TeV in both cases. The

red and blue curves are for $(c_0, c_1) = (0.001, 0.1)$ and $(c_0, c_1) = (0.1, 0.001)$, corresponding to the Z' and Z dominance, respectively, in the inelastic scattering between DM and target nucleus. The latter case is similar to the MSSM version of inverse seesaw. To translate the differential rates to experimental quantities, namely the electron equivalent recoil energies in germanium detector and the S_1 signal in xenon detector, we have used the quenching factor and scintillation efficiencies from CoGeNT [230] and XENON100 [228] experiments respectively. One can see from the first two plots in Fig. 5.6 that a peak shows up if the scattering is dominated by inelastic interactions. Furthermore, one can see from the third and fourth plots that for inelastic case, the annual modulation can be larger than 100% in some energy region. Also from the solid blue curves in the first and third plots, one can see that the energy regions for large recoil energy and large modulation can be separated from each other, which provides a chance to fit the anomaly observed by the CoGeNT experiment. In these plots, A_0 and A_1 are the zeroth and first Fourier modes of the differential scattering rate; for a detailed definition, see Ref. [231].

5.2.5   Comments on Indirect Detection

As noted earlier, there exists a domain in the parameter space for which the dominant annihilation channel of the DM is to lepton-anti-lepton final states. The relative branching fractions depend on the masses of the RH neutrinos and are somewhat model-dependent. If we take the model in Ref. [120] as a guide, we expect them to be of similar order. These dominantly-leptonic annihilation modes can, in principle, be important in understanding signals from the galactic center, radio filaments as well as WMAP haze [232]. Also the iDM capture in Sun could lead to significant flux of high energy neutrinos and/or electron/muons [233]. However, we expect these effects to be suppressed in our model due

104
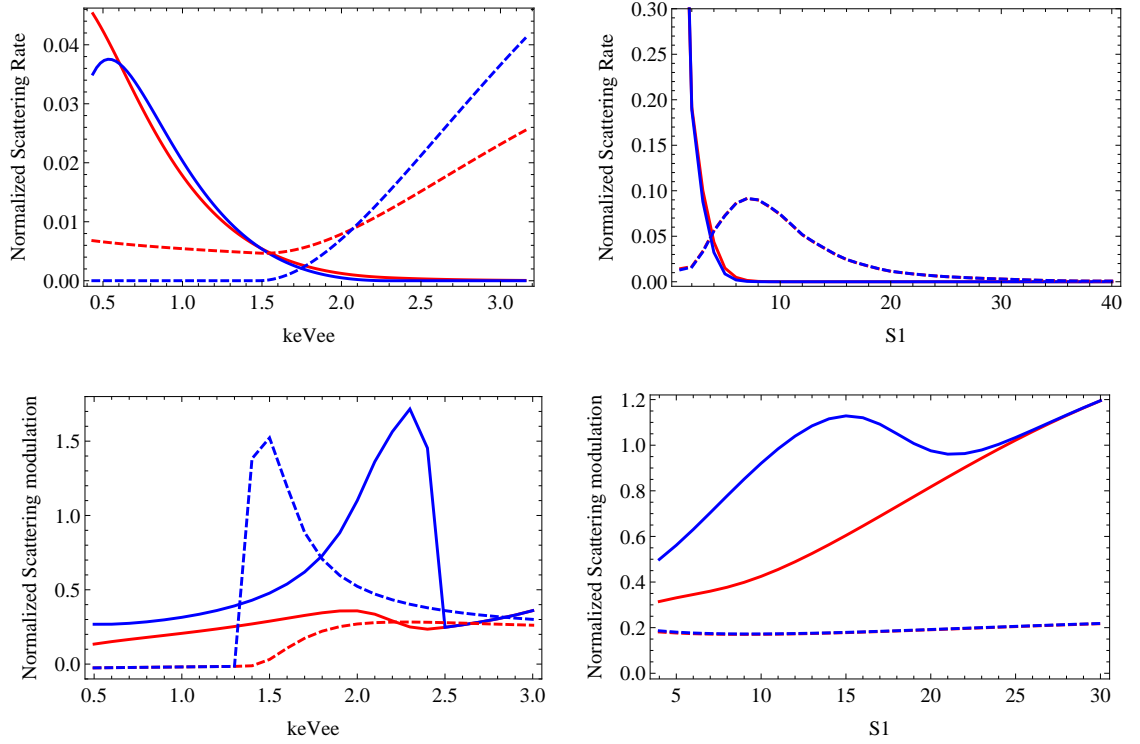
Figure 5.6: The model prediction for differential scattering rates and annual modulations for germanium and xenon detectors. The upper two plots show the differential scattering rate for germanium (left) and xenon (right) detectors. The lower two plots show the annual modulation in the same detectors. Red and blue curves are for $(c_0, c_1) = (0.001, 0.1)$ and $(c_0, c_1) = (0.1, 0.001)$, respectively, while the solid and dashed curves are for $(M_\chi, \delta) = (10\text{GeV}, 20\text{keV})$ and $(50\text{GeV}, 60\text{keV})$, respectively.

to the p-wave nature of the dominant DM annihilation channels. Thus the exclusion range of 4-90 GeV for sneutrino mass from Kamiokande Collaboration [234] does not apply in this case.

5.2.6   Collider Signatures

There exist upper limits on the direct DM detection cross section from monojet plus missing energy searches in colliders [235]. However, for light spin zero dark matter only weakly interacting with the nucleons, the collider limits on the spin-independent cross sections are weaker than the direct search bounds and our model predictions are within these bounds.

Depending on the sparticle spectrum prediction of the model, the sneutrino LSP can have distinctive collider signatures. This could be used to distinguish a sneutrino LSP from a neutralino LSP in SUSY, for instance. In particular, as has been noted in Ref. [142], sneutrino DM models in general have a characteristic LHC signal of type $pp \to \widetilde{q}\widetilde{q} \to \widetilde{W} + \widetilde{W} + \text{dijet} \to \text{charged dilepton} + \text{dijet} + \text{MET}$, or $pp \to \widetilde{g}\widetilde{g} \to \widetilde{q}\widetilde{q} + \text{dijet} \to \widetilde{W}\widetilde{W} + \text{four jets} \to \text{charged dilepton} + \text{four jets} + \text{MET}$, which can be useful in testing the model. In SUSY inverse seesaw models, the mass of the lightest sneutrino relates directly to the sneutrino soft masses if all the sfermion soft masses and the chargino masses share common origins like in most of the SUSY breaking scenarios.

5.2.7   Sneutrino LSP Parameter Space

From the form of the mass matrices as given in Appendix E, it can be seen that for a universal gaugino mass and TeV scale v_R, the sneutrino DM must be light (below 100 GeV or so), otherwise the lightest neutralino or chargino becomes the LSP. Fig. 5.7 shows the allowed $m_0 - m_{1/2}$ plane for sneutrino and neutralino LSP, shaded red and green respectively.

Requiring the lightest sneutrino to be the LSP induces a constraint that, in a large part of the parameter space, the mass of gluino is larger than the mass of lightest squark,
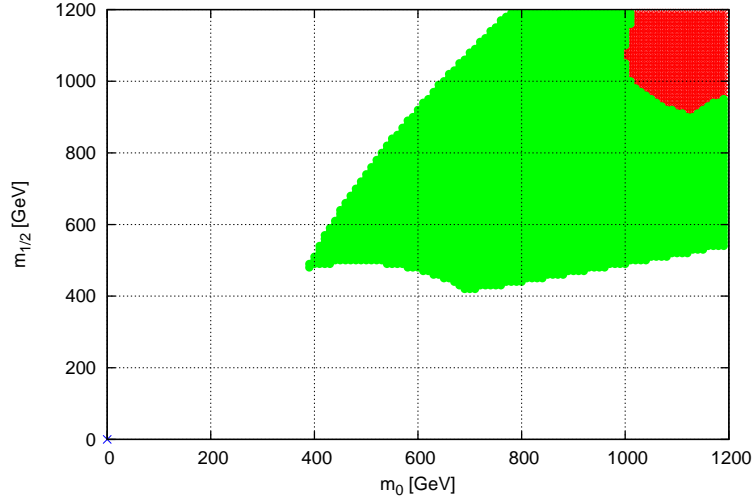
Figure 5.7: Allowed $m_0 - m_{1/2}$ plane for sneutrino (red) and neutralino (green) LSP in our SUSYLR model. Here we have assumed a mSUGRA-type scenario with $A_0 = 0, \mu > 0$. Also we have chosen $\tan\beta = 35, \tan\theta = 10$ and $v_R = 1$ TeV.

as shown in Fig. 5.8. In these regions, the signal from LHC is dominated by $pp \rightarrow$ same sign charged dilepton + dijet + MET [142], as discussed in the previous section. Furthermore, in most of the SUSY models, stop is the lightest squark, so one can also do b-tagging for these events.

To summarize, we have shown that the supersymmetric inverse seesaw model for neutrinos naturally leads to an inelastic scalar dark matter. Allowing for some fine tuning of the SUSY parameters, the dark matter can be light with mass easily in the 5-20 GeV range. A novel feature of the model is that the splitting between the LSP and NLSP states is directly related to the lepton number violating singlet fermion mass parameter responsible for small neutrino masses and is naturally of order of a few tens of KeVs due to inverse seesaw constraint. In the presence of right handed gauge symmetry, the relic density calculation is dominated by the right handed Higgsino exchange in the t-channel.
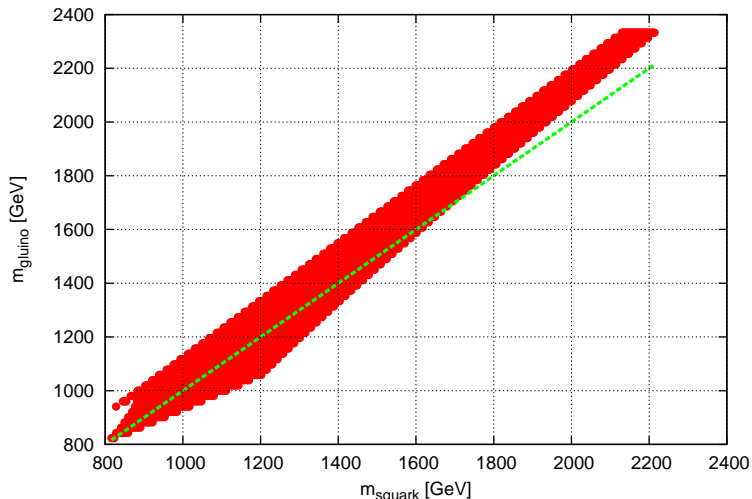
Figure 5.8: Squark-gluino spectrum for sneutrino LSP in SUSYLR.

For reasonable values of the parameters, this leads to the desired relic DM density. The direct detection cross section is dominated by the inelastic channel due to Z exchange. The differential scattering rate and annual modulation for direct detection predicted in these models might be tested in future direct detection experiments. The dark matter particle mass is found to be strongly constrained by the current XENON bounds, and for keV scale mass splitting for the real scalar LSP states (as required by neutrino mass constraints), we find an upper limit of around 20 GeV on the dark matter mass. This is consistent with the model prediction for the sneutrino LSP mass which is required to be below ~ 100 GeV from universality arguments.

Therefore, we might be able to identify SUSY inverse seesaw if from the collider search, we can confirm that the sneutrino is a long lived particle, and then from direct detection experiments, we observe an inelastic WIMP from the differential scattering rate and the annual modulation.

Chapter 6

Signatures of Inverse Seesaw

In this chapter, we discuss various experimental signatures to identify inverse seesaw. These include collider as well as other low-energy experiments.

6.1   Collider Signals

The heavy RH neutrinos, being SM singlets, can be produced at colliders only via $\nu - N$ mixing after virtual $W(Z)$'s produced in parton collision decay to $\ell(\bar{\nu}) + \nu$. Once produced, the N's decay to multi-lepton final states which could be used as a distinct signal for seesaw [112, 236]. In type I seesaw, N, being a Majorana particle, decays equally likely to both charged leptons and anti-leptons, thus giving the distinct collider signature of like-sign di-lepton final states[1]. However, the mixing in type-I seesaw is typically given by $\theta_{\nu N} \sim \sqrt{m_\nu M_N^{-1}} \lesssim 10^{-6}$ (barring cancellations [110]), and hence, the production of the N's is highly suppressed. A detailed collider simulation shows that the minimal type I seesaw can be tested at colliders only if $\theta_{\nu N}$ is large ($\gtrsim 10^{-2}$) or M_N is small (up to a few hundred GeV) [114].

In case of inverse seesaw, because of the presence of new lepton number breaking mass scale in the theory which is directly proportional to the light neutrino mass, the seesaw scale M_N can be naturally very low (within the range of colliders) even for "large" Dirac Yukawa couplings. This also allows for a large mixing $\theta_{\nu N} \simeq v_{\mathrm{wk}} h_\nu M_N^{-1}$, and makes

---

[1]This is a collider analogue of neutrinoless double beta decay to probe the lepton number violation.

the collider tests of this possibility much more feasible. However, due to the pseudo-Dirac nature of the RH neutrinos, the "smoking gun" signal for type I seesaw, namely the lepton number violating same-sign di-lepton signal [114] is absent in this case. Instead, the lepton flavor violating tri-lepton signal [112, 115, 116] can be used to test these models. In this section, we will mainly focus on these SM singlet RH neutrinos and present a detailed collider study of the multi-lepton final states in order to distinguish the heavy Dirac neutrinos from their Majorana counterparts at the LHC [116]. For reasons already discussed earlier, we will mostly work within a LR-symmetric framework at TeV-scale.

Before discussing the collider studies, we present a brief overview of the mixing between light and heavy states in LR inverse seesaw.

6.1.1 Mixing in the LR Gauge Sector and Neutrino Sector

The charged gauge bosons $W_{L,R}^{\pm}$ in the weak eigenstate mix in the mass eigenstates W, W' [30]:

$$
\begin{aligned}
W &= \cos \zeta_W W_L + \sin \zeta_W W_R, \\
W' &= -\sin \zeta_W W_L + \cos \zeta_W W_R,
\end{aligned}
\tag{6.1}
$$

where $\tan 2\zeta_W = 2\kappa\kappa'/(v_R^2 - v_L^2)$. The current bound on the mixing angle is as low as $\zeta_W < 0.013$ [237, 238]; hence for our purposes, we can safely assume the mass eigenstates as the weak eigenstates, and recognize W_L as the pure SM W-boson. The lower bound on the W' mass comes from a variety of low-energy constraints, e.g. $K_L - K_S$ mass difference, $B_{d,s} - \bar{B}_{d,s}$ mixing, weak CP violation etc (For a recent update on the old results, see Ref. [194, 198]). The most stringent limit on W_R mass in LR models is for the case of same CKM mixing angles in the left and right sectors: $M_{W_R} > 2.5$ TeV [194]; however, this

limit can be significantly lowered if there is no correlation between the mixing angles in the two sectors [237, 239]. The current collider bound on W' mass is around 1 TeV [203].

The neutral gauge bosons in LR model are mixtures of $W^3_{L,R}$ and B and the mixing between the weak eigenstates of these massive neutral bosons is parameterized as

$$
\begin{aligned}
Z &= \cos\zeta_Z Z_1 + \sin\zeta_Z Z_2, \\
Z' &= -\sin\zeta_Z Z_1 + \cos\zeta_Z Z_2
\end{aligned}
\tag{6.2}
$$

where Z, Z' are the mass eigenstates, and in the limit $v_L \ll \kappa, \kappa' \ll v_R$, the mixing angle is given by $\tan 2\zeta_Z \simeq 2\sqrt{\cos 2\theta_W}(M_Z/M_{Z'})^2$. Current experimental data constrain the mixing parameter to $< \mathcal{O}(10^{-4})$ and the Z' mass to values $> \mathcal{O}(\text{TeV})$ [238, 240]. The current collider limit on the LR Z' mass is > 998 GeV [203].

In the neutrino sector of LR models, due to the presence of the RH neutrinos, the neutrino mass eigenstates (ν_i, N_i) are mixtures of the flavor eigenstates (ν_α, N_α) where $i = 1, 2, 3$ and $\alpha = e, \mu, \tau$ for three generations. For type I seesaw with only one additional set of SM singlets, this mixing can be parameterized as

$$
\begin{pmatrix} \nu_\alpha \\ N_\beta \end{pmatrix} = \mathcal{V}_I \begin{pmatrix} \nu_i \\ N_j \end{pmatrix}
\tag{6.3}
$$

where $\mathcal{V}_I$ is a 6×6 unitary matrix diagonalizing the full neutrino mass matrix in Eq. (2.11). Similarly, for inverse seesaw case in which we have two sets of SM singlet heavy neutrinos, the mixing is given by

$$
\begin{pmatrix} \nu_\alpha \\ N_\beta \\ S_\gamma \end{pmatrix} = \mathcal{V}_{\text{inv}} \begin{pmatrix} \nu_i \\ N_j \\ N_k \end{pmatrix}
\tag{6.4}
$$

where $\mathcal{V}_{\text{inv}}$ is a 9×9 unitary matrix given by Eq. (3.4) diagonalizing the neutrino mass matrix in Eq. (3.3). Thus the weak interaction currents of light and heavy neutrinos are

modified as follows:

$$
\begin{aligned}
\mathcal{L}_{\mathrm{CC}} &= \frac{g}{\sqrt{2}} \left[W_L^\mu \bar{\ell}_\alpha \gamma^\mu P_L \nu_\alpha + W_R^\mu \bar{\ell}_\beta \gamma^\mu P_R N_\beta \right] + \text{h.c.} \\
&= \frac{g}{\sqrt{2}} \left[W_L^\mu \bar{\ell}_\alpha \gamma^\mu P_L (\mathcal{V}_{\alpha i} \nu_i + \mathcal{V}_{\alpha j} N_j) + W_R^\mu \bar{\ell}_\beta \gamma^\mu P_R (\mathcal{V}_{\beta i} \nu_i + \mathcal{V}_{\beta j} N_j) + \text{h.c.} \right], (6.5) \\
\mathcal{L}_{\mathrm{NC}} &\simeq \frac{g}{2 \cos\theta_W} \left[Z_\mu \bar{\nu}_\alpha \gamma^\mu P_L \nu_\alpha + \sqrt{\cos 2\theta_W} Z'_\mu \overline{N}_\beta \gamma^\mu P_R N_\beta \right] \\
&= \frac{g}{2 \cos\theta_W} \left[Z_\mu \left\{ \mathcal{V}^*_{\alpha i_1} \mathcal{V}_{\alpha i_2} \bar{\nu}_{i_1} \gamma^\mu P_L \nu_{i_2} + (\mathcal{V}^*_{\alpha i} \mathcal{V}_{\alpha j} \bar{\nu}_i \gamma^\mu P_L N_j + \text{h.c.}) \right. \right. \\
&\quad \left. + \mathcal{V}^*_{\alpha j_1} \mathcal{V}_{\alpha j_2} \overline{N}_{j_1} \gamma^\mu P_L N_{j_2} \right\} + \sqrt{\cos 2\theta_W} Z'_\mu \left\{ \mathcal{V}^*_{\beta j_1} \mathcal{V}_{\beta j_2} \overline{N}_{j_1} \gamma^\mu P_R N_{j_2} \right. \\
&\quad \left. \left. + (\mathcal{V}^*_{\beta i} \mathcal{V}_{\beta j} \bar{\nu}_i \gamma^\mu P_R N_j + \text{h.c.}) + \mathcal{V}^*_{\beta i_1} \mathcal{V}_{\beta i_2} \bar{\nu}_{i_1} \gamma^\mu P_R \nu_{i_2} \right\} \right]
\end{aligned}
\tag{6.6}
$$

where we have dropped the subscript for $\mathcal{V}$ which now generically represents both $\mathcal{V}_I$ and $\mathcal{V}_{\mathrm{inv}}$ in Eqs. (6.3) and (6.4) respectively. Thus, in general, $\mathcal{V}$ is a $(3+n) \times (3+n)$ unitary matrix, where n stands for the number of SM singlets (3 for type-I and 6 for inverse seesaw). This can be decomposed into the following blocks:

$$
\mathcal{V} = \begin{pmatrix} U_{3\times 3} & V_{3\times n} \\ X_{n\times 3} & Y_{n\times n} \end{pmatrix}
\tag{6.7}
$$

where U is the usual PMNS mixing matrix for the light neutrinos. The unitarity of $\mathcal{V}$ implies that

$$
U U^\dagger + V V^\dagger = U^\dagger U + X^\dagger X = I_{3\times 3},
$$

$$
X X^\dagger + Y Y^\dagger = V^\dagger V + Y^\dagger Y = I_{n\times n}.
\tag{6.8}
$$

with $U U^\dagger, Y^\dagger Y \sim \mathcal{O}(1)$ and $V V^\dagger, X^\dagger X \sim \mathcal{O}(M_D^2/M_N^2)$. Thus in Eqs. (6.5) and (6.6), the mixing between the light states, $\mathcal{V}_{\alpha i} \equiv U_{\alpha i}$, and between the heavy states, $\mathcal{V}_{\beta j} \equiv Y_{\beta j}$ both are of order $\mathcal{O}(1)$, whereas the mixing between the light and heavy states, $\mathcal{V}_{\alpha j} \equiv V_{\alpha j}, \mathcal{V}_{\beta i} \equiv X_{\beta i} \sim \mathcal{O}(M_D M_N^{-1})$ for both type I and inverse seesaw cases, which, in principle, could be large for TeV mass RH neutrinos and large Dirac Yukawa case. Henceforth, we will

generically denote this mixing between light and heavy neutrinos by $V_{\ell N}$, and assume the other mixing elements in Eqs. (6.5) and (6.6) to be $\mathcal{O}(1)$.

The electroweak precision data constrain the mixing $V_{\ell N}$ involving a single charged lepton [241] and the current 90% C.L. limits are summarized below:

$$\sum_{i=1}^{3} |V_{eN_i}|^2 \le 3.0 \times 10^{-3}, \quad \sum_{i=1}^{3} |V_{\mu N_i}|^2 \le 3.2 \times 10^{-3}, \quad \sum_{i=1}^{3} |V_{\tau N_i}|^2 \le 6.2 \times 10^{-3} \quad (6.9)$$

These limits are crucial for our analysis since they determine the decay rate of the heavy neutrinos to multi-lepton final states, as discussed in next section. One can also get constraints on the mixing involving two charged leptons from lepton-flavor violating (LFV) processes [242] [2]:

$$\left| \sum_{i=1}^{3} V_{eN_i} V_{\mu N_i}^* \right| \le 1.0 \times 10^{-4}, \quad \left| \sum_{i=1}^{3} V_{eN_i} V_{\tau N_i}^* \right| \le 1.0 \times 10^{-2}, \quad \left| \sum_{i=1}^{3} V_{\mu N_i} V_{\tau N_i}^* \right| \le 1.0 \times 10^{-2}$$

For the heavy neutrino mass below 100 GeV, the updated limits are summarized in Ref. [243].

Another constraint for the manifest LR model comes from neutrino-less double beta decay as there is a new contribution involving the heavy gauge boson W_R and RH Majorana neutrino [244, 133]. For a TeV mass RH neutrino, this puts a lower bound on $M_{W_R} \ge 1.1$ TeV which increases as $M_N^{-1/4}$ for smaller RH neutrino mass. In this paper, we therefore mainly focus on a TeV mass RH neutrino.

---

[2]However, these constraints can be easily evaded if, for example, each heavy neutrino mixes with a different charged lepton.

6.1.2 Production and Decay of Heavy Neutrinos

At a proton-proton collider, a single heavy neutrino can be produced at the parton-level, if kinematically allowed, in

$$q\bar{q}' \to W_L^*/W_R \to \ell^+ N(\ell^- \overline{N}), \tag{6.10}$$

which has lepton-number conserving (LNC) or violating (LNV) decay modes depending on whether N is Dirac or Majorana[3]. Since τ-lepton identification may be rather complicated in hadron colliders [245], we restrict our analysis to only the light charged-leptons ($\ell = e, \mu$). The parton-level production cross sections, generated using `CalcHEP` [246] and with the `CTEQ6L` parton distribution function [247], are shown in Fig. 6.1 as a function of the mass of N for 1.5, 2 and 2.5 TeV W_R mass (solid lines) at $\sqrt{s} = 14$ TeV LHC. We also show the normalized production cross section $\sigma/|V_{\ell N}|^2$ (normalized to $|V_{\ell N}|^2 = 1$) for SM W_L-boson mediation (dashed line), which is generated only through the mixing $V_{\ell N}$ between the LH and RH neutrinos. We can clearly see that the W_L-mediated production is highly suppressed by the mixing; even for large mixing, the cross section for a heavy RH neutrino with $M_{W_R} > M_N \gg M_{W_L}$ is mostly dominated by the W_R-channel because W_R can always decay on-shell whereas the W has to be highly off-shell to produce N.

The heavy RH neutrino decays to SM leptons plus a gauge or Higgs boson through its mixing with the left sector: $N \to \ell W, \nu Z, \nu H$. So all these decay rates are suppressed by the mixing parameter $|V_{\ell N}|^2$. In LR models, N can also have a three-body decay mode: $N \to \ell W_R^* \to \ell j j$ (and similarly for Z') which is not suppressed by mixing, but by mass of W_R. Note that the decay mode $N \to \ell W_R^* \to \ell \ell \nu$ will be suppressed by mixing as well as W_R-mass and hence the di-jet mode is always the dominant final state for the

---

[3]In Eq. (6.10) and following, $\overline{N}$ should be replaced by N for a Majorana RH neutrino.
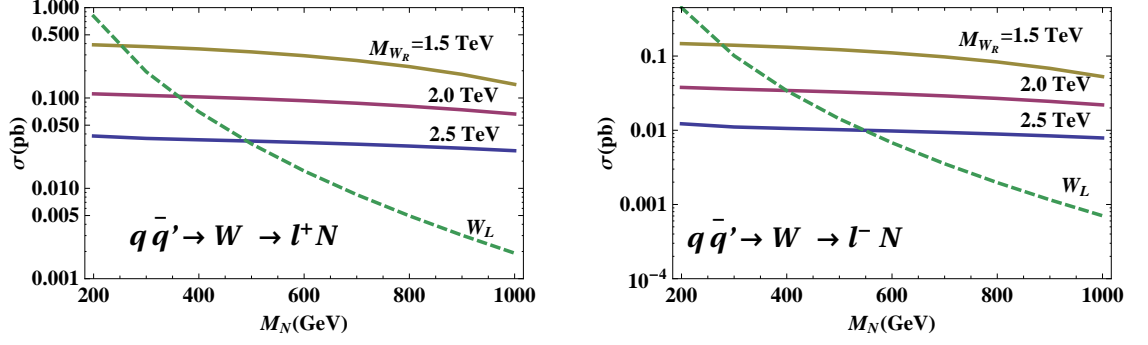
Figure 6.1: The cross section for $q\bar{q}' \to W_L/W_R \to N\ell^{\pm}$ for various values of W_R mass (solid lines). Also shown is the normalized cross section $\sigma/|V_{\ell N}|^2$ for W_L-mediated s-channel (dashed line).

three-body decay of N. The various partial decay widths of N are shown in Fig. 6.2 for a mixing parameter $|V_{\ell N}|^2 = 0.001$ and Higgs mass of 125 GeV. It is clear that for mixing larger than $\mathcal{O}(10^{-4})$, N mainly decays into the SM gauge or Higgs boson which could subsequently lead to multi-lepton final states.
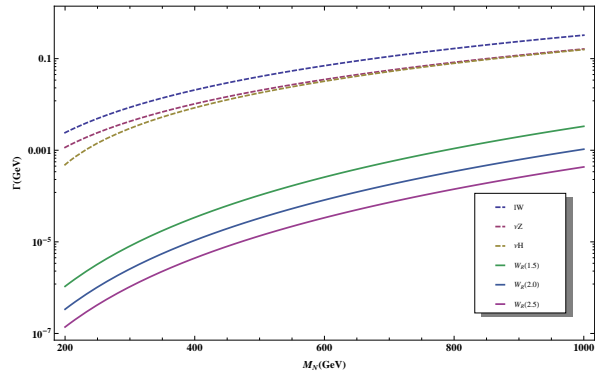
Figure 6.2: The partial decay widths of the RH neutrino into $\ell W, \nu Z, \nu H$ (dashed lines) as a function of its mass for a mixing parameter $|V_{\ell N}|^2 = 0.001$. Also shown are the three-body decay widths for $N \to \ell W_R \to \ell jj$ (solid lines) for $M_{W_R} = 1.5$, 2.0 and 2.5 TeV.

115

It should be emphasized here that the LR symmetry provides a unique channel for the production of RH neutrino through the W_R gauge boson, without any mixing suppression, and multi-lepton final states through the decay of N to SM gauge bosons, which even though suppressed by the mixing, still offer a promising channel to study the Dirac or Majorana nature of N. Without the LR symmetry (and hence W_R), the production of N (through SM W/Z) will also be suppressed by mixing, which limits its observability to only a few hundred GeV masses, mainly due to the large SM background [114]. On the other hand, LR-symmetric models provide much higher mass reach at the LHC in the multi-lepton channel, as we discuss in the next section.

We further note that a single N can also be produced in $q\bar{q} \to Z/Z' \to \bar{\nu}N$ but the resulting final state has either one charged lepton or opposite-sign di-leptons, and is buried under the huge LHC background [4]. One could also produce the RH neutrinos in pairs through a Z'-exchange: $q\bar{q} \to Z' \to N\overline{N}$, if kinematically allowed; however, the decay of two N's will be suppressed by $|V_{\ell N}|^4$, and hence, negligible.

(a) Majorana N (b) Dirac N
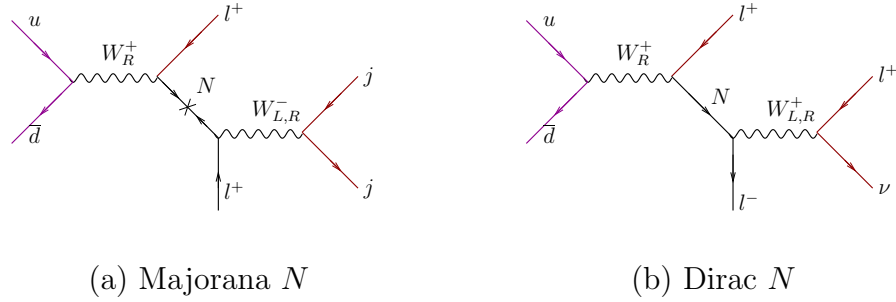
Figure 6.3: The golden channels for heavy Majorana and Dirac neutrino signals at the LHC.

Thus we conclude from this study that for a hadron collider analysis, the most

[4]This could, however, be important in cleaner environments, e.g. e^+e^- [248] and $e\gamma$ [249] colliders.

suitable production channel for a Dirac RH neutrino in LR models is through W_R-exchange and the N decay mode through SM W. We note that this particular channel was not considered in the previous studies of RH neutrino signals in LR models [198, 197], because they only considered a heavy Majorana neutrino (in type I seesaw) for which the golden channel is the same-sign di-lepton mode in Fig. 6.3(a): $q\bar{q}' \to W_R^\pm \to N\ell^\pm \to W_R^*\ell^\pm l^\pm \to jj\ell^\pm\ell^\pm$ [196]. In this case, the 3-body decay mode of $N \to \ell W_R^* \to \ell jj$ is dominant over the 2-body decay $N \to \ell W$ because the latter is suppressed by mixing which is usually very small in type I seesaw. However, for a heavy Dirac neutrino, this same-sign di-lepton mode is absent and the corresponding opposite-sign di-lepton mode $q\bar{q}' \to W_R^\pm \to N\ell^\pm \to W_R^*\ell^\mp l^\pm \to jj\ell^\mp\ell^\pm$ has large SM background. So the golden channel for a heavy Dirac neutrino is the tri-lepton mode in Fig. 6.3(b) where the W/W_R^* decays to leptonic final states: $pp \to W_R^\pm \to N\ell^\pm \to W/W_R^*\ell^\mp\ell^\pm \to \nu\ell^\pm\ell^\mp\ell^\pm$ [112, 115]. As discussed earlier in this section, the N decay to SM W is dominant over the 3-body decay through W_R for mixing $|V_{\ell N}| \lesssim 10^{-4}$, which is easily satisfied in inverse seesaw models, for instance. This is also true for type I seesaw with large mixing [110, 111], in which case the 2-body decay of N to SM gauge bosons (W, Z, H) will be dominant over the three-body decay through a virtual W_R.

6.1.3 Multi-Lepton Signals and SM Background

We perform a full LHC analysis of the multi-lepton final states given in Fig.3 and the SM background associated with it. The signal and background events are calculated at parton-level using `CalcHEP` [246] which are then fed into `PYTHIA` [250] to add initial and final state radiation and pile up, and perform hadronization of each event. Finally, a fast detector simulation is performed using `PGS` [251] to simulate a generic LHC detector. We

use the more stringent L2 trigger [252] in order to reduce the SM background. We note that the signal strength remains the same, if we use the low threshold L1 trigger, which is very close to the actual values used by the CMS detector. The L2 trigger has high enough thresholds to reduce all the SM background below the signal and therefore we do not need to impose any additional cuts on the events.

The major SM background for the di-lepton signal comes from the semi-leptonic decay of a $t\bar{t}$ pair,

$$q\bar{q}, g\bar{g} \rightarrow t\bar{t} \rightarrow W^+ b W^- \bar{b} \rightarrow jjb\ell^- \bar{\nu}\bar{b}, \tag{6.11}$$

and the b-quark giving the second lepton: $b \rightarrow c\ell\nu$. Similarly, tri-lepton background is produced in the fully leptonic decay of $t\bar{t}$ and the third lepton coming from b-quark. Though the charged leptons from b-quark decay typically have small transverse momentum, the large $t\bar{t}$ production cross section (compared to the production of N) is responsible for the dominant background, and must be taken into account in the detector simulation. The other dominant SM backgrounds for multi-lepton channels at the LHC arise from the production of $WZ, WW, ZZ, WWW, Wt\bar{t}, Zb\bar{b}, Wb\bar{b}$ etc.. A detailed discussion of the background analysis for multi-lepton final states can be found in Ref. [112, 253]. We find that by implementing the L2 trigger, most of this SM background can be eliminated, and the remaining background is dominantly due to $t\bar{t}$, WW, WZ and ZZ (which we collectively denote as 'SM background' in the following).

The invariant mass of the final state particles is used to reconstruct the mass of W_R. The selected events for the tri-lepton $(\ell^\pm \ell^\mp \ell^\pm) + \slashed{E}_T$ final state is shown in Fig. 6.4 (thick lines) as a function of the invariant mass (100 GeV bins) for $\sqrt{s} = 14$ TeV LHC and integrated luminosity, $\mathcal{L} = 8$ fb^{-1}. The expected SM background events $(t\bar{t} + VV)$ are also shown (thin lines). Here we have chosen $M_{W_R} = 2$ TeV and $M_N = 1$ TeV.

We have also taken the mixing parameter $V_{\ell N}$ just below the experimental upper bound: $|V_{\ell N}|^2 = 0.0025$ (For a lower value of mixing, the cross section and hence the total number of events, will decrease as $|V_{\ell N}|^2$). We find that the invariant mass of W_R is reconstructed nicely and the tri-lepton channel is virtually background free above 1 TeV or so. We also plot the invariant mass of $(\ell^\pm \ell^\mp \ell^\pm)$ in Fig. 6.5 which has the sharp end point at W_R mass. We note here that the tri-lepton final states with two positively charged (anti)leptons has more likelihood to be produced than those with one positively charged, which is naively expected for a proton-proton collision.
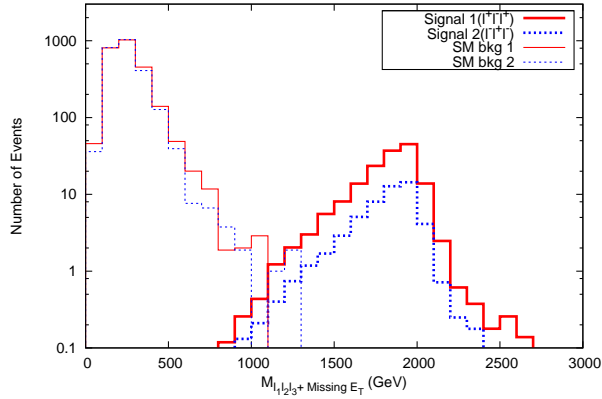
Figure 6.4: Selected events for the tri-lepton final state as a function of the invariant mass of $\ell^\pm \ell^\mp \ell^\pm + \not{E}_T$ (100 GeV bins) for $\sqrt{s} = 14$ TeV and $\mathcal{L} = 8$ fb^{-1}. We have chosen $M_{W_R} = 2, M_N = 1$ TeV and $|V_{\ell N}|^2 = 0.0025$ for this plot. The dominant SM background $(t\bar{t} + WW + WZ + ZZ)$ is also shown here (thin lines).

For comparison, we have also performed similar analysis for a heavy Majorana neutrino, similar to those in Ref. [198, 197], but with a large mixing $|V_{\ell N}|^2 = 0.0025$. Hence, as we discussed in Sec. III, N mostly decays to SM gauge bosons and charged leptons, and not through the 3-body decay involving W_R. The resulting events are shown in Figs. 6.6 and 6.7 for the invariant mass of $\ell^\pm \ell^\pm jj$ and $\ell^\pm \ell^\pm$ respectively. The parameters
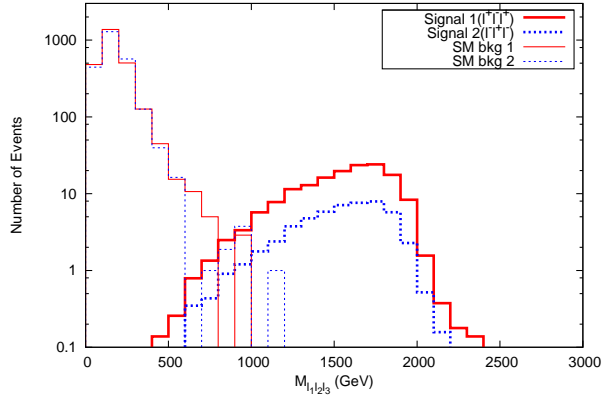
Figure 6.5: Selected events for tri-lepton final state as a function of the invariant mass of $\ell^{\pm}\ell^{\mp}\ell^{\pm}$ for the same parameters as in the Fig. 6.4 caption.

chosen are the same as for Figs. 6.4 and 6.5. We note that the number of same-sign di-lepton events passing the L2 trigger are roughly one order of magnitude larger than the tri-lepton events. This is because of the overall enhancement of the cross section for the di-lepton final state because the branching fraction for hadronic decay modes of $W \to jj$ is roughly thrice that of the light leptonic decay modes $W \to \ell\nu$.
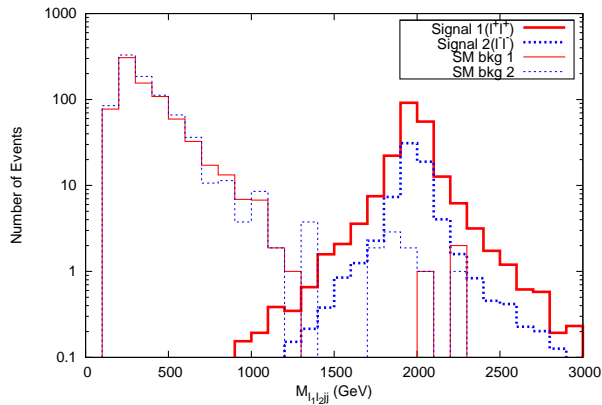
Figure 6.6: Selected events for the same-sign di-lepton final state as a function of the invariant mass of $\ell^{\pm}\ell^{\pm}jj$ for the same parameters as in the Fig. 6.4 caption.

To conclude this section, we have discussed the collider signatures of a heavy SM
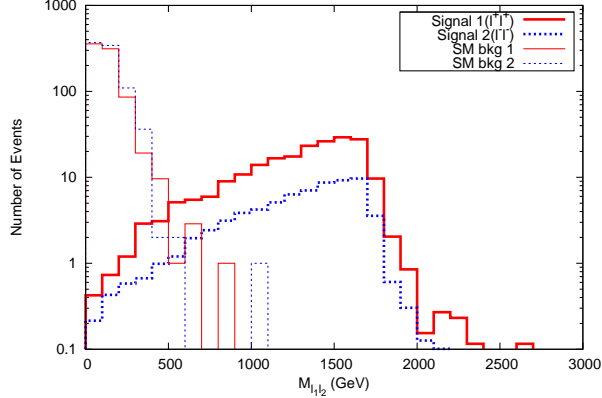
Figure 6.7: Selected events for same-sign di-lepton final state as a function of the invariant mass of $\ell^\pm \ell^\pm$ for the same parameters as in the Fig. 6.4 caption.

singlet neutrino in a minimal LR framework, which can be of either Majorana or Dirac nature depending on the mechanism for neutrino mass generation. In particular, we have analyzed the multi-lepton signals to distinguish a TeV scale Dirac neutrino from a Majorana one at the LHC. We perform a detailed collider simulation to show that, in LR models, a TeV-scale heavy neutrino can be produced at the LHC dominantly through a W_R exchange, which subsequently decays dominantly via SM gauge boson exchange. The invariant mass of the final state particles can be used to nicely reconstruct the mass of W_R in multi-lepton channels which are virtually background free above a TeV. We observe that if the heavy neutrino is of Majorana-type, there will be distinct lepton-number violating signals, including the same-sign di-lepton signal discussed here. However, in the absence of the same-sign di-lepton signal, the tri-lepton signal can be used to establish the Dirac nature of the heavy neutrino. This provides a direct way of probing the seesaw mechanism and the associated new physics at TeV-scale, and can be used to distinguish type-I seesaw (with purely Majorana heavy neutrinos) from inverse seesaw (with pseudo-Dirac ones) at the LHC.

6.2 Non-unitarity effects in the lepton mixing matrix

The 3×3 light neutrino mass matrix in flavor basis can be diagonalized by a unitary transformation:

$$U_{\text{PMNS}}^T m_\nu U_{\text{PMNS}} = \text{diag}(m_1, m_2, m_3) \equiv m_{\hat{\nu}} \qquad (6.12)$$

where U_{PMNS} is the standard PMNS mixing matrix given by Eq. (1.22). In the inverse seesaw formula [cf. Eq. (3.5)], however, since the above diagonalization of m_ν does not diagonalize the matrices M_N and μ, there will be off-diagonal mixing between the different light neutrinos even after diagonalization of m_ν due to their mixing with the heavy neutrinos. In other words, in the basis where the charged-lepton mass matrix is diagonal, U is only a part of the full mixing matrix responsible for neutrino oscillations. We have to examine the full 9×9 unitary matrix $\mathcal{V}$ in Eq. (3.4) which diagonalizes the full neutrino mass matrix $\mathcal{M}_\nu$ given by Eq. (3.3). If we block-decompose $\mathcal{V}$ as in Eq. (6.7), the upper-left sub-block $U_{3\times3}$ will represent the full (non-unitary) PMNS mixing matrix. For $\mu \ll M_D \ll M_N$, it is sufficient to consider only up to the leading order in $M_D M_N^{-1} \equiv F$ in Eq. (3.4). Then using Eq. (3.5), we can write new PMNS matrix up to second order if F [254]:

$$U_{3\times3} \simeq \left(1 - \frac{1}{2}FF^\dagger\right) U_{\text{PMNS}} \equiv \mathcal{N} \qquad (6.13)$$

In the commonly used parametrization [125], $\mathcal{N} = (1 - \eta)U_{\text{PMNS}}$, and hence, all the non-unitarity effects are determined by the Hermitian matrix

$$\eta = \frac{1}{2}FF^\dagger = \frac{1}{2}\left(M_D M_N^{-1}\right)\left(M_D M_N^{-1}\right)^\dagger \qquad (6.14)$$

which depends only on the mass ratio $M_D M_N^{-1}$ and not on the parameterization of the PMNS matrix.

The LH neutrinos entering the charged-current interactions of the SM now become superpositions of the nine mass eigenstates $(\hat{\nu}_i, N_j, N'_k)$ and at the leading order in F, the light neutrino entering the SM weak interaction Lagrangian becomes

$$\nu \simeq \mathcal{N}\hat{\nu} + \mathcal{K}P \tag{6.15}$$

where $\mathcal{K} \equiv V_{3\times6} \simeq (0, F)V_{6\times6}$ and $P = (N_1, N_2, N_3, N'_1, N'_2, N'_3)$. Then the charged-current Lagrangian in the mass basis, Eq. (1.21), is given by

$$\mathcal{L}_{\mathrm{CC}} = -\frac{g}{\sqrt{2}}\bar{l}_L\gamma^\mu\nu W^-_\mu + \mathrm{h.c.} \simeq -\frac{g}{\sqrt{2}}\bar{l}_L\gamma^\mu(\mathcal{N}\hat{\nu} + \mathcal{K}P)W^-_\mu + \mathrm{h.c.} \tag{6.16}$$

This mixing between the doublet and singlet components in the charged-current sector has several important phenomenological consequences for LFV processes, as discussed later in this section.

6.2.1   Bounds on $|\eta|$

The non-unitarity parameter η was defined in Eq. (6.14). Choosing a basis in which M_N is diagonal, and motivated by resonant leptogenesis (See Chapter 4), assuming degenerate eigenvalues for M_N equal to m_N, we have

$$\eta = \frac{1}{2m_N^2}M_D M_D^\dagger \tag{6.17}$$

With a typical form of M_D fixed by $SO(10)$ symmetry, Eq. (3.36), and extrapolated to the weak scale by neutrino RGEs [255][5], we can readily calculate the elements of η:

$$\eta \simeq \frac{1\ \mathrm{GeV}^2}{m_N^2}\begin{pmatrix} 0.1 & 0.0412 - 0.4144i & 1.5134 - 17.247i \\ 0.0412 + 0.4144i & 1.78 & 72.6794 - 0.0005i \\ 1.5134 + 17.247i & 72.6794 + 0.0005i & 3024.93 \end{pmatrix} \tag{6.18}$$

[5]The running effects are estimated to be small (within a few percent) for normal hierarchy of neutrino masses.

This is to be compared with the present bounds on $|\eta_{ij}|$ (at the 90% C.L.) [256]:

$$|\eta| < \begin{pmatrix} 2.0 \times 10^{-3} & 3.5 \times 10^{-5} & 8.0 \times 10^{-3} \\ 3.5 \times 10^{-5} & 8.0 \times 10^{-4} & 5.1 \times 10^{-3} \\ 8.0 \times 10^{-3} & 5.1 \times 10^{-3} & 2.7 \times 10^{-3} \end{pmatrix} \qquad (6.19)$$

This gives a *lower* bound on the mass of the RH neutrino:

$$m_N \gtrsim 1.06 \text{ TeV}, \qquad (6.20)$$

which is still kinematically accessible at the LHC to be produced on-shell and it decay to trilepton final states can be used to identify its pseudo-Dirac nature and test the inverse seesaew model [116].

With this lower bound on m_N, we get the following improved bounds on $|\eta_{\alpha\beta}|$ [120]:

$$|\eta_{ee}| < 8.9 \times 10^{-8}, \quad |\eta_{e\mu}| < 3.7 \times 10^{-7}, \quad |\eta_{e\tau}| < 1.5 \times 10^{-5},$$

$$|\eta_{\mu\mu}| < 1.6 \times 10^{-6}, \quad |\eta_{\mu\tau}| < 6.5 \times 10^{-5} \qquad (6.21)$$

At least one of these bounds, namely $|\eta_{e\mu}|$, is reachable at future neutrino factories from the improved branching ratio of $\mu \to e\gamma$ down to 10^{-16}, reachable in the proposed PRISM/PRIME project [257]. We note that relaxing the condition of degenerate RH neutrinos but fitting the neutrino masses affects the values of $\eta_{\alpha\beta}$; we present these results in Table-2. It appears that $|\eta_{e\mu}|$ values are all accessible to the future $\mu \to e\gamma$ searches; The largest value of $|\eta_{\mu\tau}|$ in this table may also be accessible to neutrino oscillation experiments, preferably with short baseline ($L \lesssim 100$ km) [121].

m_{N_1}	m_{N_2}	m_{N_3}	$|\eta_{e\mu}|$	$|\eta_{e\tau}|$	$|\eta_{\mu\tau}|$
1100	1100	1100	3.7×10^{-7}	1.5×10^{-5}	6.5×10^{-5}
100	100	1100	7.9×10^{-7}	1.6×10^{-5}	8.9×10^{-5}
50	50	1200	2.5×10^{-6}	2.2×10^{-5}	1.6×10^{-4}
30	30	2100	6.7×10^{-6}	4.4×10^{-5}	3.2×10^{-4}

Table 6.1: Predictions for the non-unitarity parameter $|\eta_{\alpha\beta}|$ for various RH neutrino masses (given in GeVs).

6.2.2 CP-violation effects

The CP-violation effects in the leptonic sector will be governed by the full PMNS matrix $\mathcal{N}$ instead of U_{PMNS} through the Jarlskog invariant [43]

$$J_{\alpha\beta}^{ij} = \mathrm{Im}\left(\mathcal{N}_{\alpha i}\mathcal{N}_{\beta j}\mathcal{N}_{\alpha j}^{*}\mathcal{N}_{\beta i}^{*}\right) \tag{6.22}$$

where the indices $\alpha \neq \beta$ run over e, μ and τ, while $i \neq j$ can be 1, 2 and 3. In the standard PMNS parametrization of U by the three mixing angles θ_{ij} and the Dirac CP-phase δ, one can expand Eq. (6.22) up to second order in $\eta_{\alpha\beta}$ and $s_{13} \equiv \sin\theta_{13}$ (assuming those to be small) to obtain

$$J_{\alpha\beta}^{ij} \simeq J + \Delta J_{\alpha\beta}^{ij}, \tag{6.23}$$

where the first term governs the CP-violating effects in the unitary limit and the second term gives the contribution coming from the non-unitarity effect:

$$J = c_{12}c_{13}^{2}c_{23}s_{12}s_{13}s_{23}\sin\delta, \tag{6.24}$$

$$\Delta J_{\alpha\beta}^{ij} \simeq -\sum_{\gamma=e,\mu,\tau}\mathrm{Im}\left(\eta_{\alpha\gamma}U_{\gamma i}U_{\beta j}U_{\alpha j}^{*}U_{\beta i}^{*} + \eta_{\beta\gamma}U_{\alpha i}U_{\gamma j}U_{\alpha j}^{*}U_{\beta i}^{*}\right.$$

$$+ \eta^*_{\alpha\gamma} U_{\alpha i} U_{\beta j} U^*_{\gamma j} U^*_{\beta i} + \eta^*_{\beta\gamma} U_{\alpha i} U_{\beta j} U^*_{\alpha j} U^*_{\gamma i} \Big) \qquad (6.25)$$

Note that the unitary term J vanishes if either $s_{13} \to 0$ or $\delta \to 0$. However, $\Delta J^{ij}_{\alpha\beta}$ depends on the off-diagonal elements of η (generally complex) and does not necessarily vanish even if both s_{13} and δ are zero; in fact, it might even dominate the CP-violating effects in the leptonic sector.

Note that $\Delta^{ij}_{\alpha\beta}$ is non-zero in our case as η is a complex matrix (the phases arising from the Dirac neutrino sector). Using the values of θ_{ij} from neutrino oscillation data given in Table 1.3 and the structure of η determined in Eq. (6.18) with $m_N = 1.1$ TeV, we obtain the following values for $\Delta J^{ij}_{\alpha\beta}$:

$$\Delta J^{12}_{e\mu} \simeq -2.4 \times 10^{-6},$$

$$\Delta J^{23}_{e\mu} \simeq -2.7 \times 10^{-6},$$

$$\Delta J^{23}_{\mu\tau} \simeq 2.7 \times 10^{-6},$$

$$\Delta J^{31}_{\mu\tau} \simeq 2.7 \times 10^{-6},$$

$$\Delta J^{12}_{\tau e} \simeq 7.1 \times 10^{-6} \qquad (6.26)$$

and $\Delta J^{23}_{e\mu} = \Delta J^{31}_{e\mu} = -\Delta J^{12}_{\mu\tau} = \Delta J^{23}_{\tau e} = \Delta J^{31}_{\tau e}$. Note that these values are just one order of magnitude smaller than the quark sector value, $J_{\text{CKM}} = \left(2.91^{+0.19}_{-0.11}\right) \times 10^{-5}$ [123], and can be the dominant source of CP-violation in the leptonic sector, even for vanishing Dirac CP phase, thus leading to distinctive CP-violating effects in neutrino oscillations [125]. For instance, the transition probability for the "golden channel" $\nu_\mu \to \nu_\tau$ with non-unitarity effects is given by [125]

$$P_{\mu\tau} \simeq 4|\eta_{\mu\tau}|^2 + 4s^2_{23}c^2_{23} \sin^2\left(\frac{\Delta m^2_{31}L}{4E}\right) - 4|\eta_{\mu\tau}| \sin\delta_{\mu\tau} s_{23} c_{23} \sin\left(\frac{\Delta m^2_{31}L}{2E}\right) \qquad (6.27)$$

where the last term is CP-odd due to the phase $\delta_{\mu\tau}$ of the element $\eta_{\mu\tau}$ which, in our model,

126

is $\sim 7 \times 10^{-6}$ [cf. Eq. (6.18)]. Hence, the CP-violating effects should be pronounced for long-baseline neutrino factories.

6.3 LFV decay rates

Lepton flavor violating decays such as $\mu \to e\gamma$, $\tau \to e\gamma$ and $\tau \to \mu\gamma$ could be a signature of seesaw models for neutrino masses. The LFV decays mediated by the heavy RH neutrinos have branching ratios [131]

$$\mathrm{BR}(l_\alpha \to l_\beta\gamma) \simeq \frac{\alpha_W^3 s_W^2 m_{l_\alpha}^5}{256\pi^2 M_W^4 \Gamma_\alpha} \left| \sum_{i=1}^{6} \mathcal{K}_{\alpha i}\mathcal{K}_{\beta i}^* I\left(\frac{m_{N_i}^2}{M_W^2}\right) \right|^2 \tag{6.28}$$

where $\mathcal{K}$ is defined below Eq. (6.15), Γ_α is the total decay width of l_α and the function $I(x)$ is defined by

$$I(x) = -\frac{2x^3 + 5x^2 - x}{4(1-x)^3} - \frac{3x^3 \ln x}{2(1-x)^4} \tag{6.29}$$

For degenerate RH neutrino masses, Eq. (6.28) becomes

$$\mathrm{BR}(l_\alpha \to l_\beta\gamma) \simeq \frac{\alpha_W^3 s_W^2 m_{l_\alpha}^5}{256\pi^2 M_W^4 \Gamma_\alpha} \left| \left(\mathcal{K}\mathcal{K}^\dagger\right)_{\alpha\beta} I\left(\frac{m_N^2}{M_W^2}\right) \right|^2, \tag{6.30}$$

Note that the amplitude is proportional to $\left(\mathcal{K}\mathcal{K}^\dagger\right)_{\alpha\beta} \sim \left(FF^\dagger\right)_{\alpha\beta}$, and hence, for sizeable F and TeV-scale RH sector in inverse seesaw, one could expect appreciable rates in the LFV channels [128, 129, 130]. On the other hand, in the conventional type I seesaw model, one has approximately $\mathcal{K}\mathcal{K}^\dagger = \mathcal{O}\left(m_\nu M_R^{-1}\right)$, and therefore, the branching ratio, $\mathrm{BR}(l_\alpha \to l_\beta\gamma) \propto \mathcal{O}\left(m_\nu^2\right)$ is strongly suppressed [131].

In our model [120], knowing all the three 3×3 mass matrices entering the inverse seesaw formula given by Eq. (3.3), we can easily determine the structure of the full unitary matrix $\mathcal{V}$ by diagonalizing the 9×9 neutrino mass matrix $\mathcal{M}_\nu$, and hence, obtain $\mathcal{K}$ to estimate the branching ratios given by Eq. (6.30).

The total decay width Γ_α entering Eq. (6.30) is given by $\hbar/\tau_\alpha$ where the mean life for μ and τ are, respectively [22]

$$
\begin{aligned}
\tau_\mu &= (2.197019 \pm 0.000021) \times 10^{-6} \text{ sec.,} \\
\tau_\tau &= (290.6 \pm 1.0) \times 10^{-15} \text{ sec.}
\end{aligned}
\tag{6.31}
$$

Using these values, we obtain the following branching ratios for the rare LFV decays [120]

$$
\begin{aligned}
\text{BR}(\mu \to e\gamma) &\simeq 3.5 \times 10^{-16}, \\
\text{BR}(\tau \to e\gamma) &\simeq 1.1 \times 10^{-13}, \\
\text{BR}(\tau \to \mu\gamma) &\simeq 2.0 \times 10^{-12}
\end{aligned}
\tag{6.32}
$$

We have also estimated the contribution to $\mu \to e\gamma$ branching ratio from the off diagonal Dirac Yukawa coupling contribution to slepton masses and find that for universal scalar mass of 500 GeV and $\tan\beta \simeq 5$, it is comparable to this value or less [258]. Such values for $\mu \to e\gamma$ branching ratio are accessible to future experiments such as PRISM/PRIME, capable of reaching sensitivities down to 10^{-16} [257]. They can be used to test the model.

In our model we assume that squark and slepton masses are above a TeV so that their contribution to the FCNC effects are negligible. The predictions for $\mu \to 3e$ and $\mu \to e$ conversion [132] for a TeV-scale slepton mass, as in our model, are much smaller than what can be probed in planned experiments.

Chapter 7

Proton Decay

Proton decay is the smoking gun signature of baryon number violation and hence grand unification [259]. Although there is no evidence for proton decay till now, current experimental lower bounds on the partial lifetimes of various proton decay modes tend to put severe constraints on the GUT models and suggest possible modifications of such models [260]. They also constrain the choices of Higgs multiplets that can be used for model building with $SO(10)$ group [261]. In the $SO(10)$ models we are interested in [120, 151], due to the fact that all the Yukawa couplings responsible for proton decay are constrained by the fermion mass fits, it is possible to estimate the partial life times for the various modes as functions of the squark and gaugino masses.

In non-SUSY GUTS, proton decay occurs via dimension-6 operators involving the superheavy X and Y gauge bosons, and are suppressed by $(1/M_{X,Y}^2)$ where $M_{X,Y}$ are of the order of the GUT-scale. The proton decay lifetime in a non-SUSY $SU(5)$ GUT, for instance, is given by [68]

$$\tau_p \approx \frac{M_G^4}{\alpha_G^2 m_p^5} \tag{7.1}$$

The dominant decay mode is $p \rightarrow e^+ \pi^0$. The present experimental lower bound on this mode, $\tau_{(p \rightarrow e^+ \pi^0)} > 8.2 \times 10^{33}$ years [156], has already ruled out such non-SUSY GUTs, which predict a unification scale of $\sim 10^{15}$ GeV. In SUSY-GUTs, the GUT scale is significantly higher $\sim 2 \times 10^{16}$ GeV (see Chapter 2), and hence the dimension-6 proton decay operators are significantly suppressed in SUSY-GUTs with $\tau_p \sim 10^{34-38}$ years [262].

129

However, in SUSY-GUTs, we could also have dimension-4 and -5 contributions to baryon-number violation [263]. The $d = 4$ operators are very dangerous for SUSY-GUTs as they make the proton extremely unstable. However, they could be eliminated by imposing R-parity [70]; in other words, R-parity must be a symmetry in any effective low-energy theory of SUSY-GUT. The $d = 5$ operators are generated by color triplet Higgsino exchange. Since the higgsino-mediated decay rate depends on Yukawa couplings, in SUSY GUTs, the proton preferentially decays to kaon ($p \rightarrow K^+ \bar{\nu}$) rather than to pion as in non-SUSY GUTs. The exact decay rate for this operator is model dependent, as it depends on the whole SUSY spectrum and on the structure of the Higgs sector. However, the current experimental lower bound, $\tau_{(p \rightarrow K^+ \bar{\nu})} > 1.6 \times 10^{33}$ years [156] is sufficiently strong to rule out the minimal SUSY $SU(5)$ [264], though non-minimal Higgs sectors in SUSY $SU(5)$ (see e.g. Ref. [265, 260]) and $SO(10)$ (see e.g. Ref. [266]) still survive the Super-K bounds.

In the following, we first discuss the various proton decay operators in a generic SUSY-GUT, and then we estimate the proton decay rates induced by $d = 5$ operators in our $SO(10)$ model [120, 151].

7.1   Proton decay operators

As mentioned above, in generic SUSY-GUTs with R-parity, there exist two main sources for proton decay:

- D-type (dimension-6) operators that may arise from exchange of gauge boson exchange:

$$\frac{1}{M_G^2} \int d^2\theta \, d^2\bar{\theta} \, \Phi\Phi\Phi\Phi, \qquad (7.2)$$

130

where Φ denotes a chiral superfield. For a unification scale $\gtrsim 10^{16}$ GeV, these contributions to proton decay are sufficiently small and well beyond the range of current experiments. Hence, we will not discuss them further.

- F-type (dimension-5) operators that may arise from the exchange of color triplet Higgsino fields in **10**-Higgs fields as shown in Fig. 7.1(a):

$$\frac{1}{M_G} \int d^2\theta \ \Phi\Phi\Phi\Phi \tag{7.3}$$

In the component language, they give rise to dimension-5 operators of the form $(QQ)(\widetilde{Q}\widetilde{L})$ and $(QL)(\widetilde{Q}\widetilde{Q})$. As these operators involve squark and slepton fields, they cannot induce proton decay in the lowest-order. Proton decay occurs by converting the squark and slepton legs into quarks and leptons by exchanging a gaugino, as shown in the box diagram of Fig. 7.1(b).
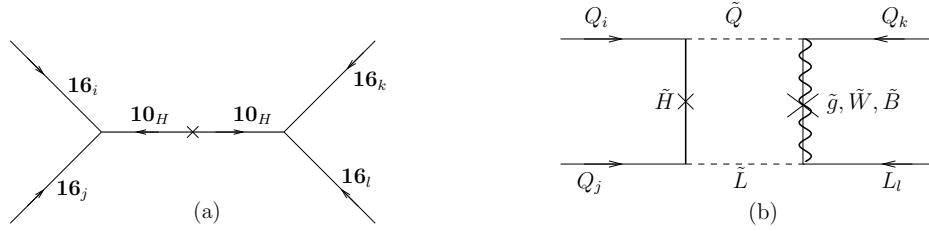
Figure 7.1: (a) Supergraph giving rise to effective dimension-5 proton decay operators, and (b) Box diagram involving gaugino exchange that converts the dimension-5 operator of Fig. 3(a) into an effective four- Fermi operator that induces proton decay.

There are two types of effective dimension-5 operators given by Eq. (7.3): $LLLL$ type that involve only left-handed quark and lepton fields and a corresponding $RRRR$ type,

both invariant under MSSM [263]. In super-space notation, these are explicitly given by

$$\mathcal{O}_L = \int d^2\theta \, \epsilon^{\alpha\beta\gamma}\epsilon^{ab}\epsilon^{cd} \, Q_{\alpha ai}Q_{\beta bj}Q_{\gamma ck}L_{dl} \ , \tag{7.4}$$

$$\mathcal{O}_R = \int d^2\theta \, \epsilon^{\alpha\beta\gamma} \, (Q^c)_{\alpha i} \, (Q^c)_{\beta j} \, (Q^c)_{\gamma k} \, (L^c)_l \tag{7.5}$$

where $\alpha, \beta, \gamma = 1, 2, 3$ are $SU(3)_c$ color indices; $a, b, c, d = 1, 2$ are $SU(2)_L$ isospin indices; and $i, j, k, l = 1, 2, 3$ are generation indices. It is clear from the form of these operators that they break baryon number by one unit, but preserve the $B - L$ symmetry, leading to the proton decay to a pseudoscalar and an anti-lepton. As argued in Ref. [267] for kinematical reasons and explicitly shown in Ref. [268] for small to moderate $\tan\beta$ region of the SUSY parameter space, the $RRRR$ contributions are at least an order of magnitude smaller than the $LLLL$ contributions. We also verify this in our model, as shown later; for the time being therefore, we concentrate only on the $LLLL$ operator.

In component form, the effective superpotential due to the $LLLL$ operator is explicitly given by [269]

$$\mathcal{W}_{\Delta B=1} = \frac{1}{M_T}\epsilon^{\alpha\beta\gamma} \left[(C_{ijkl} - C_{kjil}) \, u_{\alpha i}d_{\beta j}u_{\gamma k}e_l - (C_{ijkl} - C_{ikjl}) \, u_{\alpha i}d_{\beta j}d_{\gamma k}\nu_l \right] \tag{7.6}$$

where M_T is the effective mass of the color triplet Higgs field belonging to the $\mathbf{10}_H$ representation, and in our model, is of the order of the unification scale M_G (see Appendix A). The coefficients C_{ijkl} associated with the superpotential given by Eq. (7.6) can be expressed in terms of the products of the GUT-scale Yukawa couplings (see Section 7.3). This superpotential leads to the effective dimension-5 operators involving two fermions and two sfermions as shown in Fig. 7.1(b), which lead to proton decay by four-Fermi interactions when "dressed" via the exchange of gauginos, namely gluinos, binos and winos. A typical diagram for the effective four-Fermi interaction induced by this dressing is shown in Fig. 7.2.
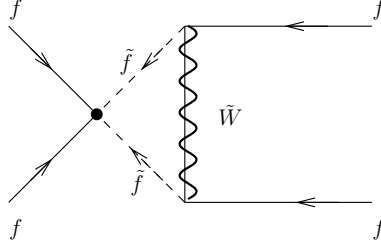
Figure 7.2: The effective four-Fermi interaction diagram induced by the gaugino dressing of the effective dimension-5 operator given by Fig. 7.1(b).

It can be shown that [270] in the limit of all squark masses being degenerate as in typical mSUGRA type models, the gluino and bino contributions to the dressing of the dimension-5 operators vanish. This basically follows from the use of Fierz identity for the chiral two component spinors representing quarks and leptons. In realistic models, the FCNC constraints allow only very small deviations from universality of squark masses. Hence, these gluino and bino contributions are expected to be small compared to the wino contributions, and can be ignored altogether. The charged wino dressing diagrams have been evaluated earlier [271], and in the limit of degenerate squark masses, this leads to the effective Lagrangian [269]

$$\mathcal{L}_{\Delta B=1} = 2I\epsilon^{\alpha\beta\gamma}(C_{kjil} - C_{ijkl})[u_{\alpha k}^T C d_{\beta j} d_{\gamma i}^T C\nu_l + u_{\beta j}^T C d_{\gamma k} u_{\alpha i}^T Ce_l], \qquad (7.7)$$

where C denotes the charge-conjugation matrix and I is given by

$$I = \frac{\alpha_2}{4\pi} \frac{m_{\widetilde{W}}}{M_{\tilde{f}}^2}, \qquad (7.8)$$

$m_{\widetilde{W}}$ being the wino mass and $M_{\tilde{f}}$ the sfermion mass. Using this expression and adding a similar contribution from the neutral wino exchange diagram, we can write down the total contribution to various proton decay channels. This is summarized in Table 7.1. We note that the proton decay operators with s-quark lead to K-meson final states whereas the

133

ones without s lead to π final states. As shown in Table 7.1, the amplitude for non-strange quark final states will be Cabibbo-suppressed compared to the strange quark final states. It is also important to mention here that the total amplitude for final states involving neutrinos is the incoherent sum of the rates for all three neutrino states. This leads to large decay rates for $p \to K^+\bar{\nu}$ and $p \to \pi^+\bar{\nu}$ channels compared to the other decay channels due to the large Yukawa couplings of the third generation.

Decay channel	$\mathcal{C}$-coefficient
$p \to K^+\bar{\nu}_l$	$(C_{112l} - C_{121l})$
$p \to K^0 e^+$	$(C_{1121} - C_{1211})$
$p \to K^0 \mu^+$	$(C_{1122} - C_{1212})$
$p \to \pi^+\bar{\nu}_l$	$\sin\theta_C(C_{211l} - C_{112l})$
$p \to \pi^0 e^+$	$\sin\theta_C(C_{2111} - C_{1121})$
$p \to \pi^0 \mu^+$	$\sin\theta_C(C_{2112} - C_{1122})$

Table 7.1: The coefficients for various $\Delta B = 1$ dimension-5 operators obtained from the effective Lagrangian to leading order. Here θ_C is the Cabibbo angle (with $\sin\theta_C \sim 0.22$) and the C_{ijkl}'s are products of the Yukawa couplings, as defined in Eqs. (7.17) and (7.18).

7.2   Yukawa Couplings

Model (A): The model discussed in Chapter 3 is defined by the vev pattern of the bi-doublets $\Phi_{1,2}$ given by Eq. (3.16), leading to the fermion mass matrices given by

Eq. (3.30). Note that the contribution from the effective $\mathbf{126}_H$ operator is assumed to be the same for both up and down sectors, i.e. $\tilde{f} = \kappa_u f_u = \kappa_d f_d$; as a result, we have the relation $f_d = f_u \tan\beta$. Using the RG analysis for the fermion masses and mixing in the SUSYLR model (see Appendix B), we obtain the GUT-scale fermion masses starting from the experimentally known values at the weak scale (see Eqs. (3.19)). Using these mass values, we obtain a fit for the coupling matrices at the GUT scale defined in Eq. (3.30). Here we give the results in a down quark mass diagonal basis for two values of $\tan\beta$:

(a) $\tan\beta(M_{\text{SUSY}}) = 10$: In this case, the GUT-scale values of the charged fermion masses are given by Eq. (3.19). With these mass eigenvalues, we find a fit for the GUT-scale couplings of the form [151]

$$
\begin{aligned}
f_u &= \text{diag}\left(1.26 \times 10^{-6}, -0.0001, -9.48 \times 10^{-6}\right), \quad f_d = f_u \tan\beta, \\
h_d &= \text{diag}\left(4.86 \times 10^{-5}, 0.0019, 0.0752\right), \\
h_u &= \begin{pmatrix} 7.46 \times 10^{-5} & 0.0002 - 6.51 \times 10^{-5}i & 0.0002 - 0.0028i \\ 0.0002 + 6.51 \times 10^{-5}i & 0.0015 & 0.0118 + 1.26 \times 10^{-6}i \\ 0.0002 + 0.0028i & 0.0118 - 1.26 \times 10^{-6}i & 0.4908 \end{pmatrix}
\end{aligned}
\tag{7.9}
$$

Note that for simplicity we have chosen the f-couplings to be diagonal. Our fit does not allow the off-diagonal components to be too different from zero.

(b) $\tan\beta(M_{\text{SUSY}}) = 30$: In this case, the GUT-scale values of the charged fermion masses are found to be

$$
m_u = 0.0121 \text{ GeV}, \quad m_c = 0.3269 \text{ GeV}, \quad m_t = 120.53 \text{ GeV},
$$

$$
m_d = 0.0014 \text{ GeV}, \quad m_s = 0.0277 \text{ GeV}, \quad m_b = 2.7958 \text{ GeV},
$$

$$
m_e = 0.0006 \text{ GeV}, \quad m_\mu = 0.1266 \text{ GeV}, \quad m_\tau = 2.7737 \text{ GeV}
\tag{7.10}
$$

and $\tan \beta(M_G) = 20$. With these mass eigenvalues, we obtain a fit for the couplings of the following form [151]:

$$
\begin{aligned}
f_u &= \operatorname{diag} \left(1.5 \times 10^{-6}, -0.0002, 4.2 \times 10^{-5}\right), \quad f_d = f_u \tan \beta_{\mathrm{GUT}}, \\
h_d &= \operatorname{diag} (0.0002, 0.0078, 0.4163), \\
h_u &= \begin{pmatrix}
0.0002 & 0.0003 - 0.0001i & -0.0008 - 0.0081i \\
0.0002 + 0.0001i & 0.0029 & 0.0144 + 0.0002i \\
-0.0008 + 0.0081i & 0.0144 - 0.0002i & 0.9145
\end{pmatrix}
\end{aligned}
\tag{7.11}
$$

We note that in this model, larger values of $\tan \beta$ (> 30) are not allowed. This can be seen analytically from the RGEs given in Appendix B; it can be seen from the form of the RGEs that the up-quark sector masses will increase rapidly at high energies for large $\tan \beta$ and the same effect is induced in the down-quark sector which makes the Yukawa terms dominant over the gauge terms. This makes all the quark masses to run up to unacceptably large values at the GUT-scale. We believe this is a general feature of low-scale SUSYLR models, in contrast to MSSM case [272].

Model (B): In this section, we consider an alternative mass fit within the $SO(10)$ models with low scale $B - L$ [151]. It follows from the ansatz in Ref. [273] that in generic $SO(10)$ models which do not use type I seesaw to fit neutrino masses, an alternative fit to fermion masses is possible with a rank one **10**-Higgs Yukawa coupling matrix which dominates the fermion masses while other couplings introduce small corrections; the third generation masses arise from the dominant rank one coupling matrix with smaller **126** and second **10** couplings generating the CKM mixing as well as the second and the first generation fermion masses. This idea can be applied to our case since, the neutrino mass is given by the inverse seesaw formula which involves an additional matrix μ. The main difference of model (B) as compared to model (A) resides in the vev pattern of the two

Higgs bidoublets i.e. in model (B), we have

$$\langle \Phi_1 \rangle = \begin{pmatrix} \kappa_d & 0 \\ 0 & \kappa_u \end{pmatrix}, \quad \langle \Phi_2 \rangle = \begin{pmatrix} \kappa'_d & 0 \\ 0 & \kappa'_u \end{pmatrix} \tag{7.12}$$

with $v_{\text{wk}}/\sqrt{2} = \sqrt{\kappa_u^2 + \kappa_d^2 + \kappa_u'^2 + \kappa_d'^2}$. Also we must have $\frac{\kappa_u}{\kappa_d} \neq \frac{\kappa'_u}{\kappa'_d}$ in order to get right fermion mixing pattern. In the limit $\kappa_u \gg \kappa'_u$, the RG analysis of model (A) can be applied to this case to generate fermion masses at the GUT scale as well as the symmetry breaking pattern via radiative corrections.

The resulting fermion mass formulas in terms of the appropriately redefined Yukawa couplings are given as follows [274]:

$$
\begin{aligned}
M_u &= \widetilde{h} + r_2 \widetilde{f} + r_3 \widetilde{h}', \\
M_d &= r_1(\widetilde{h} + \widetilde{f} + \widetilde{h}'), \\
M_l &= r_1(\widetilde{h} - 3\widetilde{f} + c_e \widetilde{h}'), \\
M_{\nu_D} &= \widetilde{h} - 3\widetilde{f} + c_\nu \widetilde{h}'
\end{aligned}
\tag{7.13}
$$

where

$$
\widetilde{h} = \kappa_u h, \quad \widetilde{f} = \frac{\kappa_u \kappa'_d}{\kappa_d} f, \quad \widetilde{h}' = \frac{\kappa_u \kappa'_d}{\kappa_d} h',
$$
$$
r_1 = \frac{\kappa_d}{\kappa_u}, \quad r_2 = r_3 = \frac{\kappa_d \kappa'_u}{\kappa_u \kappa'_d}.
\tag{7.14}
$$

As in the case of model (A), the f coupling above represents the effective **126** coupling arising from the $\psi\psi A_1 A_2 H_2$ term in the superpotential and h' arises from a coupling of the form $\psi\psi H_2 X$ (with a nonzero vev for the additional singlet field X). Note that if there is an additional Z_2 symmetry under which H_2, A_2, X are odd and all other fields are even, one can have a superpotential with only the h, f, h' type contributions as given above, to the fermion mass formulas. In our case with two Higgs bi-doublets, $c_e = 1$ and

$c_\nu = r_3$. With the GUT-scale mass eigenvalues obtained earlier, we obtain a fit for these couplings as follows:

(a) $\tan\beta_{\text{MSSM}} = 10$:

$$\kappa_u = 173.2 \text{ GeV}, \quad r_1 = 0.0218, \quad r_2 = 0.14, h = \text{diag}\,(0, 0, 0.45), \tag{7.15}$$

$$f = \begin{pmatrix} 0 & -0.0006 & 0.0019 \\ -0.0006 & 0.0115 & 0.0101 \\ 0.0019 & 0.0101 & 0.0001 \end{pmatrix}, \quad h' = i \begin{pmatrix} 0 & -0.0022 & 0.0005 \\ 0.0022 & 0 & 0.0181 \\ -0.0005 & -0.0181 & 0 \end{pmatrix}$$

(b) $\tan\beta_{\text{MSSM}} = 30$:

$$\kappa_u = 172.4 \text{ GeV}, r_1 = 0.0231, \quad r_2 = 0.21, h = \text{diag}\,(0, 0, 0.70), \tag{7.16}$$

$$f = \begin{pmatrix} 0 & -0.0016 & 0.0062 \\ -0.0016 & 0.0140 & 0.0111 \\ 0.0062 & 0.0111 & 0.0019 \end{pmatrix}, \quad h' = i \begin{pmatrix} 0 & -0.0022 & 0.0005 \\ 0.0022 & 0 & 0.0181 \\ -0.0005 & -0.0181 & 0 \end{pmatrix}$$

It may be noted here that in both the cases, all the fermion mass values predicted using the couplings above agree with those obtained from the RGEs within the experimental uncertainty, the only exception being the up-quark mass in case (a), where the our predicted value is about 4 times larger. Note however that in our discussion, we have not included contributions from threshold corrections or higher dimensional operators. Those contributions can generally be of order MeVs when their couplings are chosen appropriately, in which case, they will not affect the second and third generation masses but could easily bring the up quark mass into agreement with RGE predictions.

With the Yukawa couplings given by Eqs. (7.15) and (7.16), we can calculate the C-coefficients introduced in Eq. (7.6). For model (A), this is given by

$$C_{ijkl} = h_{u_{ij}}h_{u_{kl}} + x_1 h_{d_{ij}}h_{d_{kl}} + x_2 h_{u_{ij}}h_{d_{kl}} + x_3 h_{d_{ij}}h_{u_{kl}} + \frac{1}{2}\left[h_{u_{ij}}f_{u_{kl}} + f_{u_{ij}}h_{u_{kl}}\right.$$

$$+x_1\left(h_{d_{ij}}f_{d_{kl}} + f_{d_{ij}}h_{d_{kl}}\right) + x_2\left(f_{u_{ij}}h_{d_{kl}} + h_{u_{ij}}f_{d_{kl}}\right) + x_3\left(h_{d_{ij}}f_{u_{kl}} + f_{d_{ij}}h_{u_{kl}}\right)\Big]$$

$$+\frac{1}{4}\left(f_{u_{ij}}f_{u_{kl}} + x_1 f_{d_{ij}}f_{d_{kl}} + x_2 f_{u_{ij}}f_{d_{kl}} + x_3 f_{d_{ij}}f_{u_{kl}}\right) \tag{7.17}$$

while for model (B) this becomes

$$C_{ijkl} = h_{ij}h_{kl} + x_1 h'_{ij}h'_{kl} + x_2 h_{ij}h'_{kl} + x_3 h'_{ij}h_{kl}$$

$$+\frac{1}{2}\left[x_1\left(h'_{ij}f_{kl} + f_{ij}h'_{kl}\right) + x_2 h_{ij}f_{kl} + x_3 f_{ij}h_{kl}\right] + \frac{1}{4}x_1 f_{ij}f_{kl} \tag{7.18}$$

where x_i's are the ratios of the $\mathbf{10}_H$ color triplet Higgs masses and mixing and the factor $\frac{1}{2}$ is the Clebsch-Gordan coefficient for the $\mathbf{10} \cdot \mathbf{10} \cdot \mathbf{126}$ coupling. Note that there are only three mixing parameters as there are only four color triplet Higgses in the MSSM gauge group, corresponding to the two $\mathbf{10}_H$ fields in our model. As we are interested only in the upper bound for the partial lifetimes of various proton decay channels, we do not need to know the detailed form for the x_i parameters in terms of these masses and mixing. We just vary these parameters numerically to get the maximum value for the partial lifetimes.

Before proceeding to calculate the rate of proton decay induced by the $LLLL$ type operators discussed in Section 7.1, let us estimate the contribution from the $RRRR$ type operators in our model. The gluino dressing graphs do not contribute in the limit of universal sfermion masses by the same Fierz arguments as for the $LLLL$ case. Moreover, since all superfields in the $RRRR$ operator are $SU(2)_L$ singlets, there is no wino contribution to the leading order. Also the bino dressing generates an effective four-Fermi operator of the type $\epsilon^{\alpha\beta\gamma}\epsilon^{ij}\epsilon^{kl}u^{cT}_{\beta j}Cd^c_{\gamma k}u^{cT}_{\alpha i}Ce^c_l$ which, in flavor basis, is antisymmetric in the flavor indices i and j, and hence in the mass basis, must involve a charm quark. Thus to leading order, the bino contribution also vanishes due to phase space constraints. Thus the only dominant contribution comes from the Higgsino exchange and the largest amplitude in this case, which comes from stop intermediate states, is estimated to be [269] (using the

C_{ijkl} values given above)

$$C_{1323} \frac{m_t m_\tau V_{ub}}{16\pi^2 v_{\text{wk}}^2 \sin\beta \cos\beta} \sim 4.0 \times 10^{-10} \tag{7.19}$$

for $\tan\beta = 30$, as compared to the $LLLL$ contribution which is typically of order

$$C_{1123} \frac{\alpha_2}{4\pi} \sim 4.5 \times 10^{-9} \tag{7.20}$$

As the $RRRR$ contribution is proportional to $1/(\sin\beta \cos\beta)$ which is $\sim \tan\beta$ for large β, for smaller $\tan\beta$, this contribution is further suppressed. This justifies why we can ignore the $RRRR$ contributions in the following calculation of proton decay rate.

7.3 Extrapolation Factors for $d = 5$ Operators

In order to calculate the proton decay rate, we must extrapolate these dimension-5 operators defined at the GUT scale to the mass scale of proton, i.e. $m_p \simeq 1$ GeV. In our model, we can divide this whole energy range into three parts, following the breaking chain given in Section 3.4:

(a) from the GUT scale M_G to the $B - L$ breaking scale M_R (SUSYLR),

(b) from M_R to the SUSY-breaking scale M_S (MSSM), and

(c) from M_S to 1 GeV (SM).

The values of these extrapolation factors for SM and MSSM are given in the literature [267, 275, 276, 277], but not for the SUSYLR model. In this section, we derive these factors using the anomalous dimensions for the dimension-5 operators in our model [151]. We noted some discrepancies in the values of the anomalous dimensions quoted in different papers, but found that our results for the SM and MSSM cases agree with those given in Refs. [275, 267] and quoted in Appendix E of Ref. [259].

First, we have the SM sector from 1 GeV to the SUSY-breaking scale M_S in which we have the usual non-SUSY enhancement factor [275] for the $LLLL$ operator:

$$A_e^{\text{NS}} = \left[\frac{\alpha_3(1 \text{ GeV})}{\alpha_3(M_S)} \right]^{2/\left(11 - \frac{2}{3} n_f \right)} \tag{7.21}$$

where n_f is the number of quark flavors below the energy scale of interest. Here we have neglected the effects of $SU(2)_L$ and $U(1)_Y$ couplings as they are much smaller compared to that of $SU(3)_c$ (see Table 1.2). Assuming $M_S > m_t$, the enhancement factor explicitly becomes

$$A_e^{\text{NS}} = \left[\frac{\alpha_3(1 \text{ GeV})}{\alpha_3(m_c)} \right]^{2/9} \left[\frac{\alpha_3(m_c)}{\alpha_3(m_b)} \right]^{6/25} \left[\frac{\alpha_3(m_b)}{\alpha_3(m_t)} \right]^{6/23} \left[\frac{\alpha_3(m_t)}{\alpha_3(M_S)} \right]^{2/7} = 1.49 \tag{7.22}$$

using the values of $\alpha_3(Q)$ at $Q = 1$ GeV, m_c and m_b obtained by interpolating the renormalization group equation for the effective QCD coupling [278] and at $Q = m_t$ by the SM running from $Q = m_Z$.

Now above M_S, we have the usual MSSM till the $B - L$ breaking scale M_R and then the SUSYLR model till the GUT scale M_G. The extrapolation factor in this case is given by

$$A_e^{\text{S}} = A_e^{\text{MSSM}} A_e^{\text{SUSYLR}}, \quad \text{with}$$

$$A_e^{\text{MSSM}} = \prod_{i=1}^{3} \left[\frac{\alpha_i(M_S)}{\alpha_i(M_R)} \right]^{\frac{\gamma_i}{b_i}}, \quad \text{and} \quad A_e^{\text{SUSYLR}} = \prod_{j=1}^{4} \left[\frac{\alpha_j(M_R)}{\alpha_j(M_G)} \right]^{\frac{\gamma_j}{b_j}} \tag{7.23}$$

Here $b_i = \left(\frac{33}{5}, 1, -3 \right)$ for $i = \mathbf{1}_Y, \mathbf{2}_L, \mathbf{3}_c$ are the well known MSSM β-function coefficients [cf. Eq. (2.8)], $b_j = (13, 2, 4, -2)$ for $j = \mathbf{1}_{B-L}, \mathbf{2}_L, \mathbf{2}_R, \mathbf{3}_c$ are the β-function coefficients [cf. Eq. (3.9)] for the SUSYLR model, and γ_i's are the anomalous dimensions for the $LLLL$ operator, calculated below.

The derivation of the anomalous dimensions of the dimension-5 operators of the $LLLL$ type given by Eq. (7.4) is straightforward in a supersymmetric gauge due to the

fact that the operator $\mathcal{O}_L$ is purely chiral (it is an F-term [223]), and hence, it follows from non-renormalization theorems [279] that in a supersymmetric gauge, it will only have wave function renormalization. Then it is easy to show that the anomalous dimensions of any purely chiral operator are given by

$$\gamma_\mathcal{O} = \sum_r C_2(r) \tag{7.24}$$

where $C_2(r)$ is the eigenvalue of the quadratic Casimir operator in the representation r, and the sum runs over all the chiral superfields occurring in the chiral coupling. As the gauge bosons belong to the adjoint representation, we have

$$C_2(r) = \begin{cases} \frac{N^2-1}{2N} & \text{for } SU(N) \\[2mm] \frac{1}{4}X^2 & \text{for } U(1)_X \end{cases} \tag{7.25}$$

Thus we have for $SU(3)_c$,

$$\gamma_{\mathbf{3}_c} = 3 \times \frac{4}{3} = 4 \tag{7.26}$$

as there are three $SU(3)_c$ fields in the $LLLL$ operator [e.g. $(qq)(\tilde{q}\tilde{l})$]. Similarly, we have

$$\gamma_{\mathbf{2}_{L,R}} = 4 \times \frac{3}{4} = 3, \tag{7.27}$$

$$\gamma_{\mathbf{1}_Y} = \frac{1}{4}\left[3\left(\frac{1}{3}\right)^2 + 1\right]\frac{3}{5} = \frac{1}{5}, \tag{7.28}$$

$$\gamma_{\mathbf{1}_{B-L}} = \frac{1}{4}\left[3\left(\frac{1}{3}\right)^2 + 1\right]\frac{3}{2} = \frac{1}{2}, \tag{7.29}$$

where the factors $\frac{3}{5}$ and $\frac{3}{2}$ are the GUT normalization factors for $U(1)_Y$ and $U(1)_{B-L}$ respectively. Note that the same results would have been obtained in a non-supersymmetric gauge, though the calculation is much more involved. For instance, the calculation for the MSSM case in a Wess-Zumino gauge was done in Ref. [267].

Using these anomalous dimensions, we obtain from Eq. (7.23)

$$A_e^{\text{MSSM}} = \left[\frac{\alpha_3(M_S)}{\alpha_3(M_R)}\right]^{-4/3}\left[\frac{\alpha_{2_L}(M_S)}{\alpha_{2_L}(M_R)}\right]^3\left[\frac{\alpha_{1_Y}(M_S)}{\alpha_{1_Y}(M_R)}\right]^{1/33} = 0.91 \tag{7.30}$$

using the MSSM running of the gauge couplings, and similarly,

$$A_e^{\text{SUSYLR}} = \left[\frac{\alpha_3(M_R)}{\alpha_3(M_G)}\right]^{-2}\left[\frac{\alpha_{2_L}(M_R)}{\alpha_{2_L}(M_G)}\right]^{3/2}\left[\frac{\alpha_{2_R}(M_R)}{\alpha_{2_R}(M_G)}\right]^{3/4}\left[\frac{\alpha_{1_{B-L}}(M_R)}{\alpha_{1_{B-L}}(M_G)}\right]^{1/26} = 0.08$$

(7.31)

using the SUSYLR running of the gauge couplings (see Figure 3.1). Combining the results from Eqs. (7.22), (7.30) and (7.31), we get the overall extrapolation factor in bringing the $d = 5$ operators from the GUT scale down to 1 GeV:

$$A_e = A_e^{\text{NS}} A_e^{\text{MSSM}} A_e^{\text{SUSYLR}} = 0.11$$

(7.32)

7.4   QCD Effects

We also need to include the QCD effects in going from a partonic calculation involving three quarks to a hadronic bound state, i.e. the proton. As the low-energy hadrons are involved in the decay, this is a highly non- perturbative process, and it is difficult to calculate the exact form of the hadronic mixing matrix element for the process. Even though various QCD models have been constructed for the purpose, the estimates vary by a factor of $\mathcal{O}(10)$ between the smallest and the largest [280]. As the partial width of the decay is proportional to the matrix element squared, the variation in the estimate of proton lifetime in different models will be $\mathcal{O}(100)$. A different approach using lattice QCD techniques gives more consistent results [281]. We use these lattice results to estimate the chiral symmetry breaking effects which can be parameterized by two hadronic parameters D and F. Then the hadronic mixing matrix for the proton decay can be written as $\frac{\beta}{f_\pi}f(F, D)$ where $f_\pi = (130.4 \pm 0.04 \pm 0.2)$ MeV [22] is the pion decay constant and $|\beta| = 0.0120(26)$ GeV^3 [281] is a low-energy parameter of the $SU(3)_f$ baryon chiral Lagrangian with the baryon number violating interaction. The hadronic

matrix elements $f(F, D)$ can be obtained for different decay channels in the approximation $m_{u,d} \ll m_s \ll m_p$ as well as $-q^2 \ll m_p^2$ where q_μ is the momentum transfer (the momentum of the anti-lepton for physical decays), and summarized in Table 7.2. Here we have chosen the low-energy parameters D and F to be the same as the analogous parameters in weak semileptonic decays [13]. Then $D + F = g_A^{(np)} = 1.27$ is the nucleon axial charge, while $D - F = g_A^{(\Sigma^- n)} = 0.33 - 0.34$ [22]. This gives $D = 0.8$ and $F = 0.47$ which are used in Table 7.2.

Decay mode	$f(F, D)$	$|f(F, D)|^2$
$p \to \pi^0 l^+$	$\frac{1}{\sqrt{2}}(1 + D + F)$	2.58
$p \to \pi^+ \overline{\nu}_l$	$1 + D + F$	5.15
$p \to K^0 l^+$	$1 - \frac{m_N}{m_B}(D - F)$	0.53
$p \to K^+ \overline{\nu}_l$	$\frac{m_N}{m_B}\frac{2D}{3}$	0.19

Table 7.2: The hadronic factors $f(F, D)$ for different proton decay modes. Here we have used $m_N = 0.94$ GeV for the mass of nucleon and $m_B = 1.15$ GeV for the average baryon mass ($m_B \simeq m_\Sigma \simeq m_\Lambda$).

7.5 Proton Decay Rates

Finally, combining all the factors discussed above, the proton decay rate for a given decay mode $p \to Ml$ (M denotes the meson and l the lepton) is given by [269]

$$
\begin{aligned}
\Gamma_p(Ml) &\simeq \frac{m_p}{32\pi M_T^2} \frac{|\beta|^2}{f_\pi^2} \left(\frac{\alpha_2}{4\pi}\right)^2 \left(\frac{m_{\widetilde{W}}}{M_{\widetilde{f}}^2}\right)^2 4|\mathcal{C}|^2 |A_e|^2 |f(F, D)|^2 \\
&\simeq \left(1.6 \times 10^{-49} \text{ GeV}\right) \left(\frac{2 \times 10^{16} \text{ GeV}}{M_T}\right)^2 \left(\frac{m_{\widetilde{W}}}{200 \text{ GeV}}\right)^2 \left(\frac{1 \text{ TeV}}{M_{\widetilde{f}}}\right)^4
\end{aligned}
$$

$$\times \ |\mathcal{C}|^2 |A_e|^2 |f(F,D)|^2 \tag{7.33}$$

where the coefficients $\mathcal{C}$ are given in Table 7.1, the hadronic factors $f(F,D)$ are listed in Table 7.2, and the extrapolation factor A_e is given by Eq. (7.32). Using the triplet Higgsino mass, $M_T \simeq M_G \simeq 4 \times 10^{16}$ GeV in our model [cf. Eq. (3.11)], we obtain the partial lifetimes of different decay modes:

$$\tau_p(Ml) = \frac{\hbar}{\Gamma_p} \simeq \frac{(4.42 \times 10^{33} \text{ years})}{|f(F,D)|^2} \left(\frac{10^{-14}}{|\mathcal{C}|^2} \right) \left(\frac{200 \text{ GeV}}{m_{\widetilde{W}}} \right)^2 \left(\frac{M_{\widetilde{f}}}{1 \text{ TeV}} \right)^4 \tag{7.34}$$

The wino mass, $m_{\widetilde{W}}$, has been constrained at LEP to be larger than ~ 100 GeV [219], essentially independent of any specific model. As a typical value, we choose the universal gaugino mass, $m_{1/2} = 200$ GeV, which when extrapolated to the weak scale gives $m_{\widetilde{W}} \simeq 134$ GeV for the wino mass.

With the Yukawa couplings completely fixed in our model, we can analyze the predictions for the proton decay rate which is discussed below for both models (A) and (B), proposed earlier in this Chapter.

Model (A): As we are interested in obtaining an upper bound on the partial lifetimes of various proton decay modes, we adopt the strategy of varying the mixing parameters x_i's defined by Eq. (7.17) to maximize the expression (7.34) and simultaneously satisfying the present experimental lower bounds [156]. As expected for a SUSY-GUT, we find that the most stringent constraint comes from the $p \to K^+ \bar{\nu}$ decay mode, and for this decay rate to be consistent with the present experimental bound, we must have the sfermion mass $M_{\widetilde{f}} \geq 1.2$ (2.1) TeV for the MSSM $\tan \beta = 10$ (30). This value of $M_{\widetilde{f}}$, when extrapolated to the GUT-scale, puts a lower limit on the universal squark mass m_0 for a given value of $m_{1/2}$. The allowed region in the $m_0 - m_{1/2}$ plane satisfying the proton decay constraints and also satisfying the EWSB constraints is shown in Fig. 7.3. It is clear

that this model favors low values of $\tan\beta$. The model predictions for the upper bound
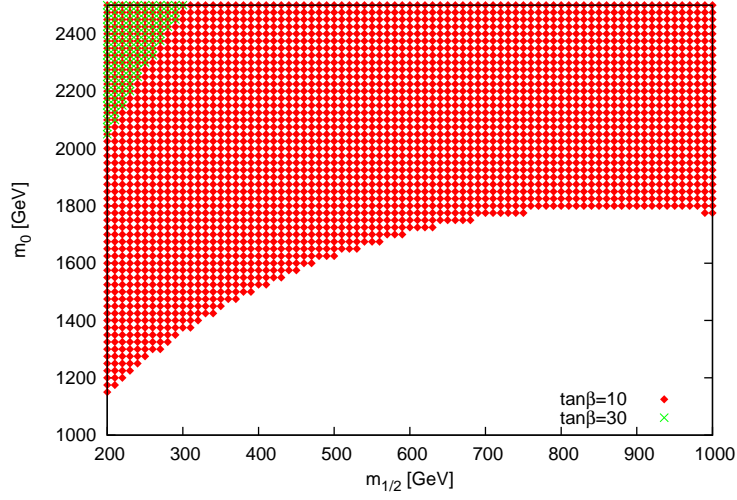
Figure 7.3: Model (A) allowed region in the $m_0 - m_{1/2}$ plane satisfying the proton decay and EWSB constraints for $\tan\beta = 10$ (red) and $\tan\beta = 30$ (green).

Decay mode	Experimental lower limit ($\times 10^{33}$ yr)	Predicted upper limit ($\times 10^{33}$ yr)	
		$\tan\beta = 10$	$\tan\beta = 30$
$p \rightarrow K^+\overline{\nu}$	2.3	2.3	2.3
$p \rightarrow K^0\mu^+$	1.3	399.3	738.8
$p \rightarrow K^0 e^+$	1.0	1.3×10^3	49.7
$p \rightarrow \pi^0 e^+$	10.1	5.8×10^3	230.0
$p \rightarrow \pi^0\mu^+$	6.6	2.4×10^4	1.3×10^4
$p \rightarrow \pi^+\overline{\nu}$	0.025	1.5	0.8

Table 7.3: Model (A) predictions for proton lifetime and present experimental limits.

on partial lifetime of various proton decay modes are given in Table 7.3. We also list the

146

present experimental lower bounds for comparison. As noted above, the most stringent constraint on the parameter space comes from the $p \to K^+ \bar{\nu}$ decay mode; this is due to the fact that the neutrino final states add incoherently for the three generations, and hence, the decay rate for the neutrino final states will be much larger compared to the rates of other decay modes due to the third generation Yukawa coupling dominance. This also explains why the $p \to \pi^+ \bar{\nu}$ decay rate is so large, even though it is Cabibbo-suppressed. The predicted upper bounds for these neutrino final states may be testable in the future proton decay searches, as in the next round of Super-Kamiokande [156] or megaton type detectors such as Hyper-Kamiokande [282].

Model (B): As in the model (A), we maximize the function $|C|^{-2}$ given by Eq. (7.18) with respect to the x_i parameters to find an upper bound on the proton decay lifetime. However, due to the particular structure of the Yukawa matrices in this model, as given by Eqs. (7.16) and (7.17), the parameters x_2 and x_3 have no effect on the amplitude and the only effective mixing parameter is x_1. The experimental lower bounds on the lifetime of various proton decay modes will then put a lower bound on the ratio $\frac{M_{\tilde{f}}^2}{x_1 m_{\widetilde{W}}}$. It turns out that the most stringent bound is $p \to K^+ \bar{\nu}$ ($\pi^0 \mu^+$) for $\tan\beta = 10$ (30) and we must have

$$\frac{M_{\tilde{f}}^2}{x_1 m_{\widetilde{W}}} \geq 1.44 \ (1.06) \times 10^5 \ \text{GeV} \tag{7.35}$$

As an example, for $m_{1/2} = 200$ GeV and $x_1 = 0.1$, it puts a lower bound on the first and second generation squark masses to be $M_{\tilde{f}} \geq 1.4$ (1.2) TeV for $\tan\beta = 10$ (30). The model predictions for $x_1 = 0.1$ for various decay modes are given in Table 7.4. We note that the observation of one of the decay modes in the last two columns of Table 7.4 at a given rate will fix x_1 and the rates for remaining modes (the ones without stars) are then predicted and should provide a test of this model. It should also be noted here that within

147

Decay	Experimental	Predicted upper limit ($\times 10^{33}$ yr)	
mode	lower limit ($\times 10^{33}$ yr)	$\tan\beta = 10$	$\tan\beta = 30$
$p \to K^+\overline{\nu}$	2.3	2.3	3.5
$p \to K^0\mu^+$	1.3	2.3	1.6
$p \to K^0 e^+$	1.0	*	*
$p \to \pi^0 e^+$	10.1	*	*
$p \to \pi^0\mu^+$	6.6	9.8	6.6
$p \to \pi^+\overline{\nu}$	0.025	1.7	2.7

Table 7.4: Model (B) predictions for proton lifetime. Note that in this case, the model does not have any predictions for the decay modes $p \to K^0 e^+$ and $p \to \pi^0 e^+$, because the C coefficients for both these modes involve products of (1,1) elements of the Yukawa coupling matrices, and by construction, these elements are zero for all the three coupling matrices; hence these modes have vanishing decay rates.

the mSUGRA framework at low $\tan\beta$, Tevatron has put a lower limit of 375 GeV for the squark mass based on an integrated luminosity of 1 fb^{-1}. We expect our predicted lower bound on the squark mass which is of order 1 TeV to be testable at higher luminosities within the reach of LHC.

7.6   Effect of R-parity breaking

Another class of dimension-5 operators arising from R-parity breaking Planck suppressed operators These operators are absent in models where **126** Higgs fields break

$B - L$, but are present in our model where the $B - L$ is broken by a $\mathbf{16} \oplus \overline{\mathbf{16}}$ Higgs field. In this section we discuss the implications of these operators on proton life time in our model. This is an interesting exercise in view of the fact that in MSSM embedding into $SU(5)$, relaxing R-parity (or matter parity) conservation leads to new contributions to baryon number violation with arbitrary strength, so that in principle, such models are not viable without matter parity assumption. We would like to study in this section the situation in the case of our $SO(10)$ model.

The most general R-parity violating interactions upto dimension-5 operators in our model are the following:

$$W' = M'_a \psi_a \bar{\psi}_H + \lambda \psi_a \psi_H H + \frac{\lambda_{abc}}{M_{\text{Pl}}} \psi_a \psi_b \psi_c \psi_H + S_a S_b S_c + \mu'^2 S_a \qquad (7.36)$$

where $\psi_{a,b,c}$ denote matter spinors and ψ_H and $\bar{\psi}_H$ are Higgs spinor fields. Before proceeding to discuss their implications, note that M'_a must be of order TeV otherwise the right handed neutrino field would decouple from the low energy sector and break the gauge multiplet required to implement inverse seesaw. There are the following classes of R-parity violating operators that follow from this in conjunction with the superpotential given by Eq. (3.12) at the TeV scale:

$$W'(\text{TeV}) = M'_a L_a^c \bar{\chi}^c + \lambda L \Phi \chi^c + \frac{\lambda_{abc}}{M_{Pl}} \chi^c \left[Q_a^c Q_b^c Q_c^c + L_a Q_b Q_c^c + L_a^c L_b L_c + \cdots \right] \qquad (7.37)$$

Note that the terms within the square bracket, after $B - L$ breaking, give rise to the familiar MSSM R-parity breaking terms with however couplings determined to be of order $\frac{v_{BL}}{M_{\text{Pl}}}$ which is of order 10^{-15}. Hence their contribution to proton decay is negligible. Note this would not be the case with $SO(10)$ models where $B - L$ symmetry is broken at the GUT scale.

Chapter 8

Summary

As we discussed in Chapter 1, there are solid experimental as well as theoretical reasons to believe that even though the standard model has been phenomenally successful in describing all the electroweak precision data, the discovery of its last missing piece, i.e. the Higgs boson would not make it a complete theory of Nature all the way up to the Planck scale. If the SM is indeed just a low-energy effective field theory, the main challenge for us is to understand what lies beyond the SM, and if any of this new physics could solve *all* the problems posed by the SM, while being consistent with the existing low-energy data.

We argued in Chapter 2 that low-energy SUSY is one of the strongest candidates for the new physics and its minimal version solves some major issues unanswered in the SM such as gauge hierarchy problem, coupling unification, electroweak symmetry breaking, dark matter, baryogenesis etc.. However, in order to explain the observed non-zero but small neutrino masses, the minimal supersymmetric standard model must be extended and it is certainly desirable to to construct supersymmetric models for neutrino masses, thus preserving all the nice features of SUSY, and, at the same time, connecting it to the neutrino sector.

A simple paradigm to understand the small neutrino masses is by the "seesaw mechanism" where one adds extra SM gauge singlets which break the $B - L$ symmetry of the SM. The simplest version of seesaw (Type-I), where one adds only one set of heavy Majorana neutrinos, usually requires very large mass $\sim 10^{13-14}$ GeV for these heavy neutrinos

(with $\mathcal{O}(1)$ Yukawa couplings) in order to account for the smallness of the left-handed (LH) neutrinos (hence the name "seesaw"). This makes it impossible to probe this type of seesaw physics at colliders. Lowering the seesaw scale to TeV-range requires tiny Yukawa couplings ($\sim 10^{-6}$), which again makes it difficult to produce these heavy neutrinos at colliders. In Chapter 3, we discussed a different realization of the seesaw mechanism, namely the inverse seesaw, where one adds two sets of SM singlet fermions – one Dirac and one Majorana, in which the smallness of the LH neutrino can be directly attributed to the smallness of the Majorana mass term. Hence, $\mathcal{O}(1)$ Dirac Yukawa couplings can be obtained naturally even at TeV-scale, thus making them "collider-friendly", and extending the scope of the LHC physics search to the neutrino sector.

We noted [120, 151] that the inverse seesaw mechanism can be naturally realized by extending the SM gauge group to the Left-Right symmetric gauge group which restores the parity symmetry and has many interesting phenomenological consequences. We also showed that a TeV-scale supersymmetric version of the LR model with inverse seesaw for neutrino masses leads to a successful gauge coupling unification, unlike its type-I counterpart. We propose this model as a realistic extension of MSSM for neutrino masses, while still preserving all its nice features. We also show this model to be a low-energy realization of an $SO(10)$ SUSY-GUT.

In Chapter 4, we observed [147] that a low-scale LR model with inverse seesaw can also successfully explain the observed baryon asymmetry in our universe by the mechanism of leptogenesis. This result makes the case stronger for the heavy gauge boson searches at the LHC. This is in contrast with the type-I LR models which require the LR scale to be well beyond the reach of colliders for successful leptogenesis.

In Chapter 5, we showed [140] that our model provides a new Dark Matter candidate

151

which is allowed to be light (a few GeV) by the experimental constraints. This might be an important point, if the Dark Matter mass indeed turns out to be in a few GeV range, as suggested by some recent experiments, since the only MSSM candidate, namely the lightest neutralino, is severely constrained by relic density and collider data to be no lighter than 20 GeV or so. Moreover, we established [140] that the light scalar DM candidate in inverse seesaw must be inelastic in nature, with the mass splitting closely connected to the Majorana mass of neutrinos.

We also analyzed [116, 120] the testability of the inverse seesaw mechanism at various experiments at energy and intensity frontiers. At colliders, the striking signal for inverse seesaw is the trilepton final state from the production and decay of the pseudo-Dirac heavy neutrino which could provide a clean signal against a very small background at the LHC. At the intensity frontier, inverse seesaw induces various non-unitarity and LFV effects which might be accessible to the next generation low-energy experiments.

Finally, we discussed [151] proton decay in this class of supersymmetric $SO(10)$ GUTs, and found that the decay rates of the dominant channels are below the experimental bounds for a reasonable squark mass of order TeV which is within reach of the LHC.

In conclusion, a supersymmetric inverse seesaw mechanism for neutrino masses could be considered as an alternative extension to the minimal supersymmetric standard model and offers a rich phenomenology for colliders as well as other low-energy experiments.

Appendix A

Masses of the $SO(10)$ Higgs multiplets

As discussed in Section 3.3.2, we obtain the gauge coupling unification at an acceptable scale only after including the contribution from the color triplets δ, δ^c. This pair of Higgs fields is contained in the **45** representation of Higgs in a generic $SO(10)$ model. However, in principle, there could be other light gauge multiplets of **45** and/or **54** that might contribute to the gauge coupling running as well. Here we argue that in a generic $SO(10)$ model with only $\mathbf{45}_H$ and $\mathbf{54}_H$ representations of Higgs (apart from the essential $\mathbf{10}_H$ and $\mathbf{16}_H$), it is possible to have only the δ's as light states (TeV scale) whereas all the other states are very heavy at GUT scale, and hence, do not contribute to the RG running. It turns out that we need to have at least two $\mathbf{45}_H$'s in our model in order to have these light color triplets.

The most general Higgs superpotential with two $\mathbf{A} \equiv \mathbf{45}$'s and a $\mathbf{E} \equiv \mathbf{54}$ Higgs fields is given by

$$W_H \;\; = \;\; \frac{1}{2} m_1 \mathbf{A}^2 + \frac{1}{2} m_1' \mathbf{A}'^2 + \frac{1}{2} m_2 \mathbf{E}^2 + \lambda_1 \mathbf{E}^3 + \lambda_2 \mathbf{E}\mathbf{A}^2 + \lambda_2' \mathbf{E}\mathbf{A}'^2 + \lambda_3 \mathbf{E}\mathbf{A}\mathbf{A}' \tag{A.1}$$

where we have absorbed the $\mathbf{A}\mathbf{A}'$ term by a redefinition of the fields. The Higgs fields $\mathbf{A}$, $\mathbf{A}'$ and $\mathbf{E}$ contain three directions of singlets (with $\mathbf{A}$ and $\mathbf{A}'$ VEVs parallel) under the SM subgroup $\mathbf{3}_c \mathbf{2}_L \mathbf{1}_Y$ [283]. The corresponding VEVs are defined by

$$\langle \mathbf{A} \rangle = \sum_{i=1}^{2} A_i \widehat{A}_i, \quad \langle \mathbf{A}' \rangle = \sum_{i=1}^{2} A_i' \widehat{A'}_i, \quad \langle \mathbf{E} \rangle = E \widehat{E} \tag{A.2}$$

where in the notation of Ref. [283], the unit directions $\widehat{A}_i$ and $\widehat{E}$ in the Y-diagonal basis

are given by

$$
\begin{aligned}
\widehat{A}_1 &= \widehat{A}^{(1,1,0)}_{(1,1,3)} = \frac{i}{2}[78 + 90] = \widehat{A'}_1, \\
\widehat{A}_2 &= \widehat{A}^{(1,1,0)}_{(15,1,1)} = \frac{i}{\sqrt{6}}[12 + 34 + 56] = \widehat{A'}_2, \\
\widehat{E} &= \widehat{E}^{(1,1,0)}_{(1,1,1)} = \frac{1}{\sqrt{60}}\left(-2 \times [12 + 34 + 56] + 3 \times [78 + 90]\right) \quad\quad\text{(A.3)}
\end{aligned}
$$

where the upper and lower indices denote the $\mathbf{3}_c\mathbf{2}_L\mathbf{1}_Y$ and $\mathbf{4}_c\mathbf{2}_L\mathbf{2}_R$ quantum numbers respectively. The unit directions in Eq. (A.2) satisfy the orthonormality relations

$$
\widehat{A}_i \cdot \widehat{A}_j = \delta_{ij} \quad \text{and} \quad \widehat{E} \cdot \widehat{E} = 1 \quad\quad\text{(A.4)}
$$

The superpotential of Eq. (A.1) calculated at the VEVs in Eq. (A.2) is given by

$$
\begin{aligned}
\langle W_H \rangle &= \frac{1}{2}m_1\langle A \rangle^2 + \frac{1}{2}m_1'\langle A' \rangle^2 + \frac{1}{2}m_2\langle E \rangle^2 \\
&\quad + \lambda_1\langle E \rangle^3 + \lambda_2\langle E \rangle\langle A \rangle^2 + \lambda_2'\langle E \rangle\langle A' \rangle^2 + \lambda_3\langle E \rangle\langle A \rangle\langle A' \rangle \\
&= \frac{1}{2}m_1(A_1^2 + A_2^2) + \frac{1}{2}m_1'(A_1'^2 + A_2'^2) + \frac{1}{2}m_2 E^2 + \frac{\lambda_1}{2\sqrt{15}}E^3 \\
&\quad + \frac{E}{2\sqrt{15}}\left[\lambda_2(3A_1^2 - 2A_2^2) + \lambda_2'(3A_1'^2 - 2A_2'^2) + \lambda_3(3A_1 A_1' - 2A_2 A_2')\right] \text{(A.5)}
\end{aligned}
$$

using the definitions in Eqs. (A.3) and the orthonormality relations given by Eqs. (A.4). The VEVs are determined by the minimization of the superpotential with respect to the fields:

$$
\left\{\frac{\partial}{\partial A_1}, \ \frac{\partial}{\partial A_2}, \ \frac{\partial}{\partial A_1'}, \ \frac{\partial}{\partial A_2'}, \ \frac{\partial}{\partial E}\right\}\langle W_H \rangle = 0 \quad\quad\text{(A.6)}
$$

This yields a set of five equations for A_1, A_2, A_1', A_2' and E:

$$
\begin{aligned}
0 &= m_1 A_1 + \frac{3}{\sqrt{15}}\lambda_2 E A_1 + \frac{3}{2\sqrt{15}}\lambda_3 E A_1', \\
0 &= m_1 A_2 - \frac{2}{\sqrt{15}}\lambda_2 E A_2 - \frac{2}{2\sqrt{15}}\lambda_3 E A_2', \\
0 &= m_1' A_1' + \frac{3}{\sqrt{15}}\lambda_2' E A_1' + \frac{3}{2\sqrt{15}}\lambda_3 E A_1, \quad\quad\text{(A.7)}
\end{aligned}
$$

$$
\begin{aligned}
0 &= m_1' A_2' - \frac{2}{\sqrt{15}} \lambda_2' E A_2' - \frac{2}{2\sqrt{15}} \lambda_3 E A_2, \\
0 &= m_2 E + \frac{1}{2\sqrt{15}} \left[3\lambda_1 E^2 + \lambda_2(3A_1^2 - 2A_2^2) + \lambda_2'(3A_1'^2 - 2A_2'^2) + \lambda_3(3A_1 A_1' - 2A_2 A_2') \right]
\end{aligned}
$$

As in our model, the $SO(10)$ symmetry is broken by the $\mathbf{45}$ and $\mathbf{54}$ VEVs to $\mathbf{3}_c \mathbf{2}_L \mathbf{2}_R \mathbf{1}_{B-L}$ gauge group at the scale M_G, we are interested in the $\mathbf{3}_c \mathbf{2}_L \mathbf{2}_R \mathbf{1}_{B-L}$ symmetry solutions [283] $A_1 = A_1' = 0$, $A_2 \neq 0$, $A_2' \neq 0$, $E \neq 0$. Hence it follows from Eqs. (A.7) that

$$
m_1 - \frac{2\lambda_2 E}{\sqrt{15}} = \frac{\lambda_3 E}{\sqrt{15}} \frac{A_2'}{A_2}, \quad m_1' - \frac{2\lambda_2' E}{\sqrt{15}} = \frac{\lambda_3 E}{\sqrt{15}} \frac{A_2}{A_2'} \tag{A.8}
$$

In order to study the mass matrices, it is convenient to decompose the Higgs representations under the SM gauge group $\mathbf{3}_c \mathbf{2}_L \mathbf{1}_Y$. In Table-3 we present the explicit decompositions of all the Higgs representations under the chain of subgroups

$$
\mathbf{4}_c \mathbf{2}_L \mathbf{2}_R \supset \mathbf{3}_c \mathbf{2}_L \mathbf{2}_R \mathbf{1}_{B-L} \supset \mathbf{3}_c \mathbf{2}_L \mathbf{1}_Y.
$$

Using the Clebsch-Gordan coefficients given in Ref. [283], we obtain the masses of these multiplets as follows. The basis designating the columns (c) of the mass matrices is given in the same way as in Table-3 while the rows (r) are designated by the corresponding complex conjugated $\mathbf{3}_c \mathbf{2}_L \mathbf{1}_Y$ multiplets.

First, we obtain the masses of the multiplet $\left[\left(3, 1, \frac{4}{3} \right) + \text{c.c.} \right]$ in the basis

$$
\text{c} : \widehat{A}_{(15,1,1)}^{\left(3,1,\frac{4}{3}\right)}, \ \widehat{A'}_{(15,1,1)}^{\left(3,1,\frac{4}{3}\right)}; \quad \text{r} : \widehat{A}_{(15,1,1)}^{\left(\bar{3},1,-\frac{4}{3}\right)}, \ \widehat{A'}_{(15,1,1)}^{\left(\bar{3},1,-\frac{4}{3}\right)}
$$

$$
M_\delta^{\left(3,1,\frac{4}{3}\right)} = \begin{pmatrix} m_1 - \frac{2\lambda_2 E}{\sqrt{15}} & -\frac{\lambda_3 E}{\sqrt{15}} \\ -\frac{\lambda_3 E}{\sqrt{15}} & m_1' - \frac{2\lambda_2' E}{\sqrt{15}} \end{pmatrix} = \frac{\lambda_3 E}{\sqrt{15}} \begin{pmatrix} \frac{A_2'}{A_2} & -1 \\ -1 & \frac{A_2}{A_2'} \end{pmatrix} \tag{A.9}
$$

using Eq. (A.8). It is obvious that $\det(M_\delta) = 0$, and hence, one of the two eigenvalues is zero while the other eigenvalue is given by

$$
\text{Tr}(M_\delta) = \frac{\lambda_3 E}{\sqrt{15}} \left(\frac{A_2'}{A_2} + \frac{A_2}{A_2'} \right), \tag{A.10}
$$

155

The zero eigenvalues (six in total) are easily identified as the longitudinal Nambu-Goldstone modes as the $SU(4)_c$ gauge group breaks to $SU(3)_c \times U(1)_{B-L}$ and they acquire mass of order M_G by the usual Higgs mechanism once the $\mathbf{45}_H$ gets VEV at the GUT scale. We keep the other six eigenvalues given by Eq. (A.10) at TeV scale by fine-tuning the coupling λ_3. In what follows, we explicitly calculate the mass eigenvalues for all the other multiplets given by Table-3 and show that it is possible to have only the above six massive δ's at the TeV scale while all the other states of $\mathbf{45}$ and $\mathbf{54}$ are heavy at the GUT-scale.

We note that once we assume λ_3 to be small, the effect of the second $\mathbf{45}_H$ multiplet becomes negligible and we can as well drop the primed terms in the superpotential. For simplicity, we also assume that $A_2 = E \sim M_G$. Then the VEV conditions given by Eqs. (A.7) yield

$$m_1 \simeq \frac{2\lambda_2 E}{\sqrt{15}}, \quad m_2 \simeq \frac{E}{\sqrt{15}}\left(\lambda_2 - \frac{3}{2}\lambda_1\right) \tag{A.11}$$

We list below the mass eigenvalues for all the multiplets given in Table-3.

- (1,1,0) : We have three such states and the mass matrix is given by

$$\text{c} : \widehat{A}^{(1,1,0)}_{(1,1,3)}, \ \widehat{A}^{(1,1,0)}_{(15,1,1)}, \ \widehat{E}^{(1,1,0)}_{(1,1,1)}; \quad \text{r} : \widehat{A}^{(1,1,0)}_{(1,1,3)}, \ \widehat{A}^{(1,1,0)}_{(15,1,1)}, \ \widehat{E}^{(1,1,0)}_{(1,1,1)}$$

$$\begin{pmatrix} m_1 + \frac{3\lambda_2 E}{\sqrt{15}} & 0 & \frac{3\lambda_2 A_1}{\sqrt{15}} \\ 0 & m_1 - \frac{2\lambda_2 E}{\sqrt{15}} & -\frac{2\lambda_2 A_2}{\sqrt{15}} \\ \frac{3\lambda_2 A_1}{\sqrt{15}} & -\frac{2\lambda_2 A_2}{\sqrt{15}} & m_2 + \frac{3\lambda_1 E}{\sqrt{15}} \end{pmatrix} = \frac{E}{\sqrt{15}} \begin{pmatrix} 5\lambda_2 & 0 & 0 \\ 0 & 0 & -2\lambda_2 \\ 0 & -2\lambda_2 & \lambda_2 + \frac{3}{2}\lambda_1 \end{pmatrix}$$

So the mass eigenvalues are

$$M_1^{(1,1,0)} = \frac{5E}{\sqrt{15}}\lambda_2 \neq 0,$$

$$M_2^{(1,1,0)} = \frac{E}{2\sqrt{15}}\left[\left(\lambda_2 + \frac{3}{2}\lambda_1\right) + \sqrt{\left(\lambda_2 + \frac{3}{2}\lambda_1\right)^2 + 16\lambda_2^2}\right] \neq 0,$$

$$M_3^{(1,1,0)} = \frac{E}{2\sqrt{15}}\left[\left(\lambda_2 + \frac{3}{2}\lambda_1\right) - \sqrt{\left(\lambda_2 + \frac{3}{2}\lambda_1\right)^2 + 16\lambda_2^2}\right] \neq 0 \tag{A.12}$$

- $[(1, 1, 2) + \text{c.c.}]$: There is only one such multiplet and its mass is

$$\text{c} \; : \; \widehat{A}^{(1,1,2)}_{(1,1,3)}, \quad \text{r} \; : \; \widehat{A}^{(1,1,-2)}_{(1,1,3)}$$

$$M^{(1,1,2)} = m_1 + \frac{3}{\sqrt{15}}\lambda_2 E = \frac{5E}{\sqrt{15}}\lambda_2 \neq 0 \tag{A.13}$$

- $\left[\left(3, 2, -\frac{5}{3}\right) + \text{c.c.}\right]$: There are two such multiplets and the mass matrix is

$$\text{c} \; : \; \widehat{A}^{\left(3,2,-\frac{5}{3}\right)}_{(6,2,2)}, \; \widehat{E}^{\left(3,2,-\frac{5}{3}\right)}_{(6,2,2)}; \quad \text{r} \; : \; \widehat{A}^{\left(\bar{3},2,\frac{5}{3}\right)}_{(6,2,2)}, \; \widehat{E}^{\left(\bar{3},2,\frac{5}{3}\right)}_{(6,2,2)}$$

$$\begin{pmatrix} m_1 + \frac{\lambda_2 E}{2\sqrt{15}} & -\frac{\lambda_2 A_1}{2} - \frac{\lambda_2 A_2}{\sqrt{6}} \\ -\frac{\lambda_2 A_1}{2} - \frac{\lambda_2 A_2}{\sqrt{6}} & m_2 + \frac{3\lambda_1 E}{2\sqrt{15}} \end{pmatrix} = \frac{\lambda_2 E}{\sqrt{15}}\begin{pmatrix} 3 & -\sqrt{\frac{5}{2}} \\ -\sqrt{\frac{5}{2}} & 1 \end{pmatrix}$$

with the eigenvalues

$$M^{\left(3,2,-\frac{5}{3}\right)}_{1,2} = \frac{E\lambda_2}{2\sqrt{15}}\left[4 \pm \sqrt{14}\right] \neq 0 \tag{A.14}$$

- $\left[\left(3, 2, \frac{1}{3}\right) + \text{c.c.}\right]$: There are two of them and the mass matrix is

$$\text{c} \; : \; \widehat{A}^{\left(3,2,\frac{1}{3}\right)}_{(6,2,2)}, \; \widehat{E}^{\left(3,2,\frac{1}{3}\right)}_{(6,2,2)}; \quad \text{r} \; : \; \widehat{A}^{\left(\bar{3},2,-\frac{1}{3}\right)}_{(6,2,2)}, \; \widehat{E}^{\left(\bar{3},2,-\frac{1}{3}\right)}_{(6,2,2)}$$

$$\begin{pmatrix} m_1 + \frac{\lambda_2 E}{2\sqrt{15}} & \frac{\lambda_2 A_1}{2} - \frac{\lambda_2 A_2}{\sqrt{6}} \\ \frac{\lambda_2 A_1}{2} - \frac{\lambda_2 A_2}{\sqrt{6}} & m_2 + \frac{3\lambda_1 E}{2\sqrt{15}} \end{pmatrix} = \frac{\lambda_2 E}{\sqrt{15}}\begin{pmatrix} 3 & -\sqrt{\frac{5}{2}} \\ -\sqrt{\frac{5}{2}} & 1 \end{pmatrix}$$

with the same eigenvalues as the previous one:

$$M^{\left(3,2,\frac{1}{3}\right)}_{1,2} = \frac{E\lambda_2}{2\sqrt{15}}\left[4 \pm \sqrt{14}\right] \neq 0 \tag{A.15}$$

- $(1,3,0)$: There are also two of them and the mass matrix is

$$\text{c} \; : \; \widehat{A}^{(1,3,0)}_{(1,3,1)}, \; \widehat{E}^{(1,3,0)}_{(1,3,3)}; \quad \text{r} \; : \; \widehat{A}^{(1,3,0)}_{(1,3,1)}, \; \widehat{E}^{(1,3,0)}_{(1,3,3)}$$

$$\begin{pmatrix} m_1 + \frac{3\lambda_2 E}{\sqrt{15}} & \lambda_2 A_1 \\ \lambda_2 A_1 & m_2 + \frac{9\lambda_1 E}{\sqrt{15}} \end{pmatrix} = \frac{E}{\sqrt{15}}\begin{pmatrix} 5\lambda_2 & 0 \\ 0 & \lambda_2 + \frac{15}{2}\lambda_1 \end{pmatrix}$$

So the mass eigenvalues are

$$M^{(1,3,0)}_1 = \frac{5E}{\sqrt{15}}\lambda_2 \neq 0, \quad M^{(1,3,0)}_2 = \frac{E}{\sqrt{15}}\left(\lambda_2 + \frac{15}{2}\lambda_1\right) \neq 0 \tag{A.16}$$

- $[(1, 3, 2) + \text{c.c.}]$: There is only one such multiplet whose eigenvalue is given by

$$\text{c} \; : \; \widehat{E}^{(1,3,2)}_{(1,3,3)}, \quad \text{r} \; : \; \widehat{E}^{(1,3,-2)}_{(1,3,3)}$$

$$M^{(1,3,2)} = m_2 + \frac{9}{\sqrt{15}}\lambda_1 E = \frac{E}{\sqrt{15}}\left(\lambda_2 + \frac{15}{2}\lambda_1\right) \neq 0 \qquad \text{(A.17)}$$

- $\left[\left(6, 1, -\frac{4}{3}\right) + \text{c.c.}\right]$: Its eigenvalue is

$$\text{c} \; : \; \widehat{E}^{\left(6,1,-\frac{4}{3}\right)}_{(20',1,1)}, \quad \text{r} \; : \; \widehat{E}^{\left(6,1,\frac{4}{3}\right)}_{(20',1,1)}$$

$$M^{\left(6,1,-\frac{4}{3}\right)} = m_2 - \frac{6}{\sqrt{15}}\lambda_1 E = \frac{E}{\sqrt{15}}\left(\lambda_2 - \frac{15}{2}\lambda_1\right) \neq 0 \qquad \text{(A.18)}$$

unless $\lambda_2 = \frac{15}{2}\lambda_1$ (which we assume not to be the case).

- (8,1,0) : There are two of them and the mass matrix is

$$\text{c} : \widehat{A}^{(8,1,0)}_{(15,1,1)}, \quad \widehat{E}^{(8,1,0)}_{(20',1,1)}; \quad \text{r} : \widehat{A}^{(8,1,0)}_{(15,1,1)}, \quad \widehat{E}^{(8,1,0)}_{(20',1,1)}$$

$$\begin{pmatrix} m_1 - \frac{2\lambda_2 E}{\sqrt{15}} & \sqrt{\frac{2}{3}}\lambda_2 A_2 \\ \sqrt{\frac{2}{3}}\lambda_2 A_2 & m_2 - \frac{6\lambda_1 E}{\sqrt{15}} \end{pmatrix} = \frac{E}{\sqrt{15}} \begin{pmatrix} 0 & \sqrt{\frac{45}{2}}\lambda_2 \\ \sqrt{\frac{45}{2}}\lambda_2 & \lambda_2 - \frac{15}{2}\lambda_1 \end{pmatrix}$$

with the mass eigenvalues

$$M^{(8,1,0)}_{1,2} = \frac{E}{2\sqrt{15}}\left[\left(\lambda_2 - \frac{15}{2}\lambda_1\right)^2 \pm \sqrt{\left(\lambda_2 - \frac{15}{2}\lambda_1\right)^2 + 90\lambda_2^2}\right] \neq 0 \qquad \text{(A.19)}$$

Thus we see that all the other multiplets have non-zero masses, and moreover, all these masses are of order $E \sim M_G$. Hence, none of these multiplets will contribute to the running of gauge coupling up to the unification scale M_G except the color triplets since these color triplets have masses of order of the SUSY breaking scale.

Note that the $\mathbf{10}_H$-Higgs field also has a color triplet pair $\left[\left(3, 1, -\frac{2}{3}\right) + \text{c.c.}\right]$ under the SM gauge group, apart from the TeV-scale bi-doublet fields $\Phi_{1,2}$ used in the SUSYLR model in Section 4 which reduce to $(1, 2, \pm 1)$ under the SM gauge group. At the GUT-scale, the $\mathbf{H} \equiv \mathbf{10}_H$ field interacts with the $\mathbf{E} \equiv \mathbf{54}_H$ field by the following term in the

superpotential:

$$W_{10} = \frac{1}{2}m_3 \mathbf{H}^2 + \lambda_3 \mathbf{E}\mathbf{H}^2 \tag{A.20}$$

After the $\mathbf{54}_H$ acquires a VEV, this gives rise to the color triplet mass

$$\mathrm{c} \ : \ \widehat{H}_{(6,1,1)}^{\left(3,1,-\frac{2}{3}\right)}; \quad \mathrm{r} \ : \ \widehat{H}_{(6,1,1)}^{\left(\bar{3},1,\frac{2}{3}\right)}$$

$$M^{\left(3,1,\frac{2}{3}\right)} = m_3 - \frac{2\lambda_3 E}{\sqrt{15}} \tag{A.21}$$

while the doublet mass is

$$\mathrm{c} \ : \ \widehat{H}_{(1,2,2)}^{(1,2,1)}; \quad \mathrm{r} \ : \ \widehat{H}_{(1,2,2)}^{(1,2,-1)}$$

$$M^{(1,2,1)} = m_3 + \sqrt{\frac{3}{5}}\lambda_3 E \tag{A.22}$$

We see that the $(1,2,\pm1)$ field can be made light by fine-tuning $m_3 + \sqrt{\frac{3}{5}}\lambda_3 E \sim$ TeV which still leaves the $\left(3,1,\frac{2}{3}\right)$ field heavy (of order M_G).

Finally, let us discuss how only the right handed doublets fields (ϕ_u^c, ϕ_d^c) from $\mathbf{16}_H$-Higgs fields (ψ_H) remain massless at the GUT scale. Note that in the left-right language, the fields in $\mathbf{16}$ are Q_H $(3,2,1,\frac{1}{3}) \oplus Q_H^c$ $(\bar{3},1,2,-\frac{1}{3})$ and ϕ_d^c $(1,2,1,-1) \oplus \phi_u^c(1,1,2,+1)$, and similarly for $\overline{\mathbf{16}}_H \equiv \bar{\psi}_H$ field. The superpotential involving these fields is

$$W_{16} \ = \ M_{16}\bar{\psi}_H\psi_H + \lambda\bar{\psi}_H A\psi_H \tag{A.23}$$

The second coupling has been worked out explicitly in Ref. [284]. On substituting the VEV of the $\mathbf{45}$-Higgs field (A), we get the following masses for the Q_H $(3,2,1,\frac{1}{3}) \oplus Q_H^c$ $(\bar{3},1,2,-\frac{1}{3})$ and ϕ_d^c $(1,2,1,-1) \oplus \phi_u^c(1,1,2,+1)$ fields:

$$M_{Q_H - \overline{Q}_H} = M_{16} + \lambda A_2; \quad M_{Q_H^c - \overline{Q}_H^c} = M_{16} - \lambda A_2;$$

$$M_{\phi_d - \phi_u} = M_{16} - 3\lambda A_2; \quad M_{\phi_d^c - \phi_u^c} = M_{16} + 3\lambda A_2 \tag{A.24}$$

From this we see that to get only the ϕ^c fields light, we have to fine-tune $M_{16} + 3\lambda A_2 \sim$ TeV. With this assumption, all other fields remain heavy at the GUT scale.

$SO(10)$	$\mathbf{4}_c, \mathbf{2}_L, \mathbf{2}_R$	$\mathbf{3}_c, \mathbf{2}_L, \mathbf{2}_R, \mathbf{1}_{B-L}$	$\mathbf{3}_c, \mathbf{2}_L, \mathbf{1}_Y$
10	(1,2,2)	(1,2,2,0)	$(1,2,\pm 1)$
	(6,1,1)	$\left(3,1,1,-\frac{2}{3}\right)$ $\left(\bar{3},1,1,\frac{2}{3}\right)$	$\left(3,1,-\frac{2}{3}\right)$ $\left(\bar{3},1,\frac{2}{3}\right)$
16	(4,2,1)	$\left(3,2,1,\frac{1}{3}\right)$ $(1,2,1,-1)$	$\left(3,2,\frac{1}{3}\right)$ $(1,2,-1)$
	$(\bar{4},1,2)$	$\left(\bar{3},1,2,-\frac{1}{3}\right)$	$\left(\bar{3},1,\frac{2}{3}\right)$ $\left(\bar{3},1,-\frac{4}{3}\right)$
		(1,1,2,1)	(1,1,2) (1,1,0)
45	(1,1,3)	(1,1,3,0)	(1,1,2) (1,1,0) $(1,1,-2)$
	(1,3,1)	(1,3,1,0)	(1,3,0)
	(6,2,2)	$\left(3,2,2,-\frac{2}{3}\right)$	$\left(3,2,\frac{1}{3}\right)$ $\left(3,2,-\frac{5}{3}\right)$
		$\left(\bar{3},2,2,\frac{2}{3}\right)$	$\left(\bar{3},2,\frac{5}{3}\right)$ $\left(\bar{3},2,-\frac{1}{3}\right)$
	(15,1,1)	(1,1,1,0) $\left(3,1,1,\frac{4}{3}\right)$ $\left(\bar{3},1,1,-\frac{4}{3}\right)$ (8,1,1,0)	(1,1,0) $\left(3,1,\frac{4}{3}\right)$ $\left(\bar{3},1,-\frac{4}{3}\right)$ (8,1,0)
54	(1,1,1)	(1,1,1,0)	(1,1,0)
	(1,3,3)	(1,3,3,0)	(1,3,2) (1,3,0) $(1,3,-2)$
	(6,2,2)	$\left(3,2,2,-\frac{2}{3}\right)$	$\left(3,2,\frac{1}{3}\right)$ $\left(3,2,-\frac{5}{3}\right)$
		$\left(\bar{3},2,2,\frac{2}{3}\right)$	$\left(\bar{3},2,\frac{5}{3}\right)$ $\left(\bar{3},2,-\frac{1}{3}\right)$
	$(20',1,1)$	$\left(6,1,1,-\frac{4}{3}\right)$ $\left(\bar{6},1,1,\frac{4}{3}\right)$ (8,1,1,0)	$\left(6,1,-\frac{4}{3}\right)$ $\left(\bar{6},1,\frac{4}{3}\right)$ (8,1,0)

Table A.1: Decomposition of the **10**, **16**, **45** and **54** Higgs representations under the chain of $SO(10)$ subgroups $\mathbf{4}_c\mathbf{2}_L\mathbf{2}_R \supset \mathbf{3}_c\mathbf{2}_L\mathbf{2}_R\mathbf{1}_{B-L} \supset \mathbf{3}_c\mathbf{2}_L\mathbf{1}_Y$.

Appendix B

RGEs for fermion masses and mixing

Given the form of the bi-doublets VEVs as in Eq. (3.16), it immediately follows from the first two terms of the superpotential Eq. (3.13) that the fermion mass matrices can be written as

$$M_u = \frac{1}{\sqrt{2}} v_u y_2, \quad M_d = \frac{1}{\sqrt{2}} v_d y_1, \quad M_e = \frac{1}{\sqrt{2}} v_d y_1', \quad \text{and } M_D = \frac{1}{\sqrt{2}} v_u y_2' \tag{B.1}$$

Henceforth, for clarity, we will denote the Yukawa couplings as

$$h_U \equiv y_2, \quad h_D \equiv y_1, \quad h_E \equiv y_1', \quad h_N \equiv y_2'$$

Then using Eqs. (3.14, 3.15) and (3.17, 3.18) the RGEs for the fermion mass matrices can be written as

$$
\begin{aligned}
16\pi^2 \frac{dM_u}{dt} &= M_u \left[4 h_U^\dagger h_U + 2 h_D^\dagger h_D - \sum_i \tilde{C}_i^{(q)} g_i^2 \right] \\
&\quad + M_d \tan\beta \left[\mathrm{Tr} \left(3 h_D^\dagger h_U + h_E^\dagger h_N \right) + 2 h_D^\dagger h_U + C_{12}^\Phi \right] \tag{B.2} \\
16\pi^2 \frac{dM_d}{dt} &= M_d \left[4 h_D^\dagger h_D + 2 h_U^\dagger h_U - \sum_i \tilde{C}_i^{(q)} g_i^2 \right] \\
&\quad + \frac{M_u}{\tan\beta} \left[\mathrm{Tr} \left(3 h_U^\dagger h_D + h_N^\dagger h_E \right) + 2 h_U^\dagger h_D + C_{21}^\Phi \right] \tag{B.3} \\
16\pi^2 \frac{dM_e}{dt} &= M_e \left[4 h_E^\dagger h_E + 2 h_N^\dagger h_N + C^\phi - \sum_i \tilde{C}_i^{(l)} g_i^2 \right] \\
&\quad + \frac{M_D}{\tan\beta} \left[\mathrm{Tr} \left(3 h_U^\dagger h_D + h_N^\dagger h_E \right) + 2 h_N^\dagger h_E + C_{21}^\Phi \right] \tag{B.4} \\
16\pi^2 \frac{dM_D}{dt} &= M_D \left[4 h_N^\dagger h_N + 2 h_E^\dagger h_E + C^\phi - \sum_i \tilde{C}_i^{(l)} g_i^2 \right] \\
&\quad + M_e \tan\beta \left[\mathrm{Tr} \left(3 h_D^\dagger h_U + h_E^\dagger h_N \right) + 2 h_E^\dagger h_N + C_{12}^\Phi \right] \tag{B.5}
\end{aligned}
$$

where $C_{ab}^{\Phi} = 4\left(\mu_{\alpha}^{\Phi\dagger}\mu_{\alpha}^{\Phi}\right)_{ab}$, $C^{\phi} = y_{S_{\alpha}}^{\dagger}y_{S_{\alpha}}$, and for $i = \mathbf{3}_c$, $\mathbf{2}_L$, $\mathbf{2}_R$, $\mathbf{1}_{B-L}$,

$$\tilde{C}_i^{(q)} = \left(\frac{16}{3}, \frac{3}{2}, \frac{3}{2}, \frac{1}{6}\right), \quad \tilde{C}_i^{(l)} = \left(0, \frac{3}{2}, \frac{3}{2}, \frac{3}{2}\right) \tag{B.6}$$

Note that the second line in each of the above mass RGEs, Eqs. (B.2-B.5), is characteristic of the left-right models, and does not appear in MSSM.

Not all the parameters of the Yukawa matrices are physical. Under an arbitrary unitary transformation on the left(right)-handed fermion fields, $\mathcal{F}_{L(R)} \rightarrow L(R)_f \mathcal{F}_{L(R)}$ (where $\mathcal{F} = U, D, E, N$), the Yukawa matrices undergo a bi-unitary transformation, $h_f \rightarrow L_f h_f R_f^{\dagger}$ and the charged current becomes off-diagonal, with the CKM mixing matrix $L_U L_D^{\dagger}$. We will also have a leptonic counterpart of the CKM matrix that represents the mixing between the charged lepton and Dirac neutrino sector. However, as the running of lepton masses is very mild and we are working only to the one-loop order, we can safely ignore this mixing in the leptonic sector. Moreover, if we assume the CP phase in the Higgs VEV to be zero, then the mass matrices are Hermitian and $L_f = R_f$ (manifest left-right). Thus we may perform scale-dependent unitary transformations $L_f(\mu)$ on the fermion bases so as to diagonalize the Yukawa matrices, and hence the mass matrices, at each scale:

$$\widehat{h}_f(\mu) = L_f(\mu)h_f(\mu)L_f^{\dagger}(\mu), \text{ and } \widehat{M}_f = L_f(\mu)M_f(\mu)L_f^{\dagger}(\mu), \tag{B.7}$$

where $\widehat{h}_f$ and $\widehat{M}_f$ denote the diagonalized Yukawa and mass matrices, respectively.

The RGEs for the physically relevant quantities, namely the mass eigenvalues $\widehat{M}_f(\mu)$ and the scale-dependent CKM matrix $V_{\mathrm{CKM}}(\mu) = L_U(\mu)L_D^{\dagger}(\mu)$, are both contained in the RGEs of $\widehat{M}_f^2(\mu) = L_f^{\dagger}(\mu)M_f(\mu)M_f^{\dagger}(\mu)L_f(\mu)$:

$$\begin{aligned}
\frac{d}{dt}\left(\widehat{M}_u^2\right) &= \left[\dot{L}_U L_U^{\dagger}, \widehat{M}_u^2\right] + \frac{1}{16\pi^2}\left[4\widehat{h}_U^2 + 2\widehat{h}_D^2 - \sum_i \tilde{C}_i^{(q)}g_i^2\right]2\widehat{M}_u^2 \\
&\quad + \frac{1}{16\pi^2}\tan\beta\left[\left\{\mathrm{Tr}\left(3V_{\mathrm{CKM}}\widehat{h}_D V_{\mathrm{CKM}}^{\dagger}\widehat{h}_U\right) + C_{12}^{\Phi}\right\}\left(V_{\mathrm{CKM}}\widehat{M}_d V_{\mathrm{CKM}}^{\dagger}\widehat{M}_u\right)\right.
\end{aligned}$$

$$+2V_{\text{CKM}}\widehat{M}_d\hat{h}_D V_{\text{CKM}}^\dagger \hat{h}_U \widehat{M}_u + \text{h.c.}\Big] \tag{B.8}$$

$$\frac{d}{dt}\left(\widehat{M}_d^2\right) = \left[\dot{L}_D L_D^\dagger, \widehat{M}_d^2\right] + \frac{1}{16\pi^2}\left[4\hat{h}_D^2 + 2\hat{h}_U^2 - \sum_i \tilde{C}_i^{(q)} g_i^2\right] 2\widehat{M}_d^2$$

$$+ \frac{1}{16\pi^2}\frac{1}{\tan\beta}\left[\left\{\text{Tr}\left(3V_{\text{CKM}}\hat{h}_D V_{\text{CKM}}^\dagger \hat{h}_U\right) + C_{12}^\Phi\right\}\left(\widehat{M}_d V_{\text{CKM}}^\dagger \widehat{M}_u V_{\text{CKM}}\right)\right.$$

$$+ 2\widehat{M}_d \hat{h}_D V_{\text{CKM}}^\dagger \hat{h}_U \widehat{M}_u V_{\text{CKM}} + \text{h.c.}\Big] \tag{B.9}$$

$$\frac{d}{dt}\left(\widehat{M}_e^2\right) = \left[\dot{L}_E L_E^\dagger, \widehat{M}_e^2\right] + \frac{1}{16\pi^2}\left[4\hat{h}_E^2 + 2\hat{h}_N^2 + \Re\left(C^\phi\right) - \sum_i \tilde{C}_i^{(l)} g_i^2\right] 2\widehat{M}_e^2 \tag{B.10}$$

$$\frac{d}{dt}\left(\widehat{M}_D^2\right) = \left[\dot{L}_N L_N^\dagger, \widehat{M}_D^2\right] + \frac{1}{16\pi^2}\left[4\hat{h}_N^2 + 2\hat{h}_E^2 + \Re\left(C^\phi\right) - \sum_i \tilde{C}_i^{(l)} g_i^2\right] 2\widehat{M}_D^2 \tag{B.11}$$

where $\dot{L} \equiv \frac{dL}{dt}$ and $\Re\left(C^\phi\right)$ denotes the real part of C^ϕ. The commutator $\left[\dot{L}_f L_f^\dagger, \widehat{M}_f^2\right]$ has vanishing diagonal elements because $\widehat{M}_f^2$ is diagonal. Thus the RGEs for the mass eigenvalues m_f^2 follow immediately from the diagonal entries of Eqs. (B.8-B.11). Using dominance of Yukawa couplings of the third generation over the first two, i.e.

$$y_t^2 \gg y_c^2 \gg y_u^2, \quad y_b^2 \gg y_s^2 \gg y_d^2, \quad y_\tau^2 \gg y_\mu^2 \gg y_e^2, \quad y_{N_3}^2 \gg y_{N_2}^2 \gg y_{N_1}^2,$$

we obtain the following RGEs for the mass eigenvalues of the fermions:

$$16\pi^2 \frac{dm_u}{dt} \simeq \left(4y_u^2 + 2y_d^2 - \sum_i \tilde{C}_i^{(q)} g_i^2\right) m_u + \tan\beta\left[3|V_{tb}|^2 y_b y_t + r_q\right]\sum_{j=d,s,b}|V_{uj}|^2 m_j$$

$$16\pi^2 \frac{dm_c}{dt} \simeq \left(4y_c^2 + 2y_s^2 - \sum_i \tilde{C}_i^{(q)} g_i^2\right) m_c + \tan\beta\left[3|V_{tb}|^2 y_b y_t + r_q\right]\sum_{j=d,s,b}|V_{cj}|^2 m_j$$

$$16\pi^2 \frac{dm_t}{dt} \simeq \left(4y_t^2 + 2y_b^2 - \sum_i \tilde{C}_i^{(q)} g_i^2\right) m_t + \tan\beta\left[\left(3|V_{tb}|^2 + 2\right) y_b y_t + r_q\right]|V_{tb}|^2 m_b$$

$$16\pi^2 \frac{dm_d}{dt} \simeq \left(4y_d^2 + 2y_u^2 - \sum_i \tilde{C}_i^{(q)} g_i^2\right) m_d + \frac{1}{\tan\beta}\left[3|V_{tb}|^2 y_b y_t + r_q\right]\sum_{j=u,c,t}|V_{jd}|^2 m_j$$

$$16\pi^2 \frac{dm_s}{dt} \simeq \left(4y_s^2 + 2y_c^2 - \sum_i \tilde{C}_i^{(q)} g_i^2\right) m_s + \frac{1}{\tan\beta}\left[3|V_{tb}|^2 y_b y_t + r_q\right]\sum_{j=u,c,t}|V_{js}|^2 m_j$$

$$16\pi^2 \frac{dm_b}{dt} \simeq \left(4y_b^2 + 2y_t^2 - \sum_i \tilde{C}_i^{(q)} g_i^2\right) m_b + \frac{1}{\tan\beta}\left[\left(3|V_{tb}|^2 + 2\right) y_b y_t + r_q\right]|V_{tb}|^2 m_t$$

$$16\pi^2 \frac{dm_e}{dt} \simeq \left(4y_e^2 + 2y_{N_1}^2 + r_l - \sum_i \tilde{C}_i^{(l)} g_i^2\right) m_e$$

$$16\pi^2 \frac{dm_\mu}{dt} \simeq \left(4y_\mu^2 + 2y_{N_2}^2 + r_l - \sum_i \tilde{C}_i^{(l)} g_i^2\right) m_\mu$$

$$16\pi^2 \frac{dm_\tau}{dt} \simeq \left(4y_\tau^2 + 2y_{N_3}^2 + r_l - \sum_i \tilde{C}_i^{(l)} g_i^2\right) m_\tau$$

$$16\pi^2 \frac{dm_{N_1}}{dt} \simeq \left(4y_{N_1}^2 + 2y_e^2 + r_l - \sum_i \tilde{C}_i^{(l)} g_i^2\right) m_{N_1}$$

$$16\pi^2 \frac{dm_{N_2}}{dt} \simeq \left(4y_{N_2}^2 + 2y_\mu^2 + r_l - \sum_i \tilde{C}_i^{(l)} g_i^2\right) m_{N_2}$$

$$16\pi^2 \frac{dm_{N_3}}{dt} \simeq \left(4y_{N_3}^2 + 2y_\tau^2 + r_l - \sum_i \tilde{C}_i^{(l)} g_i^2\right) m_{N_3} \tag{B.12}$$

where $r_q = \Re\left(C_{12}^\Phi\right)$ and $r_l = \Re\left(C^\phi\right)$.

The VEV RGEs, Eqs. (3.18) and (3.17), for third generation dominance become

$$16\pi^2 \frac{dv_u}{dt} \simeq v_u \left[\frac{3}{2}g_{2L}^2 + \frac{3}{2}g_{2R}^2 - 3y_t^2 - y_{N_3}^2 - C_{22}^\Phi\right], \tag{B.13}$$

$$16\pi^2 \frac{dv_d}{dt} \simeq v_d \left[\frac{3}{2}g_{2L}^2 + \frac{3}{2}g_{2R}^2 - 3y_b^2 - y_\tau^2 - C_{11}^\Phi\right] \tag{B.14}$$

The RGE for the CKM matrix $V_{\text{CKM}} = L_U L_D^\dagger$ is given by

$$\frac{d}{dt}V_{\text{CKM}} = \dot{L}_U L_D^\dagger + L_U \dot{L}_D^\dagger = \dot{L}_U L_U^\dagger V_{\text{CKM}} - V_{\text{CKM}} \dot{L}_D L_D^\dagger,$$

$$\text{or,} \quad \frac{d}{dt}V_{\alpha\beta} = \sum_{\gamma=u,c,t} \left(\dot{L}_U L_U^\dagger\right)_{\alpha\gamma} V_{\gamma\beta} - \sum_{\gamma=d,s,b} V_{\alpha\gamma} \left(\dot{L}_D L_D^\dagger\right)_{\gamma\beta} \tag{B.15}$$

However, the diagonal elements of $\dot{L}_{U,D} L_{U,D}^\dagger$ are not determined by Eqs. (B.8) and (B.9). This is because Eq. (B.7) determines $L_{U,D}$ only up to right multiplication by a diagonal matrix of scale-dependent phases. These undetermined phases contribute arbitrary imaginary functions to the diagonal elements of $\dot{L}_{U,D} L_{U,D}^\dagger$. But the off-diagonal elements are unambiguously determined because they receive no contribution from the phases. We can, nevertheless, make the diagonal entries of $\dot{L}_{U,D} L_{U,D}^\dagger$, which are manifestly imaginary, vanish by an appropriate choice of phases. With this choice of phases, we can then obtain the RGEs for the CKM matrix elements using Eq. (B.15):

$$\frac{d}{dt}V_{\alpha\beta} = \sum_{\substack{\gamma=u,c,t \\ \gamma\neq\alpha}} \left(\dot{L}_U L_U^\dagger\right)_{\alpha\gamma} V_{\gamma\beta} - \sum_{\substack{\gamma=d,s,b \\ \gamma\neq\beta}} V_{\alpha\gamma} \left(\dot{L}_D L_D^\dagger\right)_{\gamma\beta}$$

$$
= \frac{1}{16\pi^2} \left(\sum_{\substack{\gamma=u,c,t \\ \gamma\neq\alpha}} \left[\frac{\tan\beta}{m_\alpha - m_\gamma} \left\{ \mathrm{Tr}\left(3V\widehat{h}_D V^\dagger \widehat{h}_U\right) + r_q \right\} \left(V\widehat{M}_d V^\dagger\right)_{\alpha\gamma} \right.\right.
$$

$$
\left. + \frac{4}{v_d^2} \frac{m_\alpha^2 + m_\gamma^2}{m_\alpha^2 - m_\gamma^2} \left(V\widehat{M}_d^2 V^\dagger\right)_{\alpha\gamma} \right] V_{\gamma\beta}
$$

$$
- \sum_{\substack{\gamma=d,s,b \\ \gamma\neq\beta}} V_{\alpha\gamma} \left[\frac{1}{\tan\beta(m_\gamma - m_\beta)} \left\{ \mathrm{Tr}\left(3V\widehat{h}_D V^\dagger \widehat{h}_U\right) + r_q \right\} \left(V^\dagger \widehat{M}_u V\right)_{\gamma\beta} \right.
$$

$$
\left.\left. + \frac{4}{v_u^2} \frac{m_\gamma^2 + m_\beta^2}{m_\gamma^2 - m_\beta^2} \left(V^\dagger \widehat{M}_u^2 V\right)_{\gamma\beta} \right] \right) \tag{B.16}
$$

As before, we use the third generation dominance and get the following RGEs for $V_{\alpha\beta}$:

$$
16\pi^2 \frac{d}{dt} V_{ud} \simeq -\tan\beta\left(3|V_{tb}|^2 y_b y_t + r_q\right) \left[\frac{\left(V\widehat{M}_d V^\dagger\right)_{uc} V_{cd}}{m_c} + \frac{\left(V\widehat{M}_d V^\dagger\right)_{ut} V_{td}}{m_t} \right]
$$

$$
- \frac{4}{v_d^2} \left[\left(V\widehat{M}_d^2 V^\dagger\right)_{uc} V_{cd} + \left(V\widehat{M}_d^2 V^\dagger\right)_{ut} V_{td} \right]
$$

$$
- \frac{1}{\tan\beta}\left(3|V_{tb}|^2 y_b y_t + r_q\right) \left[\frac{V_{us}\left(V^\dagger \widehat{M}_u V\right)_{sd}}{m_s} + \frac{V_{ub}\left(V^\dagger \widehat{M}_u V\right)_{bd}}{m_b} \right]
$$

$$
- \frac{4}{v_u^2} \left[V_{us}\left(V^\dagger \widehat{M}_u^2 V\right)_{sd} + V_{ub}\left(V^\dagger \widehat{M}_u^2 V\right)_{bd} \right]
$$

$$
16\pi^2 \frac{d}{dt} V_{us} \simeq -\tan\beta\left(3|V_{tb}|^2 y_b y_t + r_q\right) \left[\frac{\left(V\widehat{M}_d V^\dagger\right)_{uc} V_{cs}}{m_c} + \frac{\left(V\widehat{M}_d V^\dagger\right)_{ut} V_{ts}}{m_t} \right]
$$

$$
- \frac{4}{v_d^2} \left[\left(V\widehat{M}_d^2 V^\dagger\right)_{uc} V_{cs} + \left(V\widehat{M}_d^2 V^\dagger\right)_{ut} V_{ts} \right]
$$

$$
- \frac{1}{\tan\beta}\left(3|V_{tb}|^2 y_b y_t + r_q\right) \left[-\frac{V_{ud}\left(V^\dagger \widehat{M}_u V\right)_{ds}}{m_s} + \frac{V_{ub}\left(V^\dagger \widehat{M}_u V\right)_{bs}}{m_b} \right]
$$

$$
- \frac{4}{v_u^2} \left[-V_{ud}\left(V^\dagger \widehat{M}_u^2 V\right)_{ds} + V_{ub}\left(V^\dagger \widehat{M}_u^2 V\right)_{bs} \right]
$$

$$
16\pi^2 \frac{d}{dt} V_{ub} \simeq -\tan\beta\left(3|V_{tb}|^2 y_b y_t + r_q\right) \left[\frac{\left(V\widehat{M}_d V^\dagger\right)_{uc} V_{cb}}{m_c} + \frac{\left(V\widehat{M}_d V^\dagger\right)_{ut} V_{tb}}{m_t} \right]
$$

$$
- \frac{4}{v_d^2} \left[\left(V\widehat{M}_d^2 V^\dagger\right)_{uc} V_{cb} + \left(V\widehat{M}_d^2 V^\dagger\right)_{ut} V_{tb} \right]
$$

$$
+ \frac{1}{m_b \tan\beta}\left(3|V_{tb}|^2 y_b y_t + r_q\right) \left[V_{ud}\left(V^\dagger \widehat{M}_u V\right)_{db} + V_{us}\left(V^\dagger \widehat{M}_u V\right)_{sb} \right]
$$

$$
+ \frac{4}{v_u^2} \left[V_{ud}\left(V^\dagger \widehat{M}_u^2 V\right)_{db} + V_{us}\left(V^\dagger \widehat{M}_u^2 V\right)_{sb} \right]
$$

$$
16\pi^2 \frac{d}{dt} V_{cd} \simeq -\tan\beta\left(3|V_{tb}|^2 y_b y_t + r_q\right) \left[-\frac{\left(V\widehat{M}_d V^\dagger\right)_{cu} V_{ud}}{m_c} + \frac{\left(V\widehat{M}_d V^\dagger\right)_{ct} V_{td}}{m_t} \right]
$$

$$-\frac{4}{v_d^2}\left[-\left(V\widehat{M}_d^2V^\dagger\right)_{cu}V_{ud}+\left(V\widehat{M}_d^2V^\dagger\right)_{ct}V_{td}\right]$$

$$-\frac{1}{\tan\beta}\left(3|V_{tb}|^2y_by_t+r_q\right)\left[\frac{V_{cs}\left(V^\dagger\widehat{M}_uV\right)_{sd}}{m_s}+\frac{V_{cb}\left(V^\dagger\widehat{M}_uV\right)_{bd}}{m_b}\right]$$

$$-\frac{4}{v_u^2}\left[V_{cs}\left(V^\dagger\widehat{M}_u^2V\right)_{sd}+V_{cb}\left(V^\dagger\widehat{M}_u^2V\right)_{bd}\right]$$

$$16\pi^2\frac{d}{dt}V_{cs}\simeq-\tan\beta\left(3|V_{tb}|^2y_by_t+r_q\right)\left[-\frac{\left(V\widehat{M}_dV^\dagger\right)_{cu}V_{us}}{m_c}+\frac{\left(V\widehat{M}_dV^\dagger\right)_{ct}V_{ts}}{m_t}\right]$$

$$-\frac{4}{v_d^2}\left[-\left(V\widehat{M}_d^2V^\dagger\right)_{cu}V_{us}+\left(V\widehat{M}_d^2V^\dagger\right)_{ct}V_{ts}\right]$$

$$-\frac{1}{\tan\beta}\left(3|V_{tb}|^2y_by_t+r_q\right)\left[-\frac{V_{cd}\left(V^\dagger\widehat{M}_uV\right)_{ds}}{m_s}+\frac{V_{cb}\left(V^\dagger\widehat{M}_uV\right)_{bs}}{m_b}\right]$$

$$-\frac{4}{v_u^2}\left[-V_{cd}\left(V^\dagger\widehat{M}_u^2V\right)_{ds}+V_{cb}\left(V^\dagger\widehat{M}_u^2V\right)_{bs}\right]$$

$$16\pi^2\frac{d}{dt}V_{cb}\simeq-\tan\beta\left(3|V_{tb}|^2y_by_t+r_q\right)\left[-\frac{\left(V\widehat{M}_dV^\dagger\right)_{cu}V_{ub}}{m_c}+\frac{\left(V\widehat{M}_dV^\dagger\right)_{ct}V_{tb}}{m_t}\right]$$

$$-\frac{4}{v_d^2}\left[-\left(V\widehat{M}_d^2V^\dagger\right)_{cu}V_{ub}+\left(V\widehat{M}_d^2V^\dagger\right)_{ct}V_{tb}\right]$$

$$+\frac{1}{m_b\tan\beta}\left(3|V_{tb}|^2y_by_t+r_q\right)\left[V_{cd}\left(V^\dagger\widehat{M}_uV\right)_{db}+V_{cs}\left(V^\dagger\widehat{M}_uV\right)_{sb}\right]$$

$$+\frac{4}{v_u^2}\left[V_{cd}\left(V^\dagger\widehat{M}_u^2V\right)_{db}+V_{cs}\left(V^\dagger\widehat{M}_u^2V\right)_{sb}\right]$$

$$16\pi^2\frac{d}{dt}V_{td}\simeq\frac{\tan\beta}{m_t}\left(3|V_{tb}|^2y_by_t+r_q\right)\left[\left(V\widehat{M}_dV^\dagger\right)_{tu}V_{ud}+\left(V\widehat{M}_dV^\dagger\right)_{tc}V_{cd}\right]$$

$$+\frac{4}{v_d^2}\left[\left(V\widehat{M}_d^2V^\dagger\right)_{tu}V_{ud}+\left(V\widehat{M}_d^2V^\dagger\right)_{tc}V_{cd}\right]$$

$$-\frac{1}{\tan\beta}\left(3|V_{tb}|^2y_by_t+r_q\right)\left[\frac{V_{ts}\left(V^\dagger\widehat{M}_uV\right)_{sd}}{m_s}+\frac{V_{tb}\left(V^\dagger\widehat{M}_uV\right)_{bd}}{m_b}\right]$$

$$-\frac{4}{v_u^2}\left[V_{ts}\left(V^\dagger\widehat{M}_u^2V\right)_{sd}+V_{tb}\left(V^\dagger\widehat{M}_u^2V\right)_{bd}\right]$$

$$16\pi^2\frac{d}{dt}V_{ts}\simeq\frac{\tan\beta}{m_t}\left(3|V_{tb}|^2y_by_t+r_q\right)\left[\left(V\widehat{M}_dV^\dagger\right)_{tu}V_{us}+\left(V\widehat{M}_dV^\dagger\right)_{tc}V_{cs}\right]$$

$$+\frac{4}{v_d^2}\left[\left(V\widehat{M}_d^2V^\dagger\right)_{tu}V_{us}+\left(V\widehat{M}_d^2V^\dagger\right)_{tc}V_{cs}\right]$$

$$-\frac{1}{\tan\beta}\left(3|V_{tb}|^2y_by_t+r_q\right)\left[-\frac{V_{td}\left(V^\dagger\widehat{M}_uV\right)_{ds}}{m_s}+\frac{V_{tb}\left(V^\dagger\widehat{M}_uV\right)_{bs}}{m_b}\right]$$

$$-\frac{4}{v_u^2}\left[-V_{td}\left(V^\dagger\widehat{M}_u^2V\right)_{ds}+V_{tb}\left(V^\dagger\widehat{M}_u^2V\right)_{bs}\right]$$

$$16\pi^2 \frac{d}{dt} V_{tb} \simeq \frac{\tan\beta}{m_t} \left(3|V_{tb}|^2 y_b y_t + r_q \right) \left[\left(V\widehat{M}_d V^\dagger \right)_{tu} V_{ub} + \left(V\widehat{M}_d V^\dagger \right)_{tc} V_{cb} \right]$$
$$+ \frac{4}{v_d^2} \left[\left(V\widehat{M}_d^2 V^\dagger \right)_{tu} V_{ub} + \left(V\widehat{M}_d^2 V^\dagger \right)_{tc} V_{cb} \right]$$
$$+ \frac{1}{m_b \tan\beta} \left(3|V_{tb}|^2 y_b y_t + r_q \right) \left[V_{td} \left(V^\dagger \widehat{M}_u V \right)_{db} + V_{ts} \left(V^\dagger \widehat{M}_u V \right)_{sb} \right]$$
$$+ \frac{4}{v_u^2} \left[V_{td} \left(V^\dagger \widehat{M}_u^2 V \right)_{db} + V_{ts} \left(V^\dagger \widehat{M}_u^2 V \right)_{sb} \right] \tag{B.17}$$

We have presented the results for these RGEs even though they look quite messy because we believe this is the first time such an analysis has been carried out in the SUSYLR model, and these analytical results at the one-loop level may be useful later for future work in this direction.

In order to solve these mass and mixing RGEs numerically, we need to know the initial values for all the 23 variables (12 masses, 9 CKM elements and 2 VEVs). We know the experimental values at $Q = m_Z$ for all of them except for the Dirac neutrino masses m_{N_i}. We fix these values by iterations using the GUT-scale predicted values, $m_{N_i}(M_G)$, which, in turn, are determined completely in terms of the other fermion masses at the GUT-scale in $SO(10)$ GUT models. Here we note that adjusting the GUT-scale values of m_{N_i} to fit the $SO(10)$ model prediction do not change the other fermion masses at this scale significantly even though they are all coupled equations because of the mild running of the neutrino masses. Hence the mass and mixing values given in Eqs. (3.19) can be considered as generic and independent of the specific $SO(10)$ model chosen.

We also have the free parameters r_q and r_l corresponding to the couplings μ_α^Φ and y_{S_α}. Assuming the couplings μ_α to be the same $\forall\, \alpha = 1, 2, 3$, we have

$$C_{ab}^\Phi = 4 \left(\mu_\alpha^{\Phi\dagger} \mu_\alpha^\Phi \right)_{ab} = 12 \left(\mu^{\Phi\dagger} \mu^\Phi \right)_{ab} = 12 \sum_{c=1}^{2} \mu_{ca}^{\Phi*} \mu_{cb}^\Phi$$
$$C^\phi = y_{S_\alpha}^\dagger y_{S_\alpha} = 3 y_S^\dagger y_S$$

Further assuming $\mu_{ab}^{\Phi} = \mu_{\phi} \; \forall \; a, \; b = 1, 2$, we have

$$r_q = 24|\mu_{\phi}|^2, \; r_l = 3|y_S|^2$$

where μ_{ϕ} and y_S can take values between 0 and 4π (for the theory to remain perturbative).

For the running behavior shown in Figures 3.2 and 3.3, we have chosen $\mu_{\phi} = 0.01$ and $y_S = 0.46$ (requiring $b - \tau$ unification) and the initial values of the Dirac neutrino masses

$$m_{N_1}(M_R) = 0.0031 \text{ GeV}, \quad m_{N_2}(M_R) = 0.2825 \text{ GeV}, \quad m_{N_3} = 71.86 \text{ GeV}$$

such that the masses evaluated at the GUT-scale, $m_{N_i}(M_G)$, agree with those predicted from the specific $SO(10)$ model described in Section 6. For consistency check, we note that the $SO(10)$ model predicted eigenvalues of M_D given by Eq. (3.36),

$$m_{N_i}^{\text{predicted}} = (0.0028, \; 0.2538, \; 77.8046) \text{ GeV},$$

agree quite well with those obtained from the RGEs,

$$m_{N_i}^{\text{RG}}(M_G) = (0.0028, \; 0.2538, \; 77.8106) \text{ GeV}.$$

Appendix C

RGEs for soft SUSY-breaking masses in SUSYLR model

Assuming R-parity conservation and the trilinear couplings A's and Y's in the superpotential and soft breaking Lagrangian given by Eqs. (3.13) and (3.21) to be zero, the soft breaking mass RGEs at one-loop level are given by [161]

$$
16\pi^2 \frac{d}{dt} m_Q^2 = 2m_Q^2 y_a y_a^\dagger + y_a \left(2y_a^\dagger m_Q^2 + 4m_{Q^c}^2 y_a^\dagger + 4m_{\Phi_{ab}}^2 y_b^\dagger \right)
$$
$$
- \frac{1}{3} M_1 M_1^\dagger g_1^2 - 6 M_{2L} M_{2L}^\dagger g_{2L}^2 - \frac{32}{3} M_3 M_3^\dagger g_3^2 + \frac{1}{8} g_1^2 S_2, \quad \text{(C.1)}
$$

$$
16\pi^2 \frac{d}{dt} m_{Q^c}^2 = 2m_{Q^c}^2 y_a^\dagger y_a + y_a^\dagger \left(2y_a m_{Q^c}^2 + 4m_Q^2 y_a + 4y_b m_{\Phi_{ba}}^2 \right)
$$
$$
- \frac{1}{3} M_1 M_1^\dagger g_1^2 - 6 M_{2R} M_{2R}^\dagger g_{2R}^2 - \frac{32}{3} M_3 M_3^\dagger g_3^2 - \frac{1}{8} g_1^2 S_2, \quad \text{(C.2)}
$$

$$
16\pi^2 \frac{d}{dt} m_L^2 = 2m_L^2 y_a' y_a'^\dagger + y_a' \left(2y_a'^\dagger m_L^2 + 4m_{L^c}^2 y_a'^\dagger + 4m_{\Phi_{ab}}^2 y_b'^\dagger \right)
$$
$$
- 3 M_1 M_1^\dagger g_1^2 - 6 M_{2L} M_{2L}^\dagger g_{2L}^2 - \frac{3}{8} g_1^2 S_2, \quad \text{(C.3)}
$$

$$
16\pi^2 \frac{d}{dt} m_{L^c}^2 = 2m_{L^c}^2 y_a'^\dagger y_a' + y_a'^\dagger \left(2y_a' m_{L^c}^2 + 4m_L^2 y_a' + 4y_b' m_{\Phi_{ba}}^2 \right)
$$
$$
+ 2y_S^{\alpha\dagger} \left[m_{L^c}^2 y_S^\alpha + m_{\phi_d^c}^2 y_S^\alpha + y_S^\beta \left(m_S^2 \right)_{\beta\alpha} \right]
$$
$$
- 3 M_1 M_1^\dagger g_1^2 - 6 M_{2R} M_{2R}^\dagger g_{2R}^2 + \frac{3}{8} g_1^2 S_2, \quad \text{(C.4)}
$$

$$
16\pi^2 \frac{d}{dt} m_{\phi_d^c}^2 = 2y_S \alpha^\dagger \left[m_{L^c}^2 y_S^\alpha + m_{\phi_d^c}^2 y_S^\alpha + y_S^\beta \left(m_S^2 \right)_{\beta\alpha} \right]
$$
$$
- 3 M_1 M_1^\dagger g_1^2 - 6 M_{2R} M_{2R}^\dagger g_{2R}^2 - \frac{3}{8} g_1^2 S_2, \quad \text{(C.5)}
$$

$$
16\pi^2 \frac{d}{dt} m_{\phi_u^c}^2 = -3 M_1 M_1^\dagger g_1^2 - 6 M_{2R} M_{2R}^\dagger g_{2R}^2 + \frac{3}{8} g_1^2 S_2, \quad \text{(C.6)}
$$

$$
16\pi^2 \frac{d}{dt} \left(m_S^2 \right)^{\alpha\beta} = 4y_S^{\alpha\dagger} y_S^\beta \left(m_{\phi_d^c}^2 + m_{L^c}^2 \right) + 8\text{Tr}(\mu_\Phi^{\alpha\dagger} \mu_\Phi^\rho) \left(m_S^2 \right)_{\rho\beta}, \quad \text{(C.7)}
$$

$$
16\pi^2 \frac{d}{dt} m_{\Phi_{ab}}^2 = m_{\Phi_{ac}}^2 \text{Tr} \left(3y_c^\dagger y_b + y_c'^\dagger y_b' \right) + \text{Tr} \left(3y_a^\dagger y_c + y_a'^\dagger y_c' \right) m_{\Phi_{cb}}^2
$$
$$
+ \text{Tr} \left(6y_a^\dagger y_b m_{Q^c}^2 + 6y_a^\dagger m_Q^2 y_b + 2y_a'^\dagger y_b' m_{L^c}^2 + 2y_a'^\dagger m_L^2 y_b' \right)
$$

169

$$+ \left(-6 M_{2L} M_{2L}^{\dagger} g_{2L}^2 - 6 M_{2R} M_{2R}^{\dagger} g_{2R}^2 \right) \delta_{ab} \tag{C.8}$$

where

$$S_2 \equiv 4 \left[\text{Tr} \left(m_Q^2 - m_{Q^c}^2 - m_L^2 + m_{L^c}^2 \right) + \left(m_{\phi_u^c}^2 - m_{\phi_d^c}^2 \right) \right] \tag{C.9}$$

We have ignored the RG running of the coupling y_S^α as these are higher order effects.

Appendix D

CP-Asymmetry for Leptogenesis in Inverse Seesaw

The full Majorana mass matrix in the flavor basis (N_i, S_i) is given by

$$\mathcal{M} = \begin{pmatrix} 0 & M_N \\ M_N^T & \mu_S/2 \end{pmatrix} \tag{D.1}$$

where for $i = 1, 2, 3$, both M_N and μ_S are 3×3 symmetric matrices. The Yukawa Lagrangian in this basis is given by (with $i, j = 1, 2, 3$)

$$\mathcal{L}_y = y_{i\alpha} \overline{N}_i \Phi^\dagger l_\alpha + M_{N_{ij}} N_i^T C^{-1} S_j + \frac{1}{2} \mu_{ij} S_i^T C^{-1} S_j + \text{ h.c.} \tag{D.2}$$

In order to calculate the *CP* asymmetry in this framework, it is more convenient to work in the basis in which the RH Majorana neutrino mass matrix is diagonal with real and positive eigenvalues. The Lagrangian in this basis is given by (with $i = 1, 2, \cdots, 6$)

$$\mathcal{L}_h = h_{i\alpha} \overline{\tilde{N}}_i \Phi l_\alpha + \frac{1}{2} M_i \tilde{N}_i^T C^{-1} \tilde{N}_i + \text{h.c.} \tag{D.3}$$

Analytically, the exact diagonalization of the full 6×6 mass matrix $\mathcal{M}$ is extremely involved and we cannot obtain a closed form expression for the *CP*-asymmetry in this case. However, we can study the dependence of the small *L*-violating parameter μ_S in some special cases, viz. when the μ_S-matrix is completely diagonal or completely off-diagonal, as in these cases the Majorana mass matrix reduces to a block diagonal form. In this section, we derive the analytical expression for the *CP*-asymmetry in these two limits and for two sets of RH neutrinos, i.e. for (N_i, S_i) with $i = 1, 2$. The $i = 3$ case reduces to this limit if one of the masses is much heavier and hence decouples from the other two.

We consider the 4×4 version of the Majorana mass matrix $\mathcal{M}$:

$$\mathcal{M}_{4\times 4} = \begin{pmatrix} 0 & M_{N_{2\times 2}} \\ M_{N_{2\times 2}} & \mu_{2\times 2} \end{pmatrix}, \tag{D.4}$$

where without loss of generality we choose the mass matrix M_N to be diagonal with real positive eigenvalues $M_{N_{1,2}}$. However, the elements of the μ_S-matrix are, in general, complex quantities. Now we consider two special cases:

Case I − μ_S purely diagonal: In this case, the Majorana mass matrix can be reduced to a simple block diagonal form which decouples the (N_1, S_1) and (N_2, S_2) sectors:

$$\mathcal{M} = \begin{pmatrix} 0 & 0 & M_{N_1} & 0 \\ 0 & 0 & 0 & M_{N_2} \\ M_{N_1} & 0 & \mu_{11} & 0 \\ 0 & M_{N_2} & 0 & \mu_{22} \end{pmatrix} \xrightarrow{r_2 \leftrightarrow r_3, c_2 \leftrightarrow c_3} \begin{pmatrix} 0 & M_{N_1} & 0 & 0 \\ M_{N_1} & \mu_{11} & 0 & 0 \\ 0 & 0 & 0 & M_{N_2} \\ 0 & 0 & M_{N_2} & \mu_{22} \end{pmatrix}. \tag{D.5}$$

Then in the (N_i, S_i) flavor basis, we have the 2×2 matrices

$$\tilde{M}_i = \begin{pmatrix} 0 & M_{N_i} \\ M_{N_i} & \mu_{ii} \end{pmatrix} = \begin{pmatrix} 0 & M_{N_i} \\ M_{N_i} & \varepsilon_i M_{N_i} e^{i\theta_i} \end{pmatrix}, \tag{D.6}$$

where $\varepsilon_i \equiv \mu_{ii}/M_{N_i} \ll 1$. The $\tilde{M}_i$ is diagonalized with real and positive eigenvalues by a unitary transformation $U_i^T \tilde{M}_i U_i$ where

$$U_i = \begin{pmatrix} -i\cos\alpha_i e^{i\theta_i/2} & \sin\alpha_i e^{i\theta_i/2} \\ i\sin\alpha_i e^{-i\theta_i/2} & \cos\alpha_i e^{-i\theta_i/2} \end{pmatrix}, \tag{D.7}$$

and the mixing angles are given by

$$\cos\alpha_i \simeq \frac{1}{\sqrt{2}}\left(1 + \frac{\varepsilon_i}{4}\right), \quad \sin\alpha_i \simeq \frac{1}{\sqrt{2}}\left(1 - \frac{\varepsilon_i}{4}\right), \tag{D.8}$$

up to $\mathcal{O}(\varepsilon_i)$. The corresponding mass eigenvalues are given by

$$M_j \simeq M_{N_i}\left(1 \pm \frac{\varepsilon_i}{2}\right) \quad (i = 1, 2; \; j = 1, 2, 3, 4). \tag{D.9}$$

It is clear that the mass splitting within a quasi-Dirac pair is given by μ_{ii}.

The Yukawa couplings in this diagonal mass basis are related to the couplings in the flavor basis as follows:

$$
\begin{aligned}
h_{1\alpha} &\simeq \frac{ie^{-i\theta_1/2}}{\sqrt{2}}\left(1 + \frac{\varepsilon_1}{4}\right) y_{1\alpha}, \\
h_{2\alpha} &\simeq \frac{e^{-i\theta_1/2}}{\sqrt{2}}\left(1 - \frac{\varepsilon_1}{4}\right) y_{1\alpha}, \\
h_{3\alpha} &\simeq \frac{ie^{-i\theta_2/2}}{\sqrt{2}}\left(1 + \frac{\varepsilon_2}{4}\right) y_{2\alpha}, \\
h_{4\alpha} &\simeq \frac{e^{-i\theta_2/2}}{\sqrt{2}}\left(1 - \frac{\varepsilon_2}{4}\right) y_{2\alpha}.
\end{aligned}
\tag{D.10}
$$

Note that in the L-conserving limit $\varepsilon_i \to 0$, we have $h_{i\alpha} = ih_{j\alpha}$ within a quasi-degenerate pair (i,j), as expected.

Now let us calculate the CP-asymmetry for the decay of one of the quasi-Dirac particles, say $i = 1$. We have from Eq. (4.18),

$$
\epsilon_1 = \frac{1}{8\pi} \sum_{j\neq 1} \frac{\mathrm{Im}\left[(hh^\dagger)^2_{1j}\right]}{\sum_\beta |h_{1\beta}|^2} f^v_{1j} \simeq \frac{\varepsilon_2}{16\pi \sum_\beta |y_{1\beta}|^2} \mathrm{Im}\left[e^{i(\theta_1 - \theta_2)}\left(\sum_\alpha y^*_{1\alpha} y_{2\alpha}\right)^2\right] f^v_{13} \tag{D.11}
$$

assuming $f_{13} \simeq f_{14}$. Note that the $j = 2$ term vanishes as there is no imaginary part in that case. It is clear that ϵ_1 vanishes as $\mu_{22} \to 0$. Similarly, one can show that ϵ_2 also vanishes in the limit $\mu_{22} \to 0$, and ϵ_3, ϵ_4 vanish as $\mu_{11} \to 0$.

Case II $- \mu_S$ **purely off-diagonal:** In this case, the Majorana mass matrix in the (N_i, S_i) flavor basis reduces to the following block diagonal form:

$$
\mathcal{M} = \begin{pmatrix} 0 & 0 & M_{N_1} & 0 \\ 0 & 0 & 0 & M_{N_2} \\ M_{N_1} & 0 & 0 & \mu_{12} \\ 0 & M_{N_2} & \mu_{12} & 0 \end{pmatrix} \xrightarrow{c_1 \leftrightarrow c_3, r_2 \leftrightarrow r_4} \begin{pmatrix} M_{N_1} & 0 & 0 & 0 \\ \mu_{12} & M_{N_2} & 0 & 0 \\ 0 & 0 & M_{N_1} & \mu_{12} \\ 0 & 0 & 0 & M_{N_2} \end{pmatrix}, \tag{D.12}
$$

which, however, mixes the (1,2) sectors; in the (N_1, S_2) basis, we have the 2×2 mass

matrix

$$\tilde{M} = \begin{pmatrix} M_{N_1} & 0 \\ \mu e^{i\theta} & M_{N_2} \end{pmatrix}, \tag{D.13}$$

with $\mu \ll M_{N_1}, M_{N_2}$. However, unlike in Case I, we cannot diagonalize this asymmetric matrix by a single unitary transformation; instead, we have to apply a bi-unitary transformation of the form $V^\dagger \tilde{M} U$. We find that the following forms of U and V diagonalize $\tilde{M}$:

$$U = \begin{pmatrix} \cos\alpha & \sin\alpha \\ -\sin\alpha e^{i\theta} & \cos\alpha e^{i\theta} \end{pmatrix}, \quad V = \begin{pmatrix} \cos\beta & \sin\beta \\ -\sin\beta e^{i\theta} & \cos\beta e^{i\theta} \end{pmatrix}, \tag{D.14}$$

where the mixing angles are given by

$$\begin{aligned}
\cos\alpha &= \frac{M_{N_2}^2 - M_{N_1}^2}{\sqrt{(M_{N_2}^2 - M_{N_1}^2)^2 + \mu^2 M_{N_2}^2}}, \\
\sin\alpha &= \frac{\mu M_{N_2}}{\sqrt{(M_{N_2}^2 - M_{N_1}^2)^2 + \mu^2 M_{N_2}^2}}, \\
\cos\beta &= \frac{M_{N_2}^2 - M_{N_1}^2}{\sqrt{(M_{N_2}^2 - M_{N_1}^2)^2 + \mu^2 M_{N_1}^2}}, \\
\sin\beta &= \frac{\mu M_{N_1}}{\sqrt{(M_{N_2}^2 - M_{N_1}^2)^2 + \mu^2 M_{N_1}^2}}.
\end{aligned} \tag{D.15}$$

The eigenvalues of $\tilde{M}$ are given by

$$M_i \simeq \frac{1}{\sqrt{2}} \left[M_{N_1}^2 + M_{N_2}^2 + \mu^2 \mp \sqrt{(M_{N_2}^2 - M_{N_1}^2)^2 + 2\mu^2(M_{N_1}^2 + M_{N_2}^2)} \right]^{1/2}, \tag{D.16}$$

up to order $\mathcal{O}(\mu^2)$. Note however that in the new basis, the mass matrix is still not diagonal and is of the form $\begin{pmatrix} 0 & M_i \\ M_i & 0 \end{pmatrix}$ with eigenvalues $\pm M_i$. This can be diagonalized with real and positive eigenvalues $|M_i|$ by another unitary transformation:

$$U_d = \begin{pmatrix} \cos\frac{\pi}{4} & \sin\frac{\pi}{4} \\ -\sin\frac{\pi}{4} & \cos\frac{\pi}{4} \end{pmatrix} \cdot \text{diag}\left(e^{-i\pi/2}, 1 \right) \tag{D.17}$$

174

We note here that in this case, unlike in case I, there is no mass splitting within the pair and the two quasi-Dirac RH neutrinos are exactly degenerate. This is a general result that the off-diagonal elements of μ do not contribute to the mass splitting within a pair; they just shift the eigenvalues. Hence, the splitting can be approximated by the diagonal elements of μ, as in Eq. (4.25).

Finally, the Yukawa couplings in the mass-diagonal basis with real and positive eigenvalues are given in terms of the couplings in the flavor basis as follows:

$$
\begin{aligned}
h_{1\alpha} &= \frac{i}{\sqrt{2}} \left(\cos\beta \; y_{1\alpha} + \sin\alpha e^{-i\theta} \; y_{2\alpha} \right), \\
h_{2\alpha} &= \frac{1}{\sqrt{2}} \left(\cos\beta \; y_{1\alpha} - \sin\alpha e^{-i\theta} \; y_{2\alpha} \right), \\
h_{3\alpha} &= \frac{i}{\sqrt{2}} \left(\sin\beta \; y_{1\alpha} - \cos\alpha e^{-i\theta} \; y_{2\alpha} \right), \\
h_{4\alpha} &= \frac{1}{\sqrt{2}} \left(\sin\beta \; y_{1\alpha} + \cos\alpha e^{-i\theta} \; y_{2\alpha} \right).
\end{aligned}
\tag{D.18}
$$

Note that in the L-conserving limit $\mu \to 0$, $\cos\alpha, \cos\beta \to 1$ and $\sin\alpha, \sin\beta \to 0$; it is clear from Eqs. (D.18) that in this limit, we recover the relation $h_{i\alpha} = i h_{j\alpha}$ for the (i, j) pair.

Using Eqs. (D.18), it can be shown that the CP-asymmetry, Eq. (4.18), for $i = 1$ becomes

$$
\begin{aligned}
\epsilon_1 &= \frac{\mathrm{Im}\left(e^{-i\theta} \sum_\gamma y_{1\gamma}^* y_{2\gamma} \right)}{8\pi \sum_\gamma |h_{1\gamma}|^2} \left[\sin\alpha \cos\beta \left(\cos^2\beta \sum_\gamma |y_{1\gamma}|^2 - \sin^2\alpha \sum_\gamma |y_{2\gamma}|^2 \right) f_{12}^v \right. \\
&\quad - \frac{1}{2} \left\{ \cos\alpha \sin\beta \left(\cos^2\beta \sum_\gamma |y_{1\gamma}|^2 - \sin^2\alpha \sum_\gamma |y_{2\gamma}|^2 \right) \right. \\
&\quad \left. \left. + \cos\alpha \cos\beta \left(\cos\beta \sin\beta \sum_\gamma |y_{1\gamma}|^2 - \cos\alpha \sin\alpha \sum_\gamma |y_{2\gamma}|^2 \right) \right\} f_{13}^v \right]
\end{aligned}
\tag{D.19}
$$

which clearly vanishes in the limit $\mu \to 0$ (as $\sin\alpha, \sin\beta \propto \mu$). Similarly it can be shown for other channels.

Comparing the CP-asymmetries ϵ_1 in these two cases, we find that in Case I, the contribution within the pair vanishes and the remaining term in Eq. (D.11) which is

proportional to f_{13}^v is highly suppressed as M_1 is not quasi-degenerate with the (M_3, M_4) pair. On the other hand, in case II, the dominant contribution comes from within the (M_1, M_2) pair which is enhanced due to large f_{12}^v. Hence, combining these results, we expect that in the general case with both diagonal and off-diagonal μ-entries, the dominant contribution to the CP-asymmetry ϵ_i should come from "within the pair" decay of N_i. We checked numerically that this is indeed the case.

Appendix E

Sparticle Spectrum in SUSYLR

The superpotential for the SULYLR model discussed in Chapter 3 is given by Eq. (3.12) and the relevant soft-SUSY breaking Lagrangian is given by Eq. (3.21). The $B-L$ symmetry is broken by the vev of the neutral RH-doublet fields: $\langle \phi_d^{c0} \rangle = v_{R_d}$, $\langle \phi_u^{c0} \rangle = v_{R_u}$ and we define

$$\tan\theta \equiv \frac{v_{R_u}}{v_{R_d}}, \quad v_R \equiv \sqrt{v_{R_u}^2 + v_{R_d}^2} \tag{E.1}$$

with $v_R \sim$ TeV. The electroweak symmetry is broken by the vev of the neutral bi-doublet fields: $\langle \Phi_{1d}^0 \rangle = v_d$, $\langle \Phi_{2u}^0 \rangle$ and we define

$$\tan\beta \equiv \frac{v_u}{v_d}, \quad v_{\mathrm{wk}} \equiv \sqrt{v_u^2 + v_d^2} \tag{E.2}$$

The values of $\mu_{\phi^c}^2$ and μ_Φ^2 are determined by minimizing the Higgs potential:

$$V_{\mathrm{Higgs}} \quad = \quad V_F + V_{\mathrm{soft}} + V_D, \quad \text{where} \tag{E.3}$$

$$V_F \quad = \quad \mu_{\phi^c}^2 (|\phi_d^{c0}|^2 + |\phi_u^{c0}|^2 + |\phi_d^{c-}|^2 + |\phi_u^{c+}|^2)$$

$$+ \mu_\Phi^2 (|\Phi_d^0|^2 + |\Phi_u^0|^2 + |\Phi_d^-|^2 + |\Phi_u^+|^2), \tag{E.4}$$

$$V_{\mathrm{soft}} \quad = \quad m_{\phi_d^c}^2 (|\phi_d^{c0}|^2 + |\phi_d^{c-}|^2) + m_{\phi_u^c}^2 (|\phi_u^{c0}|^2 + |\phi_u^{c+}|^2) + m_\Phi^2 (|\Phi_d^0|^2 + |\Phi_d^-|^2 + |\Phi_u^+|^2 + |\Phi_u^0|^2)$$

$$- B_{\phi^c}(\phi_d^{c0}\phi_u^{c0} - \phi_d^{c-}\phi_u^{c+} + \mathrm{h.c.}) - B_\Phi(\Phi_d^0\Phi_u^0 - \Phi_d^-\Phi_u^+ + \mathrm{h.c.}), \tag{E.5}$$

$$V_D \quad = \quad \frac{g_L^2}{8} \Big[(|\Phi_u^+|^2 - |\Phi_u^0|^2 + |\Phi_d^0|^2 - |\Phi_d^-|^2)^2 + 4(|\Phi_u^+|^2|\Phi_u^0|^2 + |\Phi_d^0|^2|\Phi_d^-|^2)$$

$$+ 4(\Phi_u^{+*}\Phi_d^{-*}\Phi_u^0\Phi_d^0 + \Phi_u^{0*}\Phi_d^{0*}\Phi_u^+\Phi_d^-) \Big]$$

$$+ \frac{g_R^2}{8} \Big[(|\Phi_d^0|^2 - |\Phi_d^-|^2 - |\Phi_u^0|^2 + |\Phi_u^+|^2 + |\phi_d^{c0}|^2 - |\phi_d^{c-}|^2 - |\phi_u^{c0}|^2 + |\phi_u^{c+}|^2)^2$$

$$+4(|\Phi_d^0|^2|\Phi_d^-|^2 + |\Phi_u^0|^2|\Phi_u^+|^2 + |\phi_d^{c0}|^2|\phi_d^{c-}|^2 + |\phi_u^{c0}|^2|\phi_u^{c+}|^2)$$

$$+4(\Phi_d^{0*}\Phi_u^{0*}\Phi_d^-\Phi_u^+ + \Phi_d^{0*}\Phi_d^-\phi_d^{c0}\phi_d^{c-*} + \Phi_d^{0*}\Phi_d^-\phi_u^{c0*}\phi_u^{c+} + \Phi_d^0\Phi_d^{-*}\phi_d^{c0*}\phi_d^{c-}$$

$$+\Phi_u^0\Phi_d^0\Phi_u^{+*}\Phi_d^{-*} + \Phi_u^0\Phi_u^{+*}\phi_d^{c0}\phi_d^{c-*} + \Phi_u^0\Phi_u^{+*}\phi_u^{c0*}\phi_u^{c+} + \Phi_u^{0*}\Phi_u^+\phi_d^{c0*}\phi_d^{c-}$$

$$+\Phi_d^0\Phi_d^{-*}\phi_u^{c0}\phi_u^{c+*} + \Phi_u^{0*}\Phi_u^+\phi_u^{c0}\phi_u^{c+*} + \phi_d^{c0*}\phi_u^{c0*}\phi_d^{c-}\phi_u^{c+} + \phi_u^{c0}\phi_d^{c0}\phi_u^{c+*}\phi_d^{c-*})\Big] \quad \text{(E.6)}$$

Minimizing this potential for the neutral fields yields

$$\begin{aligned}
\mu_\Phi^2 &= -m_\Phi^2 - \frac{v_{\text{wk}}^2}{4}(g_L^2 + g_R^2) - \frac{v_R^2 g_R^2}{4}\frac{\cos 2\theta}{\cos 2\beta}, \\
\mu_{\phi^c}^2 &= \frac{m_{\phi_d^c}^2 - m_{\phi_u^c}^2 \tan^2\theta}{\tan^2\theta - 1} - \frac{v_R^2}{4}(g_R^2 + g'^2)
\end{aligned} \quad \text{(E.7)}$$

The chargino mass matrix in the basis $\{\widetilde{W}_L^+, \widetilde{W}_R^+, \widetilde{\Phi}_u^+, \widetilde{\phi}_u^{c+}\}$ is given by

$$\mathcal{M}_{\text{charge}} = \begin{pmatrix} M_{2L} & 0 & g_L v_d & 0 \\ 0 & M_{2R} & g_R v_d & g_R v_{R_d} \\ g_L v_u & g_R v_u & -\mu_\Phi & 0 \\ 0 & g_R v_{R_u} & 0 & -\mu_{\phi^c} \end{pmatrix} \quad \text{(E.8)}$$

The neutralino mass matrix in the basis $\{\widetilde{W}_{3L}, \widetilde{W}_{3R}, \widetilde{B}, \widetilde{\Phi}_d^0, \widetilde{\Phi}_u^0, \widetilde{\phi}_d^{c0}, \widetilde{\phi}_u^{c0}\}$ is given by

$$\mathcal{M}_{\text{neutral}} = \begin{pmatrix} M_{2L} & 0 & 0 & \frac{g_L v_d}{\sqrt{2}} & -\frac{g_L v_u}{\sqrt{2}} & 0 & 0 \\ 0 & M_{2R} & 0 & \frac{g_R v_d}{\sqrt{2}} & -\frac{g_R v_u}{\sqrt{2}} & \frac{g_R v_{R_d}}{\sqrt{2}} & -\frac{g_R v_{R_u}}{\sqrt{2}} \\ 0 & 0 & M_1 & 0 & 0 & -\frac{g' v_{R_d}}{\sqrt{2}} & \frac{g' v_{R_u}}{\sqrt{2}} \\ \frac{g_L v_d}{\sqrt{2}} & \frac{g_R v_d}{\sqrt{2}} & 0 & 0 & \mu_\Phi & 0 & 0 \\ -\frac{g_L v_u}{\sqrt{2}} & -\frac{g_R v_u}{\sqrt{2}} & 0 & \mu_\Phi & 0 & 0 & 0 \\ 0 & \frac{g_R v_{R_d}}{\sqrt{2}} & -\frac{g' v_{R_d}}{\sqrt{2}} & 0 & 0 & 0 & \mu_{\phi^c} \\ 0 & -\frac{g_R v_{R_u}}{\sqrt{2}} & \frac{g' v_{R_u}}{\sqrt{2}} & 0 & 0 & \mu_{\phi^c} & 0 \end{pmatrix} \quad \text{(E.9)}$$

For the sfermion sector, the masses for first generation are given by

$$m_{\tilde{u}_L}^2 = m_{Q_1}^2 + m_u^2 + \frac{1}{4}g_L^2 v^2 \cos 2\beta - \frac{1}{12}g'^2 v_R^2 \cos 2\theta$$

178

$$m_{\tilde{d}_L}^2 = m_{Q_1}^2 + m_d^2 - \frac{1}{4}g_L^2 v^2 \cos 2\beta - \frac{1}{12}g'^2 v_R^2 \cos 2\theta$$

$$m_{\tilde{e}_L}^2 = m_{L_1}^2 + m_e^2 - \frac{1}{4}g_L^2 v^2 \cos 2\beta + \frac{1}{4}g'^2 v_R^2 \cos 2\theta$$

$$m_{\tilde{u}_R}^2 = m_{Q_1^c}^2 + m_u^2 - \frac{1}{4}g_R^2 (v^2 \cos 2\beta + v_R^2 \cos 2\theta) + \frac{1}{12}g'^2 v_R^2 \cos 2\theta$$

$$m_{\tilde{d}_R}^2 = m_{Q_1^c}^2 + m_d^2 + \frac{1}{4}g_R^2 (v^2 \cos 2\beta + v_R^2 \cos 2\theta) + \frac{1}{12}g'^2 v_R^2 \cos 2\theta$$

$$m_{\tilde{e}_R}^2 = m_{L_1^c}^2 + m_e^2 + \frac{1}{4}g_R^2 (v^2 \cos 2\beta + v_R^2 \cos 2\theta) - \frac{1}{4}g'^2 v_R^2 \cos 2\theta \qquad \text{(E.10)}$$

and similarly for the other two generations. For the sneutrino sector, the mass matrix in the basis of $\{\tilde{\nu}, \tilde{\nu}^{c\dagger}, \widetilde{S}\}$ is given by

$$\mathcal{M}_{\tilde{\nu}} = \begin{pmatrix} m_{\tilde{\nu}^\dagger \tilde{\nu}}^2 & m_{\tilde{\nu}^\dagger \tilde{\nu}^{c\dagger}}^2 & m_{\tilde{\nu}^\dagger \widetilde{S}}^2 \\ \left(m_{\tilde{\nu}^\dagger \tilde{\nu}^{c\dagger}}^2\right)^\dagger & m_{\tilde{\nu}^c \tilde{\nu}^{c\dagger}}^2 & m_{\tilde{\nu}^c \widetilde{S}}^2 \\ \left(m_{\tilde{\nu}^\dagger \widetilde{S}}^2\right)^\dagger & \left(m_{\tilde{\nu}^c \widetilde{S}}^2\right)^\dagger & m_{\widetilde{S}^\dagger \widetilde{S}}^2 \end{pmatrix} \qquad \text{(E.11)}$$

where

$$m_{\tilde{\nu}^\dagger \tilde{\nu}}^2 = m_L^2 + v_u^2 h_\nu^\dagger h_\nu + \frac{1}{4}g_L^2 v^2 \cos 2\beta + \frac{1}{4}g'^2 v_R^2 \cos 2\theta$$

$$m_{\tilde{\nu}^c \tilde{\nu}^{c\dagger}}^2 = m_{L^c}^2 + v_u^2 h_\nu h_\nu^\dagger + v_{R_d}^2 y_S y_S^\dagger - \frac{1}{4}g_R^2 (v^2 \cos 2\beta + v_R^2 \cos 2\theta) - \frac{1}{4}g'^2 v_R^2 \cos 2\theta$$

$$m_{\widetilde{S}^\dagger \widetilde{S}}^2 = m_S^2 + \mu_S^2 + v_{R_d}^2 y_S^\dagger y_S$$

$$m_{\tilde{\nu}^\dagger \tilde{\nu}^{c\dagger}}^2 = 2\mu_\Phi v_d h_\nu^\dagger$$

$$m_{\tilde{\nu}^\dagger \widetilde{S}}^2 = v_u v_{R_d} h_\nu^\dagger y_S,$$

$$m_{\tilde{\nu}^c \widetilde{S}}^2 = \mu_{\phi^c}^* v_{R_u} y_S \qquad \text{(E.12)}$$

Bibliography

[1] Some standard texts on Quantum Field Theory: I. J. R. Aitchison and A. J. G. Hey, *Gauge Theories in Particle Physics*, Adam Hilger (1982); C. Quigg, *Gauge Theories of the Strong, Weak, and Electromagnetic Interactions*, Benjamin/Cummings (1983); T. P. Cheng and L. F. Li, *Gauge theory of Elementary Particle Physics*, Oxford University Press (1984); C. Itzykson and J. B. Zuber, *Quantum Field Theory*, Mc Graw Hill (1985); D. Bailin and A. Love, *Introduction to Gauge Field Theory*, Adam Hilger (1986); F. Mandl and G. Shaw, *Quantum Field Theory*, Revised Edition, John Wiley (1993); S. Weinberg, *The Quantum Theory of Fields: Vol. I and II*, Cambridge University Press (1995); M. E. Peskin and D. V. Schroeder, *An introduction to Quantum Field Theory*, Addison-Wesley (1995); A. Lahiri and P. B. Pal, *A First Book of Quantum Field Theory*, Second Edition, Alpha Science (2005);

[2] For a textbook description of the SM, see e.g., F. Halzen and A. D. Martin, *Quarks and Leptons: an introductory course in Modern Particle Physics*, John Wiley (1984); D. J. Griffiths, *Introduction to Elementary Particles*, John Wiley (1987); J. Donoghue, E. Golowich and B. R. Holstein, *Dynamics of The Standard Model*, Cambridge University Press (1994); D. H. Perkins, *Introduction to High Energy Physics*, Fourth edition, Cambridge University Press (2000).

[3] For reviews on SM, see e.g., E. Abers and B. Lee, Phys. Rep. **9**, 1 (1973); M. A. B. Beg and A. Sirlin, Phys. Rept. **88**, 1 (1982); P. Langacker, hep-ph/9412361; M. Herrero, hep-ph/9812242; C. Quigg, hep-ph/0001145; S. F. Novaes, hep-ph/0001283; G. Altarelli, hep-ph/0011078; H. Spiesberger, M. Spira and P. M. Zerwas, hep-ph/0011255; A. Pich, hep-ph/0502002.

[4] The LEP Collaborations (ALEPH, DELPHI, L3 and OPAL), the LEP Electroweak Working Group and the SLD Heavy Flavour Group, arXiv:1012.2367 [hep-ex] [`http://lepewwg.web.cern.ch/LEPEWWG`]. For detailed analyses, see Phys. Rep. **427**, 257 (2006) [hep-ex/0509008]; hep-ex/0412015.

[5] The Tevatron Electroweak Working Group, `http://tevewwg.fnal.gov/`

[6] S. Haywood *et al.*, hep-ph/0003275; A. Straessner, *Electroweak Physics at LEP and LHC*, Springer-Verlag (2010).

[7] C. N. Yang and R. Mills, *Phys. Rev.* **96**, 191 (1954).

[8] S. Glashow, Nucl. Phys. **22**, 579 (1961); S. Weinberg, Phys. Rev. Lett. **19**, 1264 (1967); A. Salam, in *Elementary Particle Theory*, N. Svartholm (ed.), Almqvist and Wiksells (1969), p. 367.

[9] M. Gell-Mann, Phys. Lett. **8**, 214 (1964); G. Zweig, CERN-Report 8182/TH401 (1964); H. Fritzsch, M. Gell-Mann and H. Leutwyler, Phys. Lett. **B47**, 365 (1973).

[10] D. Gross and F. Wilczek, Phys. Rev. Lett. **30**, 1343 (1973); H. D. Politzer, Phys. Rev. Lett. **30**, 1346 (1973).

[11] See e.g., H. Georgi, *Lie Algebras In Particle Physics: from Isospin To Unified Theories*, 2nd edition, Westview Press (1999).

[12] G. Abbiendi *et al.* [OPAL Collaboration], Eur. Phys. J. **C52**, 767 (2007) [arXiv:0708.1311 [hep-ex]]; A. Robson [CDF and D0 Collaborations], arXiv:1201.4771 [hep-ex].

[13] See e.g., R. E. Marshak, Riazuddin and C. P. Ryan, *Theory of Weak Interactions in Particle Physics*, Wiley-Interscience (1969); H. Georgi, *Weak Interactions and Modern Particle Theory*, Benjamin/Cummings (1984).

[14] S. L. Adler and W. A. Bardeen, Phys. Rev. **182**, 1517 (1969); R. W. Jackiw, in *Lectures on Current Algebra and its Applications*, S. B. Treiman, R. W. Jackiw, and D. Gross (eds.), Princeton University Press (1972).

[15] C. Bouchiat, J. Iliopoulos and Ph. Meyer, Phys. Lett. **38B**, 519 (1972).

[16] G. 't Hooft, Nucl. Phys. **B33**, 173 (1971); *ibid.* **B35**, 167 (1971); G. 't Hooft and M. Veltman, Nucl. Phys. **B44**, 189 (1972).

[17] P. W. Higgs, Phys. Rev. Lett. **13**, 508 (1964); *ibid.*, Phys. Rev. **145**, 1156 (1966); F. Englert and R. Brout, Phys. Rev. Lett. **13**, 321 (1964); G. S. Guralnik, C. R. Hagen and T. Kibble, Phys. Rev. Lett. **13**, 585 (1965); T. Kibble, Phys. Rev. **155**, 1554 (1967).

[18] N. Cabibbo, Phys. Rev. Lett. **10**, 531 (1963); M. Kobayashi and T. Maskawa, Prog. Theor. Phys. **49**, 652 (1973).

[19] L. L. Chau and W. Y. Keung, Phys. Rev. Lett. **53**, 1802 (1984).

[20] L. Wolfenstein, Phys. Rev. Lett. **51**, 1945 (1983).

[21] S. Glashow, J. Illiopoulos and L. Maiani, Phys. Rev. **D2**, 1285 (1970).

[22] K. Nakamura *et al.* (Particle Data Group), J. Phys. **G37**, 075021 (2010).

[23] K. Potamianos [CDF and D0 Collaborations], arXiv:1201.6338 [hep-ex].

[24] The CKMFitter Group [`http://ckmfitter.in2p3.fr/`].

[25] T. van Ritbergen and R. G. Stuart, Phys. Rev. Lett. **82**, 488 (1999) [hep-ph/9808283]; *ibid.*, Nucl. Phys. **B564**, 343 (2000) [hep-ph/9904240].

[26] G. Aad *et al.* [ATLAS Collaboration], arXiv:1202.1408 [hep-ex]; S. Chatrchyan *et al.* [CMS Collaboration], arXiv:1202.1488 [hep-ex].

[27] For a review of the SM Higgs, see e.g., A. Djouadi, Phys. Rept. **457**, 1 (2008) [hep-ph/0503172].

[28] The TEVNPH Working Group [CDF and D0 Collaborations], FERMILAB-CONF-12-065-E (2012) [`http://tevnphwg.fnal.gov/`].

[29] For a review, see e.g., J. Erler and P. Langacker, in Ref. [22], p. 126.

[30] For a textbook description, see e.g., R. N. Mohapatra and P. B. Pal, *Massive Neutrinos in Physics and Astrophysics*, Third edition, World Scientific (2004).

[31] For a review, see e.g., M. C. Gonzalez-Garcia and Y. Nir, Rev. Mod. Phys. **75**, 345 (2003) [hep-ph/0202058]; K. Nakamura and S. T. Petcov, in Ref. [22], p. 164.

[32] B. Pontecorvo, Zh. Eksp. Teor. Fiz. **33**, 549 (1957); *ibid.* **34**, 247 (1958); Z. Maki, M. Nakagawa, and S. Sakata, Prog. Theor. Phys. **28**, 870 (1962).

[33] S. M. Bilenky, J. Hosek, and S. T. Petcov, Phys. Lett. **B94**, 495 (1980); J. Schechter and J. W. F. Valle, Phys. Rev. **D23**, 2227 (1980); M. Doi, T. Kotani, H. Nishiura, K. Okuda and E. Takasugi, Phys. Lett. **B102**, 323 (1981).

[34] G. L. Fogli, E. Lisi, A. Marrone, A. Palazzo and A. M. Rotunno, Phys. Rev. **D84**, 053007 (2011) [arXiv:1106.6028 [hep-ph]].

[35] F. P. An *et al.* [DAYA-BAY Collaboration], arXiv:1203.1669 [hep-ex].

[36] J. K. Ahn *et al.* [RENO Collaboration], arXiv:1204.0626 [hep-ex].

[37] For reviews, see e.g., R. N. Mohapatra *et al.*, Rept. Prog. Phys. **70**, 1757 (2007) [hep-ph/0510213]; R. N. Mohapatra and A. Y. Smirnov, Ann. Rev. Nucl. Part. Sci. **56**, 569 (2006) [hep-ph/0603118].

[38] See e.g., B. D. Fields and S. Sarkar, in Ref. [22], p. 241.

[39] E. Komatsu *et al.* [WMAP Collaboration], Astrophys. J. Suppl. **192**, 18 (2011) [arXiv:1001.4538 [astro-ph.CO]].

[40] For reviews, see e.g., A. G. Cohen, D. B. Kaplan and A. E. Nelson, Ann. Rev. Nucl. Part. Sci. **43**, 27 (1993) [hep-ph/9302210]; A. Riotto and M. Trodden, Annu. Rev. Nucl. Part. Sci. **49**, 35 (1999) [hep-ph/9901362]; M. Dine and A. Kusenko, Rev. Mod. Phys. **76**, 1 (2003) [hep-ph/0303065]; J. M. Cline, hep-ph/0609145.

[41] A. D. Sakharov, JETP Lett. **5**, 24 (1967).

[42] G. 't Hooft, Phys. Rev. Lett. **37**, 8 (1976); V. A. Kuzmin, V. A. Rubakov and M. E. Shaposhnikov, Phys. Lett. B **155**, 36 (1985).

[43] C. Jarlskog, Phys. Rev. Lett. **55**, 1039 (1985); *ibid*, Z. Phys. **C29**, 491 (1985).

[44] K. Kajantie, M. Laine, K. Rummukainen and M. E. Shaposhnikov, Phys. Rev. Lett. **77**, 2887 (1996) [hep-ph/9605288].

[45] See e.g., V. Trimble, Ann. Rev. Astron. Astrophys. **25**, 425 (1987); G. Bertone, D. Hooper and J. Silk, Phys. Rept. **405**, 279 (2005) [hep-ph/0404175].

[46] See e.g., J. R. Primack, astro-ph/9707285.

[47] See e.g. D. H. Weinberg, M. J. Mortonson, D. J. Eisenstein, C. Hirata, A. G. Riess and E. Rozo, arXiv:1201.2434 [astro-ph.CO].

[48] See e.g. S. Weinberg, Rev. Mod. Phys. **61**, 1 (1989).

[49] A. Höcker and W. J. Marciano, in Ref [22], p. 517.

[50] T. Aaltonen *et al.* [CDF Collaboration], Phys. Rev. **D83**, 112003 (2011) [arXiv:1101.0034 [hep-ex]].

[51] For a review, see e.g., G. Altarelli, in Ref. [3].

[52] S. Weinberg, Phys. Rev. **D19**, 1277 (1979); L. Susskind, Phys. Rev. **D20**, 2619 (1979).

[53] S. Weinberg, Phys. Lett. **82B**, 387 (1979); M. Veltman, Acta. Phys. Polon. **B12**, 437 (1981); C. H. Llewellyn Smith and G. G. Ross, Phys. Lett. **105B**, 38 (1981).

[54] M. Veltman, Acta. Phys. Pol. **B8**, 475 (1977); L. Susskind, Phys. Rept. **104**, 181 (1984).

[55] See e.g. M. E. Peskin, hep-ph/9705479; R. S. Chivukula, hep-ph/9803219; C. Quigg, Acta Phys. Polon. **B30**, 2145 (1999) [hep-ph/9905369].

[56] For a review, see e.g., R. Kaul, Rev. Mod. Phys. **55**, 449 (1983); K. Lane, hep-ph/0202255; C. T. Hill and E. H. Simmons, Phys. Rept. **381**, 235 (2003) [Erratum-ibid. **390**, 553 (2004)] [hep-ph/0203079]; R. S. Chivukula, M. Narain, and J. Womersley, in Ref. [22], p. 1340.

[57] For a review, see e.g., R. Sundrum, hep-th/0508134.

[58] For a review, see e.g., J. M. Maldacena, hep-th/0309246.

[59] Some standard texts on SUSY: P. West, *Introduction to Supersymmetry and Supergravity*, Second Edition, World Scientific (1990); J. Wess and J. Bagger, *Supersymmetry and Supergravity*, Second Edition, Princeton University Press (1992); S. Weinberg, *The Quantum Theory of Fields, Volume III, Supersymmetry*, Cambridge University Press (2000); R. N. Mohapatra, *Unification and Supersymmetry*, Third Edition, Springer-Verlag (2003); M. Drees, R. M. Godbole, and P. Roy, *Theory and Phenomenology of Sparticles*, World Scientific (2005); H. Baer and X. Tata, *Weak Scale Supersymmetry*, Cambridge University Press (2006); P. Binétruy, *Supersymmetry: Theory, Experiment, and Cosmology*, Oxford University Press (2006); I. J. R. Aitchison, *Supersymmetry in particle physics: an elementary introduction*, Cambridge University Press (2007); M. Dine, *Supersymmetry and String Theory*, Cambridge University Press (2007).

[60] For reviews on SUSY, see e.g. P. Fayet and S. Ferrara, Phys. Rept. **32**, 249 (1977); H. P. Nilles, Phys. Rept. **110**, 1 (1984); H. E. Haber and G. L. Kane, Phys. Rept. **117**, 75 (1985); M. F. Sohnius, Phys. Rept. **128**, 39 (1985); J. A. Bagger, hep-ph/9604232; S. P. Martin, in G. L. Kane (ed.), *Perspectives on supersymmetry II*, World Scietific, (2010), p. 1-153 [hep-ph/9709356]; N. Polonsky, Lect. Notes Phys. **M68**, 1 (2001) [hep-ph/0108236]; M. E. Peskin, arXiv:0801.1928 [hep-ph]; A. Signer, J. Phys. **G36**, 073002 (2009) [arXiv:0905.4630 [hep-ph]]; M. C. Rodriguez, Int. J. Mod. Phys. **A25**, 1091 (2010) [arXiv:0911.5338 [hep-ph]]; H. E. Haber, in Ref. [22], p. 1292.

[61] E. Witten, Nucl. Phys. **B188**, 513 (1981); *ibid.* **B202**, 253 (1982); N. Sakai, Z. Phys. **C11**, 153 (1981); S. Dimopoulos and H. Georgi, Nucl. Phys. **B193**, 150 (1981); R. K. Kaul and P. Majumdar, Nucl. Phys. **B199**, 36 (1982).

[62] L. Girardello and M. T. Grisaru, Nucl. Phys. **B194**, 65 (1982); for a review, see e.g., D. J. H. Chung *et al.*, Phys. Rept. **407**, 1 (2005) [hep-ph/0312378].

[63] R. Haag, J. T. Lopuszanski and M. Sohnius, Nucl. Phys. **B88**, 257 (1975).

[64] For a review, see e.g., M. Dine and J. D. Mason, Rept. Prog. Phys. **74**, 056201 (2011) [arXiv:1012.2836 [hep-th]].

[65] See e.g. P. Van Nieuwenhuizen, Phys. Rept. **68**, 189 (1981); P. Nath, R. Arnowitt, and A. H. Chamseddine, *Applied N=1 Supergravity*, World Scientific (1984).

[66] See e.g. M. B. Green, J. H. Schwarz, and E. Witten, *Superstring Theory, Volumes 1 and 2*, Cambridge University Press (1988); M. Kaku, *Introduction to Superstrings and M-Theory*, Second Edition, Springer-Verlag (1999).

[67] See e.g. G. G. Ross, *Grand Unified Theories*, Benjamin/Cummings (1984); S. Raby, in Ref. [22], p. 193.

[68] R. N. Mohapatra, in Ref. [59].

[69] L. E. Ibanez and G. G. Ross, Phys. Lett. **B110**, 215 (1982); K. Inoue, A. Kakuto, H. Komatsu and S. Takeshita, Prog. Theor. Phys. **68**, 927 (1982) [Erratum-*ibid.* **70**, 330 (1983)]; *ibid.* **71**, 413 (1984); J. R. Ellis, J. S. Hagelin, D. V. Nanopoulos and K. Tamvakis, Phys. Lett. **B125**, 275 (1983); L. Alvarez-Gaume, J. Polchinski and M. B. Wise, Nucl. Phys. **B221**, 495 (1983).

[70] G. R. Farrar and P. Fayet, Phys. Lett. **B76**, 575 (1978).

[71] J. Ellis *et al.*, Nucl. Phys. **B238**, 453 (1984).

[72] For a review, see e.g. G. Jungman, M. Kamionkowski and K. Griest, Phys. Rept. **267**, 195 (1996) [hep-ph/9506380]; K. Griest and M. Kamionkowski, Phys. Rept. **333**, 167 (2000).

[73] A. Salam and J. A. Strathdee, Nucl. Phys. **B76**, 477 (1974); *ibid.*, Phys. Lett. **B51**, 353 (1974).

[74] P. Fayet, Nucl. Phys. **B90**, 104 (1975); *ibid.* Phys. Lett. **B64**, 159 (1976); *ibid.* **B69**, 489 (1977); *ibid.* **B84**, 416 (1979); L. Alvarez-Gaume and E. Witten, Nucl. Phys. **B234**, 269 (1983).

[75] See e.g., A. Djouadi, Phys. Rept. **459**, 1 (2008) [hep-ph/0503173].

[76] S. Dimopoulos and D. W. Sutter, Nucl. Phys. **B452**, 496 (1995) [hep-ph/9504415].

[77] F. Gabbiani, E. Gabrielli, A. Masiero and L. Silvestrini, Nucl. Phys. **B477**, 321 (1996) [hep-ph/9604387].

[78] See e.g. A. Djouadi *et al.* [MSSM Working Group Collaboration], hep-ph/9901246.

[79] G. D'Ambrosio, G. F. Giudice, G. Isidori and A. Strumia, Nucl. Phys. **B645**, 155 (2002) [hep-ph/0207036].

[80] C. F. Berger, J. S. Gainer, J. L. Hewett and T. G. Rizzo, JHEP **0902**, 023 (2009) [arXiv:0812.0980 [hep-ph]].

[81] A. H. Chamseddine, R. Arnowitt and P. Nath, Phys. Rev. Lett. **49**, 970 (1982); R. Barbieri, S. Ferrara and C. A Savoy, Phys. Lett. **B119**, 343 (1982); L. Hall, J. Lykken and S. Weinberg, Phys. Rev. **D27**, 2359 (1983).

[82] H. P. Nilles, Phys. Lett. **B115**, 193 (1982); *ibid.* Nucl. Phys. **B217**, 366 (1983); S. K. Soni and H. A. Weldon, Phys. Lett. **B126**, 215 (1983); N. Ohta, Prog. Theor. Phys. **70**, 542 (1983).

[83] C. G. Callan, Phys. Rev. **D2**, 1541 (1970); K. Symanzik, Comm. Math. Phys. **18**, 227 (1970).

[84] M. E. Machacek and M. T. Vaughn, Nucl. Phys. **B222**, 83 (1983).

[85] D. R. T. Jones, Nucl. Phys. **B87**, 127 (1975); D. R. T. Jones and L. Mezincescu, Phys. Lett. **136B**, 242 (1984).

[86] S. Weinberg, Phys. Rev. Lett. **43**, 1566 (1979).

[87] E. Ma, Phys. Rev. Lett. **81**, 1171 (1998) [hep-ph/9805219].

[88] P. Minkowski, *Phys. Lett.* **B67** 421 (1977); T. Yanagida in *Workshop on Unified Theories*, KEK Report No. 79-18 (1979), p. 95; M. Gell-Mann, P. Ramond and

R. Slansky, in *Supergravity*, D. Freedman *et al.* (eds.), North Holland (1980), p. 315; S. L. Glashow, *1979 Cargese Summer Institute on Quarks and Leptons*, M. Levý *et al.* (eds.), Plenum Press (1980), p. 687; R. N. Mohapatra and G. Senjanovic, Phys. Rev. Lett. **44**, 912 (1980).

[89] M. Magg and C. Wetterich, Phys. Lett. **B94**, 61 (1980); J. Schechter and J. W. F. Valle, Phys. Rev. **D22**, 2227 (1980); T. P. Cheng and L. -F. Li, Phys. Rev. **D22**, 2860 (1980); G. B. Gelmini and M. Roncadelli, Phys. Lett. **B99**, 411 (1981); G. Lazarides, Q. Shafi and C. Wetterich, Nucl. Phys. **B181**, 287 (1981); R. N. Mohapatra and G. Senjanovic, Phys. Rev. **D23**, 165 (1981).

[90] R. Foot, H. Lew, X. G. He and G. C. Joshi, Z. Phys. **C44**, 441 (1989).

[91] J. Hisano, T. Moroi, K. Tobe, M. Yamaguchi and T. Yanagida, Phys. Lett. **B357**, 579 (1995) [hep-ph/9501407]; J. Hisano, T. Moroi, K. Tobe and M. Yamaguchi, Phys. Rev. **D53**, 2442 (1996) [hep-ph/9510309]; J. R. Ellis, J. Hisano, M. Raidal and Y. Shimizu, Phys. Rev. **D66**, 115013 (2002) [hep-ph/0206110].

[92] F. Borzumati and Y. Nomura, Phys. Rev. **D64**, 053005 (2001) [hep-ph/0007018].

[93] L. J. Hall, V. A. Kostelecky and S. Raby, Nucl. Phys. **B267**, 415 (1986); F. Borzumati and A. Masiero, Phys. Rev. Lett. **57**, 961 (1986); R. Barbieri and L. J. Hall, Phys. Lett. **B338**, 212 (1994) [hep-ph/9408406]; J. A. Casas and A. Ibarra, Nucl. Phys. B **618**, 171 (2001) [hep-ph/0103065]; E. Arganda, A. M. Curiel, M. J. Herrero and D. Temes, Phys. Rev. D **71**, 035011 (2005) [hep-ph/0407302]; A. Masiero, S. K. Vempati and O. Vives, New J. Phys. **6**, 202 (2004) [hep-ph/0407325].

[94] See e.g. R. Barbier *et al.*, Phys. Rept. **420**, 1 (2005) [hep-ph/0406039].

[95] See e.g. M. Hirsch, M. A. Diaz, W. Porod, J. C. Romao and J. W. F. Valle, Phys. Rev. **D62**, 113008 (2000) [Erratum-ibid. **D65**, 119901 (2002)] [hep-ph/0004115].

[96] See e.g. J. C. Romao, Nucl. Phys. Proc. Suppl. **81**, 231 (2000).

[97] M. Cvetic and J. C. Pati, Phys. Lett. **B135**, 57 (1984); R. N. Mohapatra, Phys. Rev. **D34**, 3457 (1986); R. Kuchimanchi and R. N. Mohapatra, Phys. Rev. **D48**, 4352 (1993) [hep-ph/9306290]; C. S. Aulakh, K. Benakli and G. Senjanovic, Phys. Rev. Lett. **79**, 2188 (1997) [hep-ph/9703434]; C. S. Aulakh, A. Melfo, A. Rasin and G. Senjanovic, Phys. Rev. **D58**, 115007 (1998) [hep-ph/9712551].

[98] J. C. Pati and A. Salam, Phys. Rev. **D10**, 275 (1974); R. N. Mohapatra and J. C. Pati, Phys. Rev. **D11**, 566, 2558 (1975); G. Senjanovic and R. N. Mohapatra, Phys. Rev. **D12**, 1502 (1975).

[99] G. Senjanovic, arXiv:1012.4104 [hep-ph].

[100] H. Fritzsch and P. Minkowski, Ann. Phys. **93**, 193 (1975).

[101] R. N. Mohapatra, Phys. Rev. Lett. **56**, 561 (1986); R. N. Mohapatra and J. W. F. Valle, Phys. Rev. **D34**, 1642 (1986).

[102] For a review, see e.g. J. L. Hewett and T. G. Rizzo, Phys. Rept. **183**, 193 (1989).

[103] M. Hirsch, T. Kernreiter, J. C. Romao and A. Villanova del Moral, JHEP **1001**, 103 (2010) [arXiv:0910.2435 [hep-ph]].

[104] D. Wyler and L. Wolfenstein, Nucl. Phys. **B218**, 205 (1983).

[105] G. t Hooft, in G 't Hooft *et al.* (eds.), *Proceedings of the 1979 Cargése Summer Institute on Recent Developments in Gauge Theories*, Plenum Press (1979).

[106] Y. Chikashige, R. N. Mohapatra and R. D. Peccei, Phys. Rev. Lett. **45**, 1926 (1980); *ibid.*, Phys. Lett. **B98**, 265 (1981).

[107] M. C. Gonzalez-Garcia and J. W. F. Valle, Phys. Lett. **B216**, 360 (1989).

[108] E. Ma, Phys. Rev. **D80**, 013013 (2009) [arXiv:0904.4450 [hep-ph]]; F. Bazzocchi, D. G. Cerdeno, C. Munoz and J. W. F. Valle, Phys. Rev. **D81**, 051701 (2010) [arXiv:0907.1262 [hep-ph]].

[109] N. Arkani-Hamed, L. J. Hall, D. Tucker-Smith and N. Weiner, Phys. Rev. **D63**, 056003 (2001) [hep-ph/9911421]; S. C. Park, K. Wang and T. T. Yanagida, Phys. Lett. **B685**, 309 (2010) [arXiv:0909.2937 [hep-ph]]; C. S. Fong, R. N. Mohapatra, I. Sung, Phys. Lett. **B704**, 171 (2011) [arXiv:1107.4086 [hep-ph]].

[110] J. Kersten and A. Y. Smirnov, Phys. Rev. **D76** (2007) 073005 [arXiv:0705.3221 [hep-ph]].

[111] X. -G. He, S. Oh, J. Tandean and C. -C. Wen, Phys. Rev. **D80**, 073012 (2009) [arXiv:0907.1607 [hep-ph]].

[112] F. del Aguila and J. A. Aguilar-Saavedra, Nucl. Phys. **B813**, 22 (2009) [arXiv:0808.2468 [hep-ph]].

[113] A. Datta, M. Guchait and D. P. Roy, Phys. Rev. **D47**, 961 (1993) [hep-ph/9208228]; A. Datta, M. Guchait and A. Pilaftsis, Phys. Rev. **D50**, 3195 (1994) [hep-ph/9311257]; F. M. L. Almeida, Jr. *et al.*, Phys. Rev. **D62**, 075004 (2000) [hep-ph/0002024]; O. Panella *et al.*, Phys. Rev. **D65**, 035005 (2002) [hep-ph/0107308]; P. Fileviez Perez, T. Han and T. Li, Phys. Rev. **D80**, 073015 (2009) [arXiv:0907.4186 [hep-ph]].

[114] T. Han and B. Zhang, Phys. Rev. Lett. **97**, 171804 (2006) [hep-ph/0604064]; F. del Aguila, J. A. Aguilar-Saavedra and R. Pittau, JHEP **0710**, 047 (2007) [hep-ph/0703261].

[115] F. del Aguila and J. A. Aguilar-Saavedra, Phys. Lett. **B672**, 158 (2009) [arXiv:0809.2096 [hep-ph]]; F. del Aguila, J. A. Aguilar-Saavedra and J. de Blas, Acta Phys. Polon. **B40**, 2901 (2009) [arXiv:0910.2720 [hep-ph]].

[116] C. -Y. Chen and P. S. Bhupal Dev, arXiv:1112.6419 [hep-ph].

[117] S. Mondal, S. Biswas, P. Ghosh and S. Roy, arXiv:1201.1556 [hep-ph].

[118] S. Antusch, C. Biggio, E. Fernández-Martínez, M. B. Gavela and J. López-Pavón, JHEP **0610**, 084 (2006) [hep-ph/0607020].

[119] M. Malinsky, T. Ohlsson, and H. Zhang, Phys. Rev. **D79**, 073009 (2009) [arXiv:0903.1961 [hep-ph]]; M. Malinsky, T. Ohlsson, Z. -z. Xing and H. Zhang, Phys. Lett. **B679**, 242 (2009) [arXiv:0905.2889 [hep-ph]].

[120] P. S. Bhupal Dev and R. N. Mohapatra, Phys. Rev. **D81**, 013001 (2010) [arXiv:0910.3924 [hep-ph]].

[121] S. Goswami and T. Ota, Phys. Rev. **D78**, 033012 (2008) [arXiv:0802.1434 [hep-ph]]; S. Antusch, M. Blennow, E. Fernandez-Martinez and J. Lopez-Pavon, Phys. Rev. **D80**, 033002 (2009) [arXiv:0903.3986 [hep-ph]].

[122] T. Ohlsson, C. Popa and H. Zhang, Phys. Lett. **B692**, 257 (2010) [arXiv:1007.0106 [hep-ph]]; D. V. Forero, S. Morisi, M. Tortola and J. W. F. Valle, JHEP **1109**, 142 (2011) [arXiv:1107.6009 [hep-ph]].

[123] See e.g. A. Ceccucci, Z. Ligeti, and Y. Sakai, in Ref. [22], p. 146.

[124] Y. Farzan and A. Yu. Smirnov, Phys. Rev. **D65**, 113001 (2002) [hep-ph/0201105]; P. H. Frampton and X. -G. He, Phys. Lett. **B688**, 67 (2010) [arXiv:1003.0310 [hep-ph]]; *ibid.*, Phys. Rev. **D82**, 017301 (2010) [arXiv:1004.3679 [hep-ph]]; S. -W. Li and B. -Q. Ma, Phys. Lett. **B691**, 37 (2010) [arXiv:1003.5854 [hep-ph]]; A. Dueck, S. Petcov and W. Rodejohann, Phys. Rev. **D82**, 013005 (2010) [arXiv:1006.0227 [hep-ph]].

[125] E. Fernández-Martínez, M. B. Gavela, J. López-Pavón and O. Yasuda, Phys. Lett. **B649**, 427 (2007) [hep-ph/0703098]; G. Altarelli and D. Meloni, Nucl. Phys. **B809**, 158 (2009) [arXiv:0809.1041 [hep-ph]].

[126] H. Nunokawa, S. J. Parke and J. W. F. Valle, Prog. Part. Nucl. Phys. **60**, 338 (2008) [arXiv:0710.0554 [hep-ph]]; G. C. Branco, R. G. Felipe and F. R. Joaquim, arXiv:1111.5332 [hep-ph].

[127] G. C. Branco, M. N. Rebelo and J. W. F. Valle, Phys. Lett. **B225**, 385 (1989).

[128] J. Bernabeu, A. Santamaria, J. Vidal, A. Mendez, and J. W. F. Valle, Phys. Lett. **B187**, 303 (1987); M. C. Gonzalez-Garcia and J. W. F. Valle, Mod. Phys. Lett. **A7**, 477 (1992).

[129] F. Deppisch and J. W. F. Valle, Phys. Rev. **D72**, 036001 (2005) [hep-ph/0406040].

[130] F. Deppisch, T. S. Kosmas and J. W. F. Valle, Nucl. Phys. **B752**, 80 (2006) [hep-ph/0512360]; M. B. Gavela, T. Hambye, D. Hernandez and P. Hernandez, JHEP **0909**, 038 (2009) [arXiv:0906.1461 [hep-ph]]; D. Ibanez, S. Morisi and J. W. F. Valle, Phys. Rev. **D80**, 053015 (2009) [arXiv:0907.3109 [hep-ph]]; W. Abdallah, A. Awad, S. Khalil and H. Okada, arXiv:1105.1047 [hep-ph]; A. Abada, D. Das and C. Weiland, arXiv:1111.5836 [hep-ph].

[131] A. Ilakovac and A. Pilaftsis, Nucl. Phys. **B437**, 491 (1995) [hep-ph/9403398]; A. Abada, C. Biggio, F. Bonnet, M. B. Gavela and T. Hambye, JHEP **0712**, 061 (2007) [arXiv:0707.4058 [hep-ph]].

[132] J. N. Esteves, J. C. Romao, A. Villanova del Moral, M. Hirsch, J. W. F. Valle and W. Porod, JHEP **0905**, 003 (2009) [arXiv:0903.1408 [hep-ph]]; A. Ilakovac and A. Pilaftsis, Phys. Rev. **D80**, 091902 (2009) [arXiv:0904.2381 [hep-ph]].

[133] M. Mitra, G. Senjanovic and F. Vissani, Nucl. Phys. **B856**, 26 (2012) [arXiv:1108.0004 [hep-ph]].

[134] D. Hooper, arXiv:1201.1303 [astro-ph.CO].

190

[135] S. Gopalakrishna, A. de Gouvea, W. Porod, JCAP **0605**, 005 (2006) [hep-ph/0602027]; T. Asaka, K. Ishiwata, and T. Moroi, Phys. Rev. **D75**, 065001 (2007) [hep-ph/0612211]; H.-S. Lee, K. T. Matchev, and S. Nasri, Phys. Rev. **D76**, 041302 (2007) [hep-ph/0702223]; C. Arina and N. Fornengo, JHEP **0711**, 029 (2007) [arXiv:0709.4477 [hep-ph]]; Z. Thomas, D. Tucker-Smith, and N. Weiner, Phys. Rev. **D77**, 115015 (2008) [arXiv:0712.4146 [hep-ph]]; D. G. Cerdeno, C. Munoz, and O. Seto, Phys. Rev. **D79**, 023510 (2009) [arXiv:0807.3029 [hep-ph]]; F. Deppisch and A. Pilaftsis, JHEP **0810**, 080 (2008) [arXiv:0808.0490 [hep-ph]]; R. Allahverdi, B. Dutta, K. Richardson-McDaniel, and Y. Santoso, Phys. Lett. **B677**, 172 (2009) [arXiv:0902.3463 [hep-ph]]; P. Bandyopadhyay, E. J. Chun, J. -C. Park, JHEP **1106**, 129 (2011) [arXiv:1105.1652 [hep-ph]]; D. G. Cerdeno, J. -H. Huh, M. Peiro, O. Seto, JCAP **1111**, 027 (2011) [arXiv:1108.0978 [hep-ph]].

[136] C. Arina, F. Bazzocchi, N. Fornengo, J. C. Romao, J. W. F. Valle, Phys. Rev. Lett. **101**, 161802 (2008) [arXiv:0806.3225 [hep-ph]].

[137] S. Khalil, H. Okada, T. Toma, JHEP **1107**, 026 (2011) [arXiv:1102.4249 [hep-ph]].

[138] Z. Kang, J. Li, T. Li, T. Liu, J. Yang, [arXiv:1102.5644 [hep-ph]].

[139] F.-X. Josse-Michaux, E. Molinaro, Phys. Rev. **D84**, 125021 (2011) [arXiv:1108.0482 [hep-ph]].

[140] H. An, P. S. Bhupal Dev, Y. Cai and R. N. Mohapatra, Phys. Rev. Lett. **108**, 081806 (2012) [arXiv:1110.1366 [hep-ph]].

[141] D. Tucker-Smith, N. Weiner, Phys. Rev. **D64**, 043502 (2001) [hep-ph/0101138].

[142] G. Belanger, S. Kraml and A. Lessa, JHEP **1107**, 083 (2011) [arXiv:1105.4878 [hep-ph]].

[143] M. Fukugita and T. Yanagida, Phys. Lett. **B174**, 45 (1986).

[144] W. Buchmuller, R. D. Peccei and T. Yanagida, Ann. Rev. Nucl. Part. Sci. **55**, 311 (2005) [hep-ph/0502169]; S. Davidson, E. Nardi and Y. Nir, Phys. Rept. **466**, 105 (2008) [arXiv:0802.2962 [hep-ph]];

[145] J. M. Frere, T. Hambye and G. Vertongen, JHEP **0901**, 051 (2009) [arXiv:0806.0841 [hep-ph]].

[146] S. Blanchet, Z. Chacko, S. S. Granor and R. N. Mohapatra, Phys. Rev. **D82**, 076008 (2010) [arXiv:0904.2174 [hep-ph]].

[147] S. Blanchet, P. S. Bhupal Dev and R. N. Mohapatra, Phys. Rev. **D82**, 115025 (2010) [arXiv:1010.1471 [hep-ph]].

[148] J. Garayoa, M. C. Gonzalez-Garcia and N. Rius, JHEP **0702**, 021 (2007) [hep-ph/0611311].

[149] S. Khalil, Phys. Rev. **D82**, 077702 (2010) [arXiv:1004.0013 [hep-ph]].

[150] A. Elsayed, S. Khalil and S. Moretti, arXiv:1106.2130 [hep-ph]; S. Khalil and A. Sil, Phys. Rev. **D84**, 103511 (2011) [arXiv:1108.1973 [hep-ph]].

[151] P. S. Bhupal Dev and R. N. Mohapatra, Phys. Rev. **D82**, 035014 (2010) [arXiv:1003.6102 [hep-ph]].

[152] For an extensive recent study, see J. N. Esteves, J. C. Romao, M. Hirsch, W. Porod, F. Staub and A. Vicente, JHEP **1201**, 095 (2012) [arXiv:1109.6478 [hep-ph]].

[153] N. G. Deshpande, E. Keith and T. G. Rizzo, Phys. Rev. Lett. **70**, 3189 (1993) [hep-ph/9211310].

[154] S. K. Majee, M. K. Parida, A. Raychaudhuri and U. Sarkar, Phys. Rev. **D75**, 075003 (2007) [hep-ph/0701109]; M. K. Parida, Phys. Rev. **D78**, 053004 (2008) [arXiv:0804.4571 [hep-ph]]; S. K. Majee, M. K. Parida and A. Raychaudhuri, Phys. Lett. **B668**, 299 (2008) [arXiv:0807.3959 [hep-ph]]; J. Kopp, M. Lindner, V. Niro and T. E. J. Underwood, Phys. Rev. **D81**, 025008 (2010) [arXiv:0909.2653 [hep-ph]].

[155] T. Fukuyama, A. Ilakovac, T. Kikuchi and K. Matsuda, JHEP **0506**, 016 (2005) [arXiv:hep-ph/0503114].

[156] M. Shiozawa, `http://nnn09.colostate.edu/Talks/Session02`; H. Nishino *et al.* [The Super-Kamiokande Collaboration], arXiv:1203.4030 [hep-ex].

[157] S. P. Martin and M. T. Vaughn, Phys. Rev. **D50**, 2282 (1994) [Erratum-ibid. **D78**, 039903 (2008)] [hep-ph/9311340].

[158] R. W. Robinett and J. L. Rosner, Phys. Rev. **D25**, 3036 (1982) [Erratum-ibid. **D27**, 679 (1983)]; *ibid.* **D26**, 2396 (1982); Y. Tosa, G. C. Branco and R. E. Marshak, Phys. Rev. **D28**, 1731 (1983).

[159] D. Chang, R. N. Mohapatra and M. K. Parida, Phys. Rev. Lett. **52**, 1072 (1984).

[160] C. R. Das and M. K. Parida, Eur. Phys. J. **C20**, 121 (2001) [hep-ph/0010004].

[161] N. Setzer and S. Spinner, Phys. Rev. **D71**, 115010 (2005) [hep-ph/0503244].

[162] P. Fayet and J. Iliopoulos, Phys. Lett. **51B**, 461 (1974).

[163] M. Malinsky, J. C. Romao and J. W. F. Valle, Phys. Rev. Lett. **95**, 161801 (2005) [hep-ph/0506296].

[164] C. H. Albright and S. M. Barr, Phys. Rev. **D62**, 093008 (2000) [hep-ph/0003251]; K. S. Babu, J. C. Pati and F. Wilczek, Nucl. Phys. **B566**, 33 (2000) [hep-ph/9812538]; X. -d. Ji, Y. -c. Li and R. N. Mohapatra, Phys. Lett. **B633**, 755 (2006) [hep-ph/0510353]; and references therein.

[165] R. N. Mohapatra and B. Sakita, Phys. Rev. D **21**, 1062 (1980).

[166] M. Hirsch, S. Morisi and J. W. F. Valle, Phys. Lett. **B679**, 454 (2009) [arXiv:0905.3056 [hep-ph]]; A. H. Chan, H. B. Low and Z. -z. Xing, Phys. Rev. **D80**, 073006 (2009) [arXiv:0908.0822 [hep-ph]]; L. Dorame, S. Morisi, E. Peinado, A. D. Rojas and J. W. F. Valle, arXiv:1203.0155 [hep-ph].

[167] W. Buchmuller, P. Di Bari and M. Plumacher, Phys. Lett. **B547**, 128 (2002) [hep-ph/0209301]; *ibid.*, Nucl. Phys. **B665**, 445 (2003) [hep-ph/0302092].

[168] V. A. Kuzmin, V. A. Rubakov and M. E. Shaposhnikov, Phys. Lett. **B155**, 36 (1985).

[169] M. Plumacher, Z. Phys. **C74**, 549 (1997) [hep-ph/9604229].

[170] See e.g., E. W. Kolb and M. S. Turner, *The Early Universe*, Westview Press (1989).

[171] See e.g., W. Buchmuller, P. Di Bari and M. Plumacher, Annals Phys. **315**, 305 (2005) [hep-ph/0401240].

[172] W. Buchmuller and M. Plumacher, Phys. Lett. **B389**, 73 (1996) [hep-ph/9608308].

[173] M. Fujii, K. Hamaguchi and T. Yanagida, Phys. Rev. **D65**, 115012 (2002) [hep-ph/0202210].

[174] E. W. Kolb and S. Wolfram, Nucl. Phys. **B172**, 224 (1980) [Erratum-*ibid.* **B195**, 542 (1982)]; J. A. Harvey, E. W. Kolb, D. B. Reiss and S. Wolfram, Nucl. Phys. **B201**, 16 (1982).

[175] W. Buchmüller and M. Plümacher, Phys. Lett. **B511**, 74 (2001) [hep-ph/0104189]; E. Nardi, Y. Nir, J. Racker and E. Roulet, JHEP **0601**, 068 (2006) [hep-ph/0512052].

[176] G. F. Giudice, A. Notari, M. Raidal, A. Riotto and A. Strumia, Nucl. Phys. **B685**, 89 (2004) [hep-ph/0310123].

[177] M. A. Luty, Phys. Rev. **D45**, 455 (1992); G. C. Branco *et al.*, Phys. Rev. **D67**, 073025 (2003) [hep-ph/0211001].

[178] R. Barbieri, P. Creminelli, A. Strumia and N. Tetradis, Nucl. Phys. **B575**, 61 (2000) [hep-ph/9911315].

[179] J. A. Harvey and M. S. Turner, Phys. Rev. **D42**, 3344 (1990).

[180] M. Laine and M. E. Shaposhnikov, Phys. Rev. **D61**, 117302 (2000) [hep-ph/9911473].

[181] K. Hamaguchi, H. Murayama and T. Yanagida, Phys. Rev. **D65**, 043512 (2002) [hep-ph/0109030].

[182] S. Davidson and A. Ibarra, Phys. Lett. **B535**, 25 (2002) [hep-ph/0202239].

[183] A. H. Guth, Phys. Rev. **D23**, 347 (1981); A. D. Linde, Phys. Lett. **B108**, 389 (1982).

[184] H. Pagels and J. R. Primack, Phys. Rev. Lett. **48**, 223 (1982); S. Weinberg, Phys. Rev. Lett. **48**, 1776 (1982); M. Y. Khlopov and A. D. Linde, Phys. Lett. **B138**, 265 (1984); J. R. Ellis, J. E. Kim, and D. V. Nanopoulos, Phys. Lett. **B145**, 181 (1984).

[185] T. Moroi, H. Murayama, and M. Yamaguchi, Phys. Lett. **B303**, 289 (1993); M. Bolz, A. Brandenburg, and W. Buchmuller, Nucl. Phys. **B606**, 518 (2001) [hep-ph/0012052]; J. Pradler and F. D. Steffen, Phys. Rev. **D75**, 023509 (2007) [hep-ph/0608344]; *ibid.*, Phys. Lett. **B648**, 224 (2007) [hep-ph/0612291].

[186] K. Kohri, T. Moroi, and A. Yotsuyanagi, Phys. Rev. **D73**, 123511 (2006) [hep-ph/0507245].

[187] A. Pilaftsis, Phys. Rev. **D56**, 5431 (1997) [hep-ph/9707235]; *ibid.*, Int. J. Mod. Phys. **A14**, 1811 (1999) [hep-ph/9812256]; A. Pilaftsis and T. E. J. Underwood, Nucl. Phys. **B692**, 303 (2004) [hep-ph/0309342].

[188] J. Liu and G. Segre, Phys. Rev. **D48**, 4609 (1993) [hep-ph/9304241]; M. Flanz, E. A. Paschos and U. Sarkar, Phys. Lett. **B345**, 248 (1995) [Erratum-*ibid.* **B382**, 447 (1996)] [hep-ph/9411366]; L. Covi, E. Roulet and F. Vissani, Phys. Lett. **B384**, 169 (1996) [hep-ph/9605319]; M. Flanz, E. A. Paschos, U. Sarkar and J. Weiss, Phys. Lett. **B389**, 693 (1996) [hep-ph/9607310].

[189] E. Nardi, Y. Nir, E. Roulet and J. Racker, JHEP **0601**, 164 (2006) [hep-ph/0601084]; A. Abada, S. Davidson, A. Ibarra, F. X. Josse-Michaux, M. Losada and A. Riotto, JHEP **0609**, 010 (2006) [hep-ph/0605281]; A. Abada, S. Davidson, F. X. Josse-Michaux, M. Losada and A. Riotto, JCAP **0604**, 004 (2006) [hep-ph/0601083]; S. Blanchet and P. Di Bari, JCAP **0703**, 018 (2007) [hep-ph/0607330].

[190] L. Covi and E. Roulet, Phys. Lett. **B399**, 113 (1997) [hep-ph/9611425].

[191] W. Buchmuller and M. Plumacher, Phys. Lett. **B431**, 354 (1998) [hep-ph/9710460]; A. Anisimov, A. Broncano and M. Plumacher, Nucl. Phys. **B737**, 176 (2006) [hep-ph/0511248].

[192] S. Antusch, S. Blanchet, M. Blennow and E. Fernandez-Martinez, JHEP **1001**, 017 (2010) [arXiv:0910.5957 [hep-ph]].

[193] S. K. Majee, M. K. Parida and A. Raychaudhuri, Phys. Lett. **B668**, 299 (2008) [arXiv:0807.3959 [hep-ph]].

[194] Y. Zhang, H. An, X. Ji and R. N. Mohapatra, Nucl. Phys. **B802**, 247 (2008) [arXiv:0712.4218 [hep-ph]]; D. Guadagnoli and R. N. Mohapatra, arXiv:1008.1074 [hep-ph].

[195] A. Pilaftsis and T. E. J. Underwood, Phys. Rev. **D72**, 113001 (2005) [hep-ph/0506107]; J. Garayoa, M. C. Gonzalez-Garcia and N. Rius, JHEP **0702**, 021 (2007) [hep-ph/0611311]; T. Asaka and S. Blanchet, Phys. Rev. **D78**, 123527 (2008) [arXiv:0810.3015 [hep-ph]]; M. C. Gonzalez-Garcia, J. Racker and N. Rius, JHEP **0911**, 079 (2009) [arXiv: 0909.3518 [hep-ph]].

[196] W. Y. Keung and G. Senjanovic, Phys. Rev. Lett. **50**, 1427 (1983).

[197] A Ferrari *et al.*, Phys. Rev. **D62**, 013001 (2000); S. N. Gninenko, M. M. Kirsanov, N. V. Krasnikov and V. A. Matveev, Phys. Atom. Nucl. **70**, 441 (2007) [hep-ph/0301140].

[198] A. Maiezza, M. Nemevsek, F. Nesti and G. Senjanovic, arXiv:1005.5160 [hep-ph].

[199] S. Blanchet, T. Hambye and F. X. Josse-Michaux, JHEP **1004**, 023 (2010) [arXiv:0912.3153 [hep-ph]].

[200] D. Aristizabal Sierra, M. Losada and E. Nardi, JCAP **0912**, 015 (2009) [arXiv:0905.0662 [hep-ph]].

[201] S. Blanchet and P. Di Bari, JCAP **0606**, 023 (2006) [hep-ph/0603107].

[202] Y. Burnier, M. Laine and M. Shaposhnikov, JCAP **0602**, 007 (2006) [hep-ph/0511246].

[203] M.-C. Chen and B. A. Dobrescu, in Ref. [22], p. 480.

[204] See e.g., O. Lahav and A. R. Liddle, in Ref. [22], p. 246.

[205] M. Kamionkowski and A. Kinkhabwala, Phys. Rev. **D57**, 3256 (1998) [hep-ph/9710337]; P. Salucci, F. Nesti, G. Gentile and C. F. Martins, Astron. Astrophys. **523**, A83 (2010) [arXiv:1003.3101 [astro-ph.GA]]; S. Garbari, J. I. Read and G. Lake, arXiv:1105.6339 [astro-ph.GA].

[206] See e.g., J. L. Feng, Ann. Rev. Astron. Astrophys. **48**, 495 (2010) [arXiv:1003.0904 [astro-ph.CO]].

[207] See e.g., C. Hagmann, H. Murayama, G. G. Raffelt, L. J. Rosenberg, and K. van Bibber, in Ref. [22], p. 496.

[208] See e.g., M. Drees and G. Gerbier, in Ref. [22], p. 255.

[209] See e.g., R. J. Gaitskell, Ann. Rev. Nucl. Part. Sci. **54**, 315 (2004).

[210] See e.g., J. Carr, G. Lamanna and J. Lavalle, Rept. Prog. Phys. **69**, 2475 (2006).

[211] T. Hebbeker, Phys. Lett. **B470**, 259 (1999) [hep-ph/9910326].

[212] J. S. Hagelin, G. L. Kane and S. Raby, Nucl. Phys. **B241**, 638 (1984); L. E. Ibanez, Phys. Lett. **B137**, 160 (1984).

[213] T. Falk, K. A. Olive and M. Srednicki, Phys. Lett. **B339**, 248 (1994) [hep-ph/9409270].

[214] See e.g., L. Baudis [XENON100 Collaboration], arXiv:1203.1589 [astro-ph.IM].

[215] J. Ellis and K. A. Olive, arXiv:1202.3262 [hep-ph].

[216] S. Chatrchyan *et al.* [CMS Collaboration], Phys. Rev. Lett. **107**, 221804 (2011) [arXiv:1109.2352 [hep-ex]]; G. Aad *et al.* [ATLAS Collaboration], Phys. Lett. **B710**, 67 (2012) [arXiv:1109.6572 [hep-ex]].

[217] J. R. Ellis, K. A. Olive, Y. Santoso and V. C. Spanos, Phys. Lett. **B565**, 176 (2003) [hep-ph/0303043].

[218] D. Hooper, T. Plehn, Phys. Lett. **B562**, 18 (2003) [hep-ph/0212226].

[219] J.-F. Grivaz, in Ref. [22], p. 1312.

[220] R. Bernabei *et al.* [DAMA Collaboration], Eur. Phys. J. **C56**, 333 (2008) [arXiv:0804.2741 [astro-ph]]; *ibid.* **C67**, 39 (2010) [arXiv:1002.1028 [astro-ph.GA]]; C. E. Aalseth *et al.* [CoGeNT Collaboration], Phys. Rev. Lett. **106**, 131301 (2011) [arXiv:1002.4703 [astro-ph.CO]]; G. Angloher *et al.* [CRESST-II Collaboration], arXiv:1109.0702 [astro-ph.CO].

[221] J. March-Russell, C. McCabe, M. McCullough, JHEP **1003** , 108 (2010) [arXiv:0911.4489 [hep-ph]].

[222] D. Tucker-Smith, N. Weiner, Nucl. Phys. Proc. Suppl. **124**, 197-200 (2003) [astro-ph/0208403].

[223] L. O'Raifeartaigh, Nucl. Phys. **B96**, 331 (1975).

[224] G. Belanger, F. Boudjema, A. Pukhov and A. Semenov, Comput. Phys. Commun. **180**, 747 (2009) [arXiv:0803.2360 [hep-ph]].

[225] S. P. Martin, in Ref. [60].

[226] J. L. Feng, J. Kumar, D. Marfatia, D. Sanford, Phys. Lett. **B703**, 124-127 (2011) [arXiv:1102.4331 [hep-ph]].

[227] G. J. Feldman, R. D. Cousins, Phys. Rev. **D57**, 3873-3889 (1998) [physics/9711021 [physics.data-an]].

[228] E. Aprile *et al.* [XENON100 Collaboration], arXiv:1104.2549 [astro-ph.CO]; E. Aprile *et al.* [XENON100 Collaboration], arXiv:1104.3121 [astro-ph.CO].

[229] R. Bernabei *et al.* [DAMA Collaboration], Eur. Phys. J. **C23**, 61-64 (2002); D. Y. Akimov *et al.* [ZEPLIN-III Collaboration], Phys. Lett. **B692**, 180-183 (2010) [arXiv:1003.5626 [hep-ex]]; Z. Ahmed *et al.* [CDMS-II Collaboration], Phys. Rev. **D83**, 112002 (2011) [arXiv:1012.5078 [astro-ph.CO]].

[230] C. E. Aalseth *et al.* [CoGeNT Collaboration], Phys. Rev. Lett. **107**, 141301 (2011). [arXiv:1106.0650 [astro-ph.CO]].

[231] H. An, F. Gao, [arXiv:1108.3943 [hep-ph]].

[232] M. R. Buckley, D. Hooper, J. L. Rosner, Phys. Lett. **B703**, 343 (2011) [arXiv:1106.3583 [hep-ph]]; D. Hooper, T. Linden, arXiv:1110.0006 [astro-ph.HE].

[233] S. Nussinov, L. -T. Wang and I. Yavin, JCAP **0908**, 037 (2009) [arXiv:0905.1333 [hep-ph]]; P. Schuster, N. Toro, N. Weiner and I. Yavin, Phys. Rev. **D82**, 115012 (2010) [arXiv:0910.1839 [hep-ph]].

[234] N. Sato *et al.* (Kamiokande Collaboration), Phys. Rev. **D44**, 2220 (1991).

[235] J. Goodman, M. Ibe, A. Rajaraman, W. Shepherd, T. M. P. Tait and H. -B. Yu, Phys. Rev. **D82**, 116010 (2010) [arXiv:1008.1783 [hep-ph]]; P. J. Fox, R. Harnik, J. Kopp and Y. Tsai, arXiv:1109.4398 [hep-ph].

[236] P. Nath *et al.*, Nucl. Phys. Proc. Suppl. **200-202**, 185 (2010) [arXiv:1001.2693 [hep-ph]].

[237] P. Langacker and S. Uma Sankar, Phys. Rev. **D40**, 1569 (1989).

[238] M. Czakon, J. Gluza and M. Zralek, Phys. Lett. **B458**, 355 (1999) [hep-ph/9904216].

[239] G. Bell, M. Bander and A. Soni, Phys. Rev. Lett. **48**, 848 (1982); T. Rizzo, Phys. Rev. **D50**, 325 (1994) [hep-ph/9311265]; G. Barenboim, J. Bernabeu, J. Prades and M. Raidal, Phys. Rev. **D55**, 4213 (1997) [hep-ph/9611347].

[240] J. Polak and M. Zralek, Nucl. Phys. **B363**, 385 (1991).

[241] P. Langacker and D. London, Phys. Rev. **D38**, 907 (1988); G. Bhattacharyya *et al.*, Mod. Phys. Lett. **A6**, (1991) 2921; E. Nardi, E. Roulet and D. Tommasini, Nucl. Phys. **B386** (1992) 239; *ibid.* Phys. Lett. **B327**, 319 (1994) [hep-ph/9402224]; A. Pilaftsis, Phys. Rev. **D52**, 459 (1995) [hep-ph/9502330]; S. Bergmann and A. Kagan, Nucl. Phys. **B538**, 368 (1999) [hep-ph/9803305];

B. Bekman *et al.*, Phys. Rev. **D66**, 093004 (2002) [hep-ph/0207015]; F. del Aguila, J. de Blas and M. Perez-Victoria, Phys. Rev. **D78**, 013010 (2008) [arXiv:0803.4008 [hep-ph]].

[242] J. G. Korner, A. Pilaftsis and K. Schilcher, Phys. Lett. **B300**, 381 (1993) [hep-ph/9301290]; A. Ilakovac and A. Pilaftsis, Nucl. Phys. **B437**, 491 (1995) [hep-ph/9403398]; D. Tommasini, G. Barenboim, J. Bernabeu and C. Jarlskog, Nucl. Phys. **B444**, 451 (1995) [hep-ph/9503228]; J. I. Illana and T. Riemann, Phys. Rev. **D63**, 053004 (2004) [hep-ph/0010193].

[243] A. Atre, T. Han, S. Pascoli and B. Zhang, JHEP **0905**, 030 (2009) [arXiv:0901.3589 [hep-ph]].

[244] R. N. Mohapatra, Phys. Rev. **D34**, 909 (1986); M. Hirsch, H. V. Klapdor-Kleingrothaus and O. Panella, Phys. Lett. **B374**, 7 (1996) [hep-ph/9602306]; M. Nemevsek, F. Nesti, G. Senjanovic and V. Tello, arXiv:1112.3061 [hep-ph].

[245] G. L. Bayatian *et al.* [CMS Collaboration], CERN-LHCC-2006-001.

[246] A. Pukhov *et al.*, hep-ph/9908288; A. Pukhov, hep-ph/0412191.

[247] J. Pumplin *et al.*, JHEP **0207**, 012 (2002) [hep-ph/0201195].

[248] F. M. L. Almeida, Jr. *et al.*, Eur. Phys. J. **C22**, 277 (2001) [hep-ph/0101077]; F. del Aguila *et al.*, Phys. Lett. **B613**, 170 (2005) [hep-ph/0502189]; F. del Aguila and J. A. Aguilar-Saavedra, JHEP **0505**, 026 (2005) [hep-ph/0503026];

[249] S. Bray, J. S. Lee and A. Pilaftsis, Phys. Lett. **B628**, 250 (2005) [hep-ph/0508077].

[250] T. Sjostrand, S. Mrenna and P. Z. Skands, JHEP **0605**, 026 (2006) [hep-ph/0603175].

[251] J. Conway, `http://www.physics.ucdavis.edu/~conway/research/software/pgs/pgs.html`

[252] J. Thaler, `http://www.jthaler.net/olympicswiki/doku.php?id=lhc_olympics:trigger_table#trigger_menu_for_the_lhc_olympics`

[253] Z. Sullivan and E. L. Berger, Phys. Rev. **D78**, 034030 (2008) [arXiv:0805.3720 [hep-ph]].

[254] K. Kanaya, Prog. Theor. Phys. **64**, 2278 (1980).

[255] S. Antusch, J. Kersten, M. Lindner, M. Ratz and M. A. Schmidt, JHEP **0503**, 024 (2005) [hep-ph/0501272]; M. Lindner, M. Ratz and M. A. Schmidt, JHEP **0509**, 081 (2005) [hep-ph/0506280].

[256] S. Antusch, J. P. Baumann and E. Fernández-Martínez, Nucl. Phys. **B810**, 369 (2009) [arXiv:0807.1003 [hep-ph]].

[257] R. J. Barlow, Nucl. Phys. Proc. Suppl. **218**, 44 (2011).

[258] L. Calibbi, A. Faccia, A. Masiero and S. K. Vempati, Phys. Rev. **D74**, 116002 (2006) [hep-ph/0605139].

[259] For a review, see e.g., P. Nath and P. Fileviez Pérez, Phys. Rept. **441**, 191 (2007) [hep-ph/0601023]; G. Senjanović, arXiv:0912.5375 [hep-ph].

[260] B. Bajc, P. Fileviez Perez and G. Senjanović, Phys. Rev. **D66**, 075005 (2002) [hep-ph/0204311]; I. Dorsner, P. Fileviez Perez and G. Rodrigo, Phys. Lett. **B649**, 197 (2007) [hep-ph/0610034].

[261] K. S. Babu and S. M. Barr, Phys. Rev. **D48**, 5354 (1993) [hep-ph/9306242].

[262] S. Dimopoulos, S. Raby and F. Wilczek, Phys. Rev. **D24**, 1681 (1981); L. Ibanez and G. G. Ross, Phys. Lett. **105B**, 439 (1981); N. Sakai, Z. Phys. **C11**, 153 (1981); M. B. Einhorn and D. R. T. Jones, Nucl. Phys. **B196**, 475 (1982); W. J. Marciano and G. Senjanovic, Phys. Rev. **D25**, 3092 (1982).

[263] S. Weinberg, Phys. Rev. **D26**, 287 (1982); N. Sakai and T. Yanagida, Nucl. Phys. **B197**, 533 (1982); S. Dimopoulous, S. Raby and F. A. Wilczek, Phys. Lett. **B112**, 133 (1982).

[264] H. Murayama and A. Pierce, Phys. Rev. **D65**, 055009 (2002) [hep-ph/0108104].

[265] G. Altarelli, F. Feruglio and I. Masina, JHEP **0011**, 040 (2000) [hep-ph/0007254].

[266] R. Dermisek, A. Mafi and S. Raby, Phys. Rev. **D63**, 035001 (2001) [hep-ph/0007213].

[267] L. E. Ibáñez and C. Muñoz, Nucl. Phys. **B245**, 425 (1984).

[268] T. Goto and T. Nihei, Phys. Rev. **D59**, 115009 (1999) [hep-ph/9808255].

[269] H. S. Goh, R. N. Mohapatra, S. Nasri and S-P. Ng, Phys. Lett. **B587**, 105 (2004) [hep-ph/0311330].

[270] V. M. Belyaev and M. I. Vysotsky, Phys. Lett. **B127**, 215 (1983).

[271] R. Arnowitt, A. H. Chamseddine and P. Nath, Phys. Lett. **B156**, 215 (1985); P. Nath, A. H. Chamseddine and R. Arnowitt, Phys. Rev. **D32**, 2348 (1985).

[272] S. Antusch and M. Spinrath, Phys. Rev. **D79**, 095004 (2009) [arXiv:0902.4644 [hep-ph]].

[273] B. Dutta, Y. Mimura and R. N. Mohapatra, Phys. Rev. **D80**, 095021 (2009) [arXiv:0910.1043 [hep-ph]]; *ibid.*, JHEP **1005**, 034 (2010) [arXiv:0911.2242 [hep-ph]].

[274] B. Dutta, Y. Mimura and R. N. Mohapatra, Phys. Rev. **D72**, 075009 (2005) [hep-ph/0507319].

[275] A. J. Buras *et al.*, Nucl. Phys. **B135**, 66 (1978).

[276] J. Ellis, D. V. Nanopoulos and S. Rudaz, Nucl. Phys. **B202**, 43 (1982).

[277] J. Hisano, H. Murayama and T. Yanagida, Nucl. Phys. **B402**, 46 (1993) [hep-ph/9207279].

[278] G. Dissertori and G. P. Salam, in Ref. [22], p. 114; http://www-theory.lbl.gov/~ianh/alpha/alpha.html

[279] M. T. Grisaru, W. Siegel and M. Rocek, Nucl. Phys. **B159**, 429 (1979); N. Seiberg, Phys. Lett. **B318**, 469 (1993) [hep-ph/9309335].

[280] S. Brodsky *et al.*, Nucl. Phys. **B238**, 561 (1984).

[281] Y. Aoki, C. Dawson, J. Noaki and A. Soni, Phys. Rev. **D75**, 014507 (2007) [hep-lat/0607002]; Y. Aoki *et al.* (RBC-UKQCD Collaboration), Phys. Rev. **D78**, 054505 (2008) [arXiv:0806.1031 [hep-lat]].

[282] K. Abe *et al.*, arXiv:1109.3262 [hep-ex].

[283] T. Fukuyama *et al.*, J. Math. Phys. **46**, 033505 (2005) [hep-ph/0405300].

[284] C. S. Aulakh and A. Girdhar, Int. J. Mod. Phys. **A20**, 865 (2005) [hep-ph/0204097].